THE ROLE OF FIBRO-ADIPOGENIC PROGENITORS IN RADIATION-INDUCED MUSCLE PATHOLOGY

Nicolás Collao, M.Sc.

A thesis submitted to the University of Ottawa
in partial fulfillment of the requirements for the
Doctorate in Philosophy Degree in Human Kinetics

School of Human Kinetics
Faculty of Health Sciences
University of Ottawa

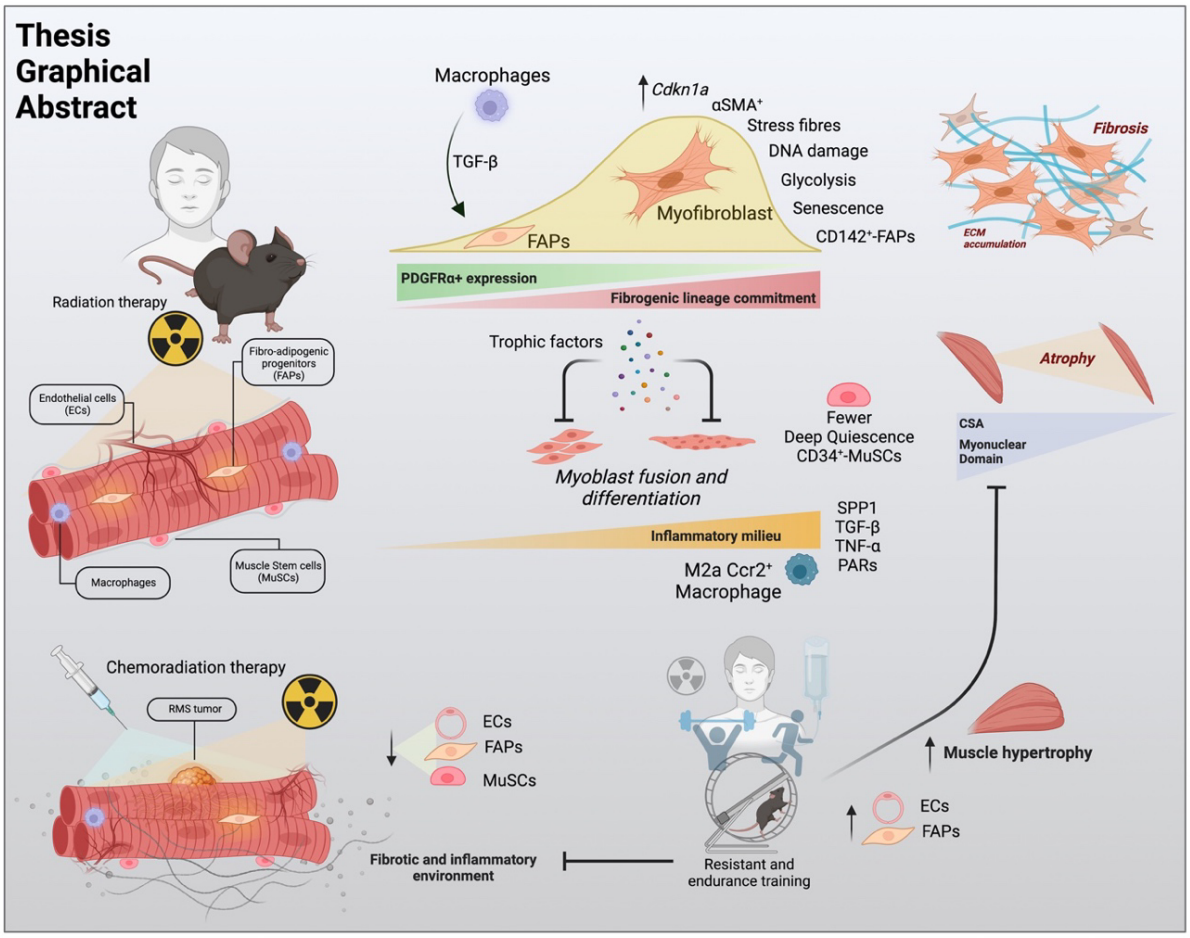

Abstract

Globally, cancer is one of the leading causes of mortality, with an estimated 18.1 million cancer cases, 10 million deaths, and 1.9 million new cases diagnosed in 2020 (Sung et al., 2021). However, during the past several decades, cancer survival has improved such that 82% of children and >2/3 of adults diagnosed with cancer will survive beyond five years (World Health Organization (WHO) - Childhood Cancer, 2021). Skeletal muscle atrophy and fibrosis are long-term adverse effects experienced by 80% of cancer survivors for which there is no available therapy (Paulino, 2004). These long-term consequences are related to the toxicity from the cancer treatment, leading to alterations in skeletal muscle function which can lead to comorbidities and increased mortality among

cancer survivors (Paulino, 2004; Williams et al., 2016). Thus, novel approaches to address the long-term effects of cancer therapy on skeletal muscle are critically needed. Exercise training is a potential non-pharmacological strategy that improves common cancer- and treatment-related side effects (Mustian et al., 2012). Specifically, exercise programs that combine resistance and endurance training (RET) have been shown to improve muscle strength and cardiovascular fitness in cancer survivors (Tong et al., 2020). The mechanisms responsible for these effects remain unknown.

The remarkable plasticity of skeletal muscle relies primarily on muscle stem (satellite) cells (MuSCs) (Lepper et al., 2011) that are regulated, in part, by muscle-resident stromal cells (Bentzinger et al., 2013). These different stromal cell types, including: vascular endothelial cells (ECs), immune cells, and mesenchymal progenitors, also known as fibro-adipogenic progenitors (FAPs), create the muscle stem cell niche (Yin et al., 2013). FAPs possess a dual role as they are involved in skeletal muscle maintenance and regeneration by secreting pro-myogenic trophic factors (Biferali et al., 2019; Joe et al., 2010; Uezumi et al., 2010; Wosczyna et al., 2019), but also contribute to fibrotic and fatty tissue accumulation in chronic degenerative conditions (Uezumi et al., 2010). The divergent features of FAPs highly depend on signals they receive from their microenvironment (Giuliani et al., 2021); however, FAP's contribution to cancer treatment-induced muscle pathology in cancer survivors remains unknown. The overall objective of this thesis is to begin to develop an understanding of the role of FAPs in cancer treatment-induced muscle pathology and to determine if RET represents an effective therapy to prevent the long-term muscle defects of juvenile cancer plus therapy.

Table of content

Acknowledgements

I want to thank my supervisor Dr. Michael De Lisio for giving me the opportunity to carry out my doctoral studies in his Laboratory. Thank you very much, Mike, for your unconditional guidance and support during these years. You taught me what a genuine commitment to science, and people looks like. Besides expanding my scientific knowledge and skills, thank you for the countless conversations that guided me through my future goals that have made me a better scientist, but above all, a better person.

I would like to thank my thesis advisory committee, Dr. Kristi Adamo and Dr. Naidine Wiper-Bergeron, for their valuable suggestion and feedback on my research projects. In addition to having given me valuable lessons that helped improve the integrity of my research and make me a better scientist.

Thank you very much to all the Lab members. To the past members, especially Matt and Eadan, for your support and friendship that continues today. To the present members, especially James, Kayleigh, and Lisa, for providing an excellent Lab environment and friendship. Thank you for all the laughs, moments, and memories we have shared, and we will continue to create. To all my friends outside the Lab, thank you for sharing incredible memories, campfires and laughs all these years. All those years in Ottawa, I am grateful for having found lifelong friendships with all of you.

Next, to my family in Chile, especially my parents, my mother, Alejandra, and my father, Eduardo, for their unconditional support and love over the years. I am grateful to have had the opportunity to show you my workplace, life, and friends in Ottawa and share incredible moments in Canada with you both. Thank you for being a fundamental pillar in my life. I love you so much.

I want to give special thank you to my partner Valentina, for having accompanied me all these years on this adventure. Thank you for the countless times you listened to me and supported me through the good and bad times during this process. I know it has not been easy for you to be away from your family during these years, and I sincerely appreciate the strength, commitment and love you have given me when I have needed it most. This achievement would not have been possible without you. Love you Vale.

List of Figures

Chapter IV

List of Supplementary Figures

List of Abbreviations

WHO: World Health Organization
RET: Resistance and endurance training
MuSCs: Muscle stem cells
FAPs: Fibro-adipogenic progenitors
ECs: Endothelial cells
RMS: Rhabdomyosarcoma
MyoD: Myoblast determination protein 1
Myf5: Myogenic factor 5
MyoG: Myogenin
Myf4: Myogenic regulatory factor 4
MHC: Myosin heavy chain
PDGFRα: Platelet-derived growth factor receptor
CD140a: Cluster of differentiation 140a
CD90: Cluster of differentiation 90
Sca-1: Stem cells antigen-1
SSB: Single DNA breaks
DSB: Doble DNA breaks
ROS: Reactive oxygen species
ECM: Extracellular matrix
SA: Synergistic muscle ablation
TGF-β1: Transforming growth factor Beta -1
Pax7: transcription factor paired box transcription factor 7
Pax3: transcription factor paired box transcription factor 3
CSA: Cross-sectional area
CreER: Cre recombinase, estrogen receptor
DTA: Diphtheria toxin fragment A
IL-4: Interleukin-4
IL-15: Interleukin-15
IL-13: Interleukin-13
FST: Follistatin
IGF-1: Insulin-like growth factor 1
WISP-1: WNT1-inducible-signaling pathway protein 1
BMP3: Bone Morphogenetic Protein 3
Tregs: Regulatory T cells
TNF-α: Tumor necrosis factor-alpha
Tie2: Angiopoietin-1 receptor
Vcam1: Vascular cell adhesion molecule 1
NGS: Next-generation sequencing
scRNA-seq: Single-cell RNA sequencing
Hic1: Hypermethylated in Cancer 1
Cxcl14: Chemokine ligand 14
Dpp4: Dipeptidyl peptidase-4
Osr1: Odd-Skipped Related Transcription Factor 1
CD55: Cluster of differentiation 55 or Complement decay-accelerating factor
CD142: Cluster of differentiation 142 or Platelet tissue factor.
ACSM: American College of Sports Medicine
Cdkn1a: Cyclin-dependent kinase inhibitor 1

CLTR: Contralateral limb
IR: Irradiation
CON: Control
Gy: Gray
Post-IR: Post-Irradiation
in vivo-IR: in vivo irradiation
in vitro-IR: in vitro irradiation
Gas/sol: Gastrocnemius/soleus
OCT: Optimal cutting temperature
FACS: Fluorescence-activated cell sorting
EdU: 5-ethynyl-2'-deoxyuridine
DAPI: 4', 6-diamidino-2-phenylindole
αSMA: alpha-smooth muscle actin
SA-β-Gal: Senescence-associated β-Galactosidase
mtDNA: mitochondria DNA
nDNA: nuclear DNA
OCR/ECAR: oxygen consumption rate/extracellular acidification
2-DG: 2-Deoxy-D-Glucose
DMD: Duchenne Muscular Dystrophy
ANID: Agencia Nacional de Investigacion y Desarrollo
CNMD: Centre for Neuromuscular Disease
SMCs: Smooth muscle cells
UMAP: Uniform Manifold Approximation and Projection
Col1a1: alpha-1 type I collagen
Acta1: Actin Alpha 1
Tnnc2: Troponin C2
Tagln: Transgelin
Cspq4: Chondroitin sulfate proteoglycan 4
CD68: Cluster of Differentiation 68
Ptprc: Protein tyrosine phosphatase, receptor type, C
S100a9: S100 calcium-binding protein A9
Ptn: Pleiotrophin
Mpz: Myelin protein zero
DEGs: Differentially expressed genes
GO: Gene Ontology
capECs1: Capillary endothelial cells 1
capECs2: Capillary endothelial cells 2
aECs: Arterial ECs
arlECs : Arteriolar endothelial cells
vECs: Venous ECs
GSEA: Gene set enrichment analysis
MSigDB: The Molecular Signatures Database
ncWNT: non-canonical WNT
NT: Neurotrophin
CALCR: Calcitonin receptor
RMS+Tx: Rhabdomyosarcoma plus treatment
GSA: Gene set analysis
MMP: Matrix metalloproteinase

Copyright Authorization

Chapter II: The manuscript is published in the Journal of Cachexia, Sarcopenia and Muscle.

Radiation induces long-term muscle fibrosis and promotes a fibrotic phenotype in fibro-adipogenic progenitors

Nicolas Collao, Donna D'Souza, Laura Messeiller, Evan Pilon, Jessica Lloyd, Jillian Larkin, Matthew Ngu, Alexanne Cuillerier, Alexander E. Green, Keir J. Menzies, Yan Burelle, and Michael De Lisio

http://doi.org/10.1002/jcsm.13320

"If you are the author of a published Wiley article, you have the right to reuse the full text of your published article as part of your thesis or dissertation. In this situation, you do not need to request permission from Wiley for this use." https://www.wiley.com/en-us/network/publishing/research-publishing/trending-stories/how-to-clear-permissions-for-a-thesis-or-dissertation

Creative Commons Attribution 4.0 International License, which allows for unrestricted use with proper citation. You can find a copy of the open access license at the following location: https://creativecommons.org/licenses/by-nd/4.0/

Chapter III: The manuscript was submitted to iScience-Cell Press.

Single-cell transcriptomic analysis of skeletal muscle cellular dynamics following radiation exposure

Nicolas Collao, Emma B Johannsen, Jesper Just, and Michael De Lisio

EMID:26ec750bda703659

Chapter IV: The manuscript is published in the Journal of Cachexia, Sarcopenia and Muscle.

Resistance endurance training improves muscle mass and the inflammatory/fibrotic transcriptome in a rhabdomyosarcoma model

Nicolas Collao†, Olivia Sanders†, Taylor Caminiti, Laura Messeiller, and Michael De Lisio

†These authors contribute equal to this work.

DOI: 10.1002/jcsm.13185

Schematic figures were created with BioRender.com under an institutional annual subscription: De Lisio Lab, University of Ottawa.

Funding Sources

Nicolás Collao Alonso was supported during his graduate program by The Chilean National Agency for Research and Development (Agencia Nacional de Investigacion y Desarrollo [ANID]), the uOttawa/CHEO Research Institute's Doctoral Fellowship for Advancement of Biological Perspectives for Exercise Interventions Across the Lifespan, and the uOttawa Eric Poulin Centre for Neuromuscular Disease (CNMD) Scholarship in Translational Research (STaR).

Chapter I

Introduction

Juvenile cancer survivors

Globally, 400,000 children and adolescents between 0 to 19 years old are diagnosed with cancer every year (World Health Organization (WHO) - Childhood Cancer, 2021). Advances in technology have led to improvements in both cancer diagnosis and treatment, increasing the survival rate of pediatric (also known as juvenile), and adult patients (Pulumati et al., 2023). In Canada, 85% of cancer patients are expected to survive beyond five years post-diagnosis, with the survival rates of juvenile cancer survivors increasing from 55% in the 1990s to 64% in 2021 (Canadian Cancer Society, 2021). Cancer survivors experience treatment-related long-term side effects which are particularly prevalent in childhood cancer survivors due to their exposure during development and long lifespan following treatment (Baskar et al., 2012; Miller et al., 2019). Patients who undergo cancer therapy can experience short-term adverse effects due to direct tissue damage; however, these acute effects are typically resolved quickly after treatment (De Ruysscher et al., 2019). Late consequences after treatment are progressive due to constant tissue deterioration, including skeletal muscle atrophy, fibrosis, hypoplasia, and contracture (Gawade et al., 2014). These adverse long-term effects on skeletal muscle manifest later in life and are associated with weakness and reduced mobility, leading to a decline in health, and functional capacity (Gawade et al., 2014). Cancer treatment during the juvenile growth stage affects physiological and cellular systems differently than in adulthood (Brand et al., 2017).

One of the more common juvenile cancers is rhabdomyosarcoma (RMS) which develops intramuscularly and comprises roughly 3 to 5% of all childhood cancers (Skapek et al., 2019). The five-year survival rate for juvenile patients with RMS is around 75% (Curry et al., 2021). RMS treatment involves multimodal therapies, including surgery and chemoradiation therapy (Skapek et al., 2019). Juvenile RMS patients can present two major RMS subtypes: embryonal and alveolar RMS (Hettmer & Wagers, 2010). Embryonal RMS is highly prevalent in children while alveolar RMS most commonly develops in adolescence (Arndt et al., 2012). The etiology of RMS is poorly understood; however, RMS tumours highly express myogenic markers such as Myoblast determination protein 1 (MyoD), Myogenic factor 5 (Myf5), and Myogenin (Keller & Guttridge, 2013), and are often located near skeletal muscle tissue suggesting that the cellular source of these tumours is myogenic (Keller & Guttridge, 2013). Indeed forced overexpression of oncogenic genes in MuSCs induces RMS development (Preussner et al., 2018). Growing evidence suggests that muscle-resident non-myogenic cells, such as mesenchymal progenitors, can develop myogenic characteristics and contribute to RMS formation and progression (Charytonowicz et al., 2009; Hettmer & Wagers, 2010). FAPs arise from mesenchymal origin (Vallecillo-García et al., 2017), and their canonical marker, Platelet-derived growth factor receptor alpha (PDGFRα) (Uezumi et al., 2010), has been detected in tumuor cells, and stromal compartments of human RMS (Ehnman et al., 2013). Lian and colleagues showed that RMS increased the production of collagen- and fibrillin-related genes that alter the surrounding microenvironment and contribute to fibrosis (Lian et al., 2021). These findings suggest that the heterogeneity among RMS subtypes may depend on the cell of origin.

Cancer and Therapy

Cancer patients are commonly treated with radiation therapy, chemotherapy, or a combination of both called chemoradiation therapy (Miller et al., 2019). Chemotherapy is a systemic anti-cancer drug treatment that is most often administered intravenously (Debela et al., 2021) in measured quantities over a specific number of intervals (Novotny & Szekeres, 2003). Radiation therapy most commonly uses ionizing radiation given in fractionated doses by a linear accelerator (De Ruysscher et al., 2019). Radiation is a common treatment modality for most cancers such as breast, lung, brain, and prostate, among others (De Ruysscher et al., 2019). The application of chemotherapy and/or radiotherapy depends on the tumuor (size, location, spread), and patient characteristics (age, health status, other related-diseases) (Sattar et al., 2018).

The main goal of cancer treatment is to prevent cell division (Baudino, 2015). Cancer treatments, such as chemo- and radiation therapy, cause direct or indirect genomic damage (Goldstein & Kastan, 2015). While radiation therapy can cause direct DNA instability leading to single- and/or double-strand DNA breaks (SSB and DSB), the primary mechanisms causing DNA damage is by generating reactive oxygen species (ROS) which then oxidize proteins, lipids, and nucleotides (Vignard et al., 2013). Chemotherapeutic agents such as vincristine, methotrexate, and doxorubicin, among others, cause DNA damage by disrupting the cytoskeleton, impairing DNA synthesis, and interfering with RNA translation (Bouwman & Jonkers, 2012). DSBs can be repaired through homologous recombination (Wright et al., 2018) or non-homologous end-joining (Lieber, 2010); however, unrepaired DNA damage can lead to cellular death (Roos et al., 2016). These cancer therapies are non-specific and negatively affect off-target tissue like

as skeletal muscle leading to long-term detrimental effects on cancer survivors (Christensen et al., 2014).

Effect of cancer treatment on skeletal muscle

Historically, it was believed that radiation had minimal effects on skeletal muscle due to its post-mitotic nature. However, recent evidence suggests that skeletal muscle is indeed sensitive to radiation damage and the skeletal muscle effects of radiation have been an emerging concern in clinical oncology (Christensen et al., 2014). The degree and complexity of the side effects of cancer treatment on skeletal muscle are multifactorial (Tisdale, 2001). The tumour type and stage, the specifics of the therapy applied, and the patient's overall health all contribute to the magnitude of the long-term adverse effects on skeletal muscle (Tisdale, 2001). In general, cancer therapy causes muscle atrophy and aberrant extracellular matrix (ECM) accumulation called fibrosis (al-Majid & McCarthy, 2001; Judge et al., 2018; Kallenbach et al., 2022) (*Figure 1*), leading to decreased muscle strength, weakness, and fatigue (Stubblefield, 2011). Indeed, 80% of juvenile cancer survivors experience muscle atrophy and fibrosis 20 years after treatment (Paulino, 2004). Hovi and colleagues showed that cancer treatment causes loss of muscle strength among juvenile patients, which persists during adulthood (Hovi et al., 1993). These long-term effects lead to poor quality of life, and an increased risk of morbidity and disability (Stubblefield, 2011).

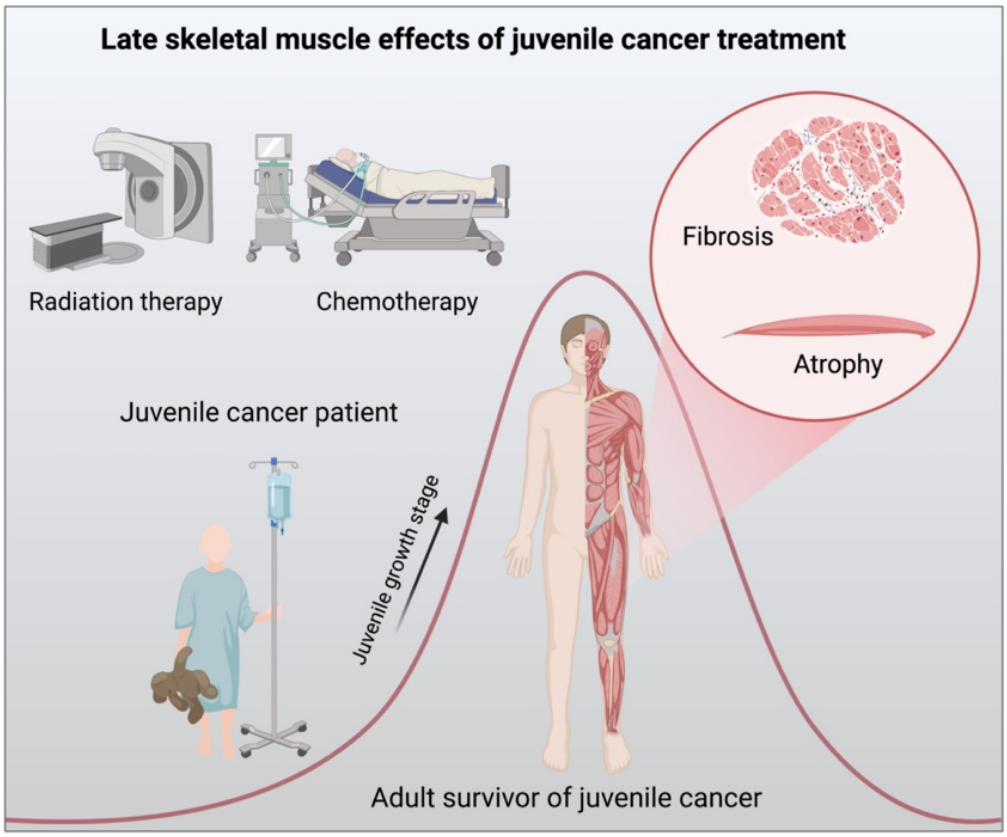

***Figure 1*. Late skeletal muscle effects of juvenile cancer treatment.** Radiation therapy, chemotherapy, or a combination of both, known as chemoradiation therapy, are common cancer treatment modalities in juvenile cancer patients. Cancer treatment during the growth period leads juvenile patients to endure long-term skeletal muscle consequences such as skeletal muscle atrophy and fibrosis.

Mechanistically, increased protein degradation, impaired protein synthesis, and reduced MuSC myogenic commitment may contribute to the loss of muscle mass in cancer survivors (Aversa et al., 2017; Bachman et al., 2020; Dale et al., 2021). However, the cause of muscle atrophy is still poorly understood. Muscle fibrosis results from an

imbalance of ECM turnover that favors synthesis over degradation (Herrera et al., 2018). While transient ECM production is essential for proper muscle regeneration (Csapo et al., 2020), ECM accumulation causes skeletal muscle dysfunction (Herrera et al., 2018). In addition to pathological ECM accumulation, a hallmark of skeletal muscle fibrosis is the disorganized matrix architecture of different ECM components, including diverse types of collagens, and fibronectin (Herrera et al., 2018). Further, persistent inflammation often accompanying fibrosis exacerbates the condition (Mack, 2018). At the cellular level, myofibroblasts which are activated fibroblasts that express highly contractile stress fibres are mainly responsible for ECM synthesis and deposition (Pakshir et al., 2020), and play a role in skeletal muscle fibrosis (Klingberg et al., 2013). FAPs give rise to myofibroblast in skeletal muscle and co-localize to fibrotic-rich areas in various myopathies (Contreras et al., 2016; Uezumi et al., 2014). Indeed, preclinical models of juvenile cancer plus therapy are characterized by skeletal muscle fibrosis and atrophy (Kallenbach et al., 2022); however, the contribution of FAPs to this process remains unknown.

Muscle satellite cells and cancer treatment

MuSCs, first discovered in 1961 (Mauro, 1961), are muscle stem cells indispensable for muscle growth, maintenance, and regeneration (Bachman & Chakkalakal, 2021; Lepper et al., 2011). MuSCs are usually in a quiescent (dormant) state, and are commonly identified by the expression of the paired box transcription factor 7 (Pax7) (Bentzinger et al., 2013). MuSCs reside between the basal lamina and the sarcolemma of the myofiber (Bentzinger et al., 2013). In response to muscle injury, MuSCs activate, enter the cell cycle, proliferate, and differentiate to fuse and donate their

nuclei with the existing myofibres (Yin et al., 2013). This process, termed myogenesis, allows for complete regeneration of the injured muscle while a small fraction of MuSCs return to a quiescence state to replenish the MuSC pool (Yin et al., 2013) (*Figure 2*). During skeletal muscle development, MuSCs are indispensable for normal muscle growth (Bachman et al., 2018a). Genetic deletion of MuSCs at 4-weeks of age, using a Pax7$^{CreER;Rosa26DTA}$ (P7DTA) mouse model, resulted in reduced cross-sectional area (CSA), myonuclear number, and force production as early as 8-weeks of age (Bachman et al., 2018a) and persisted to 18-weeks of age (Bachman et al., 2020). These results emphasize the essential role of MuSCs for muscle growth during development.

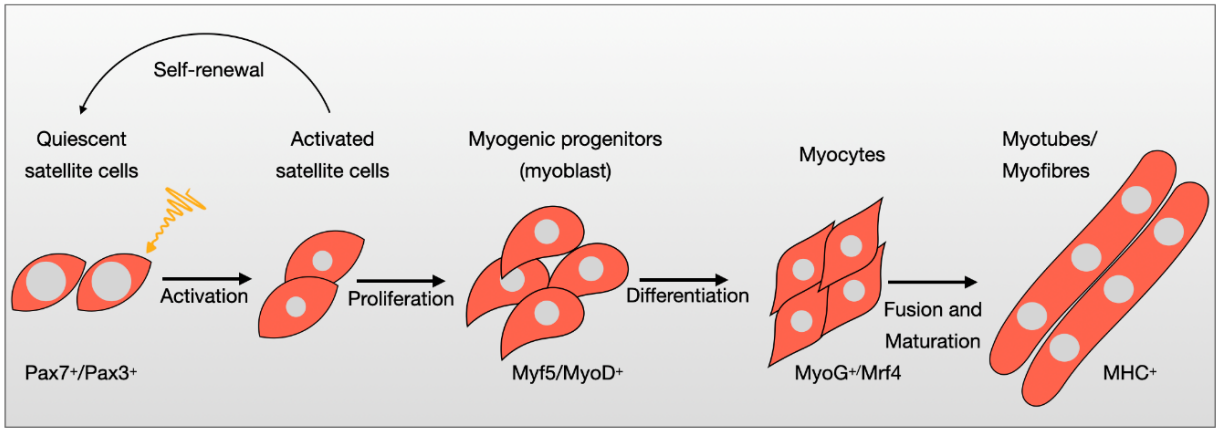

***Figure 2*. Schematic view of myogenesis.** The expression of Pax7/Pax3 identifies quiescent MuSCs. Upon muscle injury, MuSCs are activated and enter the cell cycle. MuSCs express Myogenic factor 5 (Myf5) and Myogenic differentiation factor 1 (MyoD) during proliferation and myogenic commitment. MuSCs downregulate Pax7 to differentiate and fuse to the injured myofibre. Finally, MuSCs start the process of terminal differentiation, expressing Myogenin (MyoG), Myogenic regulatory factor 4 (Mrf4) and Myosin heavy chain (MHC). To support future regenerative processes and maintain long-

term skeletal muscle function and integrity, a small fraction of MuSCs return to a quiescent state and replenish the quiescent pool.

Preclinical models have highlighted the effect of cancer treatment on MuSC content and how cancer therapy-induced alterations to MuSCs contributes to muscle pathology (Bachman et al., 2020; Paris et al., 2020). Early studies utilizing radiation exposure on skeletal muscle showed that radiation prevented increases in muscle weight and CSA following compensatory hypertrophy by synergistic muscle ablation (SA, Gastrocnemius and soleus muscles are removed, resulting in compensatory hypertrophy of the plantaris muscle) (Rosenblatt & Parry, 1992). Further, radiation exposure in one hindlimb followed by mechanical overload using SA or 90 days prevents muscle growth compared to the non-irradiated muscle (Adams et al., 2002). Findings from these early studies suggested that MuSCs are necessary for muscle hypertrophy.

Adult skeletal muscle is less susceptible to MuSC loss during cancer treatment than juvenile skeletal muscle (Bachman et al., 2020). Indeed, Scaramozza and colleagues showed a subpopulation of MuSCs in adult mice that highly express the transcription factor paired box transcription factor 3 (Pax3) be somewhat radioresistant and contribute to partial muscle regeneration following radiation exposure (Scaramozza et al., 2019). Conversely, in prepubertal/young mice, radiation therapy causes an immediate reduction in MuSC content, decreasing myonuclear number, CSA, and loss of muscle mass (Bachman et al., 2020). Radiation treatment in mice inoculated with a RMS cell line (M3-9-M cells) resulted in a decrease in MuSCs content, CSA, and myonuclear number and these effects were exacerbated when chemotherapy was combined with

radiation (Paris et al., 2020). Therefore, radiation-induced MuSC ablation in skeletal muscle has demonstrated the essential role of MuSCs for muscle growth during development (Bachman et al., 2020; Paris et al., 2020). As such, MuSC depletion has been established as a mechanism responsible for impaired skeletal muscle growth following radiation exposure.

MuSC transplantation alone has not successfully mitigated radiation-induced muscle defects, likely due to faulty MuSC engraftment (Boldrin et al., 2012). Scaramozza and colleagues showed that the radioresistant MuSC subpopulation expressing Pax3 retain their stem cell potential when transplanted into a pre-irradiated, and injured muscle; however, muscle regeneration was significantly impaired (Scaramozza et al., 2019). Further, MuSCs transplanted into irradiated skeletal muscle have significantly higher regenerative potential when transplantation occurs immediately following radiation rather than waiting several weeks (Boldrin et al., 2012). Together, these results suggest that alterations induced by radiation in the muscle niche contributes to impairments in skeletal muscle regeneration, and MuSC transplantation alone cannot resolve these alterations. Thus, identifying alterations in the muscle niche due to cancer treatment may lead to new therapies that reduce negative skeletal muscle effects of therapy.

Fibro-adipogenic progenitors in skeletal muscle homeostasis and pathology

FAPs are muscle-resident, non-myogenic progenitor cells that share phenotypic and functional characteristics with mesenchymal progenitor cells from other tissues in the body (Boppart et al., 2013). FAPs are identified in mice and humans by the expression

of PDGFRα (also known as cluster of differentiation 140a (CD140a)) (Uezumi et al., 2010), with further identification by Stem cell antigen-1 (Sca-1) in mice (Joe et al., 2010), or the cluster of differentiation 90 (CD90) in humans (Farup et al., 2021). FAPs are not myogenic themselves; however, they support muscle maintenance and regeneration by regulating MuSC proliferation and differentiation via paracrine mechanisms (Joe et al., 2010; Uezumi et al., 2010; Wosczyna et al., 2019). Indeed, genetic FAP depletion impairs muscle regeneration leading to muscle fibrosis (Santini et al., 2020). In response to muscle damage, FAPs activate and proliferate sensing cytokines, such as interleukin-4 (IL-4), IL-15, and IL-13 released by immune cells (Heredia et al., 2013; Kang et al., 2018; Moratal et al., 2018). In turn, FAPs secrete different trophic factors such as Follistatin (FST), Insulin-like growth factor 1 (IGF-1), IL-6, WNT1-inducible-signalling pathway protein 1 (WISP-1), and Bone Morphogenetic Protein 3 (BMP3) to support MuSC proliferation and differentiation (Joe et al., 2010; Lukjanenko et al., 2019; Uezumi et al., 2010, 2021). FAPs also interact with immune cells (Kastenschmidt et al., 2021; Kuswanto et al., 2016) and endothelial cells (Santini et al., 2020), to indirectly support myogenesis. Pro-regenerative immune cells prevent pathological FAP expansion during regeneration by releasing Tumour necrosis factor alpha (TNF-α), causing FAP apoptosis. (Lemos et al., 2015). Collectively, these data support the importance of FAP communication with different cell types in the muscle niche that can determine proper MuSC function and regeneration.

FAPs are multipotent cells with the capacity to differentiate into myofibroblast, adipocytes, or osteocytes/chondrocytes *in vitro* and *in vivo* (Contreras et al., 2021) (*Figure 3*). Interestingly, in muscle pathologies characterized by excessive ECM deposition, FAP

content is generally increased, and they accumulate in fibrotic areas (Gonzalez et al., 2017; Hogarth et al., 2019; Ieronimakis et al., 2016; Uezumi et al., 2014). In *mdx* mice, a model of Duchenne muscular dystrophy, FAPs differentiated into Collagen I-producing myofibroblasts confirming their fibrogenic potential *in vivo* (Uezumi et al., 2011). TGF-β1 signalling is one of the main signalling pathways involved in FAP fate decision (Giuliani et al., 2021). Immune cells secrete TGF-β1 upon muscle injury, promoting transient FAP proliferation and survival to support MuSC myogenic commitment. (Contreras et al., 2019; Juban et al., 2018; Lemos et al., 2015; Theret et al., 2022). Conversely, the persistent increase in TGF-β1 signalling in muscle pathologies promotes FAP differentiation into myofibroblast (Ismaeel et al., 2019; Piersma et al., 2015). Given the divergent roles FAPs play in muscle regeneration and pathology, recent interest in the field has focused on their heterogeneity to discriminate pro-regenerative from pro-fibrotic subpopulations.

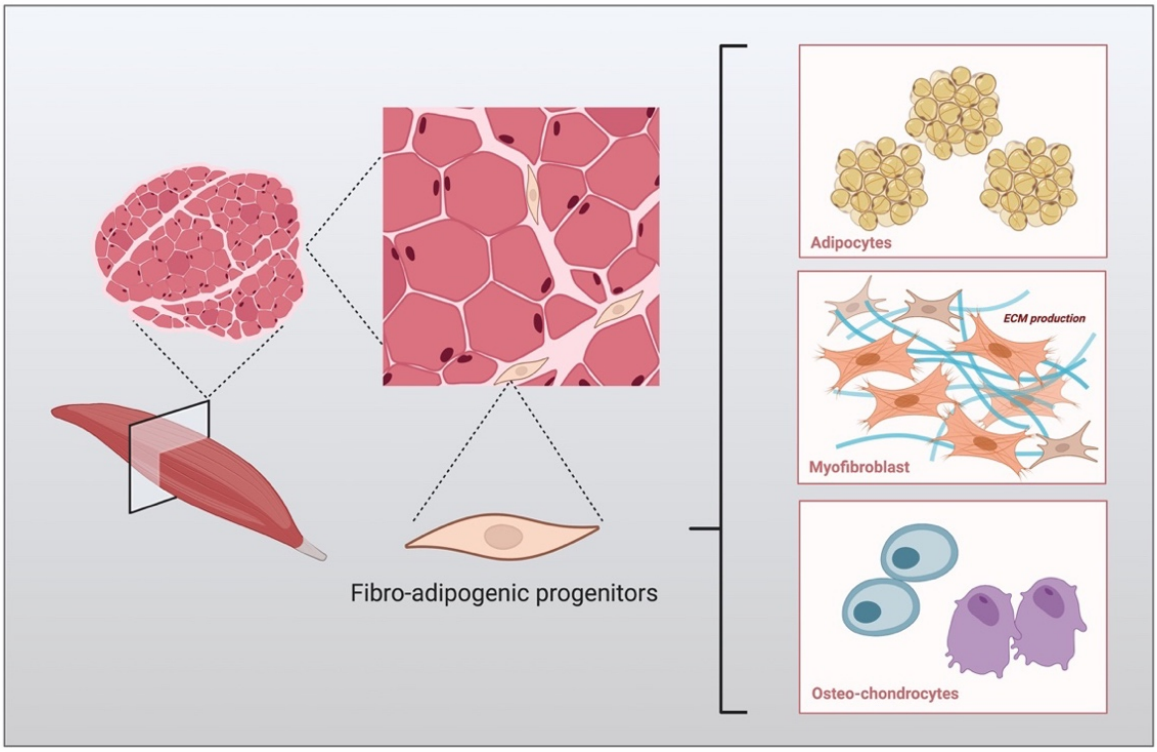

Figure 3. **Fibro-adipogenic progenitors are multipotent.** Fibro-Adipogenic Progenitors (FAPs) are muscle-resident stromal cells with multi-lineage differentiation potential. FAPs can differentiate into adipocytes, myofibroblast, or osteocytes- chondrocytes *in vitro* and *in vivo*.

FAP fate depends on signals received from their microenvironment (Camps et al., 2020; Leinroth et al., 2022). By analyzing gene expression in single cells, Puri's Lab first explored FAP heterogeneity by using a dynamic qPCR array at a single-cell level (Malecova et al., 2018). The authors showed that a $Tie2^{+}$ (Angiopoietin-1 receptor)-FAP subpopulation was associated with muscle growth and angiogenesis. Conversely, during acute and chronic muscle regeneration, an increase in activated $Vcam1^{+}$ (Vascular cell adhesion molecule 1)-FAP was associated with muscle fibrosis (Malecova et al., 2018). This study was the first to reveal the distinct cell state that FAPs exhibit during muscle growth, regeneration, and disease.

Next-generation sequencing (NGS) technology, such as single-cell RNA sequencing (scRNA-seq), has brought advantages by measuring hundreds of thousands of transcripts within individual cells, providing valuable insights into cell heterogeneity and cell-cell communication in various tissues (Vallejos, 2019) including skeletal muscle (De Micheli et al., 2020; Dell'Orso et al., 2019; Fan et al., 2021; Farup et al., 2021; Krasniewski et al., 2022; Leinroth et al., 2022; McKellar et al., 2021). The application of scRNA-seq technology in mouse models of skeletal muscle regeneration (De Micheli et al., 2020; Oprescu et al., 2020; Rubenstein et al., 2020), and human skeletal muscle (Farup et al.,

2021) has identified diverse FAP subpopulations. Oprescu and colleagues, by using scRNA-seq analysis, identified two FAP subpopulations expressing Chemokine ligand 14 (Cxcl14), and Dipeptidyl peptidase-4 (Dpp4) in uninjured muscles (Oprescu et al., 2020). After skeletal muscle injury, an activated FAP expressing Odd-skipped related transcription factor 1 (Osr1) gives rise to the Dpp4 and Cxcl14 FAP subpopulation found in uninjured muscle (Leinroth et al., 2022), confirming the previous findings described by Oprescu and colleagues. A small subpopulation of quiescence FAP has been identified by the expression of Hypermethylated in cancer 1 (Hic1) in intact skeletal muscles (Scott et al., 2019). Furthermore, genetic $Hic1^{+}$-FAP ablation leads to FAP activation and proliferation, which impairs muscle regeneration (Scott et al., 2019). Emerging scRNA-seq studies have recently focused on mouse disease models (Camps et al., 2020; Saleh et al., 2022). Interestingly, in *mdx* mice, CD55 (Complement decay-accelerating factor)-FAPs promote adipogenesis, while CD142 (Tissue factor)-FAPs inhibit adipogenesis and have a pro-fibrotic phenotype (Camps et al., 2020). In adults with type 2 diabetes, Farup and colleagues identified a FAP subpopulation expressing *CD90* with high expression of collagen genes, contributing to muscle fibrosis (Farup et al., 2021). Together, growing evidence revealed transcriptional heterogeneity in FAPs during muscle regeneration and diseases. However, radiation exposure is a type of injury that does not cause immediate structural damage to skeletal muscle, compared with the constant membrane disruption occurring during regeneration and in dystrophic muscles. Therefore, determining the extent to which FAP heterogeneity contributes to radiation-induced muscle pathology will provide cellular clues to prevent the detrimental effects of radiation in cancer survivors.

Exercise training in cancer survivors

Children who receive cancer treatment experience reductions in their daily physical activity, cardiorespiratory capacity, muscle strength, and muscle mass (Ness et al., 2009). Furthermore, cancer survivors experience increased frailty, which increases the likelihood of chronic disease, and induces a premature aging-like phenotype (Oeffinger & Hudson, 2004). As adults, 80% of juvenile cancer survivors experience health complications, such as muscle atrophy and fibrosis, due to treatment (Oeffinger et al., 2006). These long-term health complications experienced by juvenile cancer survivors have led to different strategies, such as exercise training, to prevent or mitigate the treatment-related adverse effects in the muscle niche (Garcia & Thomson, 2014).

Exercise training is an effective non-pharmacological strategy to improve muscle strength, and cardiovascular fitness among cancer survivors and patients, leading to a better quality of life (Garcia & Thomson, 2014). Resistance and endurance training are two distinct exercise modalities that exert different cellular and functional muscle responses and are potent modulators of skeletal muscle adaptation (Hughes et al., 2018). Resistance exercise programs have been applied to counteract muscle atrophy, and strength loss in cancer survivors, improving their autonomy and quality of life (al-Majid & McCarthy, 2001; Garcia & Thomson, 2014; Tong et al., 2020). On the other hand, aerobic exercise during cancer treatment improves cardiorespiratory fitness (Bourdon et al., 2018), and time to exhaustion during the maximal aerobic test in pediatric cancer survivors (Sharkey et al., 1993). The American College of Sports Medicine (ACSM) suggests that cancer patients and survivors should perform a combination of RET (Campbell et al., 2019). Unfortunately, the exercise guidelines for this type of training

modality rely on studies conducted on adult survivors of breast and prostate cancer (Campbell et al., 2019). However, no specific RET guidelines currently exist for juvenile patients and survivors, and the mechanisms for the beneficial effects of exercise in cancer survivors have yet to be determined.

In non-cancer models and patients, cellular mechanisms highlight how these two exercise modalities, in part, improve muscle function and health by providing beneficial cues to the muscle niche (Bazgir et al., 2017). Resistance training induces MuSC proliferation and promotes myonuclear accretion, contributing to muscle hypertrophy (Murach et al., 2021). Resistance training also increases FAP content in humans, which was associated with myogenic differentiation markers (Farup et al., 2015). Similarly, endurance training induces MuSC activation and proliferation; without muscle hypertrophy (Masschelein et al., 2020) and increases FAP content in juvenile mice (D'Souza et al., 2019). Interestingly, a novel murine model of RET showed a robust hypertrophic response and MuSC expansion in healthy and aged mice (Dungan et al., 2019; Englund et al., 2021). However, whether RET can prevent the long-term muscle defects of juvenile cancer and therapy remains unknown.

Statement of the Problem

Cancer treatment-induced muscle pathology among juvenile cancer survivors commonly manifests as muscle atrophy and fibrosis. Healthy muscles require FAPs for proper muscle maintenance and regeneration. Conversely, FAPs are associated with exacerbated ECM deposition in different muscle pathologies resulting in muscle fibrosis. Exercise training induces beneficial health outcomes by preventing muscle atrophy and improving cardiovascular fitness in cancer patients and survivors. It remains unknown; however, whether FAP dysfunction contributes to radiation-induced muscle pathology and whether RET represents an effective exercise modality to prevent the long-term muscle defects of juvenile cancer survivors. Therefore, identifying the cellular source and mechanisms behind radiation-induced muscle pathology is crucial for developing and implementing novel strategies to prevent or delay cancer treatment-induced muscle defects and preserving long-term health and physical performance of survivors. These findings will significantly impact Canadians by improving the health of the growing population of long-term juvenile cancer survivors.

Aims and Hypotheses

This thesis aims to understand the role of FAPs in cancer treatment-induced muscle pathology and determine if RET is an effective treatment for preventing long-term muscle defects resulting from juvenile cancer therapy. This thesis is divided into three major sub-aims:

Sub-Aim 1: To characterize the effects of radiation on skeletal muscle architecture and muscle niche cells. We hypothesize that radiation will induce long-term detriments to muscle morphology characterized by muscle atrophy, fibrosis, and FAP dysfunction.

Sub-Aim 2: To identify transcriptional changes at the single-cell level induced by radiation and how these changes may influence cell-cell communication with the muscle microenvironment. We hypothesize that radiation will increase cell-cycle arrest genes such as cyclin-dependent kinase inhibitor 1(*Cdkn1a*) in different cell types in the muscle niche. With respect to FAPs, we hypothesize that radiation will increase their long-term fibrotic gene expression. Further, we expect to identify novel intercellular signalling pathways for future interrogation that could explain radiation-induced atrophy and fibrosis.

Sub-Aim 3: To determine the role of RET in preventing skeletal muscle atrophy and fibrosis in juvenile cancer plus therapy. We hypothesize that RET will prevent muscle atrophy and fibrosis induced by juvenile RMS plus therapy by restoring cellular components and inflammatory/fibrotic gene expression in the MuSC niche.

Chapter II

Radiation induces long-term muscle fibrosis and promotes a fibrotic phenotype in fibro-adipogenic progenitors

Nicolas Collao[1,2], Donna D'Souza[1], Laura Messeiller[1], Evan Pilon[1], Jessica Lloyd[1], Jillian Larkin[1], Matthew Ngu[1], Alexanne Cuillerier[3], Alexander E. Green[3,4], Keir J. Menzies[2,3,4], Yan Burelle[3], and Michael De Lisio[1,2,5]*

[1]School of Human Kinetics, Faculty of Health Science, [2]Éric Poulin Centre for Neuromuscular Disease, [3]Interdisciplinary School of Health Sciences, [4]Ottawa Institute of Systems Biology and Department of Biochemistry, Microbiology and Immunology, University of Ottawa, Ottawa, ON, Canada, and [5]Department of Cellular and Molecular Medicine, Regenerative Medicine Program, University of Ottawa, Ottawa, ON, Canada

Keywords: skeletal muscle, atrophy, mesenchymal progenitors, differentiation, myofibroblast, extracellular matrix, metabolism.

***Correspondence to:**
Michael De Lisio, PhD
School of Human Kinetics, and Department of Cellular and Molecular Medicine
University of Ottawa
Ottawa, ON, Canada
Phone: +1 613-562-5800 ext. 6987
Email: mdelisio@uottawa.ca

Abstract

Background: Radiation-induced muscle pathology, characterized by muscle atrophy and fibrotic tissue accumulation, is the most common debilitating late effect of therapeutic radiation exposure particularly in juvenile cancer survivors. In healthy muscle, fibro/adipogenic progenitors (FAPs) are required for muscle maintenance and regeneration, while in muscle pathology FAPs are precursors for exacerbated extracellular matrix (ECM) deposition. However, the role of FAPs in radiation-induced muscle pathology has not previously been explored.

Methods: Four-week-old Male CBA or C57Bl/6J mice received a single dose (16 Gy) of irradiation (IR) to a single hindlimb with the shielded contralateral limb (CLTR) serving as a non-IR control. Mice were sacrificed 3-, 7-, 14- (acute IR response), and 56-days post-IR (long-term IR response). Changes in skeletal muscle morphology, myofiber composition, muscle niche cellular dynamics, DNA damage, proliferation, mitochondrial respiration, and metabolism and changes in progenitor cell fate where assessed.

Results: Juvenile radiation exposure resulted in smaller myofiber cross-sectional area (CSA), particularly in type I and IIA myofibres ($p<0.05$) and reduced the proportion of type I myofibres ($p<0.05$). Skeletal muscle fibrosis ($p<0.05$) was evident at 56-days post-IR. The IR-limb had fewer endothelial cells ($p<0.05$) and fibro-adipogenic progenitors (FAPs) ($p<0.05$) at 56-days post-IR. Fewer muscle satellite (stem) cells (MuSCs) were detected at 3- and 56-days in the IR-limb ($p<0.05$). IR induced FAP senescence ($p<0.05$), increased their fibrogenic differentiation ($p<0.01$), and promoted their glycolytic metabolism. Further, IR altered the FAP secretome in a manner that impaired MuSCs differentiation ($p<0.05$) and fusion ($p<0.05$).

Conclusions: Our study suggests that following juvenile radiation exposure, FAPs contribute to long-term skeletal muscle atrophy and fibrosis. These findings provide rationale for investigating FAP-targeted therapies to ameliorate the negative late effects of radiation exposure in skeletal muscle.

Introduction

Cancer survivorship is steadily increasing such that 82% of children and >2/3 of adults diagnosed with cancer will survive beyond five years.[1] Radiation therapy is a standard treatment for over 50% of cancer patients; however, the negative consequences of radiation exposure to healthy tissues results in debilitating long-term consequences in cancer survivors.[2] Skeletal muscle was traditionally believed to be radiation resistant due to its post-mitotic nature. Recent evidence indicates that radiation-induced muscle pathology, characterized by atrophy, fibrosis, hypoplasia, and contracture,[S1] is experienced by 80% of cancer survivors.[S2] These late skeletal muscle effects have serious consequences including weakness and reduced mobility leading to morbidity and disability.[S3] The lack of effective therapies to prevent the detrimental muscular consequences of radiation therapy is a critical gap in cancer survivorship that affects the long-term health and physical performance of survivors.

Skeletal muscle growth, maintenance, and repair depends on complex and dynamic interactions between muscle satellite (stem) cells (MuSCs) and their niche.[S4] MuSCs reside in a quiescence state and are located between the basal lamina and the cell membrane of the muscle fibre.[S5] During skeletal muscle development, MuSCs are indispensable for normal muscle growth,[3] and lifelong maintenance.[4] Preclinical models have shown the effect of cancer treatment on skeletal muscle and MuSC content.[4–7] In prepubertal mice, radiation therapy causes an immediate reduction in MuSC content resulting in a decrease in myonuclear number, cross-sectional area (CSA), and loss of muscle mass.[4] Strategies to mitigate radiation damage by replacing lost MuSCs via transplantation have had limited clinical success,[S6] even when a relatively small

population of radiation-resistant MuSCs are transplanted.[8] These results suggest that the alteration induced by radiation in the muscle niche contribute to impaired skeletal muscle growth in juvenile cancer survivors.

The MuSC niche consists of several mononuclear cell populations that contribute to muscle growth and regeneration. Vascular endothelial cells (ECs) are important for maintaining MuSCs stemness, and controlling the infiltration of immune cells,[S7,S8] which are critical regulators of the inflammatory and regenerative response following muscle injury.[9,S9] Mesenchymal progenitors, also known as fibro-adipogenic progenitors (FAPs), are muscle resident, non-myogenic progenitor cells identified by the expression of platelet-derived growth factor receptor alpha (PDGFRα).[10,11] FAPs provide pro-myogenic signals essential for muscle growth, maintenance, and regeneration.[11,12] First described as regulators of myogenic differentiation during regeneration,[10] recent work has identified a role for FAPs in myoblast activation,[13] muscle growth,[14,S10,S11] and maintenance.[15] FAPs regulate these processes primarily via paracrine mechanisms[16,S12] with pro-myogenic subpopulations beginning to be identified.[17,18] Specific paracrine factors secreted by FAPs that promote myogenesis include bone morphogenic protein 3B (BMP3B),[19] WNT1 inducible signaling pathway protein 1 (WISP1),[13] and follistatin.[20] Conversely, under pathological conditions, FAPs directly contribute to fibrotic and fatty tissue accumulation in skeletal muscle[10-12,15] via their differentiation into myofibroblast, adipocytes, or osteocytes/chondrocytes.[21] Indeed, in diverse muscle pathologies, with excess ECM deposition, FAPs expand, and localize in rich fibrotic areas has been observed.[22-24,S13,S14] In a murine model of pediatric cancer plus radiation therapy, an increase in inflammatory and pro-fibrotic genes was observed,[14] accompanied by lifelong muscle fibrosis.[25] At the

cellular level, activated myofibroblasts, derived from FAPs, express stress fibres with highly contractile properties, and are mainly responsible for ECM synthesis, and deposition,[S15] have been implicated in skeletal muscle fibrosis.[S16] However, FAPs' role in radiation-induced muscle pathology has not previously been examined. Thus, the present study aimed to characterize the effects of radiation on skeletal muscle architecture and different cell population in the muscle niche with a specific focus on determining the role of FAPs in a juvenile model of radiation-induced muscle fibrosis.

Methods

Additional and complete description of the protocols are included in the extended methods section available in the supporting information.

Mice and ethics statement

The present study was conducted in accordance with guidelines established by the Canadian Council on Animal Care and received ethical approval from the University of Ottawa Animal Care and Veterinary Service Committee. Mice were housed in a pathogen-free environment (22-25 °C, 30 % humidity, and a 12-hour light: dark cycle) and were supplied with food and water *ad libitum.* Four-week-old male C57Bl/6J (#000664) mice and male CBA (#000656) mice were purchased from The Jackson Laboratory. An acclimatization period of one week was allowed for mice prior to experiments.

Acute radiation exposure

One hindlimb of four to five-week-old CBA or C57Bl/6J male mice was exposed to a single dose (16 Gy)[26] of *in vivo* irradiation (*in vivo*-IR) (X-RAD 320, Precision X-Ray Irradiation, North Branford, CT); while the rest of the body was lead-shielded and contralateral limb served as the non-IR control (CLTR). Mice were anesthetized by

constant administration of isoflurane and oxygen throughout the irradiation procedure. Mice underwent daily evaluation by animal facility staff following radiation exposure and were sacrificed at 3-, 7-, 14-, and 56-days post-IR (n=6-8/day, *Figure* 1A). For *in vitro* irradiation (*in vitro*-IR) experiments, a single dose of 1 Gy was applied to cells.[S17]

Tissue collection

The gastrocnemius/soleus (Gas/sol) complex was resected and divided for immunofluorescence analysis by embedding in optimal cutting temperature (OCT, Cat# 4585, Fisher Scientific) compound prior to flash freezing in liquid nitrogen-cooled isopentane (Cat# 277258-1L, Sigma-Aldrich), or flash frozen for western blot analysis and stored immediately at -80°C, or weighed for immediate processing for fluorescence-activated cell sorting (FACS) and/or flow cytometry analysis.

Histochemical and immunofluorescent analysis

From the mid-belly of the gastrocnemius, 10 μm-thick sections were cut and mounted on a Premium Frosted Microscope Slides (Cat# 12-544-2, Fisher Scientific) using an HM 525 NX-2210 cryostat. Masson's Trichrome staining was conducted by the Histology Core and the University of Ottawa as previously described.[27] A complete description of immunofluorescent protocols for Pax7, PDGFRα, CD31, F4/80, and CD206 are provided in the extended methods.

FACS and Flow cytometer

For FACS and flow cytometry analysis, skeletal muscle was prepared as previously described with some modifications (see extended methods).[S18]

Protein extraction and western blot analysis

Western blot analysis was performed as previously described.[28]

EdU incorporation assay

For *in vitro* 5-ethynyl-2'-deoxyuridine (EdU) incorporation assay, cells were seeded and incubated with 10 μM of EdU for 72 hours. Click-iT EdU Assay Kits (Ca# C10337, Thermo Fisher Scientific) was performed according to the manufacturer's instructions. Images were acquired by CellDiscoverer7 microscope (ZEISS) and analyzed by a semi-automated pipeline using Zen Blue (v. 2.6) software.

FAPs and C3H/10T1/2 cell culture and differentiation

Sorted primary FAPs were resuspended in DMEM High Glucose (Cat# 319-005-CL, Wiset Bioproducts), 20% FBS (Cat# 12483-020, Thermo Fisher Scientific), bFGF (5 ng/ml, Cat# F0291, MilliporeSigma), and 100 U/ml penicillin/streptomycin (P/S) (Cat# 15140-122, Thermo Fisher Scientific). C3H/10T1/2, a mesenchymal stem progenitor cell line (ATCC, Clone 8 Cat# CCL-226™), was used as an *in vitro* model of FAPs. C3H/10T1/2 were culture in DMEM High Glucose, 10% FBS, and 100U/ml P/S. FAP and C3H/10T1/2 adipogenic differentiation was initiated by applying MesenCult™ Adipogenic Differentiation Kit (Cat# 05507, Stemcell Technologies) for 3 days followed by adipogenic maintenance medium for 2 additional days (1 μg/ml insulin, Cat# I9278, MilliporeSigma). Fibrogenic differentiation of FAPs and C3H/10T1/2 cells was accomplished by culturing in DMEM high glucose, 2% horse serum, 5ng/ml of TGFβ-1 (Cat# 100-21, PeproTech), and 100U/ml P/S.

MuSCs culture and differentiation

Freshly FACS sorted MuSCs were cultured in growth media consisting of DMEM high glucose, 20% FBS, bFGF (5 ng/ml, Cat# F0291, MilliporeSigma), and 100U/ml P/S. Differentiation media for primary MuSCs consisted of DMEM low glucose (Cat#319-010-

CL, Wiset Bioproducts), 2% Horse Serum (Cat# 16050122, Thermo Fisher Scientific), and 100U/ml P/S.

DNA damage assay

Cells were fix in 4% PFA at 15 minutes and 24 hours after *in vitro*-IR. Anti-phospho-Histone H2A.X (Ser139) (Cat# 9718T, Cell Signaling Technology) was applied and the nuclei were counterstained with 4', 6-diamidino-2-phenylindole (DAPI) (Cat# D9542, Sigma-Aldrich).

Stress fibres assay

Fibrogenic differentiation was induced as described above then cells were fixed with 4% PFA for 10 minutes at room temperature, and permeabilized with 0.5% Triton X-100 for 5 minutes. Cells were incubated with block solution (10% FBS, 0.1% Triton X-100 in 1x PBS) for 1 hour. Primary antibody for alpha-smooth muscle actin (αSMA) was applied and incubated overnight at 4°C. Secondary antibody Alexa Fluor 594-Goat Anti-Mouse (Cat# A11005, Invitrogen) was used to visualize stress fibre formation and nuclei were counterstained with DAPI. Stress fibre formation was analyzed from line profiles[S19] with Fiji software.

Oxidative stress assay

Cells were exposed to *in vitro*-IR and resuspended in media containing CellROX™ Green reagents (Cat# C10444, Thermo Fisher Scientific) at a final concentration of 5 μM at 37°C for 30 minutes according to manufacturer's instructions.

Senescence assay

Senescence-associated β-Galactosidase (SA-β-Gal) staining was performed according to manufacturer's instructions (Cat# 9860, Cell Signaling Technology).

MitoTracker Green

FAPs were plated at a density of 0.5 x 10^6 cells in a 35 mm glass bottom cell culture dish (Cat# 627860, Greiner Bio-One) and stained with MitoTracker Green FM (Cat# M7514, Invitrogen) according to manufacturer's instructions.

Bioenergetic analysis

FACS-isolated FAPs were immediately plated on Seahorse XFe96 Microplates (Cat# 101085-004 Agilent Technologies) at 1.0 x 10^5 cells/well. *In vitro*-IR was applied with non-irradiated FAP cell cultures used as control (CON). After 24 hours cellular bioenergetics were evaluated using the Seahorse XFe96 Analyzer as previously described.[28]

DNA isolation and qPCR

The mitochondrial to nuclear DNA ratio was determined as previously described with minor modifications (see extended methods).[S20]

Low-High glucose assay

C3H/10T1/2 cells were cultured in low glucose DMEM (1 g/L) or high glucose DMEM (4.5 g/L), respectively, for 24 hours and αSMA staining was performed for stress fibres visualization.

FAP-derived conditioned media experiment

FAPs and MuSCs were freshly isolated from the IR and the CLTR limb at 3- and 56-days post- *in vivo*-IR by FACS. After three days of culture, conditioned media (CM) from IR-FAPs or CLTR-FAPs were recovered. CM was centrifuged to remove dead cells at 600 x *g* for 5 minutes and applied to non-irradiated primary myoblast (CON) with

differentiation media (50:50 volume/volume) as previously described.[30] Following three days in culture, myotubes were fixed and stained for Myosin Heavy Chain (MyHC).

Statistical analyses

Analyses were conducted by an investigator blinded to the experimental group. Values are expressed as mean ± standard error of the mean (SEM). The number of biological replicates (n) for each experiment is indicated in the figure legend. Comparisons between IR and CLTR limbs were performed using paired Student's t-tests. Comparisons between IR and CON cells were performed using unpaired Student's t-tests. Changes over time were performed using one-way ANOVAs. A p value of <0.05 was considered statistically significant. Statistics and graphs were prepared using GraphPad Prism version 8.0.1 software (GraphPad Software).

Results

Radiation induces long-term myofibre atrophy and a lower proportion of type I muscle fibres

Myofibre characteristics were evaluated at several timepoints following *in vivo*-IR. IR significantly reduced myofibre CSA at 3-, 14-, and 56-days post-IR compared to CLTR (*Figure* 1B) with significantly more smaller diameter fibres at 3-, 14-, and 56-days post-IR (*Figure* 1C). Similarly, myonuclear domain was significantly smaller in the IR-limb at 3-, and 56-days post-IR (*Figure* 1D). Type I and type IIA fibre CSA were significantly smaller at 56-days post-IR, with no change in type IIB fibre CSA (*Figure* 1E). Further, a smaller proportion of type I fibres was detected in the IR limb at 56-days post-IR with no differences in type IIA or IIB proportion (*Figure* 1E). Mice had higher body weight at day 56 compared to 3-, 7-, and 14-days (*Figure* S1A) with no changes in Gas/sol weight per

body weight (g/g) (*Figure* S1B) or myofibre content (*Figure* S1C). There was a trend for fewer myonuclei per fibre at 56-days (p=0.09, *Figure* S1D).

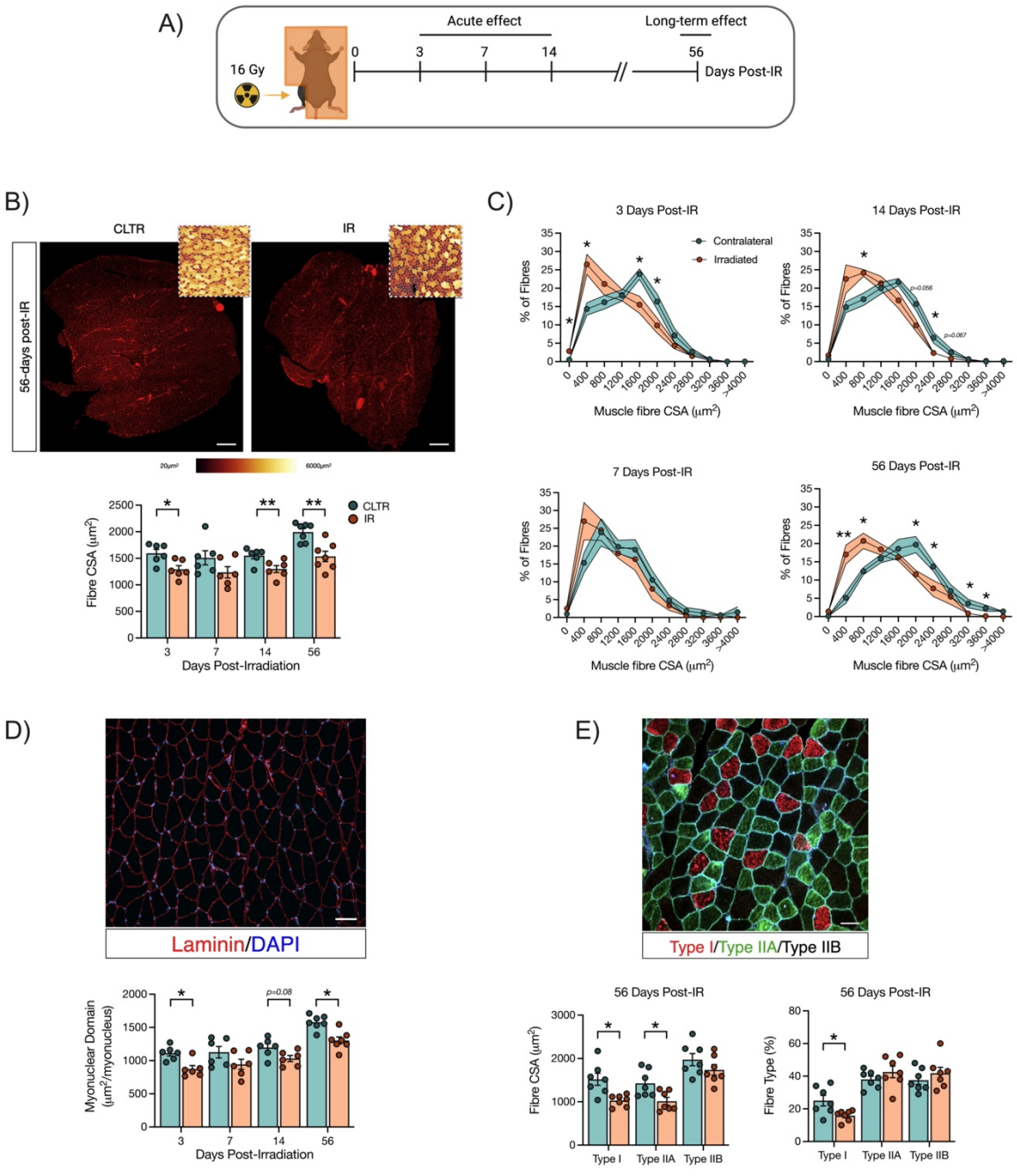

Figure 1. ***Radiation induces muscle atrophy particularly in oxidative fibres.***

(A) Experimental design. (B) Gas/sol muscle complex CSA at 56-days post-IR, Laminin staining (red), color-coded CSA to visualize changes in myofiber size. Scale bar: 500 μm, and fibre CSA (μm^2). (C) Muscle fibre distribution after 3-, 7-, 14-, and 56-days post-IR. (D) Myonuclear domain, and representative image of CSA. Laminin (red), DAPI (blue). Scale bar 100 μm. (E) Representative image of myosin heavy chain (MyHC) staining, type I fibres (red), type IIA (green), type IIB (black) at 56-days post-IR, fibre type CSA and % of muscle fibre type at 56-days post-IR. *$p < 0.05$, **$p < 0.01$; Paired Student's t-test between CLTR and IR at each timepoint (n=6-7).

Radiation induces long-term muscle fibrosis independent of sustained p-SMAD3 signalling

To confirm previous studies showing that IR-induces long-term muscle fibrosis,[25,26] Mason's trichrome staining was performed and fibrotic signalling pathways were evaluated using western blot analysis. Muscle fibrosis was significantly higher in the IR limb versus the CLTR limb at 56-days but not 14-days post-IR (*Figure* 2A). Significantly higher levels of the fibrotic markers fibronectin and α-smooth muscle actin (αSMA)[S21] were detected at 56-days post-IR (*Figure* 2B). SMAD3 phosphorylation, a well know downstream target of the transforming growth factor β1 (TGFβ-1) and a critical regulator of fibrosis,[S22] was significantly elevated at 3-days post-IR but returned to CLTR levels at 56-days post-IR (*Figure* 2B).

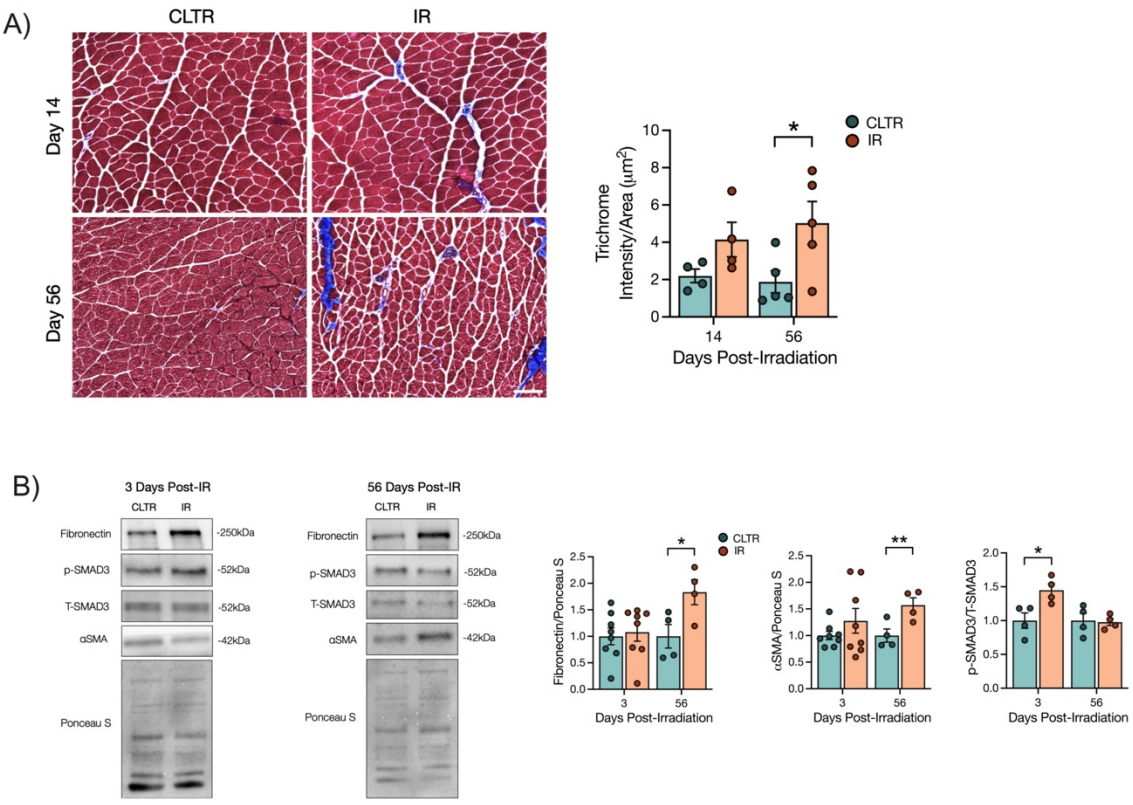

Figure 2. ***Radiation increases long-term muscle fibrosis independent of sustained p-SMAD3 signalling.***

(A) Representative image of Masson trichrome stain of muscle cryosections, and quantification of trichrome intensity per area of ROI. (B) Representative western blots of fibronectin, p-SMAD3, t-SMAD3, αSMA, and Ponceau S at 3- and 56-days post-IR. Quantification of fibronectin, αSMA, and p-SMAD3 protein expression. Scale bar: 200 μm (A). *p < 0.05, **p < 0.01; Paired Student's t-test between CLTR and IR at each timepoint (n=4-8).

Radiation depletes skeletal muscle endothelial cells, MuSCs, and FAPs

To explore the effect of juvenile radiation exposure on various mononuclear cell populations in muscle, flow cytometry analysis was performed (*Figure* S2A-B). We detected significantly fewer endothelial cells at 56-days in the IR limb with no change in hematopoietic cells versus CLTR (*Figure* 3A). We also detected significantly fewer MuSCs at 3-, and 56-days in IR versus CLTR, while FAPs were significantly lower at 56-days only in IR versus CLTR (*Figure* 3B). Our flow cytometry analyses were confirmed by immunofluorescence imaging showing significantly lower capillary to fibre ratio at 56-days in IR versus CLTR, with a trend for fewer $CD31^+$ cells/area at 56-days in IR versus CLTR (p=0.06, *Figure* S3A). Additional immunofluorescence analysis revealed significantly more macrophages in IR versus CLTR at 3-days post-IR but not at 56-days (*Figure* S3B), with significantly fewer 'M1' macrophages at 14-days in IR versus CLTR, and significantly more 'M2' macrophages at 3- and 7-days in IR versus CLTR (*Figure* S3B). Immunofluorescence further confirmed our MuSC and FAP flow analyses as significantly fewer MuSCs were present in IR versus CLTR at 7-, 14-, and 56-days (*Figure* 3C), while significantly fewer FAPs were detected at 14- and 56-days in IR versus CLTR (*Figure* 3D).

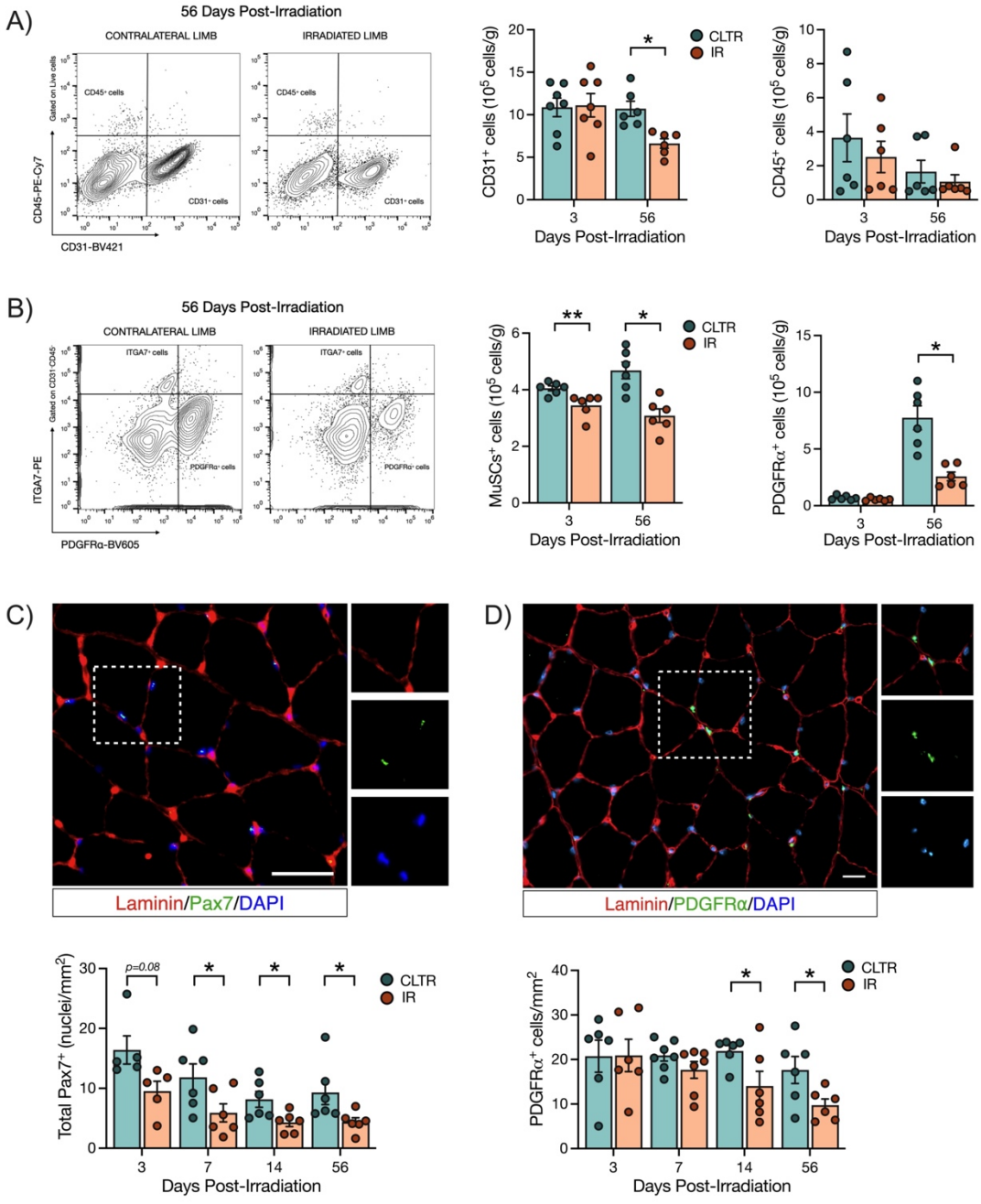

Figure 3. ***Radiation depletes endothelial cells, MuSCs, and FAPs long term.***

(A) Representative flow cytometry plots of $CD31^+$. and $CD45^+$ cells at 56-days post-IR from CLTR and IR limb. $CD31^+$. and $CD45^+$ cells per grams of muscle. (B) Representative flow cytometry plots of $ITGA7^+$. and $PDGFR\alpha^+$ cells at 56-days post-IR from CLTR and

IR limb. ITGA7$^+$, and PDGFRα$^+$ cells per grams of muscle. (C) Representative image of Pax7$^+$ cells (green), laminin (red) and DAPI (blue). Scale bar: 20 μm. Total Pax7$^+$ cells per mm^2. (D) Representative image of PDGFRα$^+$ cells (green), laminin (red) and DAPI (blue). PDGFRα cells per mm^2. *$p < 0.05$, **$p < 0.01$; Paired Student's t-test between CLTR and IR at each timepoint (n=5-8).

Radiation inhibits myoblast and FAP proliferation and induces acute DNA damage signalling and cell senescence

To functionally characterize the effects of radiation on MuSCs and FAPs, we isolated MuSCs and FAPs by FACS from *in vivo*-IR or CLTR limbs for *in vitro* characterization of cell fate (*Figure* 4A and S4A-D). MuSC proliferation was significantly impaired in IR versus CLTR at both 3-, and 56-days (*Figure* 4B). Conversely, FAP proliferation was not altered at 3-days post-IR and demonstrated a trend for impairment at 56-days in IR compared to CLTR (p=0.06, *Figure* 4B). The DNA damage (γH2AX foci) response was significantly higher in MuSCs and FAPs at 15 minutes post- *in vitro*-IR and remained elevated only in FAPs at 24 hours (*Figure* 4C). Post-*in vitro*-IR, MuSCs had significantly higher cellular oxidative stress compared to CON at 15 minutes, but not at 24 hours, while with no differences in oxidative stress levels were detected in FAPs (*Figure* 4D). Cellular senescence, as determined via SA-β-Gal staining at 24 hours post-*in vitro*-IR, was significantly higher in IR-FAPs compared to CON-FAPs (*Figure* 4E).

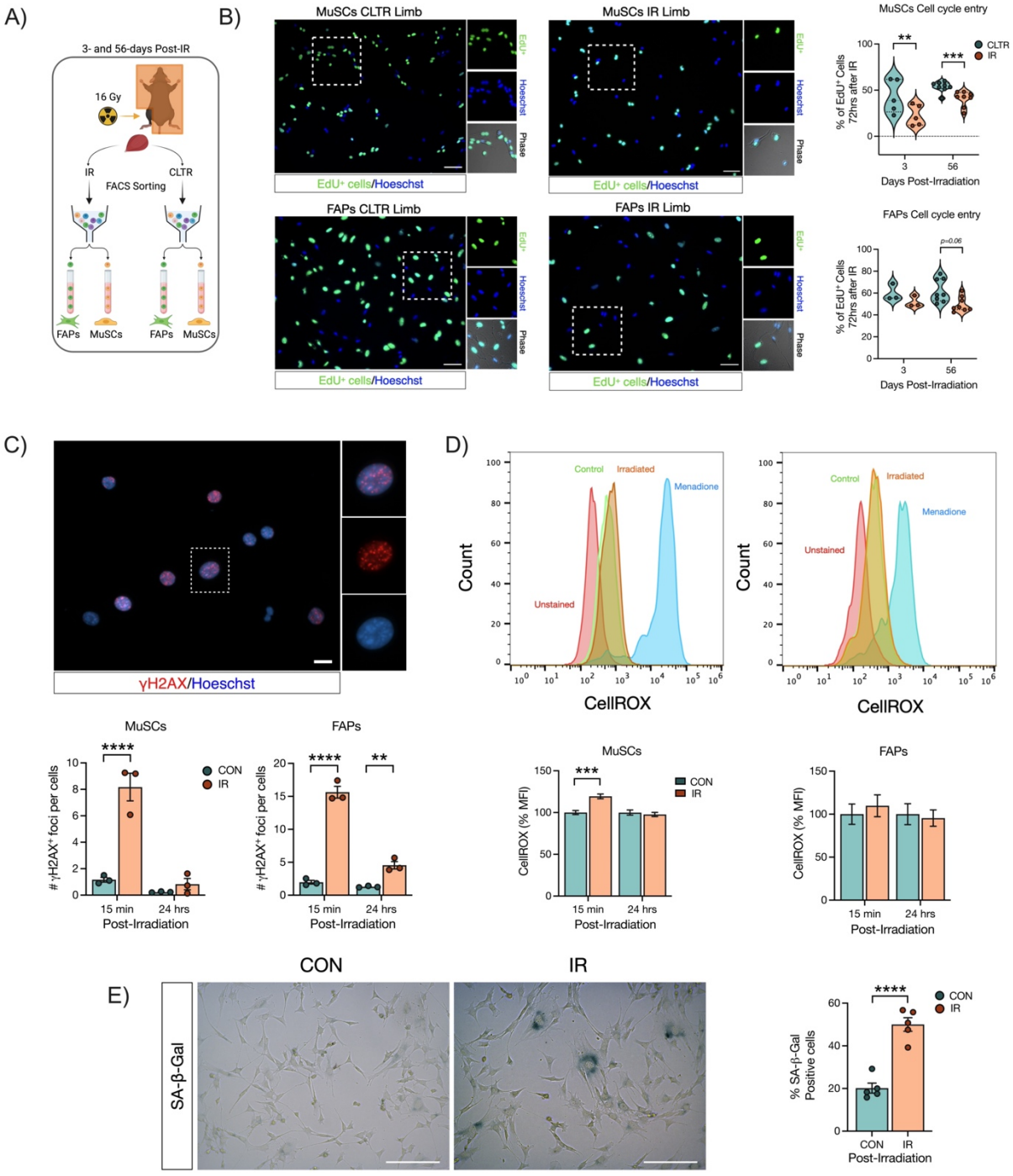

Figure 4. ***Radiation inhibits myoblast and FAP proliferation long-term and induces acute DNA damage.***

(A) Experimental design. (B) Representative image of EdU^+ MuSCs and FAPs from CLTR and IR limb from 56-days post- *in vivo*-IR. Percentage of EdU^+ MuSCs and FAPs 72 hours after *in vivo*-IR. (C) Representative image of $yH2AX^+$ foci per cell, and number of $yH2AX^+$ foci in MuSCs and FAPs 15 minutes and 24 hours post-*in vitro*-IR. (D) Representative flow cytometry histogram of CellROX fluorescence in MuSCs, and FAPs after *in vitro*-IR. Quantification of CellROX mean fluorescence intensity (MFI) as a % of MuSCs, and FAPs 15 minutes and 24 hours post-*in vitro*-IR. (E) Representative image of SA-β-Gal staining and %of SA-β-Gal^+ cells. $^{**}p < 0.01$, $^{***}p < 0.001$, $^{****}p < 0.0001$. Paired (B) and Unpaired (C-E) Student's t-test (n=3-5).

Radiation promotes a fibrotic phenotype in FAPs

Unlike other pro-fibrotic conditions,[31,S23,S24] we observed a reduction in FAP content and impaired FAP proliferation following radiation; thus, we speculated that radiation was promoting their fibrotic differentiation. *In vitro*-IR FAPs (*Figure* 5A) were evaluated for several markers of fibrotic differentiation[S25-S27] compared to CON-FAPs while FAPs treated with TGF-β1 (+TGF-β1) served as a positive control (*Figure* 5B). At 72 hours following treatment, IR-FAPs and +TGF-β1-FAPs were significantly larger (*Figure* 5B), had significantly more stress fibre formation per cell (*Figure* 5C), and had significantly elevated SMAD3 signalling than CON (*Figure* 5D). Supporting our *in vivo* findings, IR- and TGF-β1-treated FAPs had significantly lower PDGFRα content than CON (*Figure* 5D).

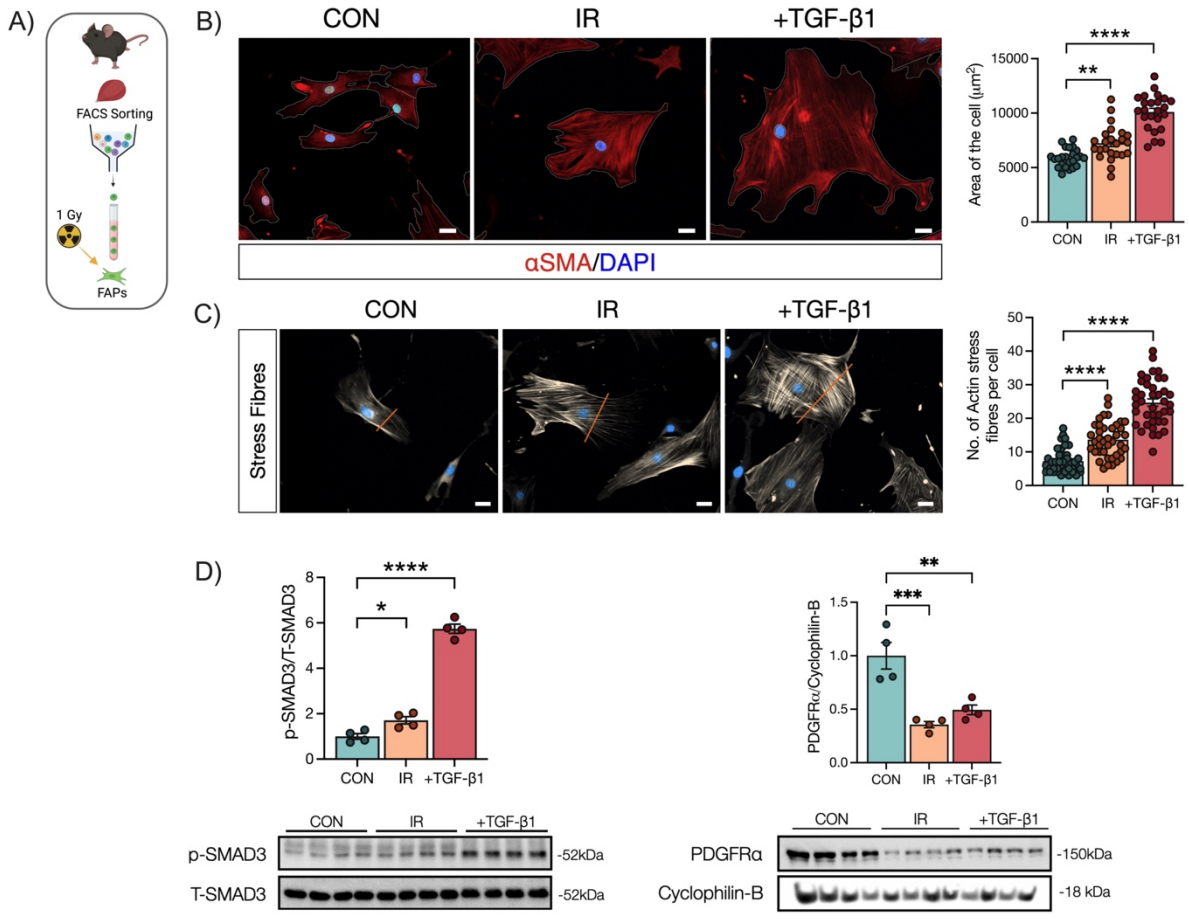

Figure 5. ***Radiation promotes fibrotic differentiation in fibro-adipogenic progenitors.***

(A) Experimental design. (B) Representative image of FAPs 72 hours post- *in vitro*-IR. Control, Irradiated and TGF-β1 (used as a positive control). αSMA (red), DAPI (blue). Scale bar: 20 μm. Average of cell area (um^2). (C) Representative image of FAPs 72 hours post- *in vitro*-IR. αSMA (gray) staining to visualize stress fibres formation. Scale bar: 20 μm. Quantification of actin stress fibres per cell. (D) Quantification and representative western blots of FAPs after 72 hours post- i*n vitro*-IR showing, p-SMAD3, T-SMAD3,

PDGFRα, and Cyclophilin-B. *p < 0.05, **p < 0.01, ****p < 0.0001. Unpaired Student's t-test (n=4).

Radiation induces a metabolic shift in FAPs to favour glycolysis and inhibiting glycolysis prevents myofibroblast differentiation

Previous work has linked radiation to alterations in skeletal muscle metabolism and mitochondrial function,[S28,S29] and metabolic changes have been found to impact FAP fate.[32,333] Thus, we evaluated FAP bioenergetics at three- and 24 hours post-*in vitro*-IR to determine if IR-induced alterations to FAP metabolism explained IR-induced alterations in FAP fate. No changes in mitochondrial mass were detected in IR-FAPs compared to CON at 24 hours post-*in vitro*-IR (*Figure* S5A). Similarly, mitochondria DNA (mtDNA) to nuclear DNA (nDNA) ratio revealed no differences in mitochondrial biogenesis (*Figure* S5B). A significant increase in mitochondrial membrane potential was observed in IR-FAPs compared to CON, being also significantly high when normalized for mitochondrial mass in IR-FAPs compared to CON (*Figure* 6A). Qualitatively, we observed consistently more fragmented mitochondria, a marker of increased glycolytic metabolism[34], at 24 hours, in IR-FAPs compared to CON (*Figure* 6A). Seahorse assay revealed that *in vitro*-IR-FAPs had higher glycolytic capacity and lower oxygen consumption rate/extracellular acidification rate (OCR/ECAR) ratio at maximal respiration versus CON (*Figure* 6B). Differences in oxidative capacity and ATP production were not detected; however, significantly lower proton leak was detected in IR-FAPs versus CON (*Figure* 6C). Next, we asked if directly altering glycolysis promoted FAP fibrotic differentiation. After inhibiting glycolysis with 2-Deoxy-D-Glucose (2-DG), we observed a significant reduction in stress fibre formation following *in vitro*-IR (*Figure* 6D). Conversely, no changes in stress fibre

formation were found when oxidative phosphorylation activity is inhibited by Oligomycin. To increase glycolysis while maintaining oxidative metabolism, as observed in our *in vitro*-IR model, we manipulated glucose levels in the media with high glucose media representing a condition where glycolysis and oxidative metabolism are activated, and low glucose media where glycolysis activity decreases while oxidative metabolism remains active.[S30,S31] Under these conditions and 24 hours post-*in vitro*-IR, we detected significantly more stress fibre formation under high glucose conditions compared to the low glucose condition (*Figure* 6E).

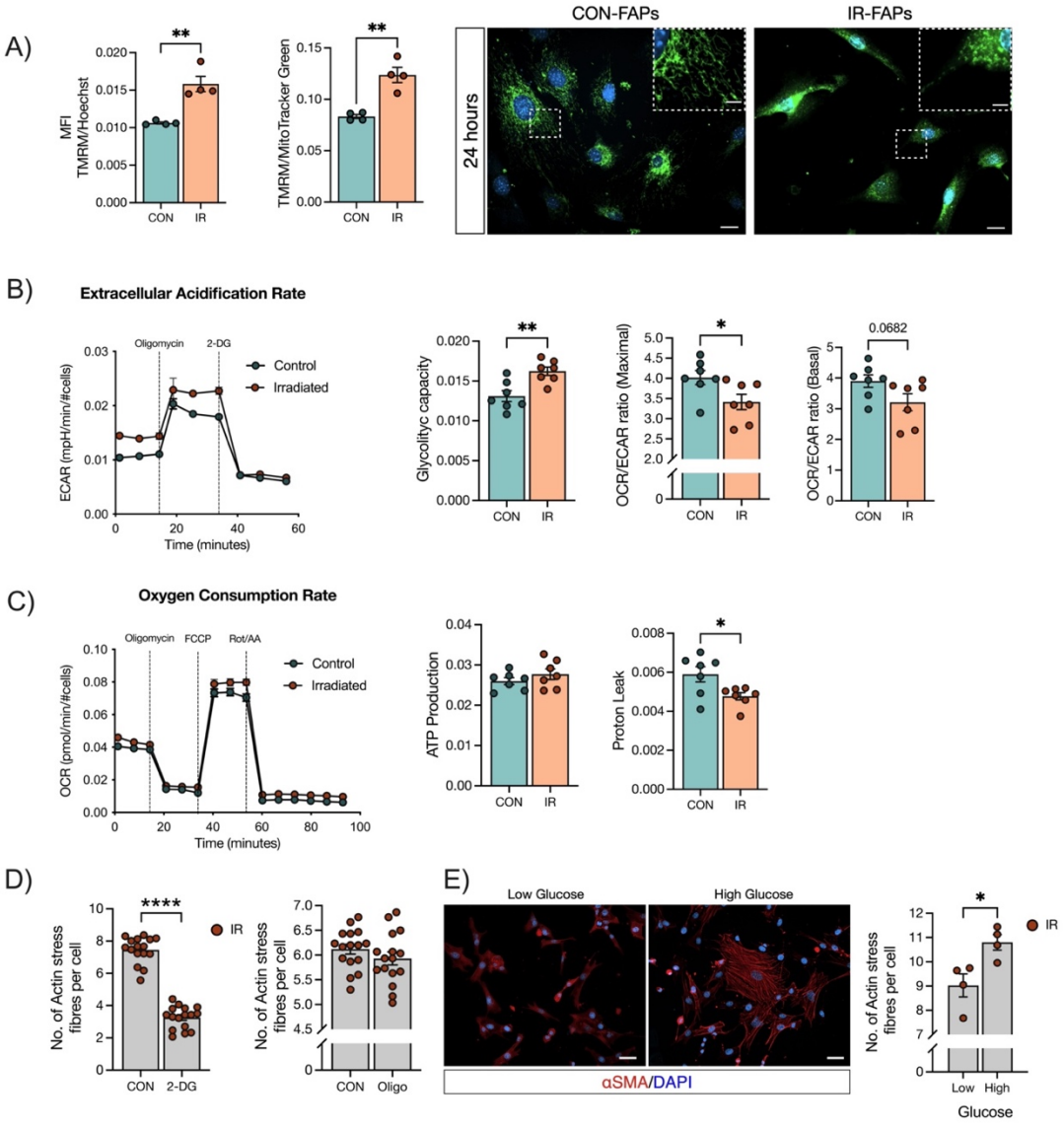

Figure 6. ***Radiation induces a metabolic shift in FAPs to favour glycolysis and inhibiting glycolysis prevents myofibroblast differentiation.***

(A) TMRM Fluorescence Intensity and TMRM Fluorescence Intensity normalized by mitochondrial mass (MitoTracker Green) from FAPs followed 24 hours post-*in vitro*-IR. Representative image of MitoTracker Green staining 24 hours post-*in vitro*-IR showing elongated and fractionated mitochondria. Scale bar: 20 μm, Scale bar Zoom in: 2 μm. (B) Extracellular acidification rate (ECAR), glycolytic capacity, OCR/ECAR ratio at maximal respiration, and OCR/ECAR ratio at basal respiration. (C) Oxygen consumption rate (OCR), ATP production, and Proton Leak. (D) Number of actin stress fibre from 24 hours post-*in vitro*-IR on C3H/10T1/2 cells treated with 2-DG or oligomycin. (E) Representative image of αSMA^+ cells and number actin stress fibre followed low or high glucose treatment on C3H/10T1/2 cells Scale bar: 50 μm. *p < 0.05, **p < 0.01, ****p < 0.0001. Unpaired Student's t-test (n=3-7).

Radiation alters the FAP secretome to inhibit myoblast differentiation and fusion

To determine if the observed cell-intrinsic changes to FAPs exposed to IR impaired their role in regulating myoblast fate via paracrine mechanisms, we conducted a conditioned media experiment where conditioned media from IR or CLTR FAPs isolated at 3- and 56-days post- *in vivo*-IR was mixed with non-irradiated primary myoblasts in differentiation media (50:50 v/v)[30] (*Figure* 7A). Myoblast differentiation and fusion was evaluated by myosin heavy chain and DAPI co-immunocytochemistry (*Figure* 7B). Conditioned media from 56-day isolated IR-FAPs impaired myoblast differentiation compared to 56-day isolated CLTR-FAPs (*Figure* 7B, $p<0.05$) with no differences between 3-day isolated IR-FAP and CLTR-FAP conditioned media. Further, conditioned

media from both 3- and 56-day isolated IR-FAPs significantly reduced the number of myotubes per area, myoblast fusion index, and the number of nuclei per myotube (*Figure* 7B) compared to CLTR. Despite these differences in myoblast differentiation and fusion, conditioned media (50:50 v/v) from 3- or 56-day isolated IR-FAPs did not reduce myoblast content, as determined by the total number of nuclei, compared to CLTR (*Figure* S6A). In a separate experiment, we applied conditioned media from the above groups to differentiated myotubes to determine if conditioned media from IR-FAPs induced myotube atrophy (*Figure* S6B). Conditioned media from IR-FAPs did not change myotube diameter or the proportion of myotubes of different diameters compared to CLTR (*Figure* S6B).

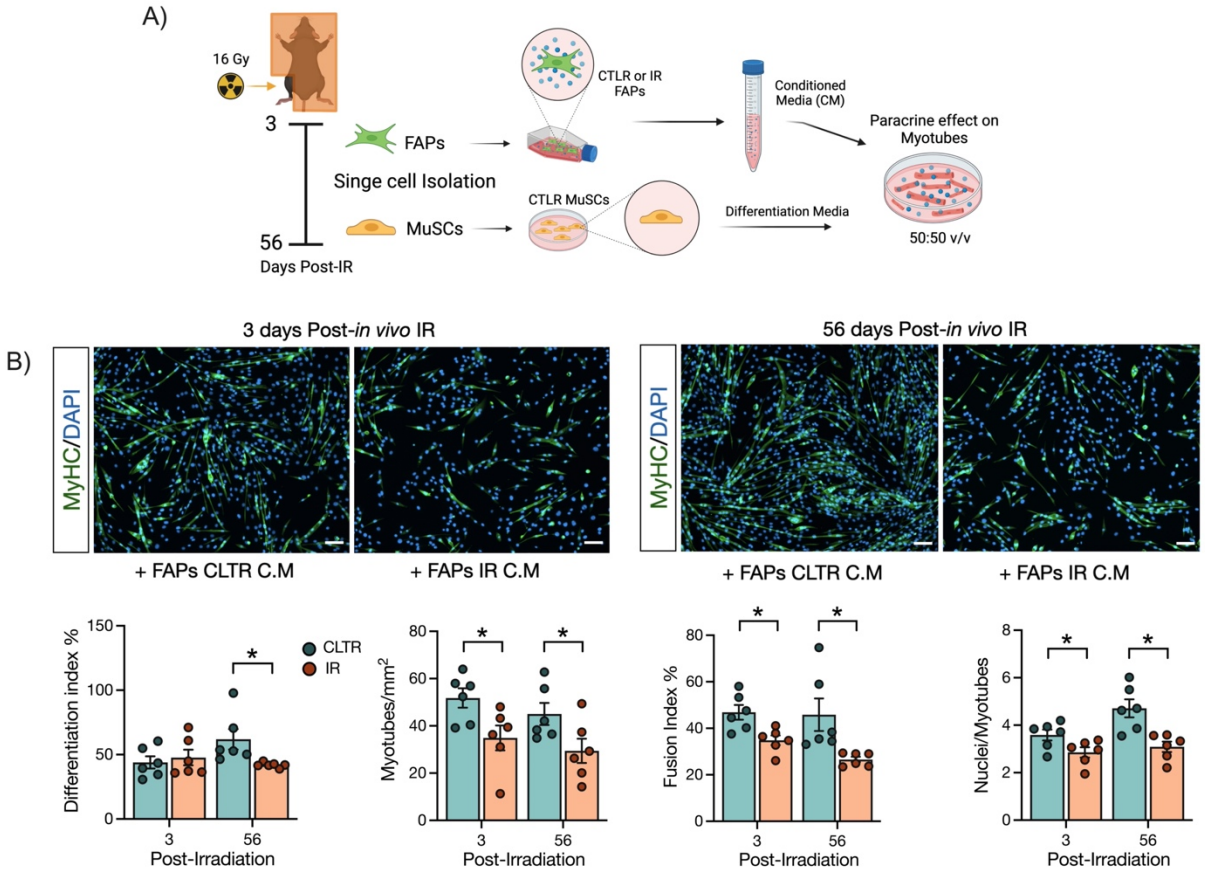

Figure 7. ***Radiation alters FAPs secretome to inhibit myoblast differentiation and fusion.***

(A) Experimental design. (B) Representative image on MyHC staining. MyHC (green), and DAPI (blue). Quantification of differentiation index, myotube per mm^2, fusion index and nuclei per myotubes. Scale bar: 100 μm. *$p < 0.05$. Unpaired Student's t-test (n=6).

Discussion

Radiation induces long-term muscle atrophy and fibrosis,[S1] and depletes MuSCs[25] resulting in long-term complications in cancer survivors, particularly juvenile cancer survivors. However, the effects of radiation on mononuclear niche cells in muscle and their role in radiation-induce fibrosis has remained relatively unexplored. The present study addresses this gap by characterizing the effects of radiation exposure on skeletal muscle morphology and skeletal muscle niche cells using a clinically relevant preclinical model.[26] Mice exposed to a single dose of radiation showed long-term muscle atrophy and fibrosis, confirming clinical findings,[S1] and reduced MuSC content as has been previously described.[4] Unlike other models of long-term skeletal muscle fibrosis,[22] we observed long-term FAP depletion in our model of radiation-induced fibrosis, similar to what is observed in aged muscle.[13,19] Interestingly, FAP depletion was associated with increased myofibroblast differentiation and a reduction in PDGFRα content, which may have been driven by increased glycolytic metabolism. Further, radiation induced FAP senescence and altered their secretome in a manner that inhibited myoblast differentiation. Collectively, our data indicate FAPs as a potential cellular source

responsible for radiation-induce muscle pathology, likely driven by radiation-induced mitochondrial defects leading to enhanced reliance on glycolysis.

Previous clinical findings indicate that 80% of childhood cancer survivors experience muscle atrophy and fibrosis,[S1-S3] a phenotype we successfully recapitulated in our preclinical model. The long-term muscle atrophy we observed was due to a lower CSA specifically in the more oxidative type I and IIA fibres, and a lower proportion of type I fibres. Radiation reacts with oxygen molecules within the cell to produce reactive oxygen species;[S32] thus, it is not surprising that oxidative fibres would be more susceptible to the effects of radiation. Indeed, our findings, align with previous studies showing that radiation reduces the percentage of oxidative type I muscle fibres,[S29] and decreases the CSA of type IIA myofibres.[26] Juvenile muscle growth requires MuSCs.[3] Similar to previous work, we show that radiation exposure decreases MuSC content as early as three days after radiation exposure and is not restored.[4,25] FAPs are also required for muscle maintenance,[15,19] and we present the novel finding that FAP content decrease persists long after radiation. Thus, radiation-induced FAP and MuSC depletion likely contributed to the lower myofibre CSA observed in this model. Since FAPs regulate muscle mass via paracrine mechanisms,[12,S33] we investigated whether radiation altered the FAP secretome. Interestingly, we showed that the *in vivo* irradiated FAP secretome impaired MuSC fusion and differentiation without impacting MuSC proliferation or inducing myotube atrophy directly *in vitro*. This finding was supported by a trend for fewer myonuclei per fibre at the latest post-IR timepoint, demonstrating a persistent alteration of the FAP secretome long after IR. These findings align with results from aged FAPs, which have a reduced capacity to regulate the myogenic program due to aging-induced

alterations in the FAP secretome.[13,19] Although we were not able to identify specific trophic factors that were altered following radiation exposure, previous work has identified several potential targets for future studies.[12] Specifically, WNT1 Inducible Signaling Pathway Protein 1 (WISP1) regulates MuSC proliferation and differentiation and is reduced in aged FAPs.[13] Further, follistatin and bone morphogenic protein 3B have also been well-described as regulators of MuSC differentiation and muscle maintenance.[19,20] Together, our findings suggest that reduced myofibre CSA following radiation exposure is due, in part, to long-term MuSC depletion and impaired FAP paracrine signalling resulting in reduced myogenic differentiation of remaining MuSCs.

Skeletal muscle fibrosis is one of the most prominent adverse effects experienced by childhood cancer survivors.[S2] Our results confirm previous work[25] by demonstrating ECM accumulation at 56-days post-IR, which was supported by an increase in pro-fibrotic markers such as fibronectin and αSMA. Gene expression data from Kallenbach and colleagues implicated TGF-β1 in radiation-induced muscle defects.[25] Similarly, we observed an early upregulation of SMAD3 signalling following radiation; however, this signalling was not maintained long-term. SMAD3 signalling is a critical regulator of myofibroblast transition;[S34] thus, the early increase in SMAD3 signalling in the whole muscle, could be the initial trigger for the myofibroblastic transition that leads to the long-term fibrosis observed in our study. One of the main contributors of ECM deposition in the skeletal muscle are myofibroblast that are driven from FAP fibrogenic differentiation.[S35] FAPs co-localize to fibrotic areas in different models of myopathy characterized by continued structural damage to the myofibres,[S13] as in human patients with Duchenne Muscular Dystrophy (DMD).[23] Conversely, FAPs were depleted in our

model suggesting that radiation-induced muscle fibrosis more closely aligns with muscle fibrosis seen in aging[S36] which is associated with reduced FAP content.[13,19] Interestingly, the putative FAP marker PDGFRα[11] is reduced when FAPs undergo fibrotic differentiation[35,36] which aligns with our *in vivo* and *in vitro* findings. Further, Yao and colleagues showed that while PDGFRα supported early fibroblast proliferation; however, PDGFRα down-regulation was necessary for fibrogenic transition into αSMA$^+$ myofibroblast.[36] We extend these findings to the context of radiation-induced fibrosis by showing that PDGFRα is reduced in FAPs during their fibrotic transition following radiation exposure. In addition, myofibroblasts exhibit a senescence-like phenotype[S37] and senescence has been associated with muscle dysfunction.[S38] Our findings show that radiation induces FAP senescence with persistent DNA damage and reduced proliferation. Our findings align with those from Moiseeva and colleagues[37], showing that senescent cells accumulate in aged skeletal muscle and are associated with fibrosis. Moreover, Zhang and colleagues showed that a FAP subpopulation present a senescence signature in old skeletal muscle,[38] and FAPs isolated from old skeletal muscles have enhanced fibrotic differentiation,[13] further supporting the notion that radiation induces a premature aging phenotype in skeletal muscle. Together, these findings suggest that radiation depletes PDGFRα$^+$ FAPs by inducing their fibrotic differentiation which contributes to radiation-induced skeletal muscle fibrosis.

Recent studies have provided a link between metabolism and FAP fate[32,33,39] and radiation has been shown to impair mitochondrial dynamics and function.[S28,S29] Thus, we examined if fibrotic differentiation in IR-FAPs was linked to alterations in FAP metabolism. Our results showed that despite an increase in mitochondrial membrane potential,

essential for ATP production, we did not detect alterations in ATP-linked respiration or oxidative capacity. Further, we did not detect any changes in mitochondrial content. Elevated mitochondrial membrane potential in cardiac mesenchymal precursors cells has been associated with increased oxidative metabolism;[S39] however, this was not the case in the present work. Rather, the increase in mitochondrial membrane potential observed in our results could be due to the decrease in proton leak[S40] observed following radiation exposure. Further, elevated membrane potential is traditionally associated with increased ROS production.[S41] Changes in mitochondrial structural integrity due to fission has been associated with increasing glycolytic metabolism[34,S42] which aligns with our qualitative observations of mitochondria from IR-FAPs. This notion is further supported by the higher glycolytic rates for energy production in *in vitro*-IR-FAPs. An increase in glycolytic metabolism, and not mitochondrial metabolism, may be a protective mechanism to prevent cellular oxidative stress while matching an elevated ATP demand.[S43] Indeed, fibroblasts treated with H_2O_2 demonstrate an increase in glycolysis and NADPH content, a cofactor associated with antioxidant activity.[S44] Further, cardiac mesenchymal progenitors with high membrane potential demonstrated higher resistance to oxidative stress and elevated SOD2.[S39] Similar mechanisms in FAPs may explain the lack of change we observed in FAP oxidative stress following radiation exposure. Together, these findings suggest that following radiation exposure, FAPs experience increased glycolytic metabolism perhaps to increase ATP production while preventing oxidative stress from mitochondria.

Growing evidence suggest the modulation of glycolysis and oxidative phosphorylation as a determinant of stem cell fate.[S45,,S46] Indeed human FAPs with

enhanced glycolytic metabolism have a fibrotic phenotype.[33] Given that radiation enhanced FAP glycolysis and induced their fibrotic differentiation, we investigated if alterations to FAP metabolism were driving the fibrotic differentiation. In line with this hypothesis, inhibiting glycolysis with 2-DG reduced FAP fibrotic differentiation. While inhibiting oxidative metabolism with oligomycin had no effect on FAP fate, we reasoned that this model did not completely recapitulate the post-IR condition as oxidative metabolism is still active following radiation. Thus, we modulated glycolysis while maintaining oxidative metabolism *in vitro* by exposing FAPs to high and low glucose conditions. Under high glucose conditions, glycolysis would be elevated and oxidative phosphorylation would also be active, similar to post-IR; however, in low glucose conditions, glycolysis is decreased while oxidative metabolism is maintained.[S30,S31] Indeed, FAP fibrotic differentiation was enhanced when glycolysis was elevated and oxidative metabolism still active, similar to the post-IR phenotype suggesting that the shift to glycolysis to maintain energy homeostasis following radiation exposure enhances FAP fibrotic differentiation. In agreement with our results, decreased fibroblast activation, proliferation and differentiation is observed, when glycolysis is inhibited.[S47,S48] Similarly, Reggio and colleagues decreased FAP proliferation by reducing glucose concentrations in the culture media.[32]

A limitation of the study is using a single radiation dose as opposed to fractionated doses as is conducted during cancer therapy. Unfortunately, given the shorter lifespan of the mice, an exact replication of the human radiation protocol would have resulted in mice being treated well-beyond their pubertal development. As such, we used the biologically equivalent dose formula[S49] to determine that a 16 Gy dose is predicted to be biologically

equivalent to 60 Gy delivered in 2 Gy fractions/day which is normally used to treat different types of common cancers.[S50] Previous work has used this dose to replicate radiation-induced pathology.[4,26] Further, the clinical phenotype of fibrosis and muscle atrophy[S1,S2,S3] was reproduced by our dosing strategy further supporting the translational relevance of our model. Another limitation of our study was the decision to irradiate mice without cancer. This decision was conducted for several reasons. First, the presence of a tumour would complicate data interpretation by adding another variable. Second, there are clinical scenarios when radiation is delivered without a tumour, such as in the adjuvant setting. Finally, previous work has shown that the presence of a tumour within the muscle microenvironment during radiation exposure produces similar outcomes as the cancer-free irradiated limb.[25] We also acknowledge that radiation is not a targeted therapy and can alter adjacent tissues. Indeed, our laboratory and others have shown that radiation alters the bone marrow.[40,S51] Future studies should address the crosstalk between bone and muscle and find potential circulatory mediators that may contribute to skeletal muscle atrophy following radiation exposure.

Together, our results indicate that juvenile radiation exposure alters the whole skeletal muscle niche long-term. Specifically, the novelty of our findings suggests that FAPs contribute to long-term skeletal muscle atrophy and fibrosis following juvenile radiation exposure. These findings suggest that FAP-targeted therapies may help mitigate the negative long-term consequences observed in cancer survivors.

Acknowledgements

We want to acknowledge the laboratory manager, Fernando Ortiz, of the Cell Sorting and Flow Cytometry Core Facility at the Ottawa Hospital Research Institute for his assistance with Cell Sorting. Also, we would like to acknowledge the services of the Behavioural Core Facility, Pre-clinical Imaging Core Facility, the Cell Biology and Image Acquisition Core, and the Louise Pelletier Histology Core Facility at the Faculty of Medicine at the University of Ottawa. Lastly, we acknowledge the important published work that were not able to be cited because of word count and references limitations.

Ethics statement

This manuscript complies with the ethical guidelines for authorship and publishing in the Journal of Cachexia, Sarcopenia and Muscle.[S55]

Conflict of interest

The authors declare no competing interests.

Funding

This work was supported by the Natural Sciences and Engineering Research Council of Canada (RGPIN-2017-04320), the Ontario Early Research Award, the Canadian Foundation for Innovation, the Canadian Institute for Health Research (PDI 184016), and discretionary research funds (M.D.). N.C is supported by The Chilean National Agency for Research and Development (Agencia Nacional de Investigacion y Desarrollo [ANID]), the uOttawa/CHEO Research Institute's Doctoral Fellowship for Advancement of Biological Perspectives for Exercise Interventions Across the Lifespan, and the uOttawa Eric Poulin Centre for Neuromuscular Disease (CNMD) Scholarship in Translational Research (STaR). A.E.G is the recipient of a University of Ottawa Brain and Mind

Research Institute uOttawa Eric Poulin Centre for Neuromuscular Disease Scholarship in Translational Research Award. K.J.M is funded by the Canadian Institutes of Health Research (MOP 159455) and the NSERC Collaborative Research and Training Experience program (Metabolomics Advanced Training and International Exchange program) and discovery grants (RGPIN 2018-06838, DGECR 2018-00012).

Supplementary information

Supplemental figures, extended methods section and extended references may be found in the supporting information section at the end of this article.

References

1. Canadian Cancer Society's Advisory Committee on Cancer Statistics. Canadian Cancer Statistics (2015).
2. Miller KD, Nogueira L, Mariotto AB, Rowland JH, Yabroff KR, Alfano CM *et al.* Cancer treatment and survivorship statistics, 2019. *CA Cancer J Clin* 2019;**69**:363–385.
3. Bachman JF, Klose A, Liu W, Paris ND, Blanc RS, Schmalz M *et al.* Prepubertal skeletal muscle growth requires Pax7-expressing satellite cell-derived myonuclear contribution. *Development* 2018;**145**:dev167197.
4. Bachman JF, Blanc RS, Paris ND, Kallenbach JG, Johnston CJ, Hernady E *et al.* Radiation-Induced Damage to Prepubertal Pax7+ Skeletal Muscle Stem Cells Drives Lifelong Deficits in Myofiber Size and Nuclear Number. *iScience* 2020;**23**:101760.
5. Rosenblatt JD, Parry DJ. Gamma irradiation prevents compensatory hypertrophy of overloaded mouse extensor digitorum longus muscle. *J Appl Physiol (1985)* 1992;**73**:2538–2543.

6. Adams GR, Caiozzo VJ, Haddad F, Baldwin KM. Cellular and molecular responses to increased skeletal muscle loading after irradiation. *Am J Physiol Cell Physiol* 2002;**283**:C1182-1195.
7. Paris ND, Kallenbach JG, Bachman JF, Blanc RS, Johnston CJ, Hernady E *et al.* Chemoradiation impairs myofiber hypertrophic growth in a pediatric tumor model. *Scientific Reports* 2020;**10**:19501.
8. Scaramozza A, Park D, Kollu S, Beerman I, Sun X, Rossi DJ *et al.* Lineage Tracing Reveals a Subset of Reserve Muscle Stem Cells Capable of Clonal Expansion under Stress. *Cell Stem Cell* 2019;**24**:944-957.e5.
9. Collao N, Rada I, Francaux M, Deldicque L, Zbinden-Foncea H. Anti-Inflammatory Effect of Exercise Mediated by Toll-Like Receptor Regulation in Innate Immune Cells - A Review. *Int Rev Immunol* 2020;**39**:39–52.
10. Joe AWB, Yi L, Natarajan A, Le Grand F, So L, Wang J *et al.* Muscle injury activates resident fibro/adipogenic progenitors that facilitate myogenesis. *Nat Cell Biol* 2010;**12**:153–163.
11. Uezumi A, Fukada S, Yamamoto N, Takeda S, Tsuchida K. Mesenchymal progenitors distinct from satellite cells contribute to ectopic fat cell formation in skeletal muscle. *Nat Cell Biol* 2010;**12**:143–152.
12. Biferali B, Proietti D, Mozzetta C, Madaro L. Fibro–Adipogenic Progenitors Cross-Talk in Skeletal Muscle: The Social Network. *Front Physiol* 2019;**10**.
13. Lukjanenko L, Karaz S, Stuelsatz P, Gurriaran-Rodriguez U, Michaud J, Dammone G et al. Aging Disrupts Muscle Stem Cell Function by Impairing Matricellular WISP1 Secretion from Fibro-Adipogenic Progenitors. Cell Stem Cell 2019;24:433-446.e7.
14. Collao N, Sanders O, Caminiti T, Messeiller L, De Lisio M. Resistance and endurance exercise training improves muscle mass and the inflammatory/fibrotic transcriptome in a rhabdomyosarcoma model. *J Cachexia Sarcopenia Muscle* 2023 doi:10.1002/jcsm.13185.
15. Wosczyna MN, Konishi CT, Perez Carbajal EE, Wang TT, Walsh RA, Gan Q *et al.* Mesenchymal Stromal Cells Are Required for Regeneration and Homeostatic Maintenance of Skeletal Muscle. Cell Rep 2019;27:2029-2035.e5.

16. Giuliani G, Rosina M, Reggio A. Signaling pathways regulating the fate of fibro/adipogenic progenitors (FAPs) in skeletal muscle regeneration and disease. FEBS J 2021 doi:10.1111/febs.16080.
17. Malecova B, Gatto S, Etxaniz U, Passafaro M, Cortez A, Nicoletti C et al. Dynamics of cellular states of fibro-adipogenic progenitors during myogenesis and muscular dystrophy. Nat Commun 2018;9:3670.
18. Leinroth AP, Mirando AJ, Rouse D, Kobayahsi Y, Tata PR, Rueckert HE et al. Identification of distinct non-myogenic skeletal-muscle-resident mesenchymal cell populations. Cell Rep 2022;39:110785.
19. Uezumi A, Ikemoto-Uezumi M, Zhou H, Kurosawa T, Yoshimoto Y, Nakatani M *et al.* Mesenchymal Bmp3b expression maintains skeletal muscle integrity and decreases in age-related sarcopenia. *J Clin Invest* 2021;**131**:139617.
20. Mozzetta C, Consalvi S, Saccone V, Tierney M, Diamantini A, Mitchell KJ et al. Fibroadipogenic progenitors mediate the ability of HDAC inhibitors to promote regeneration in dystrophic muscles of young, but not old Mdx mice. EMBO Mol Med 2013;5:626–639.
21. Soliman H, Theret M, Scott W, Hill L, Underhill TM, Hinz B *et al.* Multipotent stromal cells: One name, multiple identities. *Cell Stem Cell* 2021;**28**:1690–1707.
22. Uezumi A, Ito T, Morikawa D, Shimizu N, Yoneda T, Segawa M *et al.* Fibrosis and adipogenesis originate from a common mesenchymal progenitor in skeletal muscle. *J Cell Sci* 2011;**124**:3654–3664.
23. Uezumi A, Fukada S, Yamamoto N, Ikemoto-Uezumi M, Nakatani M, Morita M *et al.* Identification and characterization of PDGFRα+ mesenchymal progenitors in human skeletal muscle. *Cell Death Dis* 2014;**5**:e1186.
24. Lemos DR, Babaeijandaghi F, Low M, Chang C-K, Lee ST, Fiore D *et al.* Nilotinib reduces muscle fibrosis in chronic muscle injury by promoting TNF-mediated apoptosis of fibro/adipogenic progenitors. *Nat Med* 2015;**21**:786–794.
25. Kallenbach JG, Bachman JF, Paris ND, Blanc RS, O'Connor T, Furati E *et al.* Muscle-specific functional deficits and lifelong fibrosis in response to paediatric radiotherapy and tumour elimination. *J Cachexia Sarcopenia Muscle* 2022;**13**:296–310.

26. Hardee JP, Puppa MJ, Fix DK, Gao S, Hetzler KL, Bateman TA *et al.* The effect of radiation dose on mouse skeletal muscle remodeling. *Radiol Oncol* 2014;**48**:247–256.
27. Roubos S, D'Souza D, Hernández-Saavedra D, Xu G, Collao N, Emmons R *et al.* Weight loss with exercise improves muscle architecture and progenitor cell populations compared with weight loss alone in mice with preneoplastic colorectal lesions. *Appl Physiol Nutr Metab* 2021;**46**:837–845.
28. Collao N, Akohene-Mensah P, Nallabelli J, Binet ER, Askarian A, Lloyd J *et al.* The role of L-type amino acid transporter 1 (Slc7a5) during in vitro myogenesis. *Am J Physiol Cell Physiol* 2022;**323**:C595–C605.
29. Cadete VJJ, Deschênes S, Cuillerier A, Brisebois F, Sugiura A, Vincent A *et al.* Formation of mitochondrial-derived vesicles is an active and physiologically relevant mitochondrial quality control process in the cardiac system. *J Physiol* 2016;**594**:5343–5362.
30. AlSudais H, Rajgara R, Saleh A, Wiper-Bergeron N. C/EBPβ promotes the expression of atrophy-inducing factors by tumours and is a central regulator of cancer cachexia. *J Cachexia Sarcopenia Muscle* 2022;**13**:743–757.
31. Madaro L, Passafaro M, Sala D, Etxaniz U, Lugarini F, Proietti D *et al.* Denervation-activated STAT3-IL-6 signalling in fibro-adipogenic progenitors promotes myofibres atrophy and fibrosis. *Nat Cell Biol* 2018;**20**:917–927.
32. Reggio A, Rosina M, Krahmer N, Palma A, Petrilli LL, Maiolatesi G *et al.* Metabolic reprogramming of fibro/adipogenic progenitors facilitates muscle regeneration. *Life Sci Alliance* 2020;**3**:e202000646.
33. Farup J, Just J, de Paoli F, Lin L, Jensen JB, Billeskov T *et al.* Human skeletal muscle CD90+ fibro-adipogenic progenitors are associated with muscle degeneration in type 2 diabetic patients. *Cell Metab* 2021;**33**:2201-2214.e11.
34. Guido C, Whitaker-Menezes D, Lin Z, Pestell RG, Howell A, Zimmers TA *et al.* Mitochondrial fission induces glycolytic reprogramming in cancer-associated myofibroblasts, driving stromal lactate production, and early tumor growth. *Oncotarget* 2012;**3**:798–810.

35. Contreras O, Cruz-Soca M, Theret M, Soliman H, Tung LW, Groppa E *et al.* Cross-talk between TGF-β and PDGFRα signaling pathways regulates the fate of stromal fibro-adipogenic progenitors. *J Cell Sci* 2019;**132**:jcs232157.
36. Yao L, Rathnakar BH, Kwon HR, Sakashita H, Kim JH, Rackley A *et al.* Temporal control of PDGFRα regulates the fibroblast-to-myofibroblast transition in wound healing. *Cell Rep* 2022;**40**:111192.
37. Moiseeva V, Cisneros A, Sica V, Deryagin O, Lai Y, Jung S *et al.* Senescence atlas reveals an aged-like inflamed niche that blunts muscle regeneration. *Nature* 2023;**613**:169–178.
38. Zhang X, Habiballa L, Aversa Z, Ng YE, Sakamoto AE, Englund DA *et al.* Characterization of cellular senescence in aging skeletal muscle. *Nat Aging* 2022;**2**:601–615.
39. Collao N, Farup J, De Lisio M. Role of Metabolic Stress and Exercise in Regulating Fibro/Adipogenic Progenitors. *Front Cell Dev Biol* 2020;**8**:9.
40. Wright LE, Buijs JT, Kim H-S, Coats LE, Scheidler AM, John SK et al. Single-Limb Irradiation Induces Local and Systemic Bone Loss in a Murine Model. J Bone Miner Res 2015;30:1268–1279.

Chapter III

Single-cell transcriptomic analysis of skeletal muscle cellular dynamics following radiation exposure

Nicolas Collao[1,2], Emma B Johannsen[3,4], Jesper Just[3,4], and Michael De Lisio[1,2,5*]

[1]School of Human Kinetics, Faculty of Health Science, University of Ottawa, Ottawa, ON, Canada, [2]Éric Poulin Centre for Neuromuscular Disease, University of Ottawa, Ottawa, ON, Canada [3]Department of Molecular Medicine, Aarhus University Hospital, Aarhus, DK-8200, Denmark, [4]Department of Clinical Medicine, Aarhus University, Aarhus, DK-8200, Denmark, [5]Department of Cellular and Molecular Medicine, Regenerative Medicine Program, University of Ottawa, Ottawa, ON, Canada

Keywords: fibrosis, atrophy, cell-cell communication, pediatric cancer, cancer cachexia, single-cell RNA sequencing.

***Correspondence to:**
Michael De Lisio, PhD
School of Human Kinetics, and Department of Cellular and Molecular Medicine
University of Ottawa
Ottawa, ON, Canada
Phone: +1 613-562-5800 ext. 6987
Email: mdelisio@uottawa.ca

Summary

Radiation therapy causes long-term skeletal muscle atrophy and fibrosis in juvenile cancer survivors. The mechanisms responsible for the late effects of radiation therapy on skeletal muscle are not well-understood and have prevented the development of effective treatments. Using single-cell RNA sequencing (scRNAseq), we characterize cellular dynamics and cell communication in a murine model of therapeutic radiation exposure at 24-hours and 56-days post-irradiation (post-IR). We identified a quiescent muscle satellite (stem) cell (MuSC) subpopulation that was significantly reduced, and a subpopulation of type 2 macrophages that was substantially increased at 56-days post-IR. Genes related to fibroblast proliferation were up-regulated in Fibro-adipogenic progenitors (FAPs) at 24-hours post-IR, and a fibrotic phenotype persisted in FAPs at 56-days post-IR. A conserved *Cdkn1a* signature was observed in all cells post-IR and inflammatory signalling mediators were upregulated in the IR-limb at 56-days. Intercellular communication analysis revealed FAPs as the primary contributor of extracellular matrix and target of TGF-β signalling at both 24-hours and 56-days post-IR. Together, our findings provide valuable insights into the potential mechanisms and intercellular communication responsible for radiation-induced muscle late effects.

Introduction

Cancer survival in children, adolescents, and young adults has been steadily increasing such that over 80% of juvenile cancer patients are expected to survive long-term.[1] A consequence of increased juvenile cancer survival is enduring, long-term, treatment-related side-effects. Radiation therapy is a primary treatment for juvenile cancer in over 33% of cases.[2] Radiation harms non-target tissues, particularly skeletal muscle,[3] resulting in atrophy, fibrosis, weakness, reduced participation in physical activity, and impaired quality of life.[4]

Juvenile skeletal muscle growth requires myonuclear accretion from muscle satellite (stem) cells (MuSCs).[5] Lineage tracing models have shown that MuSCs directly contribute myonuclei to the growing myofiber during juvenile development.[6,7] Further, MuSC ablation during prepubertal muscle growth leads to life-long muscle impairments.[8] Radiation reduces MuSC content and function resulting in skeletal muscle atrophy and fibrosis in juvenile mice[9] and radiation prevents hypertrophy in mouse models of muscle growth due, in part, to MuSC depletion.[10–12] Interestingly, a rare population of radiation-resistant MuSCs has recently been identified; however, transplantation of these cells into previously irradiated muscle resulted in significantly reduced muscle regeneration compared to transplantation into non-irradiated muscle.[13] Similarly, myoblast transplantation efficacy into irradiated muscle decreases with time following radiation.[14] Together, these results suggest long-term changes in the muscle niche following radiation exposure that cannot be overcome by restoring myogenic cells alone.

MuSC fate is regulated by the interaction of different muscle-resident mononuclear cells such as endothelial cells (ECs), immune cells, such as macrophages, B- and T-

Lymphocytes, and fibro-adipogenic progenitors (FAPs) among other cell types.[15] Our laboratory and others have observed increased inflammatory and fibrotic gene signatures following radiation exposure in murine models of juvenile cancer.[9,16] Similarly, other groups have demonstrated impaired type 2 macrophage polarization during regeneration following radiation exposure.[17] Nevertheless, no previous works has characterized cellular dynamics in the muscle microenvironment at single-cell resolution following radiation exposure.

The application of single-cell RNA sequencing (scRNA-seq) technology in skeletal muscle has identified novel cell populations and states, molecular pathways, regulatory networks, and provided insights into potential mechanisms responsible for skeletal muscle regeneration.[18] These new findings have led to a substantial improvement in our understanding of the complexity of the skeletal muscle regeneration;[19–22] however, data from various pathological muscle conditions are lacking.[23–25] Thus, the present work aims to identify potential mechanisms contributing to the late effects of radiation in skeletal muscle. We applied scRNA-seq technology to access longitudinal muscle recovery following radiation exposure to identify i) alterations in gene expression in muscle-resident mononuclear cell populations, ii) conserved gene responses to radiation across muscle mononuclear cells, and iii) potential alterations in cellular interactions in a mouse model of juvenile radiation therapy.

Results

Short- and long-term alterations in cellular dynamics after radiation exposure

To explore changes in cellular dynamics following radiation exposure, we performed scRNA-seq at 24-hours and 56-days following radiation localized to a single

hind limb (IR). We used the non-irradiated leg as the control (CON) (Figure 1A). The time points were based on work from our lab[26] and others[9,27] that detected radiation-induced skeletal muscle fibrosis and atrophy by 56-days following radiation exposure, and acute responses within 24-hours.[8] Following quality control and normalization, 5986 cells and 17,642 total detected genes from three pooled samples were used for library generation. All samples were processed in one batch to avoid batch effects. Unsupervised clustering identified 12 distinct cell populations based on uniform manifold approximation and projection (UMAP) performed on the integrated dataset (Figure 1B). We assigned the cell identities to each cluster based on their canonical gene expression, such as endothelial cells (*Pecam1* and *Cdh5*), FAPs (*Pdgfra* and *Col1a1*), MuSCs (*Pax7* and *Myf5*), Myonuclei (*Acta1* and *Tnnc2*), Smooth muscle cells (SMCs)/Pericytes (*Tagln* and *Cspq4*), Macrophages (*Cd68* and *Ptprc*), Monocytes/Neutrophils (S100a9), B-Lymphocytes (*Cd79a*), T-Lymphocytes/Natural Killers (NK) (*Cd3d*), Glial cells (*Ptn*), Schwann cells (*Mpz*), and Erythrocytes (*Hba-a2*) (Figure 1C). These clusters were consistent with previous findings.[19,20,28] Hierarchical cluster analysis of differentially expressed genes (DEGs) in each cell type identified distinct transcriptional profiles within the twelve clusters (Figure 1D). By examining the top marker genes of each cluster, we were able to validate that the integrated UMAP successfully separated the primary populations in the dataset (Figure S1A). Relative cellular composition revealed a prominent increase in the proportion of cells in the EC cluster (60.44%) at 24-hours post-IR compared to CON; with minor increases in the proportion of cells in the FAPs (5.67%), MuSCs (3.10%), SMCs/Pericytes (6.63%) and Schwann cells (2.57%) at the same time point (Figure 1E). These acute changes were offset by a decrease in the proportion of

cells in the immune cell clusters at 24-hours post-IR (Figure 1E). Conversely, the proportion of FAPs (6.85%), MuSCs (2.81%), and Monocytes/Neutrophils (2.58%) showed a moderate decrease at 56-days post-IR compared to CON; while, ECs (50.39%), SMCs/Pericytes (7.74%) showed a moderate increase compared to CON 56-days. Together, these data suggest that radiation exposure alters the relative cellular composition in skeletal muscle.

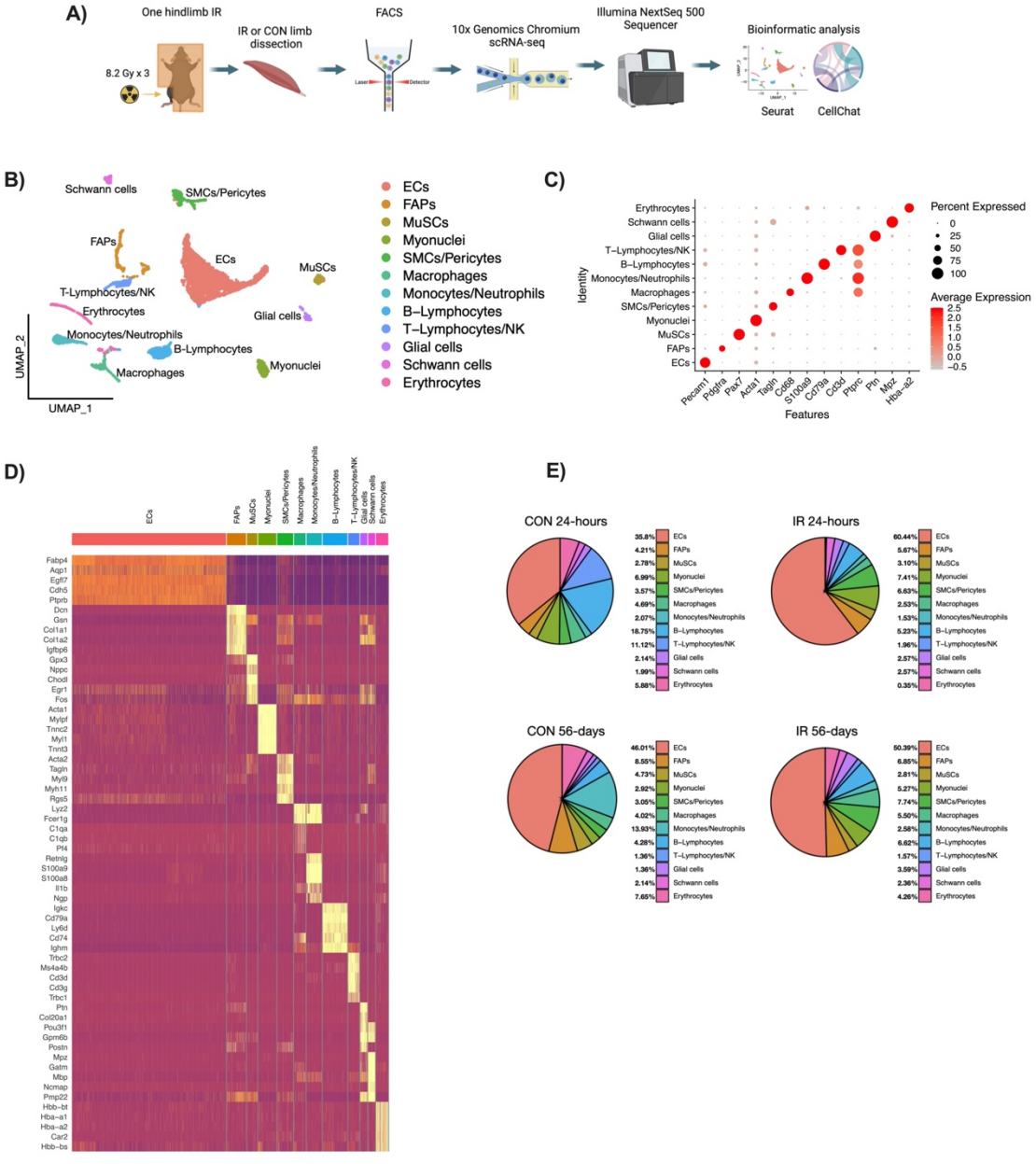

Figure 1. Single-cell RNA sequencing reveals alterations in skeletal muscle cellular dynamics after radiation exposure.

(A) Schematic representation of the sample preparation workflow for scRNA-seq experiment. (B) UMAP clustering, which identifies twelve different cell populations. (C) Feature plot of different markers identifying cell types. (D) Single cell heatmap demonstrating the top 5 differentially expressed genes (DEGs) in each cell type from the integrated data obtained from the single cell RNA-seq analysis. Colours indicate gene expression levels where yellow represents relatively high expression levels and purple represents relatively low expression levels. (E) Pie chart indicating relative cell percentage (%) of the identified cell types. The right-hand side of the pie chart indicates cell types by colour.

Radiation depletes deep quiescent MuSCs long-term.

We next investigated the transcriptional changes that occurred following radiation exposure within the different cell populations residing in the muscle niche. We identified four different MuSC clusters by re-clustering 204 cells from the integrated dataset (Figure 2A). Based on their gene expression profile, all MuSC subclusters expressed different levels of *Pax7* and *Myf5* (Figure 2B). We identified a primed quiescent MuSC subcluster expressing *Junb*, and *Hes1*, and a deep quiescent MuSC subcluster expressing *Ryr3* and *Cd34.* Also, we observed a cycling/activated MuSC subcluster expressing *Ccnd1*, *Acta2*, and *Sparc* and a committed MuSC subcluster expressing *Cdkn1a*, *Gas6*, and *Cebpb* (Figure 2B, 2C and S2A). At 24-hours post-IR, cycling/activated MuSCs were depleted compared to CON 24-hours, while committed MuSCs were relatively more abundant

(Figure 2D). At 56-days post-IR, primed quiescent MuSCs were relatively abundant compared to CON and cycling/activated and committed MuSCs were low or not detected. Interestingly at 56-days post-IR, we also observed a substantial depletion of deep quiescent MuSCs (Figure 2D). Based on the DEGs for the overall MuSC population, at 24-hours post-IR vs CON 24-hours (Figure 2E), we observed an up-regulation of enriched terms related to regulating fibroblast proliferation, kinase activity, and cytokine stimulus (GO, Biological Process). Whereas GO terms for translation, and endoplasmic reticulum (ER) were down-regulated at 24-hours (Figure 2E). Together, these findings suggest the loss of the MuSC pool, particularly deep quiescent MuSCs, following radiation exposure and fibrotic signalling in the remaining MuSCs.

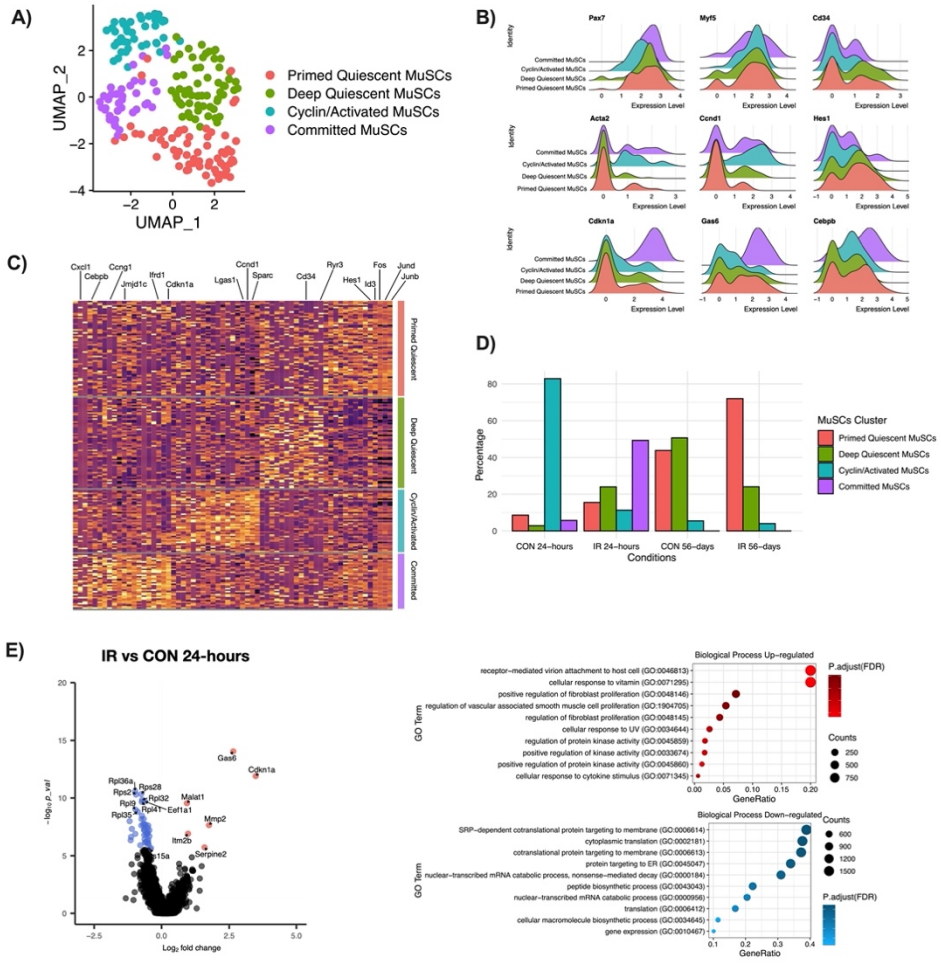

Figure 2. Radiation depletes deep quiescent MuSCs long-term.

(A) UMAP embedding of integrated MuSC populations showing the different MuSC subclusters. (B) Ridge plot showing the expression of different genes identified by the DEGs in the different MuSC subclusters. (C) Heatmap of the top 10 genes that are differentially enriched in each MuSC cluster. Colours indicate gene expression levels where yellow represents relatively high expression levels and purple represents relatively low expression levels. (D) Relative cell percentage (%) of MuSC subclusters. (E) Volcano plot showing the distribution of DEGs in the total MuSC population between IR and CON at 24 hours. Genes are plotted as $\log_2$ fold change versus the $-\log_{10}$ of the p-value. Genes in red indicate up-regulation while genes in blue indicate down-regulation in IR at 24 hours. GO enrichment analysis of the DEGs in IR versus CON at 24-hours of total MuSCs showing the up- and down-regulated biological process.

FAPs displayed a fibrotic signature following radiation exposure.

FAP normalization and clustering from the integrated dataset (n=376) was performed as described for MuSCs. Six distinct FAP clusters were identified (Figure 3A). DEGs identified distinct transcriptional profiles within the FAP subclusters (Figure 3B and S3A). We identified (1) Cxcl14$^+$-FAPs expressing *Cxcl14*, *Smoc2*, *Hmcn2*, *Spry1*, and *Fbln2*; (2) Dpp4$^+$-FAPs expressing *Dpp4*, *Pi16*, *Sema3c*, *Cd55*, and *Fn1*; (3) a pro-angiogenic FAP cluster that highly expressed *Aqp1*, *Cdh5*, *Kdr*, and *Egfl7*; (4) Dlk1$^+$-FAPs expressing *Dlk1*, *Apod*, *Lum*, and *Col14a1*; (5) Wisp1$^+$-FAPs highly expressing *Fmod*, *Thbs4*, *Tnc*, and *Post*; and (6) Tenm2$^+$-FAPs expressing *Tenm2*, I*tgb4*, *Wnt6*, and *Tagln* (Figure 3B). We observed an increase in the total FAP population at 24-hours post-IR,

followed by a substantial decrease at 56-days post-IR (Figure 3C). The pro-angiogenic FAPs and the Wisp1^{+}-FAPs were relatively enriched at 24-hours post-IR compared to CON 24-hours, while Dlk1^{+}-FAPs, Tenm2^{+}-FAPs, and pro-angiogenic FAPs were relatively enriched at 56-days post-IR compared to CON 56-days (Figure 3D). GO enrichment analysis of the DEGs in 24-hour post-IR FAPs compared to CON at 24-hours showed up-regulated fibroblast proliferation, kinase activity, and cytokines stimulus; and down-regulation of the negative regulation of WNT signalling (Figure 3E and S3B). Whereas at 56-days, IR-FAPs showed up-regulated GO terms for biological processes related to immune cells, ER, and translation compared to CON 56-days (Figure 3E). To confirm our single cell transcriptomic findings, we performed flow cytometric analysis on FAPs using previously established cell surface markers that distinguish fibrotic FAPs expressing CD142 and stem-like, pro-regenerative FAPs expressing CD55[29] (Figure S3C). No significant changes in the CD55^{+}-FAPs subpopulation were observed at 56 days post-IR compared to CON 56-days; however, a significantly higher proportion of CD142^{+}-FAPs was observed at 56-days post-IR compared to CON 56-days (Figure 3F). Together, these findings suggest that radiation exposure promotes expansion of the pro-fibrotic FAP subpopulation.

Radiation expands a subcluster of capillary endothelial cells that persists long-term.

A total of 2996 ECs were subclustered from the integrated data. We identified five ECs subpopulations (Figure 4A). Based on canonical markers[30,31] we assigned the following identities to each distinct cluster: two capillary ECs clusters: capillary 1

(capECs1) enriched for *Timp4*, *Cxcl12*, *Rgcc*, and capillary 2 (capECs2) enriched for *Cdkn1a*, *Bax*, and *Col4a1*; arterial ECs (aECs) mainly expressing, *Sema3g*, *Alpl*, and *Fbnl5*; arteriolar (arlECs) enriched for *Lars2*, and *Rpl39*; and venous ECs (vECs) expressing *Lrg1*, *Selp*, *Plvap*, and *Bgn* (Figure 4B and C). EC subpopulation proportions were changed following radiation with capECs1 relatively the most abundant cluster in CON 24-hours; however, this subcluster was decreased 24-hours post-IR with a concomitant increase in capECs2 (Figure 4D). Similarly, in CON 56-days, capECs1 were the most abundant subcluster. At 56-days post-IR, capECs1 and capECs2 were most abundant, accompanied by a doubling in aECs (Figure 4D). Unsupervised clustering showed the visual changes of the different EC subclusters, highlighting the substantial changes in EC populations following radiation exposure (Figure 4E).

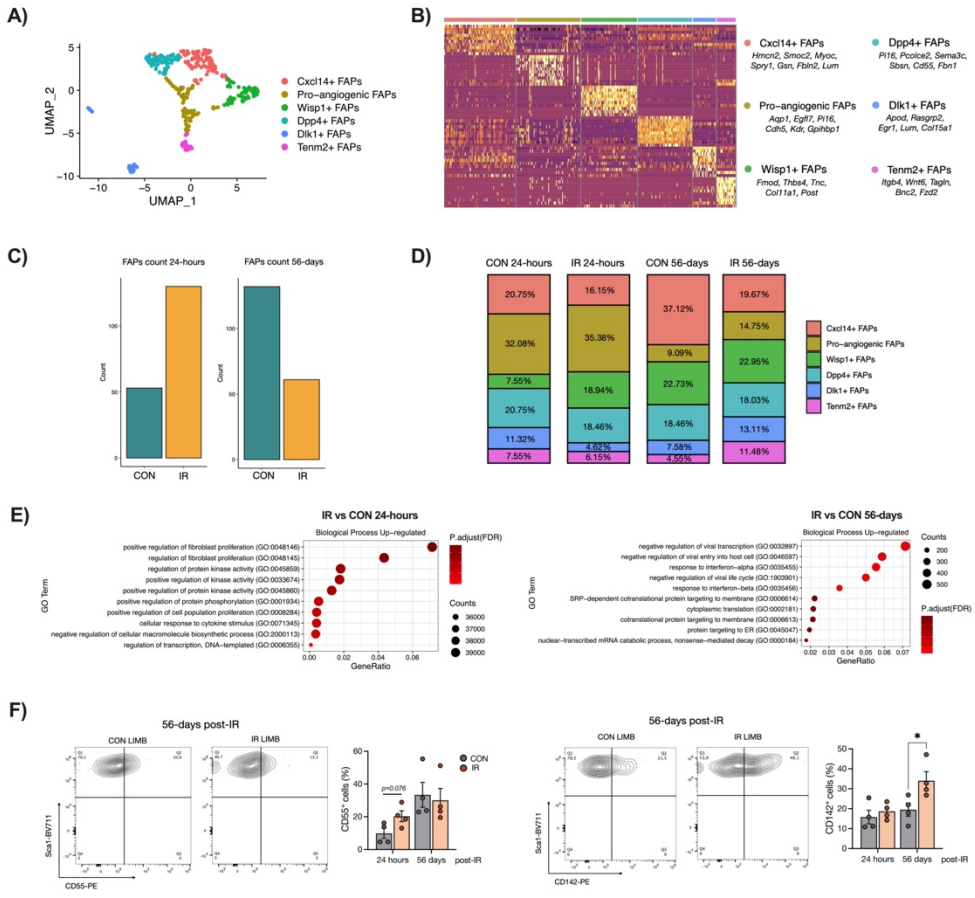

Figure 3. Fibrotic FAPs are relatively preserved following radiation exposure.

(A) UMAP embedding of integrated fibro-adipogenic progenitors (FAPs) populations showing the different FAP subclusters. (B) Heatmap of the top 10 genes that are differentially enriched in each FAP subcluster. Colours indicate gene expression levels, where yellow represents relatively high expression levels and purple represents relatively low expression levels. (C) Total FAP cell count at 24-hours, and 56-days in CON and IR. (D) Bar chart indicating relative cell percentage (%) of FAP subclusters. FAP subclusters are colour-coded on the right of the bar chart. (E) GO enrichment analysis of the DEGs in IR versus CON at 24-hours, and 56-days showing the up-regulated biological process. (F) Representative flow cytometry plots of $CD55^+$-FAPs at 56-days post-IR from CON and IR limb and quantification of $CD55^+$ cells percentage. Representative flow plot of $CD142^+$-FAPs at 56-days post-IR from CON and IR limb $CD55^+$ and quantification of $CD142^+$ cells percentage.

We further examined transcriptional changes occurring in ECs following radiation exposure. By examining the DEGs between IR and CON at 24-hours post-IR, we identified *Cdkn1a*, *Bax*, and *Gas6* among the up-regulated genes and *Fabp4*, *Malat1*, and *Cst3* among the down-regulated genes (Figure 4F). GO enrichment analysis of the DEGs at 24-hours, revealed up-regulated biological processes mainly related to DNA damage, myoblast differentiation and BMP signalling in the IR versus the CON limb. Furthermore, we conducted a gene set enrichment analysis (GSEA) using the MSigDB hallmark gene set to further investigate the underlying biological context. We observed enriched terms associated with the p53 pathway, apoptosis, TGF-β, and TNFα signalling, among others

(Figure 4F). Transcriptional changes at 56-days post-IR showed a persistent gene signature related to DNA damage, characterized by high expression of *Cdkn1a*, *Phlda3*, and *Bax*. GSEA showed an enrichment for p53 signalling, interferon alpha and gamma response, and epithelial to mesenchymal cell transition. Interestingly, biological processes related to endothelial cell proliferation, angiogenesis, and migration were down-regulated (Figure 4G). Together, these findings suggest that radiation exposure results in persistent damage to ECs suggesting decreased angiogenic potential.

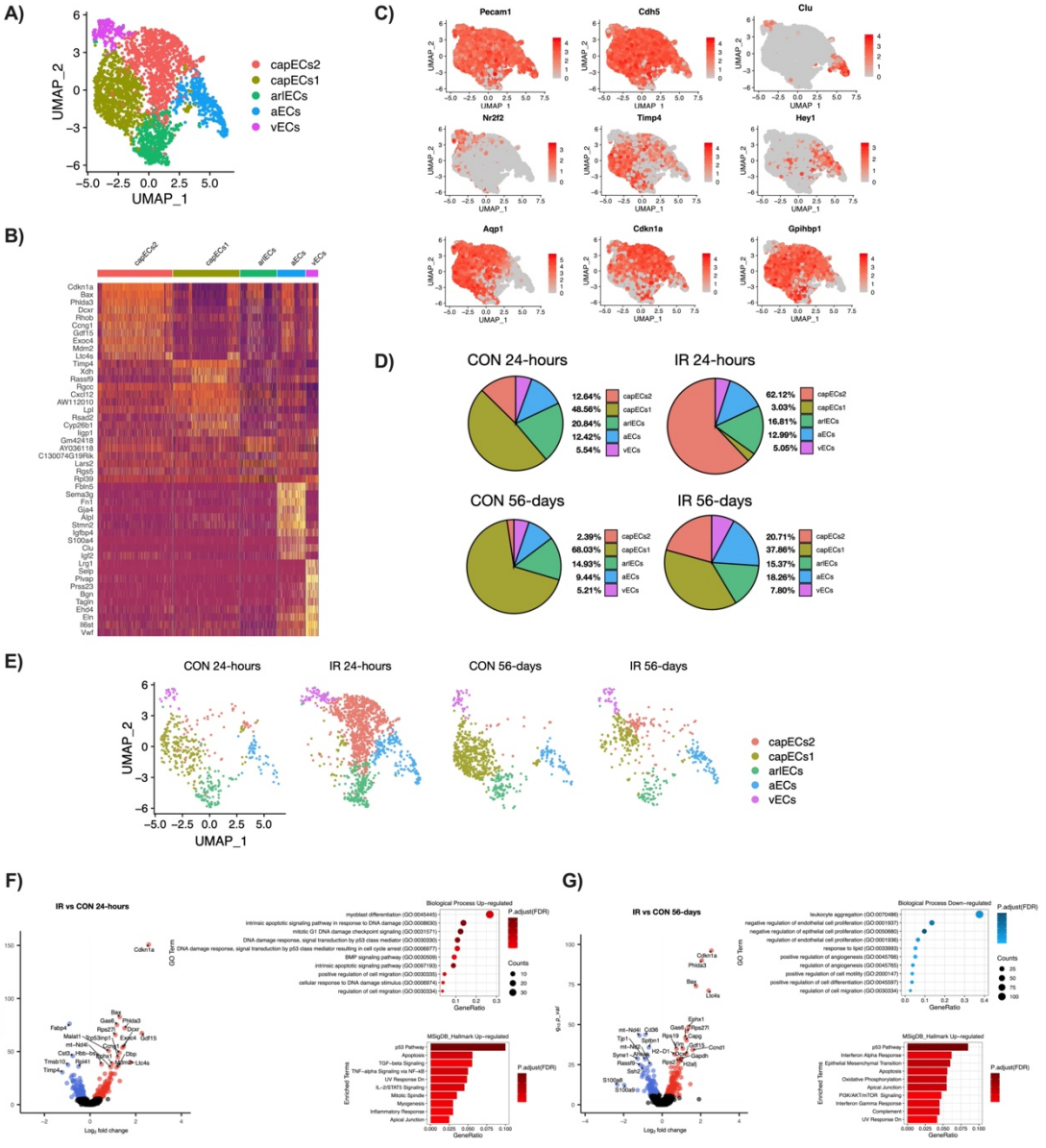

Figure 4. Radiation expands a subcluster of capillary endothelial cells that persists long-term.

(A) UMAP embedding of integrated endothelial cells (ECs) populations showing the different EC subclusters. (B) Heatmap of the top 10 genes that are differentially enriched in each EC subcluster. Colours indicate gene expression levels where yellow represents relatively high expression level and purple represents relatively low expression level. (C) UMAP plots of log-normalized count expression of signature genes identified in each EC subcluster. Expression levels of a gene are correlated with colour intensity and are indicated by scales. (D) Pie chart indicating relative cell percentage (%) of EC subclusters. EC subclusters are colour-coded on the right of the pie chart. (D) UMAP embedding of integrated ECs coloured by subcluster and identified by condition. (E) Volcano plot showing the distribution of DEGs in the total EC cluster between IR and CON at 24 hours. Genes are plotted as $\log_2$ fold change versus the $-\log_{10}$ of the p-value. Genes in red indicate up-regulation while genes in blue indicate down-regulation at 24 hours post-IR. Gene ontology (GO) enrichment analysis of the DEGs in IR versus CON at 24-hours showing the biological process and the Molecular Signatures Database (MSigDB) hallmark genes up-regulated. (F) Volcano plot showing the distribution of DEGs in the total EC cluster between IR and CON at 56 days. Biological processes that were up-downregulated and MSigDB hallmark genes up-regulated in IR and CON at 56 days.

A subcluster of type 2 macrophages persist following radiation.

We identified four macrophage subclusters; type 1a and type 1b (M1a and M1b), and type 2a, and 2b (M2a and M2b). Monocytes and neutrophils also clustered near

macrophages; thus, these cells were included in this sub-analysis (Figure 5A). All myeloid cell clusters expressed *Ptprc* and *Itgam* (Figure 5B). Monocytes were distinguished based on their high *Cxcl2* and *Ptgs2* expression, while neutrophils were distinguished based on their *S100a8*, *S100a9, and Chil3* co-expression. The M1a subcluster expressed *Fabp4* and *Fabp5*, and the M1b subcluster expressed *Cx3cr1*, *Adgre4,* and *Fabp4*. The M2a subcluster showed high expression of *Ccr2*, *Fn1*, and *H2-Ab*, whereas the M2b subcluster expressed high levels of *Lyve1, Mrc1, C1qa,* and *C1qc* (Figure 5B). The M1a subcluster was the most abundant cluster at 24-hours in the CON limb, whereas monocytes and M2a clusters expanded at 24-hours post-IR (Figure 5C). At 56-days, monocytes and neutrophils were most abundant in the CON limb. Conversely, a prominent rise in M2a macrophages was observed at 56-days post-IR compared to CON 56-days (Figure 5C). GO analysis revealed biological processes up-regulated related to apoptotic, cytokines, and MAPK signalling at 24-hours post-IR in monocytes/neutrophils. At 56-days post-IR, monocyte activation and SMAD signalling were the main up-regulated biological processes (Figure 5D). In macrophages, biological processes related to immune cells, cytokines, and kinase activity were upregulated at 24-hours post-IR, while translation and ER biological processes were up-regulated at 56 days post-IR (Figure 5E). These findings indicate alterations in macrophage polarization, and a persistent macrophage type 2 subpopulation following radiation exposure.

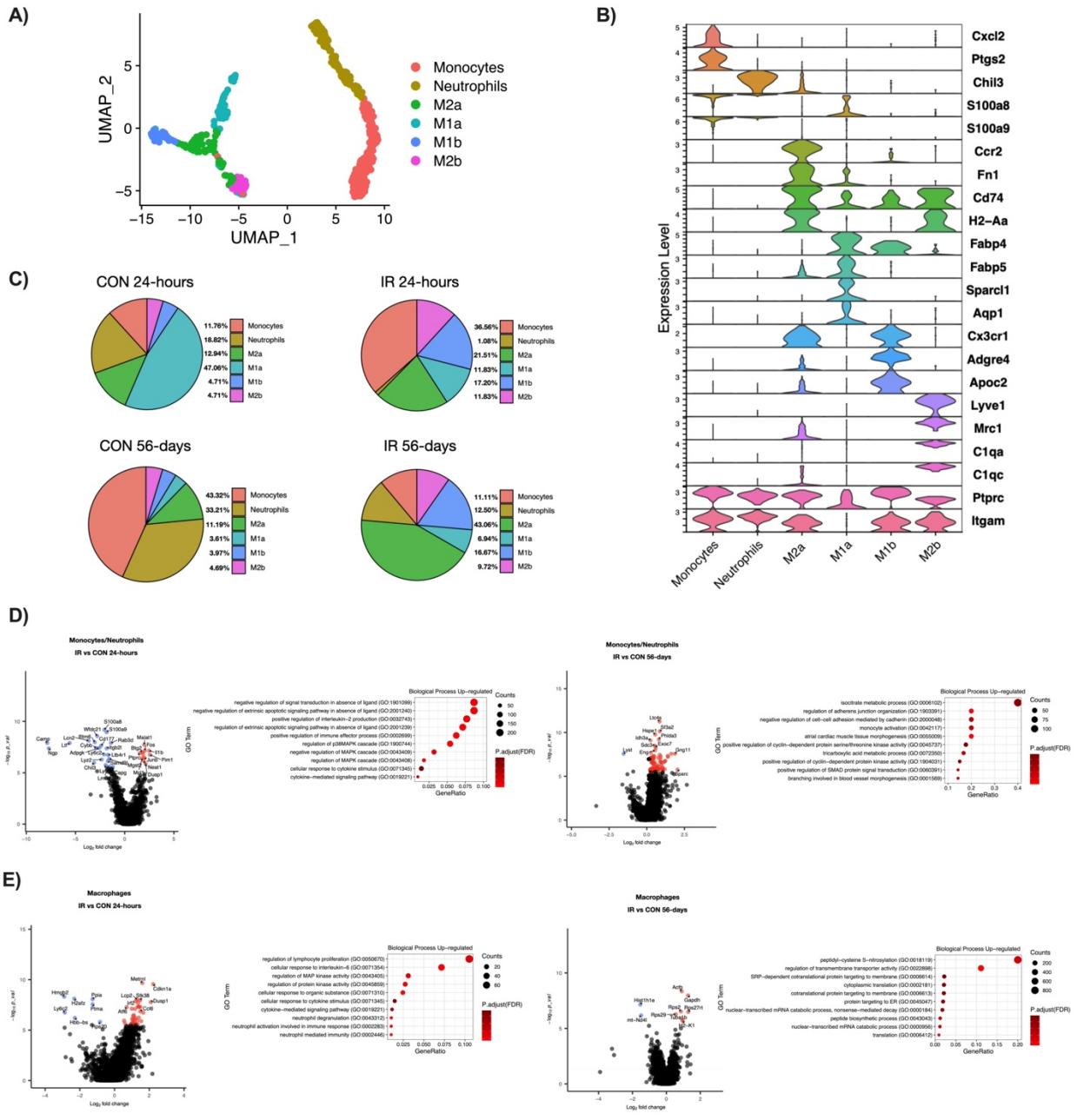

Figure 5. A subcluster of type 2 macrophages persist following radiation.

(A) UMAP embedding of integrated macrophage and monocyte/neutrophil populations showing the different subclusters. (B) Violin plot of genes identified by the DEGs in the different subclusters. (C) Pie chart indicating relative cell percentage (%) of macrophage and monocyte/neutrophil subclusters. Subclusters are colour-coded on the right of the pie

chart. (D-E) Volcano plot showing the distribution of DEGs in the total macrophage and monocyte/neutrophil population between IR and CON at 24 hours and 56-days. Genes are plotted as $\log_2$ fold change versus the $-\log_{10}$ of the p-value. Genes in red indicate up-regulation while genes in blue indicate down-regulation in IR at 24 hours. GO enrichment analysis of the DEGs in IR versus CON at 24-hours and 56-days of total macrophages and monocytes/neutrophils showing the up-regulated biological process.

Cdkn1a expression is a conserved gene signature of radiation exposure that is sustained in the muscle niche.

To identify a conserved transcriptional signature expressed collectively in muscle mononuclear cells following radiation exposure, we identified DEGs in all cell types between IR and CON at 24-hours and 56-days. We identified 1626 DEGs at 24-hours post-IR, of which 1233 genes were up-regulated, and 393 genes were down-regulated in the IR limb compared to the CON limb (Figure 6A). Among the up-regulated genes, we identified *Cdkn1a*, *Gas6*, *Bax*, and *Gdf15,* which are related to the cellular response to DNA damage, cell cycle arrest, mitochondrial membrane integrity, and differentiation. GO enrichment analysis of the DEGs revealed that biological processes related to cell-matrix adhesion, angiogenesis, cell migration, and negative regulation of cellular process were up-regulated, whereas biological processes related to translation and protein targeting to the ER were down-regulated (Figure S4A). The MSigDB hallmark gene set showed enriched terms associated with TGF-β signalling, UV Response, protein secretion, and p53 pathway with a high enrichment score (Figure 6B). Conversely, we observed a down-

regulation of the Myc target, interferon alpha response, and mTORC1 signalling (Figure 6C).

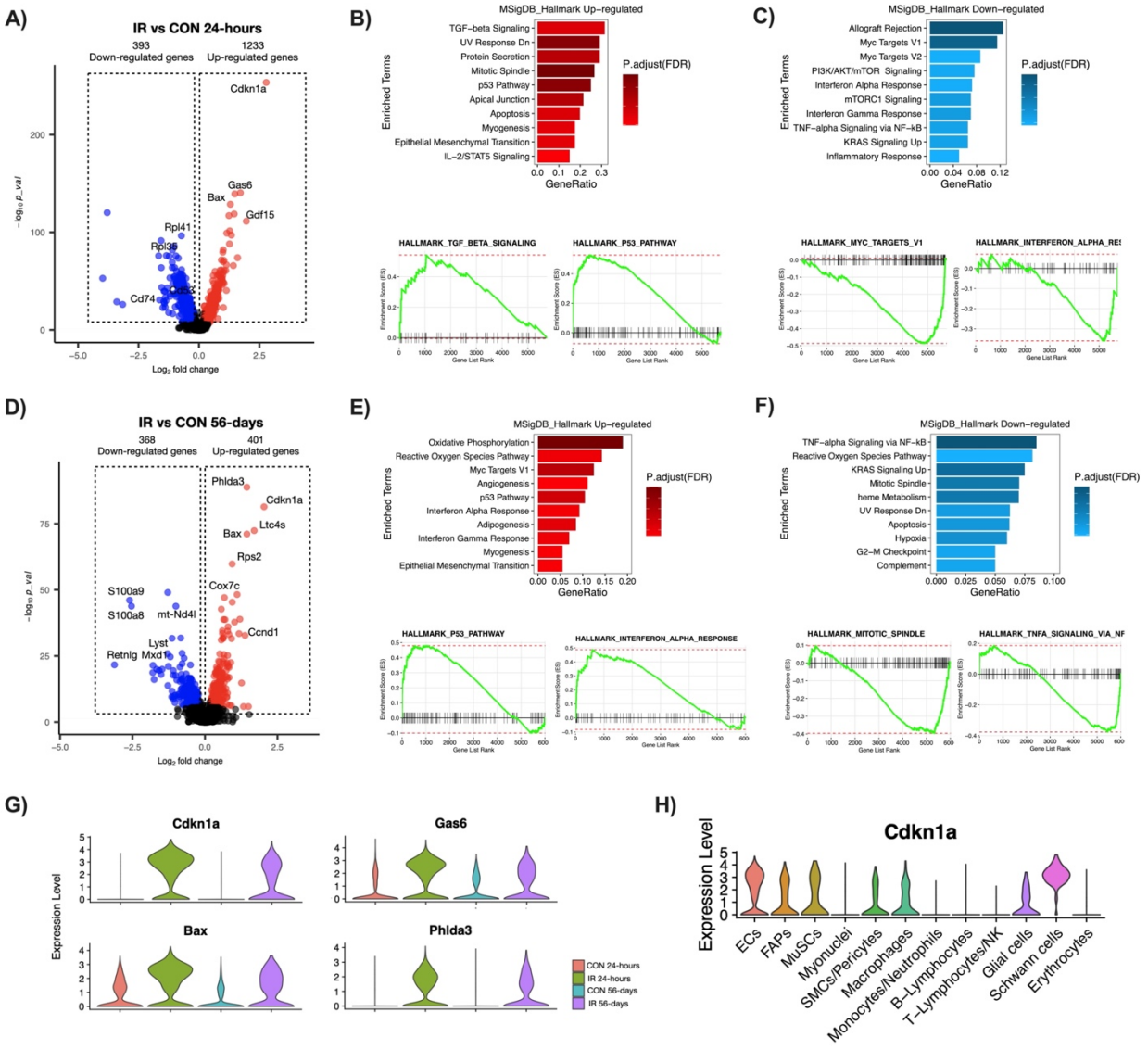

Figure 6. Cdkn1a expression is a conserved gene signature of radiation exposure that is sustained in the muscle niche.

(A) Volcano plot showing the distribution of DEGs between IR and CON at 24 hours using the entire integrated dataset. Genes are plotted as $\log_2$ fold change versus the $-\log_{10}$ of

the p-value. Genes in red indicate up-regulation while genes in blue indicate down-regulation in IR at 24 hours. (B) MSigDB hallmark genes up-regulated in the IR limb and gene set enrichment analysis (GSEA) showing different signalling and pathways from the differentially up-regulated genes. (C) MSigDB hallmark genes down-regulated in the IR limb and gene set enrichment analysis (GSEA) showing different signalling and pathways from the differentially down-regulated genes. (D) Volcano plot showing the distribution of DEGs between IR and CON at 56-days. Genes are plotted as $\log_2$ fold change versus the $-\log_{10}$ of the p-value. Genes in red indicate up-regulation while genes in blue indicate down-regulation in IR at 56-days. (B) MSigDB hallmark genes up-regulated in the IR limb and gene set enrichment analysis (GSEA) showing different signalling and pathways from the differentially up-regulated genes. (C) MSigDB hallmark genes down-regulated in the IR limb and gene set enrichment analysis (GSEA) showing different signalling and pathways from the differentially down-regulated genes. (G) Violin plot showing DEGs changes per condition. (H) Violin plot showing heterogenous gene expression of *Cdkn1a* in the different cell populations.

Transcriptional changes at 56-days post-IR showed a total of 769 DEGs, of which 401 genes were up-regulated and 368 genes were down-regulated in the IR limb compared to CON (Figure 6D). Interestingly, *Cdkn1a* and *Bax* were still up-regulated, while *Phlda3*, *Ltc4s*, *Cox7c*, and *Ccnd1*, all related to p53 target genes, inflammatory process, electron transport chain, and cellular differentiation were also up-regulated (Figure 6D). Biological processes of up-regulated genes revealed an increase in translation and metabolic processes, whereas biological processes related to

inflammation were downregulated (Figure S4B). We identified the p53 pathway, angiogenesis, and interferon alpha response with high enrichment scores while mitotic spindle and TNF-alpha signalling had lower enrichment scores in the IR limb at 56-days (Figure 6E). Radiation increased *Cdkn1a*, *Gas6*, *Bax*, and *Phlda3* expression in skeletal muscle mononuclear cells at both 24-hours and 56-days relative to CON (Figure 6G). Indeed, most cell populations had up-regulated *Cdkn1a* expression at 24-hours and 56-days in the IR limb compared to CON (Figure 6H). These results suggest that the cell cyclin-dependent kinase inhibitor, *Cdkn1a,* perhaps driven by p53 signalling, is a conserved and sustained response to radiation in most muscle cell populations.

FAPs are enriched for senescence and fibrotic gene signatures following radiation.

Based on the observation that *Cdkn1a* expression was up-regulated, and previous work demonstrating radiation-induced fibrosis in skeletal muscle,[26,27,32] we performed a multi-gene signature scoring using UCell on our scRNA-seq data first focusing on a curated senescence gene signature.[33] Based on the computed senescence score, we observed that FAPs present the most senescence-like molecular phenotype among all skeletal muscle cells, followed by Monocytes/Neutrophils, and ECs (Figure 7A). Recently, we used a murine model of juvenile cancer to identify transcriptomic changes in fibrotic and inflammatory genes using a specific CodeSet panel that included 760 genes.[16] Thus, to determine which cell types might contribute to different stages of the fibrotic and inflammatory process following radiation exposure, we repeated our UCell analysis on our integrated scRNA-seq data, this time focusing on fibrotic and inflammatory scoring.

Overall, we observed that FAPs and macrophages present the highest fibrotic and inflammatory gene score (Figure 7B).

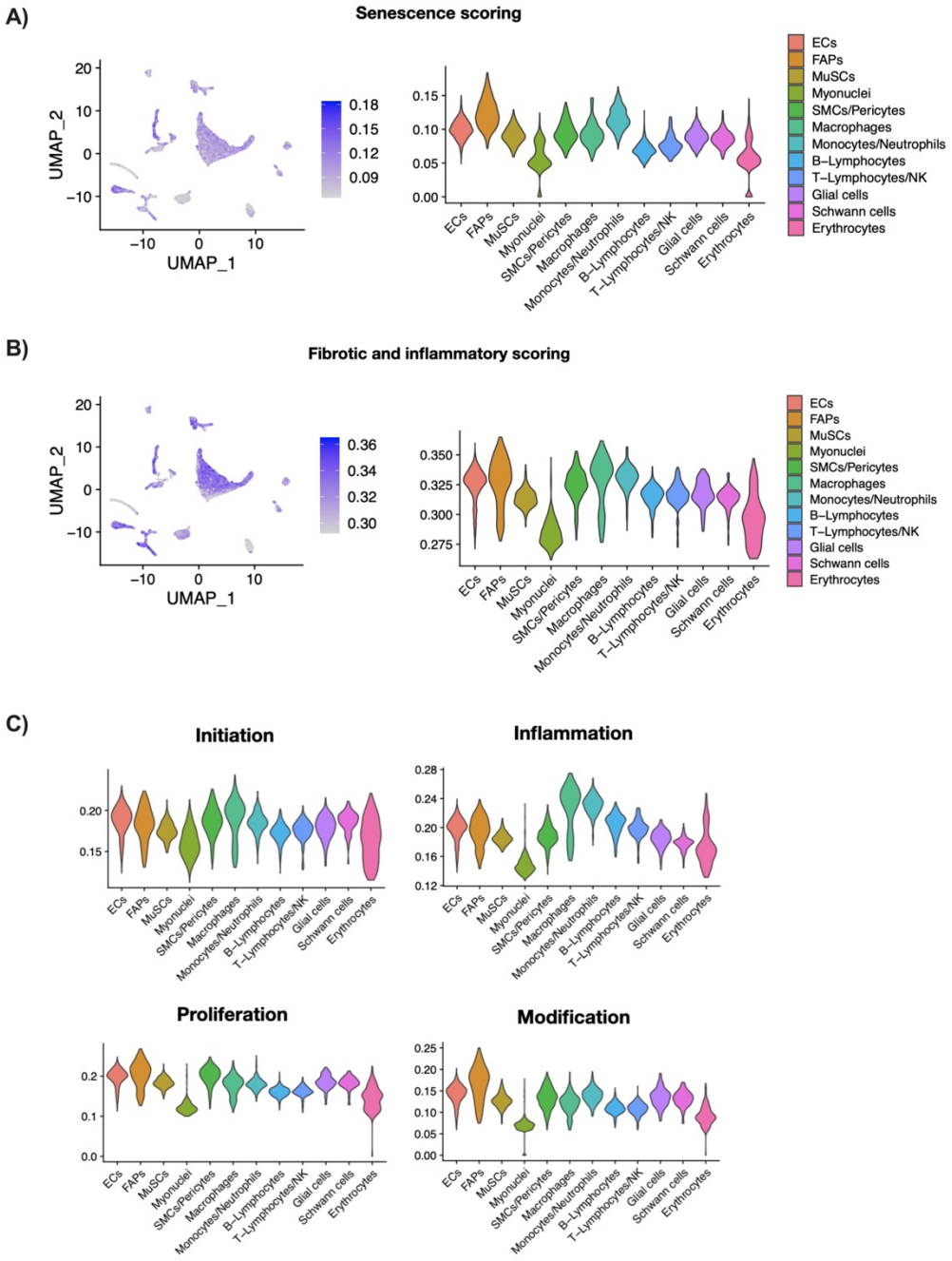

Figure 7. FAPs enriched for senescence and fibrotic gene signatures.

(A) UMAP and violin plot showing the distribution of gene signature scored by UCell based on annotated senescence genes. (B) UMAP and violin plot showing the distribution of gene signature scored by UCell based on annotated fibrotic and inflammatory genes. C) Violin plot showing the relative expression of each cell type in the different fibrotic and inflammatory process.

Next, we used the gene set to identify the cellular contribution to different stages of the fibrotic process,[34] such as (1) initiation, triggered by damaged cells that initiate stress and immune responses; (2) inflammation, a process that involves immune cells and drives expansion of fibrotic-related cells; (3) proliferation, a process related to myofibroblast proliferation and differentiation in response to damage, and lastly, (4) modification, a process associated with the contribution of myofibroblast and immune cells to ECM deposition.[34] We observed that ECs, FAPs, and macrophages contribute to the early stage of the initiation process. Further, macrophages and monocytes/neutrophils mainly contributed the inflammatory process. Finally, the proliferation and modification process score highest in FAPs (Figure 7C). Together these results suggest that FAPs are the main cells enriched in genes related to senescence and fibrosis following radiation.

Changes in cell-cell communication in the muscle niche following radiation.

To get insight into how cell communication in skeletal muscle is affected following radiation, we performed an intercellular communication network analysis using the CellChat R package.[35] Total interaction strength was similar in the IR and CON limbs at 24-hours; however, we observed a substantial decrease in interaction strength in the IR

compared to CON at 56-days (Figure 8A). Further, our analysis revealed that radiation induced the most prominent changes in FAP communication, with FAPs displaying the

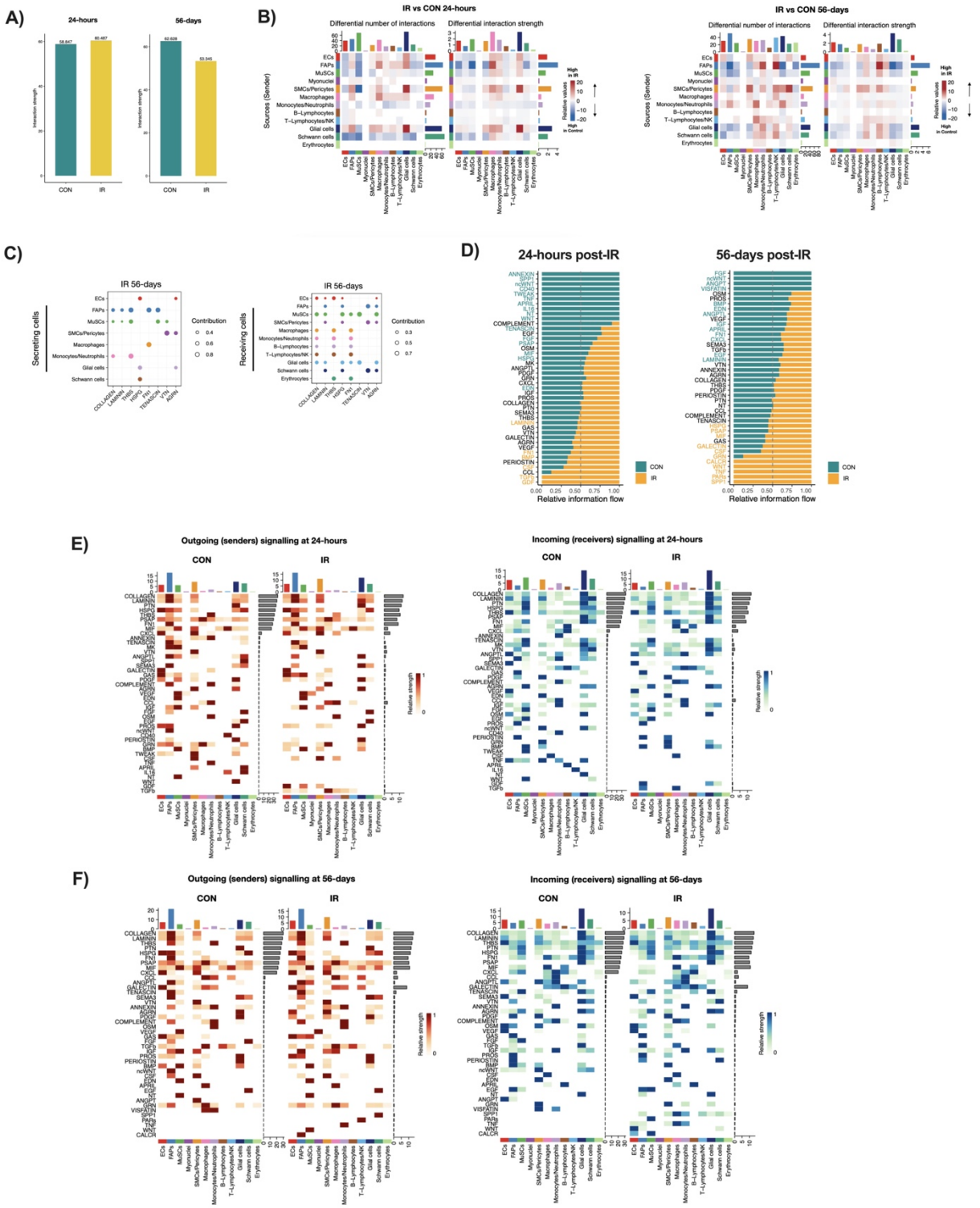

largest differential number and strength of interactions at both 24-hours and 56-days post-IR (Figure 8B). Comparing the outgoing (sender) and incoming (receiver) interactions among the different cell populations, we observed an increase in interaction strength between FAPs (sender) and macrophages and glial cells (receivers) and between SMCs/Perycites (sender) and Glial cells (receiver) at 24-hours post-IR (Figure 8B). At 56-days, the most prominent change was increased communication between FAPs (sender) and B-lymphocytes (receiver) (Figure 8B).

Figure 8. Changes in cell-cell communication in the muscle niche following radiation.

(A) Overall number of predicted paracrine interactions strength between in IR and CON at 24-hours and 56-days. (B) Number and strength of potential interactions among the different cell populations. Colour bar indicates higher (red) or lower (blue) number of interactions. (C) Dot plot indicating the expression of secreted and received ECM proteins between different cell types. (D) Overall information flow of significant signalling pathways. (E-F) Heatmap showing the outgoing (sender) and incoming (receivers) signalling pathways between IR and CON at 24-hours and 56-days. Colour bars at the top indicate the overall signalling strength of each type of cell. The summarized strength of each signalling pathway of each cell type is represented by the horizontal gray bars.

We next identified the signal changes by secreted factors and by ECM proteins. We identified a total of 36 signalling pathways that were potentially mediated by either secreted or cell surface signalling molecules (Figure S5A). Furthermore, we also

identified eight potential pathways mediated by extracellular matrix (ECM) components (Figure S5A). Interestingly, while we observed a decrease in the incoming secreted factors signalling in most cell types, monocytes/neutrophils had increased incoming interactions by **secreted factors** at 24-hours post-IR (Figure S6A). Conversely, macrophages, and B-lymphocytes showed an increase incoming secreted signals at 56-days post-IR (Figure S6A). Supporting our fibrotic gene score analysis, the ECM protein secretion analysis revealed FAPs as the major ECM contributor (Figure 8C, and S6B).

We computed the Euclidean distance to identify differences in signalling pathways between IR and CON at both time points to determine the largest contributors to alterations in the communication network. At 24-hours post-IR, the largest changes were observed in ANGPTL, VTN, BMP, and CSF signalling compared to CON (Figure S6C). Next, we wanted to identify conserved and context-specific signalling pathways following radiation exposure. An overall information flow for all significant signalling pathways showed several pathways only enriched in CON, such as ANNEXIN, SPP1, WNT, and IL16. Conversely, pathways such as GDF and TGF-β were only enriched in the IR limb at 24-hours (Figure 8D). Interestingly, TGF-β, GRN, AGRN, GAS, and IGF signalling showed a large difference in the communication network between the two data sets at 56-days post-IR (Figure S6C). At 56-days post-IR, signalling pathways enriched in CON included: FGF, non-canonical WNT (ncWNT), ANGPT, and VISFATIN, while pathways enriched in IR were: SPP1, PARs, TNF, WNT, and CALCR (Figure 8D).

We then investigated which cell populations contributed to these signalling changes (Figure 8E). We found that TGF-β was the main outgoing signal from macrophages in IR versus CON at 24-hours. Further, ECs were the main senders of GDF

signalling at 24-hours in IR versus CON and the main receiver of GDF, and TGF-β signalling, were FAPs and macrophages showing an autocrine and paracrine TGF-β signalling loop in the IR limb at 24-hours post-IR. Interestingly, FAPs were the main senders of ncWNT signalling and MuSCs were the main senders of Neurotrophin (NT) signalling in the CON limb, whereas secretion of these factors from these different cell types was not detected at 24-hours post-IR. Glial cells were the senders of WNT signalling with MuSCs as the primary receiver in the CON limb. Similar to our findings related to ncWNT and NT signalling, radiation ablated WNT signalling from glial cells to MuSCs. At 56-days post-IR (Figure 8F), FAPs remain the primary receivers of TGF-β signalling. MuSCs emerged as the main senders of BMP signalling with FAPs as the main receiver in CON; however, in IR SMCs/pericytes were the main receivers. Monocytes/neutrophils, T-lymphocytes, and glial cells were the main senders of TNF, PARs, and SPP1 signalling, in the IR limb. FAPs were the primary senders of CALCR signalling in the IR limb only, with MuSCs as the main receivers. Together, these results indicate that the FAP secretome is most sensitive to IR-induced changes with signalling pathways related to angiogenesis, inflammation, and fibrosis predominately affected. Further, FAP-macrophage crosstalk may drive fibrosis through persistent alterations in TGF-β signalling while FAPs may contribute to impaired muscle regeneration through alterations in CALCR signalling with MuSCs.

Discussion

Effective therapies for radiation-induced muscle pathology in cancer survivors are lacking due, in part, to an insufficient mechanistic understanding of the long-term effects

on the muscle niche. To begin to address this gap, we used scRNA-sequencing to characterize the cellular dynamics of muscle mononuclear cells in a model of therapeutic radiation exposure. Our findings indicate that radiation depleted muscle-resident cell populations, altered the proportions of various subclusters within each population, induced a conserved and persistent senescence molecular phenotype particularly in FAPs, and reduced cell-cell communication in the skeletal muscle niche. With respect to alterations in cellular dynamics, radiation depleted the deep quiescent MuSC subcluster long-term, and the overall FAP population. Conversely, radiation resulted in a relative expansion of the capillary endothelial cell subcluster of ECs as early as 24-hours following radiation exposure which persisted at 56-days post-IR, and expanded macrophages type 2 expressing *Ccr2*. When examining the integrated dataset, we identified a conserved and persistent gene signature that was prevalent in most skeletal muscle cell populations characterized by up-regulation of *Cdkn1a* expression and p53 signalling, and found that FAPs were the highest expressors of senescence and fibrosis-related genes in the IR-limb compared to CON at 56-days. Lastly, our cell communication analysis revealed that macrophages were the main signal receivers and FAPs were the major senders of secreted factors at 56-days post-IR with FAPs being the major contributor of extracellular matrix secretion, and the primary target of TGF-β1 signalling at 24-hours and 56-days post-IR. Collectively, our findings provide a significant advancement to our understanding of the cellular sources and the potential mechanism involved in radiation-induced muscle pathology.

Most previous work examining the effects of radiation on skeletal muscle has indicated that MuSCs are rapidly depleted following radiation resulting in impaired muscle

regeneration and hypertrophy.[8,9,11] Interestingly, our computational analysis showed an immediate increase in MuSC proportion following radiation relative to the other mononuclear cell populations in skeletal muscle which was driven by an increase in the committed MuSC subcluster at 24 hours post-IR. These findings were in apparent contrast to previous work showing an absolute decrease in MuSC content between 2- and 4-hours after radiation exposure.[8] Discrepancies in the data are likely due to our assessment relative to other cell types in muscle as absolute content of each cell populations were depleted overall in our computational analysis. The relative MuSC preservation following radiation may indicate relative radiation resistance of this stem cell population compared to mature mononuclear cells. Indeed, a subpopulation of quiescent MuSCs has been identified to be resistant to radiation or environmental stressors[13,36] and this population may account for the relative MuSC preservation we observed. The short-term increase in MuSC content following radiation may indicate a compensatory regenerative response. Indeed, we detected an upregulation in biological process for myoblast differentiation in ECs at 24-hours post-IR and an increase in the Wisp1^{+}-FAP subcluster at the same timepoint. ECs are known to support MuSC proliferation and differentiation;[37,38] WNT1 Inducible Signalling Pathway Protein 1 (WISP1) secreted from FAPs promotes MuSC proliferation and myogenic commitment.[39] Thus, the increase in committed MuSCs at 24-hours post-IR could be mediated by the relative expansion of EC and FAP subclusters that promote their myogenic commitment. Conversely, at 56 days post-IR, we observed a relative decrease in the total MuSC pool which was most evident for the deep quiescent MuSC subcluster. These results are similar to previous findings in aged mice in which the deep quiescent MuSC are depleted.[40] and may explain the

premature aging phenotype observed in skeletal muscle from juvenile cancer survivors.[32] Defective niche signalling may underlie the loss of deep quiescent MuSCs. Dlk1 expression impair MuSCs quiescence, and we observed an expansion in Dlk1^{+}-FAPs at 56-days post-IR. Further, BMP signalling is lost in FAPs at 56-days post-IR, which aligns with a previous finding that BMP3B expression in FAPs decreased during ageing and is associated with skeletal muscle atrophy.[41] Together, signals primarily from FAPs and ECs in the MuSC niche following radiation exposure appear to induce early MuSC commitment and long-term depletion of deep quiescent MuSCs. Interestingly, our analyses reveal compensatory mechanisms to preserve MuSC content may be concomitantly activated. Specifically, FAPs were the main sender of Calcitonin receptor (CALCR) signaling and MuSCs were the major receivers at 56-days post-IR. Previous work described CALCR signalling to be essential to maintain the quiescence stem cell pool,[42] indicating that FAPs may be attempting to preserve the MuSC pool following radiation exposure.

Impaired regeneration and growth in irradiated skeletal muscle is accompanied by an accumulation of ECM resulting in fibrosis. Fibrosis contributes to muscle stiffness, weakness, and reduced endurance capacity in cancer survivors.[32,43,44] In several pathological conditions, FAPs colocalize with excessive collagen and ECM production[45–49] suggesting their key role in muscle fibrosis. Indeed, FAPs were the main population enriched for ECM secretion genes and had the highest expression of the inflammatory and fibrotic transcriptomic signature. In support of their role in muscle fibrosis, we observed a decrease in PDGF signalling in FAPs at 56-days post-IR, which aligns with our previous work showing that PDGFRα expression in FAPs decreases at 56-days post-IR and is associated with a fibrotic phenotype.[26] FAPs also upregulated biological

processes related to fibroblast proliferation, cytokines, and kinase activity which are all related to fibrosis.[50,51] Additionally, regulators of WNT signalling pathways were downregulated in FAPs at 24-hours post-IR. WNT signalling has been linked to skeletal muscle fibrosis[52] mediated by TGF-β,[53] and overactivation of WNT/β-catenin signalling promotes expansion,[54] and myofibroblast differentiation of mesenchymal stem cells leading to exacerbated ECM deposition.[55,56] Thus, removing WNT signalling inhibition would promote FAP transition to myofibroblasts and contribute to muscle fibrosis. These transcriptomic findings were confirmed by our flow cytometry analysis where we detected an increase in the fibrotic[29] $CD142^{+}$-FAP subcluster at 56 days post-IR compared to CON. Together, these findings indicate intrinsic changes in FAPs that would support their role in radiation-induced fibrosis and aligns with the phenotypic changes we previously identified in our earlier work.[26]

In addition to intrinsic regulation, FAP fate is also determined by their cellular microenvironment. MuSCs regulate FAPs via paracrine mechanisms[57] during muscle hypertrophy.[58] In our study, MuSCs immediately upregulated genes associated with fibroblast proliferation following radiation suggesting similar regulation during recovery from radiation exposure. Similarly, impaired macrophage polarization and clearance also contributes to skeletal muscle fibrosis.[17] Macrophages type 2 expressing *Ccr2*, were expanded at 56-days post-IR compared to CON. This *Ccr2*-enriched subcluster of type 2 macrophages also highly expressed *Fn1*, *Ctss*, *S100a4,* and *Crp1*, which are known regulators of tissue fibrosis.[9,26,59–61] In aged muscle an increase in type M2 macrophages has been associated with enhanced ECM deposition,[62,63] and macrophage type 2 have been shown to secret high levels of TGF-β.[64] Moreover, an up-regulation of *Ccr2* gene

expression following radiation exposure has been associated with skeletal muscle inflammation and fibrosis.[9] We observed an immediate increase in interaction strength between FAPs and macrophages at 24 hours, with FAPs being the major receives of TGF-β at that timepoint. At 56-days macrophages are the major sender of TGF-β suggesting a rapid and sustained up-regulation of fibrotic signalling from macrophages to FAPs.[26] Interestingly, we observed an increase in SPP1, and TNF signalling in the IR-limb compared to CON at 56-days post-IR. These pro-inflammatory mediators have been shown to be up-regulated in different pathological conditions, promoting inflammation and fibrosis.[65,66] In addition, macrophages were the main receivers of SPP1 signalling in the IR-limb at 56-days post-IR. This finding aligns with a pro-fibrotic subset of macrophages highly expressing SPP1 following myocardial infarction, which promotes myofibroblast differentiation, contributing to ECM accumulation.[67] Our findings provide several potential mechanisms for activating the FAP/fibroblast-mediated muscle fibrosis rapidly following radiation exposure.

Disrupted tissue perfusion due to EC depletion has also been postulated as a potential mechanism contributing to radiation-induced fibrosis in several tissues[68]. In agreement with our previous work,[26] our computational analysis revealed an absolute decrease in the broader EC population, although ECs were relatively preserved compared to other cell populations. Interestingly, we observed significant alterations to EC dynamics with a relative expansion of the capEC2 subset at the expense of the capEC1 subset. Interestingly, capEC2 was defined by high expression of *Cdkn1a*, *Bax*, and *Col4a1* suggesting that this EC subcluster is senescent and fibrotic. Indeed, Bachman and colleagues showed an increased *Bax* gene expression in skeletal muscle

following 3-weeks post-IR[8] and the pro-apoptotic mediator Bax, has been correlated with radiation-induced apoptosis in carcinoma.[69] Moreover, the persistent incoming WNT signalling to ECs observed at 56-days post-IR, suggests a fibrotic transition as the WNT pathway induces endothelial to mesenchymal transition that produces myofibroblasts.[70,71] Thus, radiation likely impairs skeletal muscle perfusion by inducing a senescent, apoptotic, and fibrotic transition in ECs.

Cellular senescence is a cellular state characterized by permanent removal from the cell cycle and is induced by intrinsic and/or extrinsic damaging stimuli, including radiation exposure.[72] Growing evidence suggests that senescent cell accumulation in skeletal muscle contributes to dysfunction.[73–75] Englund and colleagues showed that p21 encoded by the *Cdkn1a* gene induces a senescence program leading to skeletal muscle atrophy and fibrosis.[74] Our findings showed a conserved and persistent *Cdkn1a* gene signature following radiation exposure that, based on previous literature, could contribute to the long-term muscle atrophy and fibrosis observed in cancer survivors. Recently, Moiseeva and colleagues showed that senescent cells present a conserved signature of fibrotic and inflammatory features decreasing their proliferative capacity and impairing muscle regeneration[76] which aligns with our results showing an up-regulation of fibrotic and inflammatory signalling, particularly in FAPs in the IR-limb compared to CON at 56-days post-IR. Zhang and colleagues identified a FAP subpopulation in aged skeletal muscle exhibiting senescence features, such as high expression of *p16*, *Tenm2*, *Apod,* and *Cq*,[77] that highly overlaps with our Tenm2^{+}-FAP subcluster which doubled in proportion in the IR-limb at 56-days post-IR. Together, these findings suggest that

radiation promotes a conserved senescence gene signature in skeletal muscle and that FAPs are the most affected cell population.

In summary, we molecularly characterized alterations to muscle-resident mononuclear cell populations, identified radiation-induced alterations to different subclusters within those populations, and discovered a conserved gene response to radiation. Additionally, we identified potential alterations in cellular communication following radiation exposure. Our findings provide valuable insights into the potential mechanisms underlying radiation-induced muscle atrophy and fibrosis. Further, characterizing the molecular response to a model of radiation therapy at the single cell level will benefit the muscle research community by providing a resource for understanding skeletal muscle cellular dynamics under pathological conditions.[23,24,78] These insights offer opportunities for further investigations into specific signalling pathways and cell populations, aiming to mitigate the long-term skeletal muscle complications experienced by cancer survivors and improve their quality of life.

Limitations of the study

One of the limiting aspects of this study was the relatively low number of cells capture by our scRNA-seq experiment. This could be explained by the known cytotoxic effects of radiation resulting in fewer cells within skeletal muscle. Regardless, our analyses, including population subclustering, were based on similar number of cells obtained in previous work,[23] we detected cellular populations that align with previous work,[19,20,28] and our subclusters largely align with previous populations observed by other groups in different muscle pathologies[23] likely due to the high read coverage we obtained per cell. We also acknowledge that *in vivo* and *in vitro* approaches are necessary to

validate our transcriptomic results and confirm the function of our subclusters; however, several of our transcriptomic findings algin with phenotypic and functional findings from previous work. Further, the experimental design precluded our ability to statistically evaluate differences in cell cluster and subcluster proportions and resulted in maturation/aging related differences between clusters in CON-24-hours and CON-56-days. Nevertheless, our study provides novel and valuable insights into a previously unexplored area of the complex transcriptional changes, cellular dynamics, and states of different muscle-resident mononuclear cell populations following radiation exposure.

ACKNOWLEDGEMENTS

We acknowledge the services of the Behavioural Core Facility at the Faculty of Medicine at the University of Ottawa. We thank the support provided by the Cell Sorting and Flow Cytometry Core Facility and the StemCore Laboratories Facility at the Ottawa Hospital Research Institute. Finally, we would also like to thank the Ottawa Bioinformatics Core Facility and Dr. David Cook for their assistance with bioinformatics analysis. This work was supported by the Natural Sciences and Engineering Research Council of Canada (RGPIN-2017-04320), the Ontario Early Research Award, the Canadian Foundation for Innovation, the Canadian Institute for Health Research (PDI 184016), Seed funding from the Faculty of Health Sciences, University of Ottawa, and discretionary research funds (M.D.). N.C is supported by The Chilean National Agency for Research and Development (Agencia Nacional de Investigacion y Desarrollo [ANID]), the uOttawa/CHEO Research Institute's Doctoral Fellowship for Advancement of Biological Perspectives for Exercise

Interventions Across the Lifespan, and the uOttawa Eric Poulin Centre for Neuromuscular Disease (CNMD) Scholarship in Translational Research (STaR).

AUTHOR CONTRIBUTION

N.C. and M.D. conceived and designed research. N.C. performed the experimental procedures. N.C., E.B.J., and J.J. performed single-cell RNA sequencing analysis. N.C. and M.D. wrote and edited the manuscript. Finally, all authors have reviewed and approved the final manuscript.

DECLARATION OF INTEREST

The authors declare no competing interests.

STAR Methods

RESOURCE AVAILABILITY

Lead contact

Further information and request for resources and reagents should be directed to and will be fulfilled by the lead contact, Michael De Lisio (mdelisio@uottawa.ca).

Materials availability

This study did not generate new unique reagents.

Data and code availability

Single-cell RNA-seq data have been deposited at GEO and are publicly available as of the date of publication. Accession numbers are listed in the key resources table. This paper does not report original code. Any additional information required to reanalyze the data reported in this paper is available from the lead contact upon request.

EXPERIMENTAL MODEL AND SUBJECT DETAILS

Mice and ethics statement

This study was conducted in accordance with the Canadian Council on Animal Care guidelines and ethical approval was provided by the Animal Care and Veterinary Service Committee at the University of Ottawa. Mice were provided food and water *ad libitum,* and mice were housed in a pathogen-free environment (22-25°C, 30% humidity, 12-hour light: dark cycle). Four-week-old male C57Bl/6J (#000664) mice were purchased from The Jackson Laboratory. Mice were acclimatized for one week before the experiments.

METHOD DETAILS

Radiation exposure

A fractionated dose of *in vivo* irradiation (*in vivo*-IR) of 8.2 Gy/dose (X-RAD 320, Precision X-Ray Irradiation, North Branford, CT) was administered for three days (Monday, Wednesday, and Friday) to one hindlimb at age five weeks (IR).[9] The rest of the body was lead-shielded, and the contralateral limb was used as a non-IR control (CON).

Tissue collection and single-cell preparation

Three independent samples (IR or CON limb) were pooled together in one batch to avoid batch effects. Briefly, the IR or the CON limb was removed at 24-hours post the final dose of radiation or 56-days post-IR (CON 24-hours, IR 24-hours, CON 56-days, and IR 56-days). Mechanical and enzymatic dissociation were used as previously described[16] to generate a single-cell suspension from the IR or the CON hindlimb at the different time points. Briefly, the IR and the CON limb were dissected and processed

separately. The connective and fat tissue was removed, and the dissected limb was subsequently transferred to a Miltenyi GentleMACS C tube (Cat# 130-093-237, Miltenyi Biotec), which contained an enzymatic solution comprised of Collagenase B (1.5U/ml, Cat# 11088831001; Roche® Life Science Products,) and Dispase II (2U/ml, Cat# 42613-33-2; Sigma Aldrich) resuspended in Ham's F10 media (Cat# 318-050-CL, Wisent Inc, St-Bruno, Canada). Using the gentleMACS Octo Dissociator (Cat# 130-096-427, Miltenyi Biotec), the muscle homogenate was passed through a 100 µm strainer (Cat# 22-363-549, Fisher Scientific). The resulting cell suspension was centrifuged at 600 x *g* at 4°C for 10 minutes. The cell pellet was treated with Red Blood Cell Lysing Buffer (Hydri-MaxTM; Cat# R7767; Sigma-Aldrich) and centrifuged at 600 x *g* at 4°C for 5 minutes. The cell pellet was then resuspended in 1 ml ice-cold FACS buffer, which consisted of 10% FBS and 3 mM EDTA in 1xPBS.

Flow cytometric analysis and Fluorescence activated cell sorting (FACS*)*

For Flow cytometric analysis, 100 µl were taken from the skeletal muscle cell suspension and incubated with primary antibodies against CD45 (FITC Rat Anti-Mouse CD45, Cat# 561088, BD Biosciences), CD31 (BV421 Rat Anti-Mouse CD31, Cat# 102423, BioLegend), ITGA7 (anti-Alpha 7 Integrin 647, Cat# 67-0010-05, AbLab Biologics), Ly-6A/E (Sca1) (BV711 Rat Anti-Mouse Ly-6A/E, Cat# 563992, BD Bioscience), CD55 (PE anti-mouse CD55, Cat# 131803, BioLegend) or CD142 (PE Mouse Coagulation Factor III/Tissue Factor, Cat# FAB3178P, R&D Systems), and SYTOX™ green (Cat# S34860, Invitrogen). The Attune™ Nxt Acoustic Focusing Flow Cytometer system (Thermo Fisher Scientific) with two excitation lasers (Violet (405 nm)

and Blue (488 nm)) was used for flow cytometeric analysis. FCS files were processed in FlowJo™ v10.8 Software (BD Life Sciences).

For FACS, cell suspension from three limbs were pooled then were labelled with a live cell nuclei stain (NucBlue™ Live ReadyProbes™ Reagent (Hoechst 33342), Cat# R37605, Thermo Fisher Scientific), and SYTOX™ AADvanced™ (Cat# S10349, Thermo Fisher Scientific) for dead cells (Figure S7A). A minimum of 10,000 live, mononucleated cells were sorted in the Cell Sorting Facility at the Ottawa Hospital Research Institute using the Beckman Coulter MoFlo XDP cell sorter (32-bit high resolution digital system with five excitation laser lines (UV, 405nm, 488nm, 561nm, and 640nm) for further scRNA-seq.

Single-cell RNA sequencing

Single-cell RNA sequencing, including droplet collection, cDNA amplification, and library preparation was conducted at the StemCore Facility at the Ottawa Hospital Research Institute using the Chromium system (10X Genomics, Chromium Single Cell Kits (v3.1 Chemistry)). Briefly, cells were loaded onto the Chromium Controller to generate single-cell gel beads in emulsion (GEMs). Within every GEM, cDNA underwent reverse transcription and barcoding. Next, PCR amplification and library preparation were conducted. The four libraries (CON 24-hours, IR 24-hours, CON 56-days, and IR 56-days) were sequenced on the Illumina NextSeq 500, with a read depth of 10,000 reads per cell. The FASTQ sequencing reads were mapped to the mouse genome (mm10), barcode processed, UMI counted, and converted to digital gene expression matrices using the CellRanger v5.0.0 Software (10x Genomics).

Bioinformatic analysis

Bioinformatic analysis of the scRNA-seq data was conducted in R/RStudio (v4.2.1) using the Seurat R package (v4.2.0) and workflow.[79] The four 10x Genomics data sets (CON 24-hours, IR 24-hours, CON 56-days, and IR 56-days) were converted into Seurat objects. For quality control and filtering, unique molecular identifier (UMI) feature counts below 200 and above 5000, and more than 10% of the UMIs that align with the mitochondrial genome were removed from the analysis (Figure S7B-C). The gene counts for individual cells were normalized based on the total gene count of each respective cell, followed by scaling using a factor of 10,000, and subsequently log-transformed. The FindVariableFeatures function was used to identify the top 2000 variable genes. The four objects were integrated using SelectIntegrationFeatures function, and biological anchors were found using the FindIntegrationAnchors function to correct for technical differences between the four objects. Anchors were merged, followed by integration using the IntegrateData function. The gene counts were subjected to scaling and dimensional reduction through principal component analysis, where variable features served as input. Subsequently, dataset dimensionality was determined using the ElbowPlot function. Seurat's graph-based clustering approach was then used, with FindNeighbors and FindClusters, to cluster cells based on the previously determined dataset dimensionality. The Uniform Manifold Approximation and Projection (UMAP) plot was used to visualize the clusters. Specific cluster markers were identified through differential expression analysis using the FindAllMarkers function. The Subset function was used to obtain the individual cell populations of MuSCs, FAPs, ECs, Macrophages, and Monocytes/Neutrophils from the integrated dataset. Filtration and normalization were performed for each individual cell population to further identified different subpopulation.

Enrichment analysis

The enrichR (v3.1), and ClusterProfiler R (v3.10.1) packages were used to performed functional enrichment analyses using Biological Processes of Gene Ontology (GO), as well as the Molecular Signatures Database (MSigDB) hallmark gene set collection, which were aligned to the mouse genome. This approach facilitated the identification of differentially expressed genes (DEGs) that were significantly enriched in each respective condition.

Gene set scoring

The R package Ucell[80] (v1.0.0) was used to score gene set signatures in our scRNA-seq data from curated-senescence gene set,[33] and from a fibrotic and inflammatory gene set.[16] UCell scores rank the expression levels of each query gene in individual cells based on the Mann-Whitney U statistic. Ranking-based scores allow interpretation of the relative ranking of gene sets within each cell's transcriptome without being affected by the cellular composition of the dataset. The AddModuleScoreUCell function was used to calculate gene signature scores.

Cell–Cell Communication Analysis

Cellular communication networks were inferred and analyzed from our scRNA-seq data. In order to visualize the communications that occur amongst various cell types, the R package CellChat (v1.6.0) was used as previously described.[35] Briefly, the merged scRNA-seq Seurat object was split into individual datasets by condition (CON 24-hours, IR 24-hours, CON 56-days, and IR 56-days) using the subset function. Then, CellChat objects were created using the createCellChatObject function. The ligand-receptor interaction database CellChatDB.mouse was used for further analysis. Using the

Wilcoxon rank sum test with a significance level of 0.05, we identified differentially expressed signalling genes within all cells in a specific object to infer cell-cell communications. Further, the computeCommunProb, computeCommunProbPathway and aggregateNet functions were applied to infer cell-cell communication networks. For more information (https://github.com/sqjin/CellChat).

QUANTIFICATION AND STATISTICAL ANALYSIS

Statistical analysis

DEGs had an adjusted p-value less than 0.05. Two-way analysis of variance (ANOVA) was used to evaluate flow cytometric analysis and a p value <0.05 was considered statistically significant. Statistics and graphs were prepared using Seurat and GraphPad Prism version 10 software (GraphPad Software). Schematic figures were created with BioRender.com.

KEY RESOURCES TABLE

REAGENT or RESOURCE	SOURCE	IDENTIFIER
Antibodies		
FITC Rat Anti-Mouse CD45	BD Biosciences	Cat# 561088
BV421 Rat Anti-Mouse CD31	BioLegend	Cat# 102423
anti-Alpha 7 Integrin 647	AbLab Biologics	Cat# 67-0010-05
BV711 Rat Anti-Mouse Ly-6A/E	BD Bioscience	Cat# 563992
PE anti-mouse CD55	BioLegend	Cat# 131803
PE Mouse Coagulation Factor III/Tissue Factor	R&D Systems	Cat# FAB3178P
Chemicals, peptides, and recombinant proteins		
NucBlue™ Live ReadyProbes™ Reagent (Hoechst 33342)	Thermo Fisher Scientific	Cat# R37605
SYTOX™ AADvanced™	Thermo Fisher Scientific	Cat# S10349
Collagenase B	Roche® Life Science Products	Cat# 11088831001
Dispase II	Sigma Aldrich	Cat# 42613-33-2
Red Blood Cell Lysing Buffer	Sigma-Aldrich	Cat# R7767
Critical commercial assays		
Chromium Next GEM Single Cell 3′ Kit v3.1	10X Genomics	Cat#PN-1000121

Deposited data		
Raw scRNA-seq data and processed matrices	This paper	GEO: GSE241675
Experimental models: Organisms/strains		
C57Bl/6J	The Jackson Laboratory	Cat#000664
Software and algorithms		
CellRanger version v5.0.0	10x Genomics	https://support.10xgenomics.com/single-cell-gene-expression/software/release-notes/3-0
R/RStudio v4.2.1	R CRAN	https://cran.r-project.org/
Seurat R package v4.2.0	R CRAN (Stuart et al.[79])	https://cran.r-project.org/web/packages/Seurat/index.html
enrichR v3.1	R CRAN	https://cran.r-project.org/web/packages/enrichR/index.html
ClusterProfiler R v3.10.1	Bioconductor	https://bioconductor.org/packages/release/bioc/html/clusterProfiler.html
CellChat v1.6.0	Jin et al.[35]	https://github.com/sqjin/CellChat
Ucell v1.0.0	Andreatta et al.[80]	https://github.com/carmonalab/UCell
FlowJo™ v10.8	BD Life Sciences	https://www.flowjo.com/
GraphPad Prism v10	GraphPad Software	https://www.graphpad.com/
Other		
X-RAD 320, Precision X-Ray Irradiation	N/A	N/A
Attune™ Nxt Acoustic Focusing Flow Cytometer system	Thermo Fisher Scientific	N/A
MoFlo XDP cell sorter	Beckman Coulter Life Sciences	N/A
Illumina NextSeq 500	Illumina	N/A
gentleMACS Octo Dissociator	Miltenyi Biotec	Cat# 130-096-427
GentleMACS C tube	Miltenyi Biotec	Cat# 130-093-237

REFERENCES

1. Effinger, K.E., Haardörfer, R., Marchak, J.G., Escoffery, C., Landier, W., Kommajosula, A., Hendershot, E., Sadak, K.T., Eshelman-Kent, D., Kinahan, K., et al. (2022). Current pediatric cancer survivorship practices: a report from the

Children's Oncology Group. J Cancer Surviv, 1–10. 10.1007/s11764-021-01157-w.

2. Boik, N., and Hall, M.D. (2020). Psychosocial Support for Pediatric Patients at Proton Therapy Institutions. Int J Part Ther *7*, 28–33. 10.14338/IJPT-20-00015.1.
3. De Ruysscher, D., Niedermann, G., Burnet, N.G., Siva, S., Lee, A.W.M., and Hegi-Johnson, F. (2019). Radiotherapy toxicity. Nat Rev Dis Primers *5*, 13. 10.1038/s41572-019-0064-5.
4. Goodenough, C.G., Partin, R.E., and Ness, K.K. (2021). Skeletal Muscle and Childhood Cancer: Where are we now and where we go from here. Aging Cancer *2*, 13–35. 10.1002/aac2.12027.
5. Bachman, J.F., and Chakkalakal, J.V. (2021). Insights into muscle stem cell dynamics during postnatal development. FEBS J. 10.1111/febs.15856.
6. Bachman, J.F., Klose, A., Liu, W., Paris, N.D., Blanc, R.S., Schmalz, M., Knapp, E., and Chakkalakal, J.V. (2018). Prepubertal skeletal muscle growth requires Pax7-expressing satellite cell-derived myonuclear contribution. Development *145*, dev167197. 10.1242/dev.167197.
7. Pawlikowski, B., Pulliam, C., Betta, N.D., Kardon, G., and Olwin, B.B. (2015). Pervasive satellite cell contribution to uninjured adult muscle fibers. Skeletal Muscle *5*, 42. 10.1186/s13395-015-0067-1.
8. Bachman, J.F., Blanc, R.S., Paris, N.D., Kallenbach, J.G., Johnston, C.J., Hernady, E., Williams, J.P., and Chakkalakal, J.V. (2020). Radiation-Induced Damage to Prepubertal Pax7+ Skeletal Muscle Stem Cells Drives Lifelong Deficits in Myofiber Size and Nuclear Number. iScience *23*, 101760. 10.1016/j.isci.2020.101760.
9. Kallenbach, J.G., Bachman, J.F., Paris, N.D., Blanc, R.S., O'Connor, T., Furati, E., Williams, J.P., and Chakkalakal, J.V. (2022). Muscle-specific functional deficits and lifelong fibrosis in response to paediatric radiotherapy and tumour elimination. J Cachexia Sarcopenia Muscle *13*, 296–310. 10.1002/jcsm.12902.
10. Adams, G.R., Caiozzo, V.J., Haddad, F., and Baldwin, K.M. (2002). Cellular and molecular responses to increased skeletal muscle loading after irradiation. Am J Physiol Cell Physiol *283*, C1182-1195. 10.1152/ajpcell.00173.2002.

11. Rosenblatt, J.D., Yong, D., and Parry, D.J. (1994). Satellite cell activity is required for hypertrophy of overloaded adult rat muscle. Muscle Nerve *17*, 608–613. 10.1002/mus.880170607.
12. Rosenblatt, J.D., and Parry, D.J. (1993). Adaptation of rat extensor digitorum longus muscle to gamma irradiation and overload. Pflugers Arch *423*, 255–264. 10.1007/BF00374404.
13. Scaramozza, A., Park, D., Kollu, S., Beerman, I., Sun, X., Rossi, D.J., Lin, C.P., Scadden, D.T., Crist, C., and Brack, A.S. (2019). Lineage Tracing Reveals a Subset of Reserve Muscle Stem Cells Capable of Clonal Expansion under Stress. Cell Stem Cell *24*, 944-957.e5. 10.1016/j.stem.2019.03.020.
14. Boldrin, L., Neal, A., Zammit, P.S., Muntoni, F., and Morgan, J.E. (2012). Donor satellite cell engraftment is significantly augmented when the host niche is preserved and endogenous satellite cells are incapacitated. Stem Cells *30*, 1971–1984. 10.1002/stem.1158.
15. Evano, B., and Tajbakhsh, S. (2018). Skeletal muscle stem cells in comfort and stress. NPJ Regen Med *3*, 24. 10.1038/s41536-018-0062-3.
16. Collao, N., Sanders, O., Caminiti, T., Messeiller, L., and De Lisio, M. (2023). Resistance and endurance exercise training improves muscle mass and the inflammatory/fibrotic transcriptome in a rhabdomyosarcoma model. J Cachexia Sarcopenia Muscle. 10.1002/jcsm.13185.
17. Patsalos, A., Pap, A., Varga, T., Trencsenyi, G., Contreras, G.A., Garai, I., Papp, Z., Dezso, B., Pintye, E., and Nagy, L. (2017). In situ macrophage phenotypic transition is affected by altered cellular composition prior to acute sterile muscle injury. J Physiol *595*, 5815–5842. 10.1113/JP274361.
18. Jovic, D., Liang, X., Zeng, H., Lin, L., Xu, F., and Luo, Y. (2022). Single-cell RNA sequencing technologies and applications: A brief overview. Clin Transl Med *12*, e694. 10.1002/ctm2.694.
19. De Micheli, A.J., Laurilliard, E.J., Heinke, C.L., Ravichandran, H., Fraczek, P., Soueid-Baumgarten, S., De Vlaminck, I., Elemento, O., and Cosgrove, B.D. (2020). Single-Cell Analysis of the Muscle Stem Cell Hierarchy Identifies

Heterotypic Communication Signals Involved in Skeletal Muscle Regeneration. Cell Reports *30*, 3583-3595.e5. 10.1016/j.celrep.2020.02.067.

20. Oprescu, S.N., Yue, F., Qiu, J., Brito, L.F., and Kuang, S. (2020). Temporal Dynamics and Heterogeneity of Cell Populations during Skeletal Muscle Regeneration. iScience *23*, 100993. 10.1016/j.isci.2020.100993.
21. Dell'Orso, S., Juan, A.H., Ko, K.-D., Naz, F., Perovanovic, J., Gutierrez-Cruz, G., Feng, X., and Sartorelli, V. (2019). Single cell analysis of adult mouse skeletal muscle stem cells in homeostatic and regenerative conditions. Development *146*, dev174177. 10.1242/dev.174177.
22. Walter, L.D., Orton, J.L., Hannah Fong, E.H., Maymi, V.I., Rudd, B.D., Elisseeff, J.H., and Cosgrove, B.D. (2023). Single-cell transcriptomic analysis of skeletal muscle regeneration across mouse lifespan identifies altered stem cell states associated with senescence. bioRxiv, 2023.05.25.542370. 10.1101/2023.05.25.542370.
23. Saleh, K.K., Xi, H., Switzler, C., Skuratovsky, E., Romero, M.A., Chien, P., Gibbs, D., Gane, L., Hicks, M.R., Spencer, M.J., et al. (2022). Single cell sequencing maps skeletal muscle cellular diversity as disease severity increases in dystrophic mouse models. iScience *25*, 105415. 10.1016/j.isci.2022.105415.
24. Farup, J., Just, J., de Paoli, F., Lin, L., Jensen, J.B., Billeskov, T., Roman, I.S., Cömert, C., Møller, A.B., Madaro, L., et al. (2021). Human skeletal muscle CD90+ fibro-adipogenic progenitors are associated with muscle degeneration in type 2 diabetic patients. Cell Metab *33*, 2201-2214.e11. 10.1016/j.cmet.2021.10.001.
25. Fitzgerald, G., Turiel, G., Gorski, T., Soro-Arnaiz, I., Zhang, J., Casartelli, N.C., Masschelein, E., Maffiuletti, N.A., Sutter, R., Leunig, M., et al. (2023). MME+ fibro-adipogenic progenitors are the dominant adipogenic population during fatty infiltration in human skeletal muscle. Commun Biol *6*, 111. 10.1038/s42003-023-04504-y.
26. Collao, N., Johannsen, E.B., Just, J., and De Lisio, M. (2023). Radiation induces long-term muscle fibrosis and promotes a fibrotic phenotype in fibro-adipogenic progenitors. Accepted, Journal of Cachexia, Sarcopenia and Muscle.

27. Hardee, J.P., Puppa, M.J., Fix, D.K., Gao, S., Hetzler, K.L., Bateman, T.A., and Carson, J.A. (2014). The effect of radiation dose on mouse skeletal muscle remodeling. Radiol Oncol *48*, 247–256. 10.2478/raon-2014-0025.

28. Rubenstein, A.B., Smith, G.R., Raue, U., Begue, G., Minchev, K., Ruf-Zamojski, F., Nair, V.D., Wang, X., Zhou, L., Zaslavsky, E., et al. (2020). Single-cell transcriptional profiles in human skeletal muscle. Sci Rep *10*, 229. 10.1038/s41598-019-57110-6.

29. Camps, J., Breuls, N., Sifrim, A., Giarratana, N., Corvelyn, M., Danti, L., Grosemans, H., Vanuytven, S., Thiry, I., Belicchi, M., et al. (2020). Interstitial Cell Remodeling Promotes Aberrant Adipogenesis in Dystrophic Muscles. Cell Rep *31*, 107597. 10.1016/j.celrep.2020.107597.

30. Fan, Z., Turiel, G., Ardicoglu, R., Ghobrial, M., Masschelein, E., Kocijan, T., Zhang, J., Tan, G., Fitzgerald, G., Gorski, T., et al. (2021). Exercise-induced angiogenesis is dependent on metabolically primed ATF3/4+ endothelial cells. Cell Metab *33*, 1793-1807.e9. 10.1016/j.cmet.2021.07.015.

31. Kalucka, J., de Rooij, L.P.M.H., Goveia, J., Rohlenova, K., Dumas, S.J., Meta, E., Conchinha, N.V., Taverna, F., Teuwen, L.-A., Veys, K., et al. (2020). Single-Cell Transcriptome Atlas of Murine Endothelial Cells. Cell *180*, 764-779.e20. 10.1016/j.cell.2020.01.015.

32. Paulino, A.C. (2004). Late effects of radiotherapy for pediatric extremity sarcomas. Int J Radiat Oncol Biol Phys *60*, 265–274. 10.1016/j.ijrobp.2004.02.001.

33. Saul, D., Kosinsky, R.L., Atkinson, E.J., Doolittle, M.L., Zhang, X., LeBrasseur, N.K., Pignolo, R.J., Robbins, P.D., Niedernhofer, L.J., Ikeno, Y., et al. (2022). A new gene set identifies senescent cells and predicts senescence-associated pathways across tissues. Nat Commun *13*, 4827. 10.1038/s41467-022-32552-1.

34. El Ayadi, A., Jay, J.W., and Prasai, A. (2020). Current Approaches Targeting the Wound Healing Phases to Attenuate Fibrosis and Scarring. Int J Mol Sci *21*, 1105. 10.3390/ijms21031105.

35. Jin, S., Guerrero-Juarez, C.F., Zhang, L., Chang, I., Ramos, R., Kuan, C.-H., Myung, P., Plikus, M.V., and Nie, Q. (2021). Inference and analysis of cell-cell

communication using CellChat. Nat Commun *12*, 1088. 10.1038/s41467-021-21246-9.

36. Der Vartanian, A., Quétin, M., Michineau, S., Auradé, F., Hayashi, S., Dubois, C., Rocancourt, D., Drayton-Libotte, B., Szegedi, A., Buckingham, M., et al. (2019). PAX3 Confers Functional Heterogeneity in Skeletal Muscle Stem Cell Responses to Environmental Stress. Cell Stem Cell *24*, 958-973.e9. 10.1016/j.stem.2019.03.019.
37. Mounier, R., Chrétien, F., and Chazaud, B. (2011). Blood vessels and the satellite cell niche. Curr Top Dev Biol *96*, 121–138. 10.1016/B978-0-12-385940-2.00005-X.
38. Christov, C., Chrétien, F., Abou-Khalil, R., Bassez, G., Vallet, G., Authier, F.-J., Bassaglia, Y., Shinin, V., Tajbakhsh, S., Chazaud, B., et al. (2007). Muscle satellite cells and endothelial cells: close neighbors and privileged partners. Mol Biol Cell *18*, 1397–1409. 10.1091/mbc.e06-08-0693.
39. Lukjanenko, L., Jung, M.J., Hegde, N., Perruisseau-Carrier, C., Migliavacca, E., Rozo, M., Karaz, S., Jacot, G., Schmidt, M., Li, L., et al. (2016). Loss of fibronectin from the aged stem cell niche affects the regenerative capacity of skeletal muscle in mice. Nat Med *22*, 897–905. 10.1038/nm.4126.
40. García-Prat, L., Perdiguero, E., Alonso-Martín, S., Dell'Orso, S., Ravichandran, S., Brooks, S.R., Juan, A.H., Campanario, S., Jiang, K., Hong, X., et al. (2020). FoxO maintains a genuine muscle stem-cell quiescent state until geriatric age. Nat Cell Biol *22*, 1307–1318. 10.1038/s41556-020-00593-7.
41. Uezumi, A., Ikemoto-Uezumi, M., Zhou, H., Kurosawa, T., Yoshimoto, Y., Nakatani, M., Hitachi, K., Yamaguchi, H., Wakatsuki, S., Araki, T., et al. (2021). Mesenchymal Bmp3b expression maintains skeletal muscle integrity and decreases in age-related sarcopenia. J Clin Invest *131*, 139617. 10.1172/JCI139617.
42. Yamaguchi, M., Watanabe, Y., Ohtani, T., Uezumi, A., Mikami, N., Nakamura, M., Sato, T., Ikawa, M., Hoshino, M., Tsuchida, K., et al. (2015). Calcitonin Receptor Signaling Inhibits Muscle Stem Cells from Escaping the Quiescent State and the Niche. Cell Rep *13*, 302–314. 10.1016/j.celrep.2015.08.083.

43. Gawade, P.L., Hudson, M.M., Kaste, S.C., Neglia, J.P., Wasilewski-Masker, K., Constine, L.S., Robison, L.L., and Ness, K.K. (2014). A systematic review of selected musculoskeletal late effects in survivors of childhood cancer. Curr Pediatr Rev *10*, 249–262. 10.2174/1573400510666141114223827.

44. Stubblefield, M.D. (2011). Radiation fibrosis syndrome: neuromuscular and musculoskeletal complications in cancer survivors. PM R *3*, 1041–1054. 10.1016/j.pmrj.2011.08.535.

45. Uezumi, A., Ito, T., Morikawa, D., Shimizu, N., Yoneda, T., Segawa, M., Yamaguchi, M., Ogawa, R., Matev, M.M., Miyagoe-Suzuki, Y., et al. (2011). Fibrosis and adipogenesis originate from a common mesenchymal progenitor in skeletal muscle. J. Cell. Sci. *124*, 3654–3664. 10.1242/jcs.086629.

46. Uezumi, A., Fukada, S., Yamamoto, N., Ikemoto-Uezumi, M., Nakatani, M., Morita, M., Yamaguchi, A., Yamada, H., Nishino, I., Hamada, Y., et al. (2014). Identification and characterization of PDGFRα+ mesenchymal progenitors in human skeletal muscle. Cell Death Dis *5*, e1186. 10.1038/cddis.2014.161.

47. Lemos, D.R., Babaeijandaghi, F., Low, M., Chang, C.-K., Lee, S.T., Fiore, D., Zhang, R.-H., Natarajan, A., Nedospasov, S.A., and Rossi, F.M.V. (2015). Nilotinib reduces muscle fibrosis in chronic muscle injury by promoting TNF-mediated apoptosis of fibro/adipogenic progenitors. Nat. Med. *21*, 786–794. 10.1038/nm.3869.

48. Contreras, O., Rebolledo, D.L., Oyarzún, J.E., Olguín, H.C., and Brandan, E. (2016). Connective tissue cells expressing fibro/adipogenic progenitor markers increase under chronic damage: relevance in fibroblast-myofibroblast differentiation and skeletal muscle fibrosis. Cell Tissue Res. *364*, 647–660. 10.1007/s00441-015-2343-0.

49. Ieronimakis, N., Hays, A., Prasad, A., Janebodin, K., Duffield, J.S., and Reyes, M. (2016). PDGFRα signalling promotes fibrogenic responses in collagen-producing cells in Duchenne muscular dystrophy. J Pathol *240*, 410–424. 10.1002/path.4801.

50. Borthwick, L.A., Wynn, T.A., and Fisher, A.J. (2013). Cytokine mediated tissue fibrosis. Biochim Biophys Acta *1832*, 1049–1060. 10.1016/j.bbadis.2012.09.014.

51. Kendall, R.T., and Feghali-Bostwick, C.A. (2014). Fibroblasts in fibrosis: novel roles and mediators. Front Pharmacol *5*, 123. 10.3389/fphar.2014.00123.

52. Brack, A.S., Conboy, M.J., Roy, S., Lee, M., Kuo, C.J., Keller, C., and Rando, T.A. (2007). Increased Wnt signaling during aging alters muscle stem cell fate and increases fibrosis. Science *317*, 807–810. 10.1126/science.1144090.

53. Akhmetshina, A., Palumbo, K., Dees, C., Bergmann, C., Venalis, P., Zerr, P., Horn, A., Kireva, T., Beyer, C., Zwerina, J., et al. (2012). Activation of canonical Wnt signalling is required for TGF-β-mediated fibrosis. Nat Commun *3*, 735. 10.1038/ncomms1734.

54. Trensz, F., Haroun, S., Cloutier, A., Richter, M.V., and Grenier, G. (2010). A muscle resident cell population promotes fibrosis in hindlimb skeletal muscles of mdx mice through the Wnt canonical pathway. Am J Physiol Cell Physiol *299*, C939-947. 10.1152/ajpcell.00253.2010.

55. Cao, H., Wang, C., Chen, X., Hou, J., Xiang, Z., Shen, Y., and Han, X. (2018). Inhibition of Wnt/β-catenin signaling suppresses myofibroblast differentiation of lung resident mesenchymal stem cells and pulmonary fibrosis. Sci Rep *8*, 13644. 10.1038/s41598-018-28968-9.

56. Sun, Z., Wang, C., Shi, C., Sun, F., Xu, X., Qian, W., Nie, S., and Han, X. (2014). Activated Wnt signaling induces myofibroblast differentiation of mesenchymal stem cells, contributing to pulmonary fibrosis. International Journal of Molecular Medicine *33*, 1097–1109. 10.3892/ijmm.2014.1672.

57. Biferali, B., Proietti, D., Mozzetta, C., and Madaro, L. (2019). Fibro–Adipogenic Progenitors Cross-Talk in Skeletal Muscle: The Social Network. Front Physiol *10*. 10.3389/fphys.2019.01074.

58. Fry, C.S., Kirby, T.J., Kosmac, K., McCarthy, J.J., and Peterson, C.A. (2017). Myogenic Progenitor Cells Control Extracellular Matrix Production by Fibroblasts during Skeletal Muscle Hypertrophy. Cell Stem Cell *20*, 56–69. 10.1016/j.stem.2016.09.010.

59. Yoo, Y., Choi, E., Kim, Y., Cha, Y., Um, E., Kim, Y., Kim, Y., and Lee, Y.-S. (2022). Therapeutic potential of targeting cathepsin S in pulmonary fibrosis. Biomed Pharmacother *145*, 112245. 10.1016/j.biopha.2021.112245.

60. Li, Z., Li, Y., Liu, S., and Qin, Z. (2020). Extracellular S100A4 as a key player in fibrotic diseases. J Cell Mol Med *24*, 5973–5983. 10.1111/jcmm.15259.

61. Järvinen, P.M., Myllärniemi, M., Liu, H., Moore, H.M., Leppäranta, O., Salmenkivi, K., Koli, K., Latonen, L., Band, A.M., and Laiho, M. (2012). Cysteine-rich protein 1 is regulated by transforming growth factor-β1 and expressed in lung fibrosis. J Cell Physiol *227*, 2605–2612. 10.1002/jcp.23000.

62. Cui, C.-Y., Driscoll, R.K., Piao, Y., Chia, C.W., Gorospe, M., and Ferrucci, L. (2019). Skewed macrophage polarization in aging skeletal muscle. Aging Cell *18*, e13032. 10.1111/acel.13032.

63. Wang, Y., Wehling-Henricks, M., Samengo, G., and Tidball, J.G. (2015). Increases of M2a macrophages and fibrosis in aging muscle are influenced by bone marrow aging and negatively regulated by muscle-derived nitric oxide. Aging Cell *14*, 678–688. 10.1111/acel.12350.

64. Stepien, D.M., Hwang, C., Marini, S., Pagani, C.A., Sorkin, M., Visser, N.D., Huber, A.K., Edwards, N.J., Loder, S.J., Vasquez, K., et al. (2020). Tuning macrophage phenotype to mitigate skeletal muscle fibrosis: Macrophage and FAP Crosstalk in Muscular Polytrauma. J Immunol *204*, 2203–2215. 10.4049/jimmunol.1900814.

65. Mori, R., Shaw, T.J., and Martin, P. (2008). Molecular mechanisms linking wound inflammation and fibrosis: knockdown of osteopontin leads to rapid repair and reduced scarring. J Exp Med *205*, 43–51. 10.1084/jem.20071412.

66. Grounds, M.D., and Torrisi, J. (2004). Anti-TNFalpha (Remicade) therapy protects dystrophic skeletal muscle from necrosis. FASEB J *18*, 676–682. 10.1096/fj.03-1024com.

67. Hoeft, K., Schaefer, G.J.L., Kim, H., Schumacher, D., Bleckwehl, T., Long, Q., Klinkhammer, B.M., Peisker, F., Koch, L., Nagai, J., et al. (2023). Platelet-instructed SPP1+ macrophages drive myofibroblast activation in fibrosis in a CXCL4-dependent manner. Cell Rep *42*, 112131. 10.1016/j.celrep.2023.112131.

68. Williams, J.P., Calvi, L., Chakkalakal, J.V., Finkelstein, J.N., O'Banion, M.K., and Puzas, E. (2016). Addressing the Symptoms or Fixing the Problem? Developing Countermeasures against Normal Tissue Radiation Injury. Radiat Res *186*, 1–16. 10.1667/RR14473.1.

69. Ohno, T., Nakano, T., Niibe, Y., Tsujii, H., and Oka, K. (1998). Bax protein expression correlates with radiation-induced apoptosis in radiation therapy for cervical carcinoma. Cancer *83*, 103–110. 10.1002/(SICI)1097-0142(19980701)83:1<103::AID-CNCR14>3.0.CO;2-0.

70. Liebner, S., Cattelino, A., Gallini, R., Rudini, N., Iurlaro, M., Piccolo, S., and Dejana, E. (2004). β-Catenin is required for endothelial-mesenchymal transformation during heart cushion development in the mouse. J Cell Biol *166*, 359–367. 10.1083/jcb.200403050.

71. Lee, W.J., Park, J.H., Shin, J.U., Noh, H., Lew, D.H., Yang, W.I., Yun, C.O., Lee, K.H., and Lee, J.H. (2015). Endothelial-to-mesenchymal transition induced by Wnt 3a in keloid pathogenesis. Wound Repair Regen *23*, 435–442. 10.1111/wrr.12300.

72. Tabasso, A.F.S., Jones, D.J.L., Jones, G.D.D., and Macip, S. (2019). Radiotherapy-Induced Senescence and its Effects on Responses to Treatment. Clin Oncol (R Coll Radiol) *31*, 283–289. 10.1016/j.clon.2019.02.003.

73. Dungan, C.M., Murach, K.A., Zdunek, C.J., Tang, Z.J., VonLehmden, G.L., Brightwell, C.R., Hettinger, Z., Englund, D.A., Liu, Z., Fry, C.S., et al. (2022). Deletion of SA β-Gal+ cells using senolytics improves muscle regeneration in old mice. Aging Cell *21*, e13528. 10.1111/acel.13528.

74. Englund, D.A., Jolliffe, A., Aversa, Z., Zhang, X., Sturmlechner, I., Sakamoto, A.E., Zeidler, J.D., Warner, G.M., McNinch, C., White, T.A., et al. (2023). p21 induces a senescence program and skeletal muscle dysfunction. Molecular Metabolism *67*, 101652. 10.1016/j.molmet.2022.101652.

75. Sousa-Victor, P., Gutarra, S., García-Prat, L., Rodriguez-Ubreva, J., Ortet, L., Ruiz-Bonilla, V., Jardí, M., Ballestar, E., González, S., Serrano, A.L., et al. (2014). Geriatric muscle stem cells switch reversible quiescence into senescence. Nature *506*, 316–321. 10.1038/nature13013.

76. Moiseeva, V., Cisneros, A., Sica, V., Deryagin, O., Lai, Y., Jung, S., Andrés, E., An, J., Segalés, J., Ortet, L., et al. (2023). Senescence atlas reveals an aged-like inflamed niche that blunts muscle regeneration. Nature *613*, 169–178. 10.1038/s41586-022-05535-x.

77. Zhang, X., Habiballa, L., Aversa, Z., Ng, Y.E., Sakamoto, A.E., Englund, D.A., Pearsall, V.M., White, T.A., Robinson, M.M., Rivas, D.A., et al. (2022). Characterization of cellular senescence in aging skeletal muscle. Nat Aging *2*, 601–615. 10.1038/s43587-022-00250-8.

78. Liu, L., Kim, S., Buckley, M.T., Reyes, J.M., Kang, J., Tian, L., Wang, M., Lieu, A., Mao, M., Rodriguez-Mateo, C., et al. (2023). Exercise reprograms the inflammatory landscape of multiple stem cell compartments during mammalian aging. Cell Stem Cell *30*, 689-705.e4. 10.1016/j.stem.2023.03.016.

79. Stuart, T., Butler, A., Hoffman, P., Hafemeister, C., Papalexi, E., Mauck, W.M., Hao, Y., Stoeckius, M., Smibert, P., and Satija, R. (2019). Comprehensive Integration of Single-Cell Data. Cell *177*, 1888-1902.e21. 10.1016/j.cell.2019.05.031.

80. Andreatta, M., and Carmona, S.J. (2021). UCell: Robust and scalable single-cell gene signature scoring. Comput Struct Biotechnol J *19*, 3796–3798. 10.1016/j.csbj.2021.06.043.

Chapter IV

Resistance endurance training improves muscle mass and the inflammatory/fibrotic transcriptome in a rhabdomyosarcoma model

Nicolas Collao[1†], Olivia Sanders[1†], Taylor Caminiti[1], Laura Messeiller[1], and Michael De Lisio[1,2*]

[1]School of Human Kinetics, and [2]Department of Cellular and Molecular Medicine, Regenerative Medicine Program, University of Ottawa, Ottawa, ON, Canada

†These authors contribute equal to this work.

*Correspondence to: Michael De Lisio, School of Human Kinetics, and Department of Cellular and Molecular Medicine, Regenerative Medicine Program, University of Ottawa, Ottawa, ON, Canada. Phone: +1 613-562-5800 ext. 6987. Email: mdelisio@uottawa.ca

Abstract

Background: Rhabdomyosarcoma (RMS) is an aggressive soft tissue sarcoma that most often develops in children. Chemoradiation therapy is a standard treatment modality; however, the detrimental long-term skeletal muscle consequences of these therapies in juvenile cancer survivors include muscle atrophy and fibrosis resulting in decreased physical performance. Using a novel model of murine resistance endurance training, we investigate its role in preventing the long-term effects of juvenile RMS plus therapy.

Methods: Four-week-old Male (n=10) and Female (n=10) C57Bl/6J mice were injected with M3-9-M RMS cell into the left gastrocnemius with the right limb serving as an internal control (CON). Mice received a systemic vincristine injection then five doses of 4.8 Gy of gamma radiation localized to the left hindlimb (RMS+Tx). Mice were then randomly divided into either sedentary (SED) or resistance and endurance exercise training (RET) groups. Changes in exercise performance, body composition, myocellular adaptations, and the inflammatory/fibrotic transcriptome were assessed.

Results: RET improved endurance performance ($p<0.0001$) and body composition ($p=0.0004$) compared to SED. RMS+Tx resulted in significantly lower muscle weight ($p=0.015$), and significantly smaller myofibre cross-sectional area (CSA) ($p=0.014$). Conversely, RET resulted in significantly higher muscle weight ($p=0.030$) and significantly larger Type IIA ($p=0.014$) and IIB ($p=0.015$) fibre CSA. RMS+Tx resulted in significantly more muscle fibrosis ($p=0.028$) which was not prevented by RET. RMS+Tx resulted in significantly fewer mononuclear cells ($p<0.05$) and muscle satellite (stem) cells (MuSCs) ($p<0.05$), and significantly more immune cells ($p<0.05$) compared to CON. RET resulted in significantly more fibro-adipogenic progenitors (FAPs) ($p<0.05$), a trend for more

MuSCs (p=0.076) compared to SED, and significantly more endothelial cells specifically in the RMS+Tx limb. Transcriptomic changes revealed significantly higher expression of inflammatory and fibrotic genes in RMS+Tx, which was prevented by RET. In the RMS+Tx model, RET also significantly altered expression of genes involved in extracellular matrix (ECM) turnover.

Conclusions: Our study suggests that RET preserves muscle mass and performance in a model of juvenile RMS survivorship while partially restoring cellular dynamics and the inflammatory and fibrotic transcriptome.

Keywords: Fibrosis, Radiation, Chemotherapy, Muscle Satellite cells, Fibro-adipogenic progenitors, Inflammation, Cachexia, Exercise, Cancer

Introduction

Rhabdomyosarcoma (RMS) is an intramuscular cancer and is the most common juvenile soft-tissue sarcoma.[1] While survival is as high as 90%[1], chemoradiation therapy used to treat RMS causes muscle atrophy and fibrosis in 80% survivors.[2] As a result, juvenile sarcoma survivors experience a high prevalence of muscle weakness, fatigue, exercise intolerance, and disability.[3] A reduction in muscle stem (satellite) cells (MuSCs),[4,5] increased expression of fibrotic genes, and inflammation have been implicated as mechanisms responsible for these late effects in skeletal muscle.[6] MuSCs are quiescent myogenic cells, located in the periphery of the muscle fibre between the sarcolemma and the basal lamina[7] and are required for pre-pubertal skeletal muscle growth.[8] Proper MuSC regulation requires a functioning niche consisting of vascular endothelial cells (ECs), immune cells, and fibro-adipogenic progenitors (FAPs), among other cell types.[9] Cancer therapy is known to deplete endothelial cells in several tissues[10] and alters immune cell phenotype and function in skeletal muscle which contributes to impaired muscle regeneration.[11] The effects of cancer therapy on FAPs has received relatively less attention; however, early evidence suggests that cancer therapy does not impact FAP content in mice.[6] As such, interventions to prevent deleterious alterations to niche-mediated MuSC dysfunction in juvenile cancer survivors may improve long-term outcomes.

Resistance and endurance exercise training (RET) are recommended for cancer survivors as an effective non-pharmacological strategy to improves muscle strength, endurance performance, and quality of life in cancer survivors.[12] These recommendations are derived primarily from adult survivors of breast, prostate, and colorectal cancer with

no specific recommendations for juvenile cancer survivors.[12] Mechanistically, endurance exercise training reduces radiation-induced oxidative stress in skeletal muscle[13,14] and increases MuSC and FAP content in post-pubertal mice.[15] Whether exercise training can improve long-term, skeletal muscle late effects in a preclinical model of juvenile RMS plus therapy survival remains unknown.

To begin to elucidate the mechanisms responsible for RET-induced improvements in skeletal muscle in cancer survivors, we combine these newly established models of juvenile RMS plus therapy,[5] and progressive RET,[16] to examine the extent to which RET improves skeletal muscle quality and quantity. We hypothesized that RET would prevent several of the skeletal muscle defects induced by juvenile RMS plus therapy by improving cellular components and gene expression of soluble factors in the MuSC niche.

Methods

Experimental design

Ethical approval for this project was obtained from the University of Ottawa Animal Care and Veterinary Service Committee and performed according to the Canadian Council on Animal Care's guidelines. Mice were housed under specific pathogen-free conditions in a controlled facility (temperature 22-25 °C, 30% humidity and 12-hour light: dark cycle) and food and water were provided *ad libitum*. Four-week-old male (n=10) and female (n=10) C57Bl/6 mice (Jackson Laboratory) acclimatized to the animal facility for one week prior to use in any experiments.

The RMS+Tx model was conducted as previously described (Figure 1A).[5] All mice were injected with 100,000 M3-9-M cells in sterile PBS into the left gastrocnemius

(RMS+Tx).[17] The contralateral right gastrocnemius was injected with sterile PBS as an internal control (CON). Mice recovered for three days then received an intraperitoneal injection of vincristine sulfate (1 mg/kg Cat#V8388, Sigma Aldrich). At five weeks of age, all mice were exposed to fractioned radiation of five doses of 4.8 Gy (X-RAD 320, Precision X-Ray Irradiation) localized to the RMS-injected (left) limb (RMS+Tx). The rest of the body was protected using a lead murine abdomen shield and the contralateral non-RMS-injected, non-irradiated (right) limb was used as an internal control (CON).

At six weeks of age, mice were randomly assigned into either a RET or sedentary (SED) group. Mice in the RET group were individually housed with weighted running wheels while mice in the SED group were housed with no wheel for 8 weeks.[16] After one week of wheel acclimatization with no weight, RET began with a 2 g resistance in week 1 which progressed by 1 g/week until a weight of 5 g was maintained for 2 weeks (weeks 4-5) and then increased to 6 g which was maintained for the final 3 weeks (weeks 6-8) as previously described.[16] Running distance (km/day) was tracked using low profile wireless running wheels (ENV-044, ENV-047, Med Associates) and associated software packages (Wheel Manager Software SOF-860, Med Associates). The design resulted in four groups with the within factors (i.e., contralateral limbs of the same mouse) of CON and RMS+Tx and the between factors (i.e., independent mice) of SED and RET: (1) CON-SED, (2) CON-EX, (3) RMS+Tx-SED, and (4) RMS+Tx-RET. Animals were euthanized 4 days after the final exercise session with CO_2 asphyxiation followed by cervical dislocation. The left (RMS+Tx) and right (CON) gastrocnemius were resected, weighed, and partitioned into thirds for downstream analyses.

Rabdomyosarcoma cell line

M3-9-M RMS cells (gift MacKall Lab, Stanford) were cultured in RPMI media 1640 (Cat# 350-000-CL, Wisent Inc) containing 1% L-glutamine (Cat# 07100; StemCell Technologies), 10% heat-inactivated fetal bovine serum (Cat# 12483-020; Gibco), HEPES (Cat# 15630-080, Gibco), 1% non-essential amino acids (Cat# 11140-050, Gibco), 1% sodium pyruvate (Cat# 11360-070, Gibco), 1% penicillin/streptomycin (P/S) (Cat# 15140-122, Thermo Fisher Scientific), and 50 mM 2-mercaptoethanol (Cat# 21985-023, Gibco).[17]

Body composition and performance testing

Body composition and body weight was assessed by EchoMRI-900 (EchoMRI LLC) and an electronic scale as previously described.[18,19] Endurance performance was evaluated on a motorized treadmill as previously described without electric shock.[19] Testing ceased when mice met one of the following three criteria to end the test: 1) resisted stimulation with rubberized tweezers, 2) remained stationary on the treadmill platform off of the belt for greater than 2 minutes, or 3) remained one body length away from the platform for greater than 5 seconds and could not increase speed when stimulated.[19] Maximal grip strength of fore- and hindlimbs combined was measured as previously described[19] using a Chantillion DFE II (Columbus Instruments). A total of five grip strength tests were performed on each mouse with each mouse grasping the force grid with all four limbs. The highest and lowest force values were discarded and an average of the remaining three values were used to score each mouse. Body composition and performance tests were conducted before treatment (Pre-Tx), before RET (Pre-RET) and after RET (Post-RET).

Histochemical, immunostaining, and microscopy

The distal third of the gastrocnemius was then embedded in tissue-embedding medium (OCT, Cat# 4585, Fisher Scientific) prior to freezing in liquid nitrogen-cooled isopentane (Cat# 277258-1L, Sigma-Aldrich). 10 μm transverse sections were collected using a HM 525 NX-2210 cryostat (Leica, Wezlar, Germany) and placed onto glass slides (Cat# 12-544-2, Fisher Scientific). An average of 482 ± 22.5 myofibres per mouse were analyzed for CSA, fibre type proportion, and myonuclear domain. Masson's Trichrome[15,20] and Myosin Heavy Chain (MyHC)[21] staining and analysis were conducted as previously described. The following isotype-specific anti-mouse primary antibodies were used: MyHC-I, IgG-2b (1:100, Cat# BA-D5, DSHB), MyHC-IIA, IgG1 (1:100, Cat# SC-71, DSHB), MyHC-IIB, IgM (1:25, Cat# BF-F3, DSHB), and anti-laminin (IgG, 1:50, Cat # MA1-06100 Monoclonal Antibody (A5), Thermo Fisher Scientific) with their corresponding secondary antibodies: Alexa Fluor® 647 AffiniPure Goat Anti-Mouse IgG, Fcγ subclass 2b specific (1:100, Cat# 115-605-207, Cedarlane Laboratories), Alexa Fluor® 488 AffiniPure Goat Anti-Mouse IgG, Fcγ subclass 1 specific (1:100, Cat# 115-545-205, Cedarlane Laboratories), Cy™3 AffiniPure Fab Fragment Goat Anti-Mouse IgM, μ chain specific (1:50, Cat# 115-167-020, Cedarlane Laboratories), and Alexa Fluor 594 (Cat # A11005, Invitrogen). Type IIx fibres were identified as unstained for MyHC I, IIA, or IIB. Hybrid fibres were identified as those staining for >1 MyHC isoform. Myonuclei were identified as nuclei with at least 50% of their area beneath the basal lamina. Myonuclear domain was calculated by dividing the number of myonuclei by the CSA (μm^2) per fibre. Images for Masson's Trichrome staining were acquired using an EVOS-FL2 Automated Microscope (Thermo Fisher Scientific), while a ZEISS CellDiscoverer7 (ZEISS)

automated microscope was used to capture fluorescent images. Brightness and color contrast was adjusted, and images analyzed using ImageJ software.

Flow cytometry

The proximal third of the gastrocnemius was immediately processed for flow cytometry.[22] Briefly, muscles were digested in Miltenyi GentleMACS C tube (Cat# 130-093-237, Miltenyi Biotec) containing Collagenase B (1.5U/ml, Cat# 11088831001; Sigma-Aldrich) and Dispase II, (2U/ml, Cat# 42613-33-2; Sigma Aldrich) in Ham's F10 media (Cat# 318-050-CL, Wisent Inc) by gentleMACS Octo Dissociator (Cat# 130-096-427, Miltenyi Biotec). The resulting muscle slurry was filtered (100 µm; Cat# 22-363-549, Fisher Scientific) then treated with Red Blood Cell Lysing Buffer (Cat# R7767; Sigma-Aldrich). Cells were incubated with FITC Rat Anti-Mouse CD45 (Cat# 561088, BD Biosciences), BV510 Rat Anti-Mouse CD31 (Cat# 563089, BD Biosciences), anti-Alpha 7 Integrin (ITGA7) 647 (Cat# 67-0010-05, AbLab), and BV711 Rat Anti-Mouse Ly-6A/E (Sca1) (Cat# 563992, BD Biosciences) in flow buffer (10% FBS, 3 mM of EDTA in 1xPBS) for 35 minutes. Cell viability was assessed with SYTOX™ green (Cat# S34860, Invitrogen). Cell populations of interest were hematopoietic ($CD31^-/CD45^+$), endothelial ($CD45^-/CD31^+$), MuSCs ($CD45^-/CD31^-/ITGA7^+$), and FAPs ($CD45^-/CD31^-/ITGA7^-/Sca1^+$). Analysis was performed using a NxT flow cytometer and processed in FlowJo™ v10.8 Software (BD Life Sciences) with gates and compensation established using fluorescence minus one and single-stained controls.

NanoString nCounter assay and data analysis

Total RNA isolation from flash frozen gastrocnemius was performed using MicroKit (Cat# 74004, Qiagen) according to manufacturer's instructions. RNA purity and

concentration were measured with a Nanodrop 2000c spectrophotometer (Thermo Fisher Scientific). Targeted transcriptomic analysis of a specific CodeSet panel of genes involved in muscle fibrosis and inflammation was performed with a Nanostring nCounter Mouse Fibrosis V2 panel (Cat# 115000388, NanoString Technologies). Samples (100 ng of RNA) were prepared and analyzed on the multiplexed digital nCounter® platform (NanoString Technologies) according to the manufacturer's instructions. Reporter code counts (RCC) and reporter library file (RFL) were generated, and quality control, background subtraction, and normalization were performed using the nSolver 4.0 Software (NanoString Technologies). Normalized RCC files were analyzed using ROSALIND® nCounter Data Analysis Software (https://rosalind.bio/), with a HyperScale architecture developed by OnRamp BioInformatics, Inc. A multidimensional scaling (MDS) plot was generated and the cell type profiling module quantified cell populations, fold changes, and p-values were calculated based on the fast method (nCounter Advanced Analysis MAN-10030-03). The Benjamini-Hochberg method of estimating false discovery rates (FDR) was used for the adjusted p-value. Genes clusters for heatmaps of differentially expressed genes (DEGs) were created using the PAM (Partitioning Around Medoids) method using the fpc R library.[23] Hypergeometric distribution was performed to analyze the enrichment of pathways, gene ontology (GO), and other ontologies. The topGO R library[24] was used to determine local similarities and dependencies between GO terms. Gene set analysis (GSA) and GO terms were performed using the DEGs.

Statistical analyses

Analyses were blinded. Data are expressed as mean ± standard error of the mean (SEM) with $p \leq 0.05$ considered significant. A three-way mixed analysis (time x group x treatment) of variance or a two-way mixed analysis (treatment x group) of variance were used where appropriate followed by Sidak posthoc tests using GraphPad Prism version 8.0.1 software (GraphPad Software).

Results

Mouse survival and tumor recurrence

Four mice, two males and one female in RET and one male in SED, perished during the intervention. Three male mice likely died due to tumor recurrence and metastases, while the female mice sustained an injury during RET that required sacrificed. Therefore, a total of 16 mice (SED=9 and RET=7) were used for downstream analyses except for immunohistochemistry where muscles for six mice in the RET group (n=6) and eight in the SED group (n=8) were of sufficient quality to use for myonuclear and MyHC analyses.

Resistance and endurance exercvise training improves endurance performance and body composition after rhabdomyosarcoma plus therapy

Mice in the RET group ran approximately 5.86 ± 0.44 km per day which was consistent across the 8-week intervention (Supplementary Figure 1A). RET had higher endurance performance compared to SED at Post-RET (Figure 1B, group effect $p<0.0001$, with no sex-difference (Supplementary Figure 1B $p=0.004$). Absolute and relative grip strength increased at Pre-RET compared to Pre-Tx, and further increased at

Post-RET (Supplementary Figure 1C and D, time effect p<0.0001). Body weight increased between baseline and Post-RET (Figure 1C, time effect p<0.0001). RET had less body fat percentage than SED at Post-RET (Figure 1D, group effect p=0.0004). Lean mass increased between Pre-RET and Pre-Tx, and was further increased post-RET (Figure 1E, time effect p<0.0001).

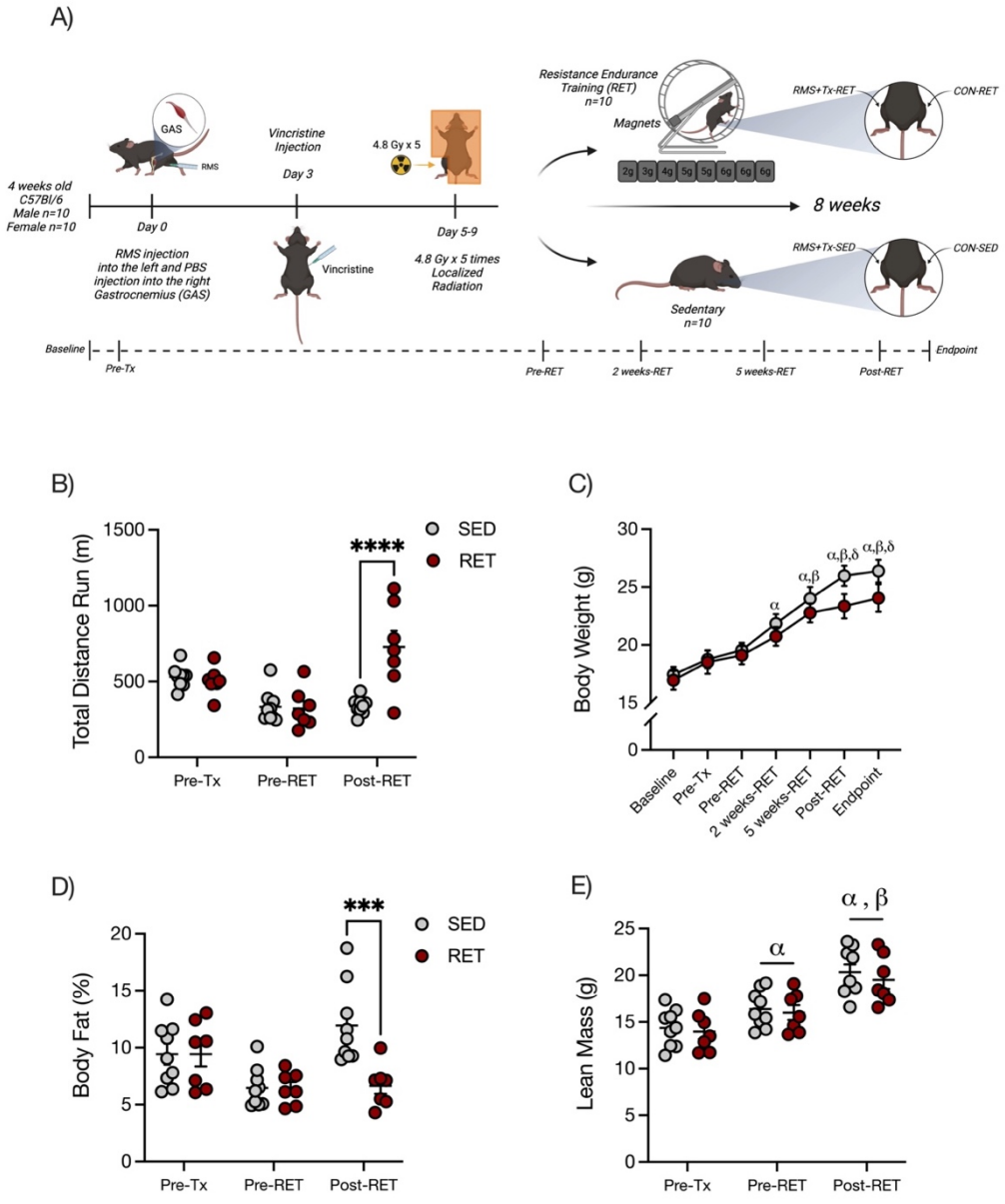

Figure 1. ***Resistance and endurance exercise training (RET) improves endurance performance, body composition, and muscle weight following rhabdomyosarcoma (RMS) plus therapy.***

(A) Study design. Four-week-old Male (n=10) and Female (n=10) C57Bl/6 mice received M3-9-M Rhabdomyosarcoma (RMS) cell injections into the left gastrocnemius to generate the tumors with the left limb serving injected with phosphate-buffered saline (PBS) as an internal control (CON). After three days, all mice received systemic vincristine treatment administered by I.P. injection. Two days post-chemotherapy, mice were administered five doses of 4.8 Gy of gamma radiation localized to the left hindlimb only (RMS+Tx). Following treatment, mice were randomly divided into either sedentary (SED) or resistance endurance trained (RET) groups for eight weeks. Figure created with Biorender.com. (B) Endurance performance assessed by total distance run (m) until volitional exhaustion. (C) Body weight (g). (D) Body fat percentage, and (E) Lean Mass (g). ***P < 0.001, ****P < 0.0001; SED vs RET. In Figure 1C, α = significantly different than baseline, Pre-Tx and Pre-RET; β = significantly different than 2 weeks-RET; σ = significantly different than 5 weeks-RET. In (E), α = significantly different than baseline, Pre-Tx; β = significantly different than Pre-RET. Three-way ANOVA or Two-way ANOVA (E), Sidak posthoc test. N = 7-9 per group.

Rhabdomyosarcoma plus therapy induced muscle atrophy and fibrosis

Gastrocnemius weight was lower in RMS+Tx compared to CON (Figure 2A, treatment effect $p<0.05$) and higher in RET versus SED (Figure 2A, group effect $p<0.05$).

More extracellular matrix accumulated in RMS+Tx versus CON (Figure 2B, treatment effect p=0.028). Representative Masson's trichrome images are presented (Figure 2C).

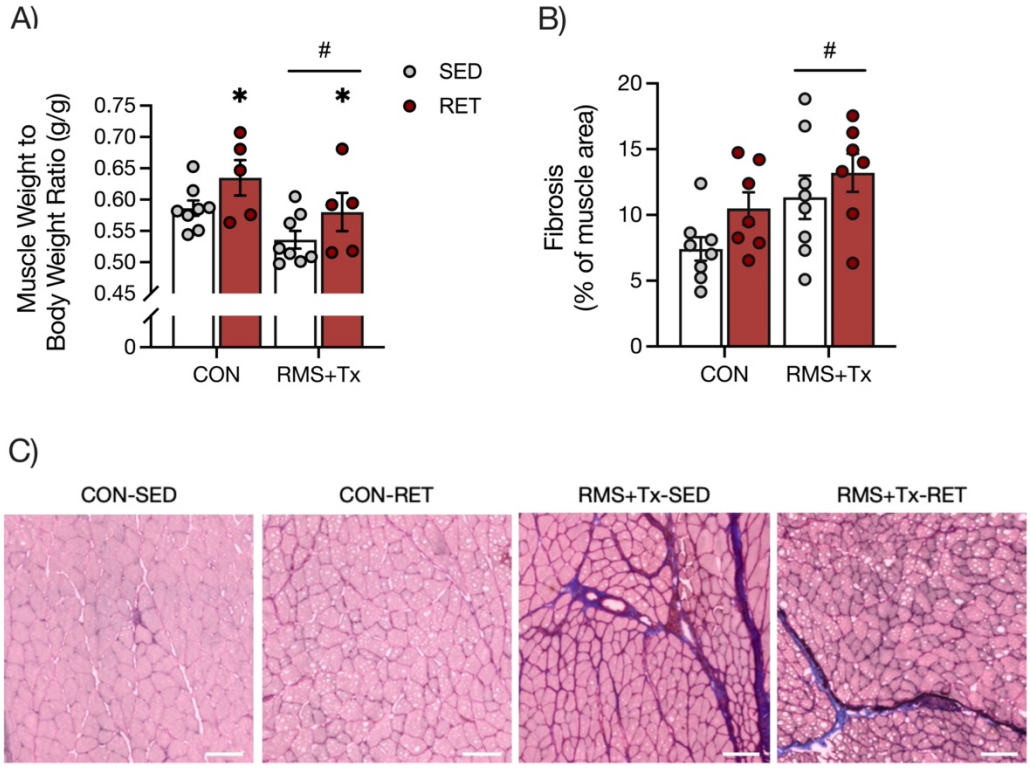

Figure 2. *Rhabdomyosarcoma* (*RMS) plus therapy induce muscle atrophy and fibrosis.*

(A) Muscle weight relative to total body weight (g/g). (B) Quantification of Trichrome stain for intramuscular fibrosis and collagen content as a % of total muscle area. (C) Representative images of Trichrome staining for intramuscular fibrosis and collagen content. Scale = 100 μm. #P< 0.05 RMS+Tx vs. CON. *P < 0.05 SED vs RET. Two-way ANOVA, Sidak posthoc test. N = 7-9 per group.

Resistance and endurance exercise training induced myofibre hypertrophy and alterations in fibre-type distribution independent of rhabdomyosarcoma plus therapy

Representative MyHC images are presented (Figure 3A). MyHC Type I and hybrid fibres were inconsistently detected across samples, thus were excluded from final analyses. Total fibre CSA was larger in RET versus SED (Figure 3B, group effect p=0.0087). SED had more 2000-2400 μm^2 fibres than RET in the CON limb (Supplementary Figure 2A, p=0.011), and a trend for more fibres <400 μm^2 in SED versus RET in the RMS+Tx limb (Supplementary Figure 2B, p=0.065). Type IIA CSA was larger in RET versus SED (Figure 3C, group effect p=0.014). Type IIB CSA was smaller in RMS+Tx versus CON (Figure 3D, treatment effect p=0.006) and was larger in RET versus SED (Figure 3D, group effect p=0.015). Type IIX CSA was not altered (Supplementary Figure 2C). The proportion of type IIA fibres was higher in RMS+Tx versus CON (Figure 3E, treatment effect p=0.004), and was also higher in RET versus SED (Figure 3E, group effect p=0.025). Fewer type IIB fibres were observed in RMS+Tx versus CON (Figure 3F, treatment effect p=0.006) as well as in RET versus SED (Figure 3F, group effect p=0.025). No differences in type IIX fibre proportion were observed (Supplementary Figure 2D).

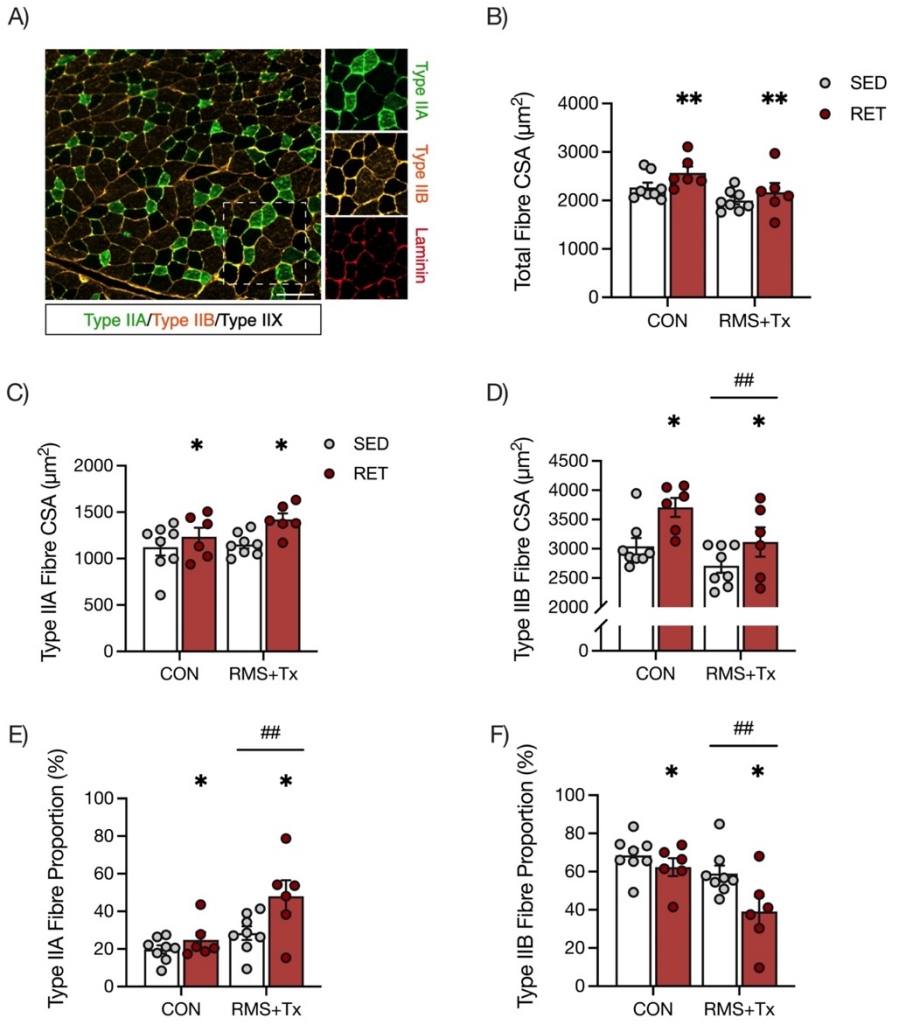

Figure 3. ***Rhabdomyosarcoma (RMS) plus therapy reduced Type IIB cross-sectional area (CSA) and proportion whereas resistance and endurance exercise training (RET) enlarged myofibre CSA and induced alterations in fibre-type distribution independent of RMS plus therapy.*** (A) Representative image of myosin heavy chain stain immunofluorescence (Type IIA: green, Type IIB: orange, Type IIX: black, laminin: red). (B) Total fibre CSA (μm^2). (C) Type IIA fibre specific CSA (μm^2). (D) Type IIB fibre specific CSA (μm^2). (E) Proportion of Type IIA fibres (% of total fibre #). (F)

Proportion of Type IIB fibres (% of total fibre #). *P < 0.05, **P<0.01; SED vs RET group. ##P < 0.01; RMS+Tx vs CON. Two-way ANOVA, Sidak post hoc test. N=6-8 per group. Scale = 100 μm.

Increase in myonuclear domain with no changes in myonuclear accretion followed rhabdomyosarcoma plus therapy and resistance and endurance exercise training

Representative myonuclear and laminin staining is presented (Figure 4A). Total myonuclear domain was larger in CON-RET versus RMS+Tx-RET (Figure 4B, p<0.001). Type IIA myonuclear domain was larger in RET versus SED (Figure 4C, group effect p=0.001). A larger domain was observed in Type IIB fibres in CON-RET versus CON-SED (p=0.013) and RMS+Tx-RET (p=<0.001) (Figure 4D). A trend for greater myonuclear domain size was also observed in RET versus SED for Type IIX fibres (Figure 4E, group effect p=0.086). No differences in nuclei per fibre were observed (Supplementary Figure 3A-D).

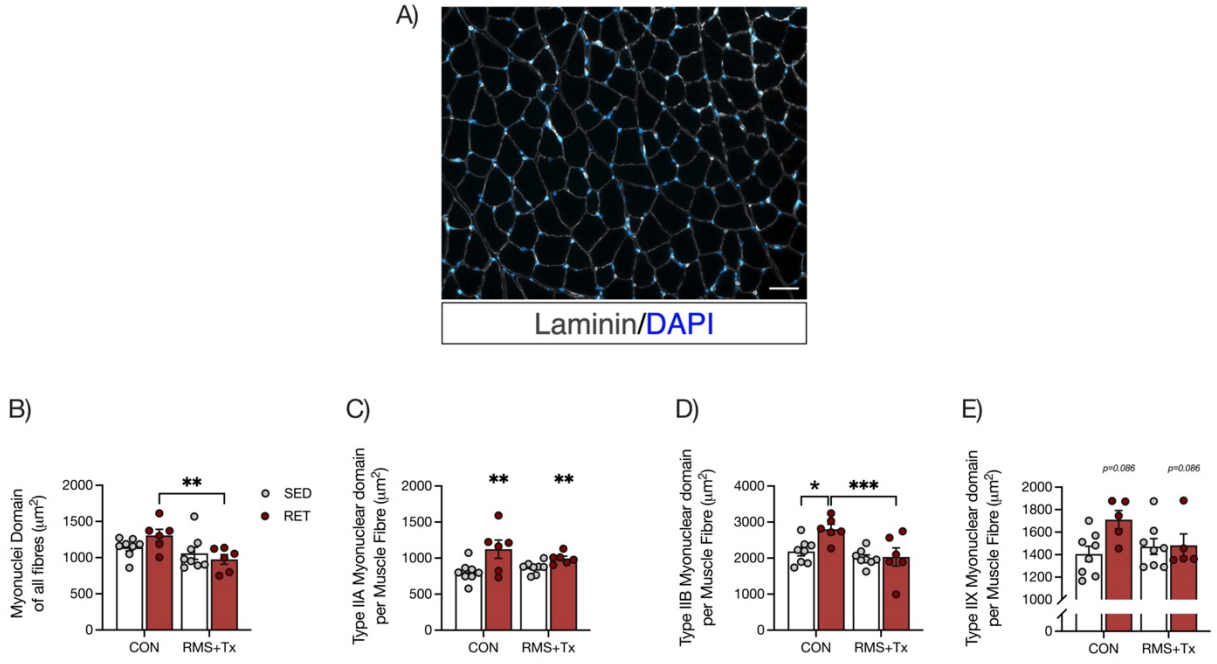

Figure 4. ***Resistance and endurance training (RET) enlarged myonuclear domain with no changes in myonuclear accretion followed rhabdomyosarcoma (RMS) plus therapy.***

(A) Representation of images used for quantifying myonuclei and myonuclear domain. (B) Myonuclear domain of all fibres (μm^2). (C) Type IIA fibre specific myonuclear domain (μm^2). (D) Type IIB fibre specific myonuclear domain (μm^2). (E) Type IIX fibre specific myonuclear domain (μm^2). *P < 0.05, **P < 0.01, ***P < 0.001. Two-way ANOVA, Sidak post hoc test. N=6-8 per group. Scale = 100 μm.

Rhabdomyosarcoma plus therapy and resistance and endurance exercise training induce changes in cellular dynamic in skeletal muscle

Representative flow plots for skeletal muscle mononuclear cell populations are presented (Supplementary Figure 4A). Total live, mononuclear cell count per muscle weight was lower in RMS+Tx versus CON (Supplementary Figure 4B, treatment effect $p<0.05$). RMS+Tx had a higher number (Figure 5A, treatment effect $p<0.05$) and proportion of $CD45^+$ cells versus CON (Supplementary Figure 4C, treatment effect $p<0.05$). More $CD31^+$ cells in RET compared to SED mice was observed in the RMS+Tx limb (Figure 5B, $p<0.05$). RET had a higher proportion of $CD31^+$ cells compared to SED (Supplementary Figure 4D, group effect $p<0.05$). RMS+Tx had fewer $\alpha7^+$ cells versus CON (Figure 5C, treatment effect $p<0.05$) with no difference in $\alpha7^+$ cell proportion (Supplementary Figure 4E). RET had more (Figure 5D, group effect $p=0.022$) and a higher proportion (Supplementary Figure 4F, group effect $p<0.05$) of $Sca1^+$ cells versus SED.

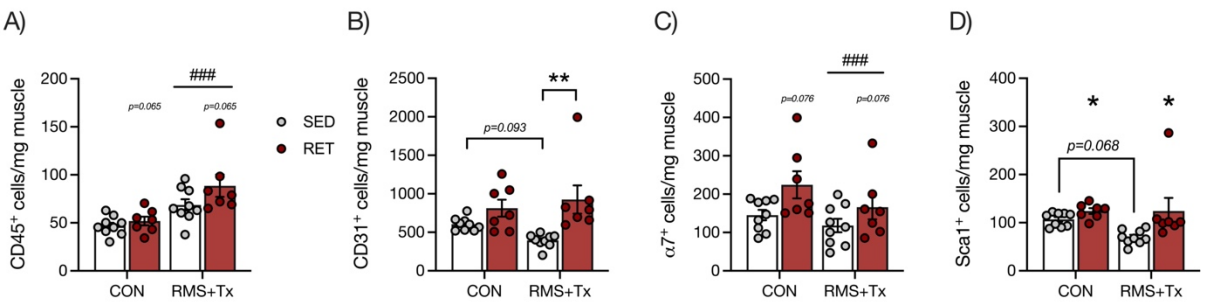

Figure 5. ***Rhabdomyosarcoma (RMS) plus therapy and resistance endurance exercise training (RET) alter cellular dynamic in skeletal muscle.***

(A) CD45$^+$ cells per mg of muscle. (B) CD31$^+$ cells per mg of muscle. (C) α7$^+$ cells per mg of muscle. (D) Sca1$^+$ cells per mg of muscle. *P < 0.05, **P < 0.01; SED vs RET. $^{\#\#\#}$P < 0.001; RMS+Tx vs CON. Two-way ANOVA, Sidak post hoc test. N=7-9 per group.

Fibrotic and inflammatory transcriptome is induced by rhabdomyosarcoma plus therapy and is partially prevented by resistance endurance exercise training

The MDS plot distinguishes CON and RMS+Tx groups independent of RET/SED condition (Supplementary Figure 5A). Cell Profiler indicates an enrichment of mast cells, macrophages, and CD45$^+$ cells in RMS+Tx versus CON (Supplementary Figure 5B). A volcano plot showing the differentially expressed genes (DEGs) up-regulated (log_2 fold change > +0.5) and down-regulated (log_2 fold change < -0.5) between CON-RET and CON-SED (Figure 6A, p<0.05). Eight genes (*Cd36, Cxcr4, Gbp3, Oasl1, Tnfsf10, Mmp12 and Angptl4*) were up-regulated and four genes were down-regulated (*Lep, Adipoq, Irf4* and *S100a4)* in the CON-RET compared with CON-SED. The Top 10 GSA revealed up-regulated genes for macrophage activation, chemokine signaling, fatty acid and cholesterol metabolism, oxidative stress, and others in CON-RET versus CON-SED

(Figure 6A). Comparing RMS-RET to RMS-SED, three genes were up-regulated (*Dapk1, Tm6fs2 and Ptger4*) and three were down-regulated (*Ccl2, Cd163 and Myd88*) (Figure 6B). The Top 10 GSA revealed down-regulated genes for cell cycle, ECM remodeling, and others with up-regulated genes for Th1 Differentiation (Figure 6B).

A total of 117 genes were up-regulated in RMS-SED versus CON-SED (Figure 6C, $p<0.05$). GSA revealed genes enriched for macrophage activation, interferon, chemokine signaling, and others (Figure 6C and Supplementary Figure 5C). Biological process Gene Ontology (GO) terms, based on the up-regulated genes showed genes involved mostly in the immune response in RMS-SED versus CON-SED (Figure 6C, FDR, adjusted p-value <0.05). Conversely, 124 genes were up-regulated and 1 down-regulated (*Ppara*) in RMS-RET versus CON-RET (Figure 6D, $p<0.05$). These genes were enriched for complement activation, collagen biosynthesis and modification, ECM degradation, and cytokine and chemokine signaling among others in RMS-RET (Figure 6D and Supplementary Figure 5D). Biological process GO terms showed genes involved in the immune response and collagen organization among others (Figure 6D, FDR, adjusted p-value <0.05). Higher *Mmp-2* ($p=0.005$) and *Col3a1* ($p=0.028$) gene expression in RMS-RET compared to CON-RET was confirmed by qPCR (Supplementary Figure 5E). Active-MMP2 ($p=0.0068$) and CCR2 ($p=0.018$) protein in RMS-RET compared to CON-RET (Figure 6E).

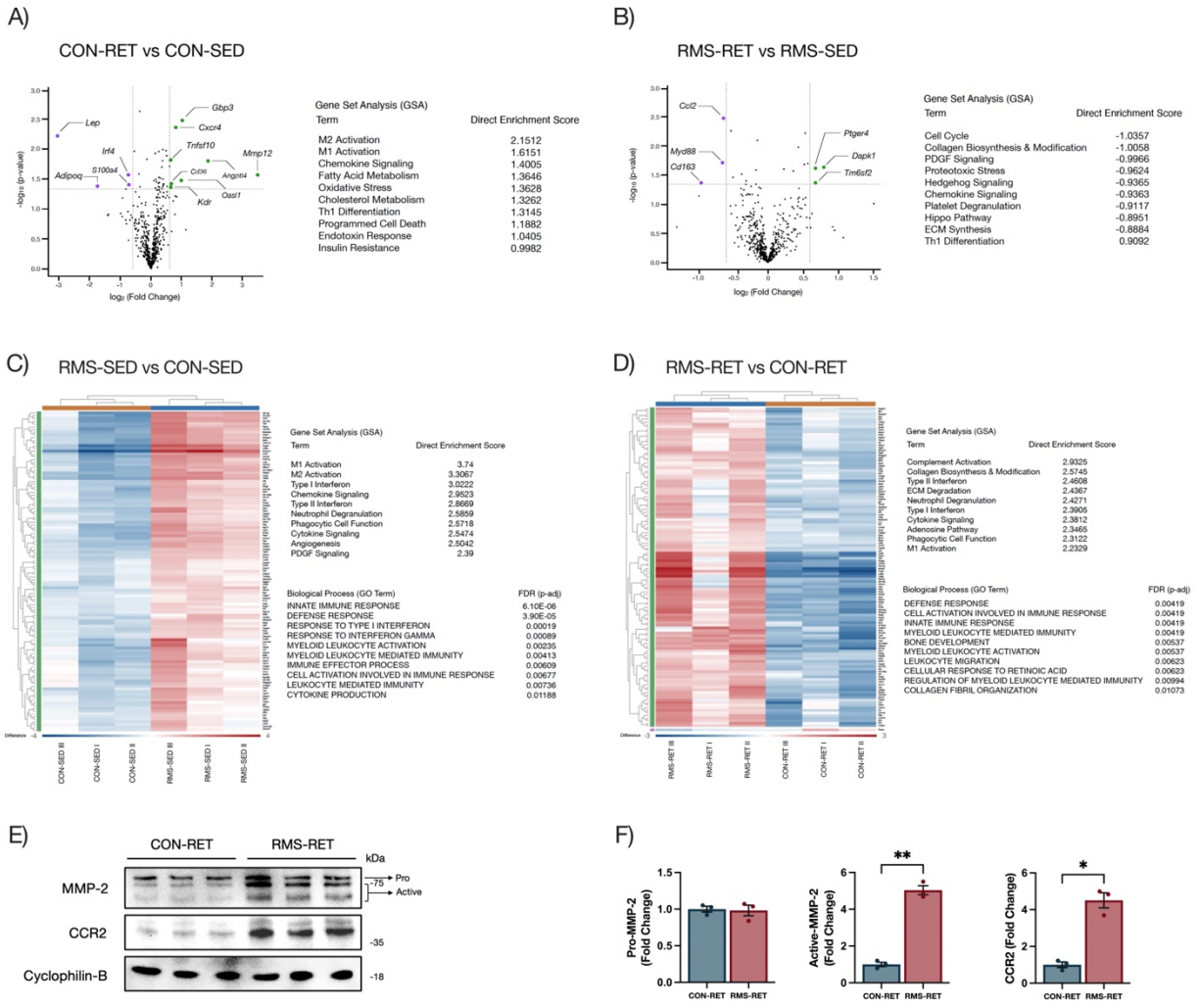

Figure 6. ***Fibrotic and inflammatory signature is induced by rhabdomyosarcoma (RMS) plus therapy and is partially reduced by resistance and endurance training (RET) in skeletal muscle.***

(A) Volcano plot of log_2-transformed fold change and $-log_{10}$-transformed P values showing up-regulated (in green) and downregulated (in purple) genes in CON-RET vs. CON-SED and the Top 10 direct enrichment score from the gene set analysis (GSA). (B) Volcano plot of log_2-transformed fold change and $-log_{10}$-transformed P values showing

up-regulated (in green) and downregulated (in purple) genes in RMS-RET vs. RMS-SED and the Top 10 direct enrichment score from the gene set analysis (GSA). (C) Heatmap of differentially expressed genes (DEGs) in RMS-SED vs. CON-SED, Top 10 (GSA) in RMS-SED vs. CON-SED and Top 10 Biological process Gene Ontology (GO) terms (FDR, adjusted p-value) in RMS-SED vs. CON-SED. (D) Heatmap of DEGs in RMS-RET vs. CON-RET, Top 10 GSA in RMS-RET vs. CON-RET and Top 10 Biological process GO terms (FDR, adjusted p-value) in RMS-RET vs. CON-RET. (E) Representative Western Blot image of MMP-2, CCR2 and Cyclophilin-B protein expression. (F) Fold-Change of Pro-MMP-2, Active-MMP-2 and CCR2 protein expression, normalized by Cyclophilin-B. *P < 0.05, **P < 0.01. N=3 per condition.

Discussion

The overall objective of this study was to determine the extent to which RET can prevent the negative long-term consequences of RMS plus therapy in skeletal muscle. Our main findings were that RET improved body composition and enhanced endurance performance, induced Type II myofibre hypertrophy, increased the number of several mononuclear cells involved in supporting muscle maintenance, and partially prevented the inflammatory/fibrotic gene signature induced by RMS plus therapy. These results suggest that RET-based interventions reduce the negative long-term effects of RMS plus therapy, in part by improving the skeletal muscle microenvironment.

Excess adiposity and impaired physical performance leading to reduced participation in physical activity is commonly reported among cancer survivors.[3] We showed that RET leads to improved body composition and exercise performance.

Adiposity did not increase in RET mice following RMS plus therapy while SED mice experienced an almost 2-fold increase in total body fat percentage which aligns with previous work from our group.[15] Conversely, RET did not alter the increases in body weight and lean mass observed over the course of the study, likely due to the period of juvenile growth and development and the effects of RET on muscle hypertrophy not being detected by less sensitive whole body measures. The increases in grip strength in our study was like due to the period of growth and development of the mice. However, a limitation of our study is that we were not able to assess a direct strength measure of the gastrocnemius due to the data collection across multiple time points in the same mice. Adherence to exercise programs in cancer survivors is often a barrier to their efficacy.[25] Mice in the RET group effectively sustained the voluntary exercise protocol for eight weeks with increasing resistance. Daily distance travelled in our RMS plus therapy model was similar to previous work in aged mice.[26,27] Thus, our preclinical juvenile RMS plus therapy model appears to show a similar premature aging response that has been described in human cancer survivor.[28] Further, the RET protocol induced a 200% increase in endurance performance following RMS plus therapy. These results agree with previous literature from our group that describe increases in muscular performance in mouse models of cancer survivorship.[19] In conclusion, these findings indicate that sustained adherence to RET leads to improvements in whole body composition and enhanced endurance performance in a model of RMS plus therapy.

Previous work has shown that RET causes myofibre hypertrophy and can lead to fibre type adaptations that favour a more oxidative profile in healthy and aged mice.[16,29] We confirm and extend these findings by showing that RET induces hypertrophy in both

Type IIA and Type IIB myofibres and supports a shift from Type IIB to Type IIA fibres in a model of juvenile cancer survivorship. Interestingly, RMS+Tx only resulted in significantly smaller fibres in Type IIB. Based on these results, RET induced hypertrophy in total fibres and in Type IIA fibres as evidenced by larger CSA with RET and no change in CSA in RMS+Tx. Conversely, in Type IIB fibres, RET likely prevented atrophy given the smaller CSA in RMS+Tx and larger CSA in RET. As such, the effects of RET and RMS+Tx in this model seem fibre type-dependent. Interestingly, our targeted gene expression analysis revealed a significant difference in genes involved in the mTOR signaling pathway and a significant down-regulation in genes involved in genes involved in the TGFβ pathway which support a combined pro-hypertrophic and anti-atrophic effect of RET. The results obtained in the present study, largely align with and extend findings from the Deminice lab which used a model of cachexia, not cancer survivorship, a different resistance training model that lacked an endurance component, a different species[30]/strain of mice[31], and did not conduct fibre type-specific analyses.[30,31] Taken together these data support the concept that a hybrid resistance-endurance exercise program can have dual effects of enhancing endurance and inducing hypertrophy.

Juvenile muscle growth requires functioning MuSCs providing for the addition of new myonuclei to myofibres.[8] Previous work using the same RMS plus therapy model showed that treatment-induced depletion of MuSCs underlies impaired muscle development.[5] Further, RET has been shown to elevate MuSC content,[16] while MuSC ablation impairs muscle adaptation to RET.[29] Our results support these findings showing that MuSCs were depleted by RMS plus therapy, with a trend for more MuSCs in RET. Intriguingly, no changes in nuclei per fibre were found between groups; however, a

significant increase in the myonuclear domain was apparent in Type IIA fibres in RET compared to SED, as well as for Type IIX fibres in the control limb of RET compared to SED. This is in contrast to previous work that reports increased number of myonuclei per fibre in RET versus SED groups in both young and aged mice.[16,29] These data suggest that the muscle hypertrophy seen in RET mice following RMS plus therapy is driven primarily by protein synthesis, independent of myonuclear accretion. Indeed, our transcriptional profiling indicated a slight down-regulation of the mechano-sensitive Hippo pathway which would be expected to activate muscle protein synthesis.[32] Further, these data suggest that the MuSC pool is still defective in RMS plus therapy even after an exercise intervention.

MuSCs are regulated by their local microenvironment which includes several cell types, including FAPs. In line with previous work[6], RMS plus therapy did not result in FAP depletion; however, we did observe a trend for fewer FAPs in RMS+Tx-SED versus CON-SED. Conversely, we observed significantly more FAPs following RET in both CON and RMS plus therapy, which aligns with previous preclinical models of endurance exercise,[15,20,33] and resistance training studies in humans.[34] Further, we detected more fibrosis in the RMS plus therapy condition[15] which aligns with our transcriptional analysis that showed an enrichment in genes involved in platelet-derived growth factor (PDGF) signalling in RMS+Tx-SED compared to CON-SED. PDGF signaling is involved in sarcoma formation[35] and promotes fibrosis by inducing FAP differentiation into myofibroblast leading to excess ECM accumulation.[36,37] Thus, the trend for a reduction in FAPs by RMS plus therapy could be due to their myofibroblast differentiation which contributed to the observed ECM accumulation in RMS+Tx. Although RET had no effect

on muscle fibrosis, which was similar to our previous work with endurance exercise following radiation exposure[15], genes involved in PDGF and Hedgehog signaling, two pro-fibrotic pathways[37,38], were down-regulated in the RMS+Tx-RET compared to RMS+Tx-SED, suggesting RET as a potential exercise intervention to decrease the fibrogenic potential of FAPs. Hypertrophic stimuli induces ECM remodelling, by stimulating pathways involved in ECM degradation and synthesis which facilitates ECM reorganization, and promotes myofibre growth.[39] Our transcriptomic data indicate ECM reorganization is ongoing in RET facilitated by diverse matrix metalloproteinases (*Mmp14, Mmp3, Mmp2*, etc.) and with collagen biosynthesis and modification and collagen degradation pathways both enriched in RMS+Tx-RET versus RMS+Tx-SED. Consistent with our results, Peck and colleagues showed that mechanical overload increased *Mmp14* gene expression which was correlated with a more macrophages and skeletal muscle adaptation in humans followed resistance exercise training.[40] Similarly, our study showed that MMP-2 protein expression was higher in RMS-RET compared to CON-RET, aligning with the increase in macrophages in RMS+Tx versus CON observed in our transcriptomic data. Similarly, CCR2 was upregulated in RMS+Tx which is also associated with muscle inflammation and impaired regeneration.[S1] Thus, MMP-2 and CCR2 are potential targets to improve the effects of RMS plus therapy on skeletal muscle.

Endothelial cells are another component of the MuSC niche and the perivascular location of FAPs and MuSCs suggest the strong communication with ECs.[S2] Endothelial cell loss is radiation dose-dependent, progressive, and contributes to myofibroblast activation and muscle fibrosis.[10] When FAPs are genetically depleted disrupting FAP-endothelial cell crosstalk results in impaired skeletal muscle revascularization and fibrosis

following hind limb ischemia.[S2] We detected a trend for fewer endothelial cells in the RMS plus therapy model which mirrors our FAP findings. Also, similar to our FAP results, RET increased ECs suggesting pro-angiogenic features of RET that could improve skeletal muscle perfusion, and facilitate crosstalk between ECs and FAPs.

Previous work suggested that long-term upregulation of inflammatory genes was involved in muscle degradation using the same RMS plus therapy model.[6] Similarly, we found an increase in cell abundance score of macrophages and hematopoietic cells; supported by flow cytometry analysis that showed higher quantity of hematopoietic cells following RMS plus therapy. Several genes involved in the immune and inflammatory response were also up-regulated in RMS+Tx in our transcriptional analyses. Immune cells, especially macrophages are a key component of muscle regeneration and adaptation but also in chronic inflammatory conditions.[S3] In our study, RMS plus therapy increased genes related to M1 (generally pro-inflammatory) and M2 (generally anti-inflammatory) macrophage activation (i.e., *Ccr2*, *Ccl2*, and *Cxcr4*, etc.) as well as genes involved in interferon signalling (i.e., *H2-Aa*, *Isg15a*, etc.) and this heightened and prolonged inflammatory response aligns with previous work.[6] Excitingly, RET downregulated *Ccl2*, *Myd88,* and *Cd163* in RMS+Tx which are all genes involved in pro-inflammatory signalling. While RET in the CON limb showed higher M1 and M2 related genes than SED, this aligns with a previous finding that shows the necessity of macrophage recruitment to induce muscle hypertrophy following mechanical overload.[S4] Thus, RET may inhibit the negative long-term late effects of RMS plus therapy by reducing inflammation.

Together, our results show that RET improves endurance performance, body composition, and induces skeletal muscle hypertrophy in a model of juvenile RMS plus therapy. These effects were mediated by positive changes in cellular dynamics, including increases in endothelial cells and FAPs and a partial reversal of the inflammatory and fibrotic gene signature. As such, our study indicates that skeletal muscles can adapt to RET following RMS plus therapy and suggests that increased protein synthesis and improvements in the muscle microenvironment may be the primary mechanisms responsible.

Acknowledgements

We acknowledge the MacKall lab at Stanford for generously providing the M3-9-M cells. We also acknowledge Katey Rayner and Michele Geoffrion from the Ottawa Heart Institute, and the Department of Biochemistry, Microbiology and Immunology, Faculty of Medicine at the University of Ottawa, for their assistance with the NanoString assay. We acknowledge the services of The Behavioural Core Facility, The Louise Pelletier Histology Core Facility, and the Pre-clinical Imaging Core Facility at the University of Ottawa. We acknowledge Isabel Rodriguez for her assistance with the myonuclear domain analysis. Finally, we also acknowledge the important published work that could not be cited due to limitations on word count and references.

Ethics statement

This manuscript complies with the ethical guidelines for authorship and publishing in the Journal of Cachexia, Sarcopenia and Muscle.[S5]

Conflict of Interest

The authors declare no conflict of interest.

Funding

This work was supported by the Natural Sciences and Engineering Research Council of Canada (NSERC), discretional funds awarded to the De Lisio lab, and the Ontario Early Research Award (M.D). N.C is supported by The Chilean National Agency for Research and Development (ANID) and the uOttawa/CHEO Research Institute's Doctoral Fellowship for Advancement of Biological Perspectives for Exercise Interventions Across the Lifespan. O.S is supported by the Ontario Graduate Scholarship (OGS).

Online supplementary material

Additional supporting information may be found online in the Supporting Information section at the end of the article.

References

1. Amer KM, Thomson JE, Congiusta D, Dobitsch A, Chaudhry A, Li M et al. Epidemiology, Incidence, and Survival of Rhabdomyosarcoma Subtypes: SEER and ICES Database Analysis. J Orthop Res 2019;37:2226–2230.
2. Paulino AC. Late effects of radiotherapy for pediatric extremity sarcomas. International Journal of Radiation Oncology, Biology, Physics 2004;60:265–274.
3. Stubblefield MD. Radiation fibrosis syndrome: neuromuscular and musculoskeletal complications in cancer survivors. PM R 2011;3:1041–1054.
4. Bachman JF, Blanc RS, Paris ND, Kallenbach JG, Johnston CJ, Hernady E et al. Radiation-Induced Damage to Prepubertal Pax7+ Skeletal Muscle Stem Cells Drives Lifelong Deficits in Myofiber Size and Nuclear Number. iScience 2020;23:101760.
5. Paris ND, Kallenbach JG, Bachman JF, Blanc RS, Johnston CJ, Hernady E et al. Chemoradiation impairs myofiber hypertrophic growth in a pediatric tumor model. Scientific Reports 2020;10:19501.
6. Kallenbach JG, Bachman JF, Paris ND, Blanc RS, O'Connor T, Furati E et al. Muscle-specific functional deficits and lifelong fibrosis in response to paediatric radiotherapy and tumour elimination. J Cachexia Sarcopenia Muscle 2022;13:296–310.
7. Mauro A. Satellite cell of skeletal muscle fibers. J Biophys Biochem Cytol 1961;9:493–495.
8. Bachman JF, Klose A, Liu W, Paris ND, Blanc RS, Schmalz M et al. Prepubertal skeletal muscle growth requires Pax7-expressing satellite cell-derived myonuclear contribution. Development 2018;145:dev167197.
9. Mashinchian O, Pisconti A, Le Moal E, Bentzinger CF. The Muscle Stem Cell Niche in Health and Disease. Curr Top Dev Biol 2018;126:23–65.
10. Williams JP, Calvi L, Chakkalakal JV, Finkelstein JN, O'Banion MK, Puzas E. Addressing the Symptoms or Fixing the Problem? Developing Countermeasures against Normal Tissue Radiation Injury. Radiat Res 2016;186:1–16.

11. Patsalos A, Pap A, Varga T, Trencsenyi G, Contreras GA, Garai I et al. In situ macrophage phenotypic transition is affected by altered cellular composition prior to acute sterile muscle injury. J Physiol 2017;595:5815–5842.
12. Campbell KL, Winters-Stone KM, Wiskemann J, May AM, Schwartz AL, Courneya KS et al. Exercise Guidelines for Cancer Survivors: Consensus Statement from International Multidisciplinary Roundtable. Med Sci Sports Exerc 2019;51:2375–2390.
13. O'Connor TN, Kallenbach JG, Orciuoli HM, Paris ND, Bachman JF, Johnston CJ et al. Endurance exercise attenuates juvenile irradiation-induced skeletal muscle functional decline and mitochondrial stress. Skelet Muscle 2022;12:8.
14. De Lisio M, Kaczor JJ, Phan N, Tarnopolsky MA, Boreham DR, Parise G. Exercise training enhances the skeletal muscle response to radiation-induced oxidative stress. Muscle & Nerve 2011;43:58–64.
15. D'Souza D, Roubos S, Larkin J, Lloyd J, Emmons R, Chen H et al. The Late Effects of Radiation Therapy on Skeletal Muscle Morphology and Progenitor Cell Content are Influenced by Diet-Induced Obesity and Exercise Training in Male Mice. Sci Rep 2019;9:6691.
16. Dungan CM, Murach KA, Frick KK, Jones SR, Crow SE, Englund DA et al. Elevated myonuclear density during skeletal muscle hypertrophy in response to training is reversed during detraining. Am J Physiol Cell Physiol 2019;316:C649–C654.
17. Meadors JL, Cui Y, Chen Q-R, Song YK, Khan J, Merlino G et al. Murine rhabdomyosarcoma is immunogenic and responsive to T-cell-based immunotherapy. Pediatric Blood & Cancer 2011;57:921–929.
18. Emmons R, Ngu M, Xu G, Hernández-Saavedra D, Chen H, DE Lisio M. Effects of Obesity and Exercise on Bone Marrow Progenitor Cells after Radiation. Med Sci Sports Exerc 2019;51:1126–1136.
19. Farber E, Kwiecien JM, Bojic D, Ngu M, Akohene-Mensah P, Vanhie JJ et al. Exercise Improves Cancer-free Survival and Health Span in a Model of Radiation-induced Cancer. Medicine & Science in Sports & Exercise 2021;53:2254–2263.

20. Roubos S, D'Souza D, Hernández-Saavedra D, Xu G, Collao N, Emmons R et al. Weight loss with exercise improves muscle architecture and progenitor cell populations compared with weight loss alone in mice with preneoplastic colorectal lesions. Appl Physiol Nutr Metab 2021;46:837–845.
21. Dyar KA, Ciciliot S, Wright LE, Biensø RS, Tagliazucchi GM, Patel VR et al. Muscle insulin sensitivity and glucose metabolism are controlled by the intrinsic muscle clock. Mol Metab 2014;3:29–41.
22. Feige P, Rudnicki MA. Isolation of satellite cells and transplantation into mice for lineage tracing in muscle. Nat Protoc 2020;15:1082–1097.
23. Hennig, C. Cran-package fpc. https://cran.rproject.org/web/packages/fpc/index.html.
24. Alexa A, Rahnenfuhrer J. topGO: Enrichment Analysis for Gene Ontology. R package version 1.38.1 (2019). .
25. Courneya KS, Friedenreich CM, Quinney HA, Fields ALA, Jones LW, Vallance JKH et al. A longitudinal study of exercise barriers in colorectal cancer survivors participating in a randomized controlled trial. Ann Behav Med 2005;29:147–153.
26. Englund DA, Murach KA, Dungan CM, Figueiredo VC, Vechetti IJ, Dupont-Versteegden EE et al. Depletion of resident muscle stem cells negatively impacts running volume, physical function, and muscle fiber hypertrophy in response to lifelong physical activity. Am J Physiol Cell Physiol 2020;318:C1178–C1188.
27. Dungan CM, Brightwell CR, Wen Y, Zdunek CJ, Latham CM, Thomas NT et al. Muscle-Specific Cellular and Molecular Adaptations to Late-Life Voluntary Concurrent Exercise. Function (Oxf) 2022;3:zqac027.
28. van Brussel M, Takken T, Lucia A, van der Net J, Helders PJM. Is physical fitness decreased in survivors of childhood leukemia? A systematic review. Leukemia 2005;19:13–17.
29. Englund DA, Figueiredo VC, Dungan CM, Murach KA, Peck BD, Petrosino JM et al. Satellite Cell Depletion Disrupts Transcriptional Coordination and Muscle Adaptation to Exercise. Function 2021;2.

30. Padilha CS, Cella PS, Chimin P, Voltarelli FA, Marinello PC, Testa MTDJ et al. Resistance Training's Ability to Prevent Cancer-induced Muscle Atrophy Extends Anabolic Stimulus. Med Sci Sports Exerc 2021;53:1572–1582.
31. Testa MT de J, Cella PS, Marinello PC, Frajacomo FTT, Padilha C de S, Perandini PC et al. Resistance Training Attenuates Activation of STAT3 and Muscle Atrophy in Tumor-Bearing Mice. Front Oncol 2022;12:880787.
32. Watt KI, Turner BJ, Hagg A, Zhang X, Davey JR, Qian H et al. The Hippo pathway effector YAP is a critical regulator of skeletal muscle fibre size. Nat Commun 2015;6:6048.
33. Saito Y, Chikenji TS, Matsumura T, Nakano M, Fujimiya M. Exercise enhances skeletal muscle regeneration by promoting senescence in fibro-adipogenic progenitors. Nat Commun 2020;11:889.
34. Farup J, De Lisio M, Rahbek SK, Bjerre J, Vendelbo MH, Boppart MD et al. Pericyte response to contraction mode-specific resistance exercise training in human skeletal muscle. J Appl Physiol (1985) 2015;119:1053–1063.
35. Heldin C-H. Targeting the PDGF signaling pathway in tumor treatment. Cell Commun Signal 2013;11:97.
36. Kendall RT, Feghali-Bostwick CA. Fibroblasts in fibrosis: novel roles and mediators. Front Pharmacol 2014;5:123.
37. Farup J, Just J, de Paoli F, Lin L, Jensen JB, Billeskov T et al. Human skeletal muscle CD90+ fibro-adipogenic progenitors are associated with muscle degeneration in type 2 diabetic patients. Cell Metab 2021;33:2201-2214.e11.
38. Horn A, Palumbo K, Cordazzo C, Dees C, Akhmetshina A, Tomcik M et al. Hedgehog signaling controls fibroblast activation and tissue fibrosis in systemic sclerosis. Arthritis Rheum 2012;64:2724–2733.
39. Brightwell CR, Latham CM, Thomas NT, Keeble AR, Murach KA, Fry CS. A glitch in the matrix: the pivotal role for extracellular matrix remodeling during muscle hypertrophy. Am J Physiol Cell Physiol 2022;323:C763–C771.
40. Peck BD, Murach KA, Walton RG, Simmons AJ, Long DE, Kosmac K et al. A muscle cell-macrophage axis involving matrix metalloproteinase 14 facilitates

extracellular matrix remodeling with mechanical loading. FASEB J 2022;36:e22155.

Chapter V

General discussion and future directions

The research projects presented in this thesis aimed to address a critical gap in the lack of knowledge regarding the cellular source and mechanisms responsible for radiation-induced muscle pathology in juvenile cancer survivors. The studies explored the extent to which FAPs are involved in cancer treatment-induced muscle pathology and characterized how radiation therapy affects cellular dynamics and communication within the muscle niche at a single-cell resolution. We also examined whether a combination of resistance and endurance exercise training can mitigate the long-term muscle defect in a juvenile model of cancer plus therapy. The major findings from the research projects presented in this thesis, were that following juvenile radiation exposure, FAPs acquire a pro-fibrotic phenotype and contribute to the long-term skeletal muscle atrophy and fibrosis observed in juvenile cancer survivors (Chapter II). Subsequently, our scRNA-seq analysis (Chapter III) revealed a conserved *Cdkn1a* gene signature across all cells and higher expression of proinflammatory signalling in the IR-limb. Furthermore, cell-cell interaction analysis revealed FAPs as the primary target of TGF-β signalling post-IR. Lastly, we demonstrated that RET preserved skeletal muscle mass and restored the inflammatory and fibrotic transcriptome in a model of juvenile RMS survivorship (Chapter IV). Collectively, these studies identify FAPs as significant cell contributors to the development of radiation-induced fibrosis in skeletal muscle. Moreover, RET emerges as a novel potential strategy that can prevent or mitigate the long-term side effects of cancer

treatment in juvenile cancer survivors. This chapter aims to connect the individual research projects in a broader global discussion beyond what was presented in the individual chapters, and offering potential directions and limitations for future work that build on the outcomes of the individual projects.

The complexity of the extracellular matrix

The extracellular matrix is a network composed of various structural proteins such as collagens, proteoglycans, and fibronectin, among others, essential during muscle development, hypertrophy, and regeneration (Brightwell et al., 2022; Csapo et al., 2020). Transient ECM deposition serves as a substrate and scaffold for various types of cells, including MuSCs, by providing a three-dimensional structure supporting their myogenic commitment (Thomas et al., 2015; W. Zhang et al., 2021). Conversely, exacerbated ECM accumulation results in skeletal muscle fibrosis. The highly dynamic fibrogenic process involves a constant communication between various cells, such as immune cells and FAPs. This fibrogenic process comprises an inflammatory response where different immune cells are activated, releasing multiple cytokines and chemokines, such as TGF-β, PDGF, CTGF, and TNF-α (Mahdy, 2019). The immune response leads to the proliferation of fibroblastic-like cells such as FAPs, initiating various intracellular processes such as phosphorylation of SMAD protein targets, leading to the activating fibrogenic genes, and contributing to excessive ECM deposition (H.-H. Hu et al., 2018; Uezumi et al., 2011). In Chapter II, we observed exacerbated ECM accumulation in skeletal muscle at 56-days post-IR. Additionally, we observed an increase in fibronectin and αSMA in the whole muscle, which are well established pro-fibrotic markers.

Furthermore, we observed early phosphorylation of SMAD3, a downstream target of TGF-β which is known as a master regulator of fibrogenesis (Biernacka et al., 2011). The early activation of SMAD3 signalling may be responsible for the early biological process related to myofibroblast proliferation in FAPs observed in our scRNA-seq study (Chapter III). Persistent SMAD3 signalling during muscle regeneration hinders MuSC fusion and differentiation (Melendez et al., 2021; Girardi et al., 2021). We also observed an impairment of MuSCs fusion and differentiation in Chapter II. A recent work by Le Grand's Lab revealed that TGF-β signalling impairs myoblast fusion, by controlling the expression of actin-related genes, leading to a reduction of myotube formation (Girardi et al., 2021). Similarly, Lamarche and colleagues showed that treating myoblast with TGF-β inhibits myoblast differentiation (Lamarche et al., 2015). Therefore, the TGF-β-SMAD3 axis has been shown to inhibit myogenic fusion (Melendez et al., 2021) and differentiation (Liu et al., 2001). This aligns with our scRNA-seq analysis, where persistent TGF-β signalling was observed in the IR-limb compared to CON at 56-days post-IR. Upregulation of TGF-β signalling has been reported in mice (Bachman et al., 2018b; Kallenbach et al., 2022) and humans (Ejaz et al., 2019; Martin et al., 2000; J. Wang et al., 2021) following radiation exposure. Thus, our findings suggest that TGF-β signaling it could be an important signalling pathway involved in skeletal muscle atrophy and fibrosis observed in cancer survivors. ıt is important to note that there was a difference in findings between Chapter II and III. In Chapter II, we did not detect an increase in SMAD3 signalling in the whole muscle 56-days post-IR, while in Chapter III, using scRNA-seq analysis, we observed increased TGF-β signalling at the same time point. This difference could be due to the

sensitivity of the two techniques used to evaluate this pro-fibrotic signalling and the different radiation protocols.

Interestingly, our scRNA-seq data reveled that macrophages were the main source of TGF-β and FAPs were the primary receiver of TGF-β signalling post-IR. Moreover, we found that FAPs were the main cellular source of ECM deposition. Together, these findings suggest an active communication between macrophages and FAPs contributing to skeletal muscle fibrosis following radiation exposure. Similarly, in the RMS plus therapy study (Chapter IV), we found an increase in macrophages compared to the control. Furthermore, an up-regulation of *Ccr2* gene expression was present in the RMS plus therapy group. These align with previous findings showing increased *Ccr2* expression associated with different fibrotic pathologies (Moore et al., 2001; Seki et al., 2009; Venosa et al., 2021). Interestingly, RET down-regulated *Ccl2* gene expression, a gene related to pro-inflammatory signalling and a specific ligand of Ccr2, which is highly expressed in macrophages (Gschwandtner et al., 2019). Blanc and colleagues showed that Ccl2 inhibits MuSC fusion and differentiation (Blanc et al., 2020). Moreover, genetic ablation of the *Ccr2* gene in MuSCs leads to enhanced muscle regeneration (Blanc et al., 2020). Thus, this data suggests that downregulation of *Ccl2* gene expression by RET might enhance skeletal muscle hypertrophy by promoting MuSCs fusion and differentiation in or RMS plus therapy model. Growing evidence has shown that persistent M2 macrophages accumulation in the skeletal muscle contributes to muscle fibrosis (Braga et al., 2015; M. Hu et al., 2023; Stepien et al., 2020) and promotes myofibroblast differentiation (Hoeft et al., 2023; Hou et al., 2018). These findings align with our scRNA-seq data in Chapter III, showing a macrophage type 2 subpopulation highly expressing

Ccr2 increases at 56-days post-IR that could contribute to skeletal muscle fibrosis and promote FAP fibrogenic lineage commitment into myofibroblast. Moreover, we observed pro-inflammatory signalling pathways enriched just in the IR-limb at 56-days post-IR, such as Protease-activated receptors (PARs), TNF, and Osteopontin (SPP1). Villalta's Lab recently found that SPP1 is highly expressed in macrophages from *mdx* mice and plays a crucial role in regulating communication between macrophages and FAPs, which is closely associated with skeletal muscle fibrosis (Coulis et al., 2023). This aligns with the observation from our scRNA-seq analysis that at 56-days post-IR, SPP1 is the most incoming interaction with macrophages. Thus, these findings suggest that SPP1 could be a potential target mediating macrophage-FAP communication associated with fibrogenic pathologies. Together, paracrine factors, such as TGF-β and SPP1, are novel factors identified in our radiation model that might regulate the activation and fate of FAPs contributing to skeletal muscle fibrosis.

In Chapter II, we characterized and identified the effect of radiation exposure on FAP phenotypic changes, suggesting their contribution to the long-term skeletal muscle atrophy and fibrosis observed following radiation exposure. In pathological conditions, FAPs are associated with progressive deterioration of skeletal muscle (Ieronimakis et al., 2016; Lemos et al., 2015; Uezumi et al., 2010, 2011). PDGFRa downregulation is involved in fibrogenic lineage commitment, which is counter-intuitive given the association with PDGFRa signal in immunofluorescence and collagen staining in *mdx* muscle (Uezumi et al., 2010). Interestingly, we observed a decrease in PDGFRα expression in Chapter II by immunofluorescence which was confirmed by flow cytometric analysis. In line with this finding, our scRNA-seq analysis in Chapter III shows that PDGF signalling

also decreases post-IR. Thus, our findings suggest that the decrease in PDGFRα expression in the context of radiation is associated with FAP differentiation into a profibrogenic lineage. Supporting this notion, elevated PDGFRα expression in skin fibroblasts delays their myofibroblast transition (Yao et al., 2022). Conversely, PDGFRα downregulation is essential for early lineage commitment into myofibroblast expressing αSMA in skin (Yao et al., 2022). These findings align with the increase in αSMA stress fibre formation observed in FAPs following radiation exposure in Chapter II. In order to confirm the contribution of FAPs to skeletal muscle fibrosis *in vivo*, future studies using a lineage tracing model are necessary. A PDGFRα$^{CreERT2/TdTomato}$ lineage tracing mouse model can be generated by crossing a mice containing Tamoxifen-inducible CreERT2 insert into the PDGFRα locus (PDGFRα^{CreERT2} mice) with a floxed TdTomato reporter gene in the Rosa26 locus (B6.Cg-Gt(ROSA)26Sor$^{tm14(CAGtdTomato)\ Hze/J}$) mice. This genetic model will allow to visualize all TdTomato^{+} cells that are either FAPs or their progeny. Thus, this genetic mouse model will provide evidence and determine FAP fate lineage commitment following *in vivo* radiation.

Exercise and the creation of a better scaffold

Skeletal muscle force generation relies on the properties of the ECM structures (Csapo et al., 2020). These functional structures depend on the balance between ECM synthesis and degradation (Csapo et al., 2020). The ECM undergoes continuous remodeling due to matrix metalloproteinase (MMP) enzymes, which are crucial for ECM degradation (Jabłońska-Trypuć et al., 2016). Our transcriptomic data in Chapter IV revealed that RET increased enrichment analysis related to ECM biosynthesis and

reorganization. We also observed an increased *Mmp14*, *Mmp3*, and *Mmp2* gene expression, which may lead to biological processes of RET-driven collagen organization. In line with our findings, Peck and colleagues found that resident macrophages highly expressing *Mmp14* facilitate ECM degradation after mechanical loading (Peck et al., 2022). Thus, RET might contribute to ECM remodeling in our RMS plus therapy model.

Exercise induces ECM adaptations that enhance skeletal muscle function (Pillon et al., 2020). Acute resistance training increases ECM-related gene expression, especially MMPs-related genes, suggesting increased ECM turnover (Wessner et al., 2019). Further, 12-weeks of endurance exercise training promotes an increase in ECM-related genes, suggesting their essential role in exercise adaptation (Hjorth et al., 2015). In Chapter IV, although we did not observe a direct effect of RET in reducing ECM accumulation based on trichrome staining analysis, we did observe that RET promotes the reduction of profibrotic and inflammatory-related genes that contribute to skeletal muscle fibrosis, such as *Ccl2*, *Cd163*, and *Myd88* (Bayer & Alcaide, 2021; Gschwandtner et al., 2019; Kowal et al., 2011). In fibrotic pathologies, the ECM possesses a disorganized structure, associated with detrimental outcomes in the affected tissue (Brashear et al., 2021; Frantz et al., 2010; Gazoti Debessa et al., 2001; Karsdal et al., 2017; Xue & Jackson, 2015). Skeletal muscles of *mdx* mice display alterations in the relationship between ECM organization, muscle contraction, and stiffness (Brashear et al., 2021). This highlights the important link between ECM structure and mechanical muscle function. Recent work suggests that targeting collagen fibre alignment to improve muscle function and stiffness, rather than solely focusing on decreasing ECM content, should be the main goal of anti-fibrotic strategies in pathologies with exacerbated ECM

deposition (Brashear et al., 2022). Brashear and colleagues showed that administering an anti-fibrotic drug in *mdx* mice significantly changes the ECM architecture in the dystrophic skeletal muscle (Brashear et al., 2022). Future studies must investigate whether RET can impact the spatial ECM organization following cancer treatment. Methods, including the nanoindentation assay, can assess tissue stiffness in muscle CSA and determine the mechanical properties of ECM remodeling following RMS plus therapy (Akhtar et al., 2009). Advances in imaging technology can also help to determine the complex structure of the ECM in pathology and following exercise training. Techniques such as rotational linearly polarized light microscopy, electron microscopy, optical microscopy, and second harmonic generation imaging can provide important insight into the micropatterning structure of the ECM (Leonard et al., 2018; Poole & Mostaço-Guidolin, 2021). Thus, combining immunofluorescence, histological, and imaging analyses, we can better understand the ECM complexity and the link between ECM structure, alignment, and tissue function in response to exercise.

A senescent cell perspective

Unrepaired DNA from cancer therapy could lead to a senescence cell state which is a state of irreversible cell growth arrest (Campisi & d'Adda di Fagagna, 2007). Senescent cells also actively secrete various soluble factors called senescence-associated secretory phenotype (SASP) (Coppé et al., 2008). The SASP consists of a variety of pro-fibrotic and inflammatory factors such as TNF-α, C/EBPβ, IL-6, and TGF-β (Coppé et al., 2008; Ohtani, 2022). In Chapter II, we observed that FAPs obtained a senescence-like phenotype following radiation exposure, characterized by the activation

of senescence-associated (SA)-β-Galactosidase (β-gal) staining, a biomarker of cellular senescence (Morgunova et al., 2015). In Chapter III, our scRNA-sequencing analysis revealed that in most mononuclear cells residing in the muscle niche, there was an increase in *Cdkn1a* gene signature and p53 signalling. These findings align with previous studies showing that cancer patients undergoing chemo- or radiation therapy present increased levels of senescence markers such as β-gal and cyclin-dependent kinase inhibitor 1 (p21, encoded by the *Cdkn1a* gene) in skeletal muscle, peripheral blood, and other tissues (Sakai et al., 2014; Amundson et al., 2004; Koster et al., 2010; Mansour et al., 2023; Roberson et al., 2005), and that irradiated, cancer-free mice also present senescence markers in different tissues (Demaria et al., 2014; Fielder et al., 2019). Nevertheless, no previous studies have shown which cell type acquires the senescence-like phenotype following radiation in skeletal muscle. Applying gene scoring to our scRNA-seq data set based on a curated-senescence gene signature called SenMayo (Saul et al., 2022), we made the novel finding that FAPs present the highest senescence-enriched genes compared to the other cell types, suggesting that they are the most affected cell population following radiation exposure. A recent study by Zhang and colleagues showed that a FAP subpopulation that aligns with the Tenm2^{+}-FAP subpopulation from our scRNAseq, presents a senescence signature in aging muscle (X. Zhang et al., 2022). The senescence phenotype acquired by FAPs suggests that FAPs may secrete the SASP. In Chapter II, we showed that radiation exposure affects FAP-derived trophic factors in a manner that inhibits MuSC fusion and differentiation. This result may be partly due to the senescence-like phenotype acquired by FAPs resulting in their secretion of SASP which would then inhibit myogenesis. Therefore, future studies

are needed to investigate the effect of cancer treatments on FAP secretory profile that may alter cellular communication with MuSCs and various other cell groups. In this context, various senolytics could mitigate the senescent cell state accumulated during ageing, cancer treatments, and various pathological states. Treatment of old mice with a combination of dasatinib and quercetin, two senotherapeutics, showed improvement in muscle function and reduced the expression of senescence markers such as *Cdkn1a*, and p53 pathway (X. Zhang et al., 2022). Another benefit of these therapies is that senolytics promote cell cycle arrest, leading to cellular senescence and ultimately preventing tumorigenesis (Bousset & Gil, 2022; L. Wang et al., 2022).

Limitations

We have considered some important limitations to the work presented herein. In Chapter II, one limitation was using a single dose of radiation rather than fractionated doses. In clinical cancer treatment, a multi-session schedule allows healthy cells to repair between treatments, reducing long-term tissue damage (Baskar et al., 2012). Because we focused on radiation treatment in a juvenile stage where MuSCs are required for normal muscle development (Bachman et al., 2018b), we could not precisely replicate the clinical radiation schedule (Cardoso-Moreira et al., 2020). Thus, our radiation dose was based on previous work from the Carson lab, showing the effect of 16 Gy on muscle morphology, and fibrosis (Hardee et al., 2014), and based on biologically equivalent dose calculations to treat different types of cancers (Voyant et al., 2014). Another limiting aspect of Chapter II and III was the use of cancer-free mice. In Chapter IV, we addressed this limitation directly by developing an RMS plus therapy model. Radiating cancer-free

muscle is clinically relevant because radiation is often used as an adjuvant therapy subsequent to cancer resection. Furthermore, Chakkalakal's Lab demonstrated that the irradiated limb alone and the irradiated limb inoculated with RMS, showed similar increases in pro-inflammatory cytokines, extracellular matrix genes, and decrease in myofiber volume and force production (Kallenbach et al., 2022), suggesting that treatment is the main driver of this phenotype, at least in the context of RMS.

In our single-cell RNA sequencing experiment (Chapter III), we obtained a low number of cells, potentially due to the cytotoxic effect of irradiation itself. This limitation could be addressed by increasing the sample collection. In addition, being able to FACS sort a greater number of cells would have helped us to discern with greater certainty some FAP subpopulations solely responsible for the long-term fibrosis observed in cancer survivors. Future studies using a lineage tracing model will allow us to confirm *in vivo* the FAP contribution to skeletal muscle fibrosis. Furthermore, genetic ablation models could be used to investigate how the FAP subpopulation might contributes to long-term skeletal muscle defects. Thus, allowing us to gain a better understanding of which FAPs subpopulation contributes to radiation-induced skeletal muscle pathology. Another limitation is that in our RMS plus therapy study (Chapter IV), we could not perform *in situ* or *in vivo* muscle stimulation measurements following RMS treatment and resistance and endurance training. Performing these measurements would have been a better approach to directly assess strength in the gastrocnemius muscle following training. Since this was an initial investigation characterizing the effects of RET in preclinical, juvenile RMS plus therapy, we focused our analysis on markers of muscle size (i.e., cross-sectional area) and fibrosis. Future work needs to investigate the direct changes in force

production in the gastrocnemius muscle following RMS plus therapy. Another limitation in Chapter IV was that four mice (two males in the RET group, one male in the SED group, and one female in the RET group) perished before the intervention was completed. Tumors recurred in two mice in the RET group and one in the SED group, while the fourth mouse had to be sacrificed after an injury that occurred during RET. This attrition prevented us from conducting planned sex-difference analyses (Beaudry et al., 2022; Binet et al., 2023; Deasy et al., 2008; Fortino et al., 2022). Thus, future work is needed to investigate sex-based comparison following resistance and endurance training in an RMS-treated murine model. Lastly, a limitation is that the analysis only focused on the gastrocnemius muscle, which does not capture the full effect of RET on various muscle groups. However, the decision to focus on the gastrocnemius muscle was made to accurately inject the RMS into the muscle due to its large surface area and to perform localized radiation due to the shape of the lead shield in the radiation machine.

Final remarks

The studies presented in this thesis identified FAPs as key contributors to radiation-induced fibrosis in skeletal muscle and identified a gene signature of radiation exposure that occur in skeletal muscle following radiation exposure. Additionally, the thesis proposes resistance and endurance exercise as a non-pharmacological strategy to mitigate the detrimental effects of cancer treatment in juvenile cancer survivors perhaps by reversing fibrotic and inflammatory signalling. Future studies are needed to further delineate the mechanisms underlying these changes in skeletal muscle due to cancer treatment. Furthermore, understanding how resistance and endurance training prevents muscle degeneration following cancer treatment could lead to novel, exercise-inspired therapies for radiation-induced fibrosis in cancer survivors. Overall, the findings presented in this thesis will positively impact Canadians' health by identifying FAPs as key contributors to radiation-induced fibrosis in skeletal muscle and RET as a novel potential therapy that can prevent or mitigate the late effects of cancer treatment in juvenile cancer survivors.

References (Chapter I and Chapter V)

Adams, G. R., Caiozzo, V. J., Haddad, F., & Baldwin, K. M. (2002). Cellular and molecular responses to increased skeletal muscle loading after irradiation. *American Journal of Physiology. Cell Physiology*, *283*(4), C1182-1195. https://doi.org/10.1152/ajpcell.00173.2002

Akhtar, R., Schwarzer, N., Sherratt, M. J., Watson, R. E. B., Graham, H. K., Trafford, A. W., Mummery, P. M., & Derby, B. (2009). Nanoindentation of histological specimens. *Journal of Materials Research*, *24*(3), 638–646. https://doi.org/10.1557/JMR.2009.0130

al-Majid, S., & McCarthy, D. O. (2001). Cancer-induced fatigue and skeletal muscle wasting: The role of exercise. *Biological Research for Nursing*, *2*(3), 186–197. https://doi.org/10.1177/109980040100200304

Amundson, S. A., Grace, M. B., McLeland, C. B., Epperly, M. W., Yeager, A., Zhan, Q., Greenberger, J. S., & Fornace, A. J. (2004). Human in vivo radiation-induced biomarkers: Gene expression changes in radiotherapy patients. *Cancer Research*, *64*(18), 6368–6371. https://doi.org/10.1158/0008-5472.CAN-04-1883

Arndt, C. A. S., Rose, P. S., Folpe, A. L., & Laack, N. N. (2012). Common musculoskeletal tumors of childhood and adolescence. *Mayo Clinic Proceedings*, *87*(5), 475–487. https://doi.org/10.1016/j.mayocp.2012.01.015

Aversa, Z., Costelli, P., & Muscaritoli, M. (2017). Cancer-induced muscle wasting: Latest findings in prevention and treatment. *Therapeutic Advances in Medical Oncology*, *9*(5), 369–382. https://doi.org/10.1177/1758834017698643

Bachman, J. F., Blanc, R. S., Paris, N. D., Kallenbach, J. G., Johnston, C. J., Hernady, E., Williams, J. P., & Chakkalakal, J. V. (2020). Radiation-Induced Damage to Prepubertal Pax7+ Skeletal Muscle Stem Cells Drives Lifelong Deficits in Myofiber Size and Nuclear Number. *IScience*, *23*(11), 101760. https://doi.org/10.1016/j.isci.2020.101760

Bachman, J. F., & Chakkalakal, J. V. (2021). Insights into muscle stem cell dynamics during postnatal development. *The FEBS Journal*. https://doi.org/10.1111/febs.15856

Bachman, J. F., Klose, A., Liu, W., Paris, N. D., Blanc, R. S., Schmalz, M., Knapp, E., & Chakkalakal, J. V. (2018a). Prepubertal skeletal muscle growth requires Pax7-expressing satellite cell-derived myonuclear contribution. *Development (Cambridge, England)*, *145*(20), dev167197. https://doi.org/10.1242/dev.167197

Bachman, J. F., Klose, A., Liu, W., Paris, N. D., Blanc, R. S., Schmalz, M., Knapp, E., & Chakkalakal, J. V. (2018b). Prepubertal skeletal muscle growth requires Pax7-expressing satellite cell-derived myonuclear contribution. *Development (Cambridge, England)*, *145*(20), dev167197. https://doi.org/10.1242/dev.167197

Baskar, R., Lee, K. A., Yeo, R., & Yeoh, K.-W. (2012). Cancer and Radiation Therapy: Current Advances and Future Directions. *International Journal of Medical Sciences*, *9*(3), 193–199. https://doi.org/10.7150/ijms.3635

Baudino, T. A. (2015). Targeted Cancer Therapy: The Next Generation of Cancer Treatment. *Current Drug Discovery Technologies*, *12*(1), 3–20. https://doi.org/10.2174/1570163812666150602144310

Bayer, A. L., & Alcaide, P. (2021). MyD88: At the heart of inflammatory signaling and cardiovascular disease. *Journal of Molecular and Cellular Cardiology*, *161*, 75–85. https://doi.org/10.1016/j.yjmcc.2021.08.001

Bazgir, B., Fathi, R., Rezazadeh Valojerdi, M., Mozdziak, P., & Asgari, A. (2017). Satellite Cells Contribution to Exercise Mediated Muscle Hypertrophy and Repair. *Cell Journal (Yakhteh)*, *18*(4), 473–484.

Beaudry, K. M., Surdi, J. C., Mari, A., & Devries, M. C. (2022). Exercise mode influences post-exercise glucose sensitivity and insulin clearance in young, healthy males and females in a sex-dependent manner: A randomized control trial. *Physiological Reports*, *10*(13), e15354. https://doi.org/10.14814/phy2.15354

Bentzinger, C. F., Wang, Y. X., Dumont, N. A., & Rudnicki, M. A. (2013). Cellular dynamics in the muscle satellite cell niche. *EMBO Reports*, *14*(12), 1062–1072. https://doi.org/10.1038/embor.2013.182

Biernacka, A., Dobaczewski, M., & Frangogiannis, N. G. (2011). TGF-β signaling in fibrosis. *Growth Factors (Chur, Switzerland)*, *29*(5), 196–202. https://doi.org/10.3109/08977194.2011.595714

Biferali, B., Proietti, D., Mozzetta, C., & Madaro, L. (2019). Fibro–Adipogenic Progenitors Cross-Talk in Skeletal Muscle: The Social Network. *Frontiers in Physiology*, *10*. https://doi.org/10.3389/fphys.2019.01074

Binet, E. R., McKenna, C. F., Salvador, A. F., Martinez, I. G., Alamilla, R. A., Collao, N., Bodnariuc, G., Khan, N. A., Paluska, S. A., Burd, N. A., & De Lisio, M. (2023). Sex-based comparisons of muscle cellular adaptations after 10 weeks of progressive resistance training in middle-aged adults. *Journal of Applied Physiology*

(Bethesda, Md.: 1985), *134*(1), 116–129. https://doi.org/10.1152/japplphysiol.00274.2022

Blanc, R. S., Kallenbach, J. G., Bachman, J. F., Mitchell, A., Paris, N. D., & Chakkalakal, J. V. (2020). Inhibition of inflammatory CCR2 signaling promotes aged muscle regeneration and strength recovery after injury. *Nature Communications*, *11*(1), 4167. https://doi.org/10.1038/s41467-020-17620-8

Boldrin, L., Neal, A., Zammit, P. S., Muntoni, F., & Morgan, J. E. (2012). Donor satellite cell engraftment is significantly augmented when the host niche is preserved and endogenous satellite cells are incapacitated. *Stem Cells (Dayton, Ohio)*, *30*(9), 1971–1984. https://doi.org/10.1002/stem.1158

Boppart, M. D., De Lisio, M., Zou, K., & Huntsman, H. D. (2013). Defining a role for non-satellite stem cells in the regulation of muscle repair following exercise. *Frontiers in Physiology*, *4*. https://doi.org/10.3389/fphys.2013.00310

Bourdon, A., Grandy, S. A., & Keats, M. R. (2018). Aerobic exercise and cardiopulmonary fitness in childhood cancer survivors treated with a cardiotoxic agent: A meta-analysis. *Supportive Care in Cancer: Official Journal of the Multinational Association of Supportive Care in Cancer*, *26*(7), 2113–2123. https://doi.org/10.1007/s00520-018-4208-z

Bousset, L., & Gil, J. (2022). Targeting senescence as an anticancer therapy. *Molecular Oncology*, *16*(21), 3855–3880. https://doi.org/10.1002/1878-0261.13312

Bouwman, P., & Jonkers, J. (2012). The effects of deregulated DNA damage signalling on cancer chemotherapy response and resistance. *Nature Reviews. Cancer*, *12*(9), 587–598. https://doi.org/10.1038/nrc3342

Braga, T. T., Agudelo, J. S. H., & Camara, N. O. S. (2015). Macrophages During the Fibrotic Process: M2 as Friend and Foe. *Frontiers in Immunology*, *6*, 602. https://doi.org/10.3389/fimmu.2015.00602

Brand, S., Wolfe, J., & Samsel, C. (2017). The Impact of Cancer and Its Treatment on the Growth and Development of the Pediatric Patient. *Current Pediatric Reviews*, *13*(1), 24–33. https://doi.org/10.2174/1573396313666161116094916

Brashear, S. E., Wohlgemuth, R. P., Gonzalez, G., & Smith, L. R. (2021). Passive stiffness of fibrotic skeletal muscle in mdx mice relates to collagen architecture. *The Journal of Physiology*, *599*(3), 943–962. https://doi.org/10.1113/JP280656

Brashear, S. E., Wohlgemuth, R. P., Hu, L.-Y., Jbeily, E. H., Christiansen, B. A., & Smith, L. R. (2022). Collagen cross-links scale with passive stiffness in dystrophic mouse muscles, but are not altered with administration of a lysyl oxidase inhibitor. *PLOS ONE*, *17*(10), e0271776. https://doi.org/10.1371/journal.pone.0271776

Brightwell, C. R., Latham, C. M., Thomas, N. T., Keeble, A. R., Murach, K. A., & Fry, C. S. (2022). A glitch in the matrix: The pivotal role for extracellular matrix remodeling during muscle hypertrophy. *American Journal of Physiology. Cell Physiology*, *323*(3), C763–C771. https://doi.org/10.1152/ajpcell.00200.2022

Campbell, K. L., Winters-Stone, K., Wiskemann, J., May, A. M., Schwartz, A. L., Courneya, K. S., Zucker, D., Matthews, C., Ligibel, J., Gerber, L., Morris, S., Patel, A., Hue, T., Perna, F., & Schmitz, K. H. (2019). Exercise Guidelines for Cancer Survivors: Consensus statement from International Multidisciplinary Roundtable. *Medicine and Science in Sports and Exercise*, *51*(11), 2375–2390. https://doi.org/10.1249/MSS.0000000000002116

Campisi, J., & d'Adda di Fagagna, F. (2007). Cellular senescence: When bad things happen to good cells. *Nature Reviews. Molecular Cell Biology*, *8*(9), 729–740. https://doi.org/10.1038/nrm2233

Camps, J., Breuls, N., Sifrim, A., Giarratana, N., Corvelyn, M., Danti, L., Grosemans, H., Vanuytven, S., Thiry, I., Belicchi, M., Meregalli, M., Platko, K., MacDonald, M. E., Austin, R. C., Gijsbers, R., Cossu, G., Torrente, Y., Voet, T., & Sampaolesi, M. (2020). Interstitial Cell Remodeling Promotes Aberrant Adipogenesis in Dystrophic Muscles. *Cell Reports*, *31*(5), 107597. https://doi.org/10.1016/j.celrep.2020.107597

Canadian Cancer Society, 2021. (n.d.).

Cardoso-Moreira, M., Sarropoulos, I., Velten, B., Mort, M., Cooper, D. N., Huber, W., & Kaessmann, H. (2020). Developmental Gene Expression Differences between Humans and Mammalian Models. *Cell Reports*, *33*(4), 108308. https://doi.org/10.1016/j.celrep.2020.108308

Charytonowicz, E., Cordon-Cardo, C., Matushansky, I., & Ziman, M. (2009). Alveolar rhabdomyosarcoma: Is the cell of origin a mesenchymal stem cell? *Cancer Letters*, *279*(2), 126–136. https://doi.org/10.1016/j.canlet.2008.09.039

Christensen, J. F., Jones, L. W., Andersen, J. L., Daugaard, G., Rorth, M., & Hojman, P. (2014). Muscle dysfunction in cancer patients. *Annals of Oncology: Official Journal of the European Society for Medical Oncology*, *25*(5), 947–958. https://doi.org/10.1093/annonc/mdt551

Contreras, O., Cruz-Soca, M., Theret, M., Soliman, H., Tung, L. W., Groppa, E., Rossi, F. M., & Brandan, E. (2019). Cross-talk between TGF-β and PDGFRα signaling

pathways regulates the fate of stromal fibro-adipogenic progenitors. *Journal of Cell Science*, *132*(19), jcs232157. https://doi.org/10.1242/jcs.232157

Contreras, O., Rebolledo, D. L., Oyarzún, J. E., Olguín, H. C., & Brandan, E. (2016). Connective tissue cells expressing fibro/adipogenic progenitor markers increase under chronic damage: Relevance in fibroblast-myofibroblast differentiation and skeletal muscle fibrosis. *Cell and Tissue Research*, *364*(3), 647–660. https://doi.org/10.1007/s00441-015-2343-0

Contreras, O., Rossi, F. M. V., & Theret, M. (2021). Origins, potency, and heterogeneity of skeletal muscle fibro-adipogenic progenitors-time for new definitions. *Skeletal Muscle*, *11*(1), 16. https://doi.org/10.1186/s13395-021-00265-6

Coppé, J.-P., Patil, C. K., Rodier, F., Sun, Y., Muñoz, D. P., Goldstein, J., Nelson, P. S., Desprez, P.-Y., & Campisi, J. (2008). Senescence-Associated Secretory Phenotypes Reveal Cell-Nonautonomous Functions of Oncogenic RAS and the p53 Tumor Suppressor. *PLOS Biology*, *6*(12), e301. https://doi.org/10.1371/journal.pbio.0060301

Coulis, G., Jaime, D., Guerrero-Juarez, C., Kastenschmidt, J. M., Farahat, P. K., Nguyen, Q., Pervolarakis, N., McLinden, K., Thurlow, L., Movahedi, S., Hughes, B. S., Duarte, J., Sorn, A., Montoya, E., Mozaffar, I., Dragan, M., Othy, S., Joshi, T., Hans, C. P., … Villalta, S. A. (2023). Single-cell and spatial transcriptomics identify a macrophage population associated with skeletal muscle fibrosis. *Science Advances*, *9*(27), eadd9984. https://doi.org/10.1126/sciadv.add9984

Csapo, R., Gumpenberger, M., & Wessner, B. (2020). Skeletal Muscle Extracellular Matrix – What Do We Know About Its Composition, Regulation, and Physiological

Roles? A Narrative Review. *Frontiers in Physiology*, *11*. https://www.frontiersin.org/articles/10.3389/fphys.2020.00253

Curry, S. D., Jiang, Z. Y., & Jain, K. S. (2021). Population-based survival of pediatric rhabdomyosarcoma of the head and neck over four decades. *International Journal of Pediatric Otorhinolaryngology*, *142*, 110599. https://doi.org/10.1016/j.ijporl.2020.110599

Dale, B., Cheng, M., Park, K.-S., Kaniskan, H. Ü., Xiong, Y., & Jin, J. (2021). Advancing targeted protein degradation for cancer therapy. *Nature Reviews. Cancer*, *21*(10), 638–654. https://doi.org/10.1038/s41568-021-00365-x

De Micheli, A. J., Laurilliard, E. J., Heinke, C. L., Ravichandran, H., Fraczek, P., Soueid-Baumgarten, S., De Vlaminck, I., Elemento, O., & Cosgrove, B. D. (2020). Single-Cell Analysis of the Muscle Stem Cell Hierarchy Identifies Heterotypic Communication Signals Involved in Skeletal Muscle Regeneration. *Cell Reports*, *30*(10), 3583-3595.e5. https://doi.org/10.1016/j.celrep.2020.02.067

De Ruysscher, D., Niedermann, G., Burnet, N. G., Siva, S., Lee, A. W. M., & Hegi-Johnson, F. (2019). Radiotherapy toxicity. *Nature Reviews. Disease Primers*, *5*(1), 13. https://doi.org/10.1038/s41572-019-0064-5

Deasy, B. M., Schugar, R. C., & Huard, J. (2008). Sex differences in muscle-derived stem cells and skeletal muscle. *Critical Reviews in Eukaryotic Gene Expression*, *18*(2), 173–188. https://doi.org/10.1615/critreveukargeneexpr.v18.i2.60

Debela, D. T., Muzazu, S. G., Heraro, K. D., Ndalama, M. T., Mesele, B. W., Haile, D. C., Kitui, S. K., & Manyazewal, T. (2021). New approaches and procedures for cancer

treatment: Current perspectives. *SAGE Open Medicine*, *9*, 20503121211034370. https://doi.org/10.1177/20503121211034366

Dell'Orso, S., Juan, A. H., Ko, K.-D., Naz, F., Perovanovic, J., Gutierrez-Cruz, G., Feng, X., & Sartorelli, V. (2019). Single cell analysis of adult mouse skeletal muscle stem cells in homeostatic and regenerative conditions. *Development (Cambridge, England)*, *146*(12), dev174177. https://doi.org/10.1242/dev.174177

Demaria, M., Ohtani, N., Youssef, S. A., Rodier, F., Toussaint, W., Mitchell, J. R., Laberge, R.-M., Vijg, J., Van Steeg, H., Dollé, M. E. T., Hoeijmakers, J. H. J., de Bruin, A., Hara, E., & Campisi, J. (2014). An Essential Role for Senescent Cells in Optimal Wound Healing through Secretion of PDGF-AA. *Developmental Cell*, *31*(6), 722–733. https://doi.org/10.1016/j.devcel.2014.11.012

D'Souza, D., Roubos, S., Larkin, J., Lloyd, J., Emmons, R., Chen, H., & De Lisio, M. (2019). The Late Effects of Radiation Therapy on Skeletal Muscle Morphology and Progenitor Cell Content are Influenced by Diet-Induced Obesity and Exercise Training in Male Mice. *Scientific Reports*, *9*(1), 6691. https://doi.org/10.1038/s41598-019-43204-8

Dungan, C. M., Murach, K. A., Frick, K. K., Jones, S. R., Crow, S. E., Englund, D. A., Vechetti, I. J., Figueiredo, V. C., Levitan, B. M., Satin, J., McCarthy, J. J., & Peterson, C. A. (2019). Elevated myonuclear density during skeletal muscle hypertrophy in response to training is reversed during detraining. *American Journal of Physiology. Cell Physiology*, *316*(5), C649–C654. https://doi.org/10.1152/ajpcell.00050.2019

Ehnman, M., Missiaglia, E., Folestad, E., Selfe, J., Strell, C., Thway, K., Brodin, B., Pietras, K., Shipley, J., Östman, A., & Eriksson, U. (2013). Distinct effects of ligand-induced PDGFRα and PDGFRβ signaling in the human rhabdomyosarcoma tumor cell and stroma cell compartments. *Cancer Research*, *73*(7), 2139–2149. https://doi.org/10.1158/0008-5472.CAN-12-1646

Ejaz, A., Greenberger, J. S., & Rubin, P. J. (2019). Understanding the mechanism of radiation induced fibrosis and therapy options. *Pharmacology & Therapeutics*, *204*, 107399. https://doi.org/10.1016/j.pharmthera.2019.107399

Englund, D. A., Figueiredo, V. C., Dungan, C. M., Murach, K. A., Peck, B. D., Petrosino, J. M., Brightwell, C. R., Dupont, A. M., Neal, A. C., Fry, C. S., Accornero, F., McCarthy, J. J., & Peterson, C. A. (2021). Satellite Cell Depletion Disrupts Transcriptional Coordination and Muscle Adaptation to Exercise. *Function (Oxford, England)*, *2*(1), zqaa033. https://doi.org/10.1093/function/zqaa033

Fan, Z., Turiel, G., Ardicoglu, R., Ghobrial, M., Masschelein, E., Kocijan, T., Zhang, J., Tan, G., Fitzgerald, G., Gorski, T., Alvarado-Diaz, A., Gilardoni, P., Adams, C. M., Ghesquière, B., & De Bock, K. (2021). Exercise-induced angiogenesis is dependent on metabolically primed ATF3/4+ endothelial cells. *Cell Metabolism*, *33*(9), 1793-1807.e9. https://doi.org/10.1016/j.cmet.2021.07.015

Farup, J., De Lisio, M., Rahbek, S. K., Bjerre, J., Vendelbo, M. H., Boppart, M. D., & Vissing, K. (2015). Pericyte response to contraction mode-specific resistance exercise training in human skeletal muscle. *Journal of Applied Physiology (Bethesda, Md.: 1985)*, *119*(10), 1053–1063. https://doi.org/10.1152/japplphysiol.01108.2014

Farup, J., Just, J., de Paoli, F., Lin, L., Jensen, J. B., Billeskov, T., Roman, I. S., Cömert, C., Møller, A. B., Madaro, L., Groppa, E., Fred, R. G., Kampmann, U., Gormsen, L. C., Pedersen, S. B., Bross, P., Stevnsner, T., Eldrup, N., Pers, T. H., … Jessen, N. (2021). Human skeletal muscle CD90+ fibro-adipogenic progenitors are associated with muscle degeneration in type 2 diabetic patients. *Cell Metabolism*, *33*(11), 2201-2214.e11. https://doi.org/10.1016/j.cmet.2021.10.001

Fielder, E., Weigand, M., Agneessens, J., Griffin, B., Parker, C., Miwa, S., & von Zglinicki, T. (2019). Sublethal whole-body irradiation causes progressive premature frailty in mice. *Mechanisms of Ageing and Development*, *180*, 63–69. https://doi.org/10.1016/j.mad.2019.03.006

Fortino, S. A., Wageh, M., Pontello, R., McGlory, C., Kumbhare, D., Phillips, S. M., & Parise, G. (2022). Sex-Based Differences in the Myogenic Response and Inflammatory Gene Expression Following Eccentric Contractions in Humans. *Frontiers in Physiology*, *13*. https://www.frontiersin.org/articles/10.3389/fphys.2022.880625

Frantz, C., Stewart, K. M., & Weaver, V. M. (2010). The extracellular matrix at a glance. *Journal of Cell Science*, *123*(24), 4195–4200. https://doi.org/10.1242/jcs.023820

Garcia, D. O., & Thomson, C. A. (2014). Physical Activity and Cancer Survivorship. *Nutrition in Clinical Practice : Official Publication of the American Society for Parenteral and Enteral Nutrition*, *29*(6), 768–779. https://doi.org/10.1177/0884533614551969

Gawade, P. L., Hudson, M. M., Kaste, S. C., Neglia, J. P., Wasilewski-Masker, K., Constine, L. S., Robison, L. L., & Ness, K. K. (2014). A systematic review of

selected musculoskeletal late effects in survivors of childhood cancer. *Current Pediatric Reviews*, *10*(4), 249–262. https://doi.org/10.2174/1573400510666141114223827

Gazoti Debessa, C. R., Mesiano Maifrino, L. B., & Rodrigues de Souza, R. (2001). Age related changes of the collagen network of the human heart. *Mechanisms of Ageing and Development*, *122*(10), 1049–1058. https://doi.org/10.1016/s0047-6374(01)00238-x

Girardi, F., Taleb, A., Ebrahimi, M., Datye, A., Gamage, D. G., Peccate, C., Giordani, L., Millay, D. P., Gilbert, P. M., Cadot, B., & Le Grand, F. (2021). TGFβ signaling curbs cell fusion and muscle regeneration. *Nature Communications*, *12*(1), Article 1. https://doi.org/10.1038/s41467-020-20289-8

Giuliani, G., Rosina, M., & Reggio, A. (2021). Signaling pathways regulating the fate of fibro/adipogenic progenitors (FAPs) in skeletal muscle regeneration and disease. *The FEBS Journal*. https://doi.org/10.1111/febs.16080

Goldstein, M., & Kastan, M. B. (2015). The DNA damage response: Implications for tumor responses to radiation and chemotherapy. *Annual Review of Medicine*, *66*, 129–143. https://doi.org/10.1146/annurev-med-081313-121208

Gonzalez, D., Contreras, O., Rebolledo, D. L., Espinoza, J. P., van Zundert, B., & Brandan, E. (2017). ALS skeletal muscle shows enhanced TGF-β signaling, fibrosis and induction of fibro/adipogenic progenitor markers. *PloS One*, *12*(5), e0177649. https://doi.org/10.1371/journal.pone.0177649

Gschwandtner, M., Derler, R., & Midwood, K. S. (2019). More Than Just Attractive: How CCL2 Influences Myeloid Cell Behavior Beyond Chemotaxis. *Frontiers in Immunology*, *10*. https://www.frontiersin.org/articles/10.3389/fimmu.2019.02759

Hardee, J. P., Puppa, M. J., Fix, D. K., Gao, S., Hetzler, K. L., Bateman, T. A., & Carson, J. A. (2014). The effect of radiation dose on mouse skeletal muscle remodeling. *Radiology and Oncology*, *48*(3), 247–256. https://doi.org/10.2478/raon-2014-0025

Heredia, J. E., Mukundan, L., Chen, F. M., Mueller, A. A., Deo, R. C., Locksley, R. M., Rando, T. A., & Chawla, A. (2013). Type 2 innate signals stimulate fibro/adipogenic progenitors to facilitate muscle regeneration. *Cell*, *153*(2), 376–388. https://doi.org/10.1016/j.cell.2013.02.053

Herrera, J., Henke, C. A., & Bitterman, P. B. (2018). Extracellular matrix as a driver of progressive fibrosis. *The Journal of Clinical Investigation*, *128*(1), 45–53. https://doi.org/10.1172/JCI93557

Hettmer, S., & Wagers, A. J. (2010). Muscling in: Uncovering the origins of rhabdomyosarcoma. *Nature Medicine*, *16*(2), 171–173. https://doi.org/10.1038/nm0210-171

Hjorth, M., Norheim, F., Meen, A. J., Pourteymour, S., Lee, S., Holen, T., Jensen, J., Birkeland, K. I., Martinov, V. N., Langleite, T. M., Eckardt, K., Drevon, C. A., & Kolset, S. O. (2015). The effect of acute and long-term physical activity on extracellular matrix and serglycin in human skeletal muscle. *Physiological Reports*, *3*(8), e12473. https://doi.org/10.14814/phy2.12473

Hoeft, K., Schaefer, G. J. L., Kim, H., Schumacher, D., Bleckwehl, T., Long, Q., Klinkhammer, B. M., Peisker, F., Koch, L., Nagai, J., Halder, M., Ziegler, S., Liehn,

E., Kuppe, C., Kranz, J., Menzel, S., Costa, I., Wahida, A., Boor, P., … Kramann, R. (2023). Platelet-instructed SPP1+ macrophages drive myofibroblast activation in fibrosis in a CXCL4-dependent manner. *Cell Reports*, *42*(2), 112131. https://doi.org/10.1016/j.celrep.2023.112131

Hogarth, M. W., Defour, A., Lazarski, C., Gallardo, E., Diaz Manera, J., Partridge, T. A., Nagaraju, K., & Jaiswal, J. K. (2019). Fibroadipogenic progenitors are responsible for muscle loss in limb girdle muscular dystrophy 2B. *Nature Communications*, *10*(1), 2430. https://doi.org/10.1038/s41467-019-10438-z

Hou, J., Shi, J., Chen, L., Lv, Z., Chen, X., Cao, H., Xiang, Z., & Han, X. (2018). M2 macrophages promote myofibroblast differentiation of LR-MSCs and are associated with pulmonary fibrogenesis. *Cell Communication and Signaling: CCS*, *16*(1), 89. https://doi.org/10.1186/s12964-018-0300-8

Hovi, L., Era, P., Rautonen, J., & Siimes, M. A. (1993). Impaired muscle strength in female adolescents and young adults surviving leukemia in childhood. *Cancer*, *72*(1), 276–281. https://doi.org/10.1002/1097-0142(19930701)72:1<276::aid-cncr2820720148>3.0.co;2-2

Hu, H.-H., Chen, D.-Q., Wang, Y.-N., Feng, Y.-L., Cao, G., Vaziri, N. D., & Zhao, Y.-Y. (2018). New insights into TGF-β/Smad signaling in tissue fibrosis. *Chemico-Biological Interactions*, *292*, 76–83. https://doi.org/10.1016/j.cbi.2018.07.008

Hu, M., Yao, Z., Xu, L., Peng, M., Deng, G., Liu, L., Jiang, X., & Cai, X. (2023). M2 macrophage polarization in systemic sclerosis fibrosis: Pathogenic mechanisms and therapeutic effects. *Heliyon*, *9*(5), e16206. https://doi.org/10.1016/j.heliyon.2023.e16206

Hughes, D. C., Ellefsen, S., & Baar, K. (2018). Adaptations to Endurance and Strength Training. *Cold Spring Harbor Perspectives in Medicine*, *8*(6), a029769. https://doi.org/10.1101/cshperspect.a029769

Ieronimakis, N., Hays, A., Prasad, A., Janebodin, K., Duffield, J. S., & Reyes, M. (2016). PDGFRα signalling promotes fibrogenic responses in collagen-producing cells in Duchenne muscular dystrophy. *The Journal of Pathology*, *240*(4), 410–424. https://doi.org/10.1002/path.4801

Ismaeel, A., Holmes, M., Papoutsi, E., Panton, L., & Koutakis, P. (2019). Resistance Training, Antioxidant Status, and Antioxidant Supplementation. *International Journal of Sport Nutrition and Exercise Metabolism*, *29*(5), 539–547. https://doi.org/10.1123/ijsnem.2018-0339

Jabłońska-Trypuć, A., Matejczyk, M., & Rosochacki, S. (2016). Matrix metalloproteinases (MMPs), the main extracellular matrix (ECM) enzymes in collagen degradation, as a target for anticancer drugs. *Journal of Enzyme Inhibition and Medicinal Chemistry*, *31*(sup1), 177–183. https://doi.org/10.3109/14756366.2016.1161620

Joe, A. W. B., Yi, L., Natarajan, A., Le Grand, F., So, L., Wang, J., Rudnicki, M. A., & Rossi, F. M. V. (2010). Muscle injury activates resident fibro/adipogenic progenitors that facilitate myogenesis. *Nature Cell Biology*, *12*(2), 153–163. https://doi.org/10.1038/ncb2015

Juban, G., Saclier, M., Yacoub-Youssef, H., Kernou, A., Arnold, L., Boisson, C., Ben Larbi, S., Magnan, M., Cuvellier, S., Théret, M., Petrof, B. J., Desguerre, I., Gondin, J., Mounier, R., & Chazaud, B. (2018). AMPK Activation Regulates LTBP4-Dependent TGF-β1 Secretion by Pro-inflammatory Macrophages and Controls

Fibrosis in Duchenne Muscular Dystrophy. *Cell Reports*, *25*(8), 2163-2176.e6. https://doi.org/10.1016/j.celrep.2018.10.077

Judge, S. M., Nosacka, R. L., Delitto, D., Gerber, M. H., Cameron, M. E., Trevino, J. G., & Judge, A. R. (2018). Skeletal Muscle Fibrosis in Pancreatic Cancer Patients with Respect to Survival. *JNCI Cancer Spectrum*, *2*(3), pky043. https://doi.org/10.1093/jncics/pky043

Kallenbach, J. G., Bachman, J. F., Paris, N. D., Blanc, R. S., O'Connor, T., Furati, E., Williams, J. P., & Chakkalakal, J. V. (2022). Muscle-specific functional deficits and lifelong fibrosis in response to paediatric radiotherapy and tumour elimination. *Journal of Cachexia, Sarcopenia and Muscle*, *13*(1), 296–310. https://doi.org/10.1002/jcsm.12902

Kang, X., Yang, M.-Y., Shi, Y.-X., Xie, M.-M., Zhu, M., Zheng, X.-L., Zhang, C.-K., Ge, Z.-L., Bian, X.-T., Lv, J.-T., Wang, Y.-J., Zhou, B.-H., & Tang, K.-L. (2018). Interleukin-15 facilitates muscle regeneration through modulation of fibro/adipogenic progenitors. *Cell Communication and Signaling: CCS*, *16*(1), 42. https://doi.org/10.1186/s12964-018-0251-0

Karsdal, M. A., Nielsen, S. H., Leeming, D. J., Langholm, L. L., Nielsen, M. J., Manon-Jensen, T., Siebuhr, A., Gudmann, N. S., Rønnow, S., Sand, J. M., Daniels, S. J., Mortensen, J. H., & Schuppan, D. (2017). The good and the bad collagens of fibrosis—Their role in signaling and organ function. *Advanced Drug Delivery Reviews*, *121*, 43–56. https://doi.org/10.1016/j.addr.2017.07.014

Kastenschmidt, J. M., Coulis, G., Farahat, P. K., Pham, P., Rios, R., Cristal, T. T., Mannaa, A. H., Ayer, R. E., Yahia, R., Deshpande, A. A., Hughes, B. S., Savage,

A. K., Giesige, C. R., Harper, S. Q., Locksley, R. M., Mozaffar, T., & Villalta, S. A. (2021). A stromal progenitor and ILC2 niche promotes muscle eosinophilia and fibrosis-associated gene expression. *Cell Reports*, *35*(2), 108997. https://doi.org/10.1016/j.celrep.2021.108997

Keller, C., & Guttridge, D. C. (2013). Mechanisms of impaired differentiation in rhabdomyosarcoma. *The FEBS Journal*, *280*(17), 4323–4334. https://doi.org/10.1111/febs.12421

Klingberg, F., Hinz, B., & White, E. S. (2013). The myofibroblast matrix: Implications for tissue repair and fibrosis. *The Journal of Pathology*, *229*(2), 298–309. https://doi.org/10.1002/path.4104

Koster, R., di Pietro, A., Timmer-Bosscha, H., Gibcus, J. H., van den Berg, A., Suurmeijer, A. J., Bischoff, R., Gietema, J. A., & de Jong, S. (2010). Cytoplasmic p21 expression levels determine cisplatin resistance in human testicular cancer. *The Journal of Clinical Investigation*, *120*(10), 3594–3605. https://doi.org/10.1172/JCI41939

Kowal, K., Silver, R., Sławińska, E., Bielecki, M., Chyczewski, L., & Kowal-Bielecka, O. (2011). CD163 and its role in inflammation. *Folia Histochemica Et Cytobiologica*, *49*(3), 365–374. https://doi.org/10.5603/fhc.2011.0052

Krasniewski, L. K., Chakraborty, P., Cui, C.-Y., Mazan-Mamczarz, K., Dunn, C., Piao, Y., Fan, J., Shi, C., Wallace, T., Nguyen, C., Rathbun, I. A., Munk, R., Tsitsipatis, D., De, S., Sen, P., Ferrucci, L., & Gorospe, M. (2022). Single-cell analysis of skeletal muscle macrophages reveals age-associated functional subpopulations. *ELife*, *11*, e77974. https://doi.org/10.7554/eLife.77974

Kuswanto, W., Burzyn, D., Panduro, M., Wang, K. K., Jang, Y. C., Wagers, A. J., Benoist, C., & Mathis, D. (2016). Poor Repair of Skeletal Muscle in Aging Mice Reflects a Defect in Local, Interleukin-33-Dependent Accumulation of Regulatory T Cells. *Immunity*, *44*(2), 355–367. https://doi.org/10.1016/j.immuni.2016.01.009

Lamarche, É., Lala-Tabbert, N., Gunanayagam, A., St-Louis, C., & Wiper-Bergeron, N. (2015). Retinoic acid promotes myogenesis in myoblasts by antagonizing transforming growth factor-beta signaling via C/EBPβ. *Skeletal Muscle*, *5*(1), 8. https://doi.org/10.1186/s13395-015-0032-z

Leinroth, A. P., Mirando, A. J., Rouse, D., Kobayahsi, Y., Tata, P. R., Rueckert, H. E., Liao, Y., Long, J. T., Chakkalakal, J. V., & Hilton, M. J. (2022). Identification of distinct non-myogenic skeletal-muscle-resident mesenchymal cell populations. *Cell Reports*, *39*(6), 110785. https://doi.org/10.1016/j.celrep.2022.110785

Lemos, D. R., Babaeijandaghi, F., Low, M., Chang, C.-K., Lee, S. T., Fiore, D., Zhang, R.-H., Natarajan, A., Nedospasov, S. A., & Rossi, F. M. V. (2015). Nilotinib reduces muscle fibrosis in chronic muscle injury by promoting TNF-mediated apoptosis of fibro/adipogenic progenitors. *Nature Medicine*, *21*(7), 786–794. https://doi.org/10.1038/nm.3869

Leonard, A. K., Loughran, E. A., Klymenko, Y., Liu, Y., Kim, O., Asem, M., McAbee, K., Ravosa, M. J., & Sharon Stack, M. (2018). Methods for the visualization and analysis of extracellular matrix protein structure and degradation. *Methods in Cell Biology*, *143*, 79–95. https://doi.org/10.1016/bs.mcb.2017.08.005

Lepper, C., Partridge, T. A., & Fan, C.-M. (2011). An absolute requirement for Pax7-positive satellite cells in acute injury-induced skeletal muscle regeneration.

Development (Cambridge, England), *138*(17), 3639–3646. https://doi.org/10.1242/dev.067595

Lian, X., Bond, J. S., Bharathy, N., Boudko, S. P., Pokidysheva, E., Shern, J. F., Lathara, M., Sasaki, T., Settelmeyer, T., Cleary, M. M., Bajwa, A., Srinivasa, G., Hartley, C. P., Bächinger, H. P., Mansoor, A., Gultekin, S. H., Berlow, N. E., & Keller, C. (2021). Defining the Extracellular Matrix of Rhabdomyosarcoma. *Frontiers in Oncology*, *11*, 601957. https://doi.org/10.3389/fonc.2021.601957

Lieber, M. R. (2010). The mechanism of double-strand DNA break repair by the nonhomologous DNA end-joining pathway. *Annual Review of Biochemistry*, *79*, 181–211. https://doi.org/10.1146/annurev.biochem.052308.093131

Liu, D., Black, B. L., & Derynck, R. (2001). TGF-β inhibits muscle differentiation through functional repression of myogenic transcription factors by Smad3. *Genes & Development*, *15*(22), 2950–2966. https://doi.org/10.1101/gad.925901

Lukjanenko, L., Karaz, S., Stuelsatz, P., Gurriaran-Rodriguez, U., Michaud, J., Dammone, G., Sizzano, F., Mashinchian, O., Ancel, S., Migliavacca, E., Liot, S., Jacot, G., Metairon, S., Raymond, F., Descombes, P., Palini, A., Chazaud, B., Rudnicki, M. A., Bentzinger, C. F., & Feige, J. N. (2019). Aging Disrupts Muscle Stem Cell Function by Impairing Matricellular WISP1 Secretion from Fibro-Adipogenic Progenitors. *Cell Stem Cell*, *24*(3), 433-446.e7. https://doi.org/10.1016/j.stem.2018.12.014

Mack, M. (2018). Inflammation and fibrosis. *Matrix Biology*, *68–69*, 106–121. https://doi.org/10.1016/j.matbio.2017.11.010

Mahdy, M. A. A. (2019). Skeletal muscle fibrosis: An overview. *Cell and Tissue Research*, *375*(3), 575–588. https://doi.org/10.1007/s00441-018-2955-2

Malecova, B., Gatto, S., Etxaniz, U., Passafaro, M., Cortez, A., Nicoletti, C., Giordani, L., Torcinaro, A., De Bardi, M., Bicciato, S., De Santa, F., Madaro, L., & Puri, P. L. (2018). Dynamics of cellular states of fibro-adipogenic progenitors during myogenesis and muscular dystrophy. *Nature Communications*, *9*(1), 3670. https://doi.org/10.1038/s41467-018-06068-6

Mansour, M. A., Rahman, M., Ayad, A. A., Warrington, A. E., & Burns, T. C. (2023). P21 Overexpression Promotes Cell Death and Induces Senescence in Human Glioblastoma. *Cancers*, *15*(4), Article 4. https://doi.org/10.3390/cancers15041279

Martin, M., Lefaix, J.-L., & Delanian, S. (2000). TGF-β1 and radiation fibrosis: A master switch and a specific therapeutic target? *International Journal of Radiation Oncology, Biology, Physics*, *47*(2), 277–290. https://doi.org/10.1016/S0360-3016(00)00435-1

Masschelein, E., D'Hulst, G., Zvick, J., Hinte, L., Soro-Arnaiz, I., Gorski, T., von Meyenn, F., Bar-Nur, O., & De Bock, K. (2020). Exercise promotes satellite cell contribution to myofibers in a load-dependent manner. *Skeletal Muscle*, *10*(1), 21. https://doi.org/10.1186/s13395-020-00237-2

Mauro, A. (1961). Satellite cell of skeletal muscle fibers. *The Journal of Biophysical and Biochemical Cytology*, *9*, 493–495. https://doi.org/10.1083/jcb.9.2.493

McKellar, D. W., Walter, L. D., Song, L. T., Mantri, M., Wang, M. F. Z., De Vlaminck, I., & Cosgrove, B. D. (2021). Large-scale integration of single-cell transcriptomic data captures transitional progenitor states in mouse skeletal muscle regeneration.

Communications Biology, *4*(1), Article 1. https://doi.org/10.1038/s42003-021-02810-x

Melendez, J., Sieiro, D., Salgado, D., Morin, V., Dejardin, M.-J., Zhou, C., Mullen, A. C., & Marcelle, C. (2021). TGFβ signalling acts as a molecular brake of myoblast fusion. *Nature Communications*, *12*(1), Article 1. https://doi.org/10.1038/s41467-020-20290-1

Miller, K. D., Nogueira, L., Mariotto, A. B., Rowland, J. H., Yabroff, K. R., Alfano, C. M., Jemal, A., Kramer, J. L., & Siegel, R. L. (2019). Cancer treatment and survivorship statistics, 2019. *CA: A Cancer Journal for Clinicians*, *69*(5), 363–385. https://doi.org/10.3322/caac.21565

Moore, B. B., Paine, R., III, Christensen, P. J., Moore, T. A., Sitterding, S., Ngan, R., Wilke, C. A., Kuziel, W. A., & Toews, G. B. (2001). Protection from Pulmonary Fibrosis in the Absence of CCR2 Signaling1. *The Journal of Immunology*, *167*(8), 4368–4377. https://doi.org/10.4049/jimmunol.167.8.4368

Moratal, C., Raffort, J., Arrighi, N., Rekima, S., Schaub, S., Dechesne, C. A., Chinetti, G., & Dani, C. (2018). IL-1β- and IL-4-polarized macrophages have opposite effects on adipogenesis of intramuscular fibro-adipogenic progenitors in humans. *Scientific Reports*, *8*(1), 17005. https://doi.org/10.1038/s41598-018-35429-w

Morgunova, G. V., Kolesnikov, A. V., Klebanov, A. A., & Khokhlov, A. N. (2015). Senescence-associated β-galactosidase—A biomarker of aging, DNA damage, or cell proliferation restriction? *Moscow University Biological Sciences Bulletin*, *70*(4), 165–167. https://doi.org/10.3103/S0096392515040082

Murach, K. A., Fry, C. S., Dupont-Versteegden, E. E., McCarthy, J. J., & Peterson, C. A. (2021). Fusion and beyond: Satellite cell contributions to loading-induced skeletal muscle adaptation. *FASEB Journal: Official Publication of the Federation of American Societies for Experimental Biology*, *35*(10), e21893. https://doi.org/10.1096/fj.202101096R

Mustian, K. M., Sprod, L. K., Janelsins, M., Peppone, L. J., & Mohile, S. (2012). Exercise Recommendations for Cancer-Related Fatigue, Cognitive Impairment, Sleep problems, Depression, Pain, Anxiety, and Physical Dysfunction: A Review. *Oncology & Hematology Review*, *8*(2), 81–88.

Ness, K. K., Hudson, M. M., Ginsberg, J. P., Nagarajan, R., Kaste, S. C., Marina, N., Whitton, J., Robison, L. L., & Gurney, J. G. (2009). Physical Performance Limitations in the Childhood Cancer Survivor Study Cohort. *Journal of Clinical Oncology*, *27*(14), 2382–2389. https://doi.org/10.1200/JCO.2008.21.1482

Novotny, L., & Szekeres, T. (2003). Cancer therapy: New targets for chemotherapy. *Hematology (Amsterdam, Netherlands)*, *8*(3), 129–137. https://doi.org/10.1080/1024533031000112257

Oeffinger, K. C., & Hudson, M. M. (2004). Long-term complications following childhood and adolescent cancer: Foundations for providing risk-based health care for survivors. *CA: A Cancer Journal for Clinicians*, *54*(4), 208–236. https://doi.org/10.3322/canjclin.54.4.208

Oeffinger, K. C., Mertens, A. C., Sklar, C. A., Kawashima, T., Hudson, M. M., Meadows, A. T., Friedman, D. L., Marina, N., Hobbie, W., Kadan-Lottick, N. S., Schwartz, C. L., Leisenring, W., Robison, L. L., & Childhood Cancer Survivor Study. (2006).

Chronic health conditions in adult survivors of childhood cancer. *The New England Journal of Medicine*, *355*(15), 1572–1582. https://doi.org/10.1056/NEJMsa060185

Ohtani, N. (2022). The roles and mechanisms of senescence-associated secretory phenotype (SASP): Can it be controlled by senolysis? *Inflammation and Regeneration*, *42*(1), 11. https://doi.org/10.1186/s41232-022-00197-8

Oprescu, S. N., Yue, F., Qiu, J., Brito, L. F., & Kuang, S. (2020). Temporal Dynamics and Heterogeneity of Cell Populations during Skeletal Muscle Regeneration. *IScience*, *23*(4), 100993. https://doi.org/10.1016/j.isci.2020.100993

Pakshir, P., Noskovicova, N., Lodyga, M., Son, D. O., Schuster, R., Goodwin, A., Karvonen, H., & Hinz, B. (2020). The myofibroblast at a glance. *Journal of Cell Science*, *133*(13), jcs227900. https://doi.org/10.1242/jcs.227900

Paris, N. D., Kallenbach, J. G., Bachman, J. F., Blanc, R. S., Johnston, C. J., Hernady, E., Williams, J. P., & Chakkalakal, J. V. (2020). Chemoradiation impairs myofiber hypertrophic growth in a pediatric tumor model. *Scientific Reports*, *10*(1), Article 1. https://doi.org/10.1038/s41598-020-75913-w

Paulino, A. C. (2004). Late effects of radiotherapy for pediatric extremity sarcomas. *International Journal of Radiation Oncology, Biology, Physics*, *60*(1), 265–274. https://doi.org/10.1016/j.ijrobp.2004.02.001

Peck, B. D., Murach, K. A., Walton, R. G., Simmons, A. J., Long, D. E., Kosmac, K., Dungan, C. M., Kern, P. A., Bamman, M. M., & Peterson, C. A. (2022). A muscle cell-macrophage axis involving matrix metalloproteinase 14 facilitates extracellular matrix remodeling with mechanical loading. *FASEB Journal: Official Publication of*

the Federation of American Societies for Experimental Biology, *36*(2), e22155. https://doi.org/10.1096/fj.202100182RR

Piersma, B., Bank, R. A., & Boersema, M. (2015). Signaling in Fibrosis: TGF-β, WNT, and YAP/TAZ Converge. *Frontiers in Medicine*, *2*. https://www.frontiersin.org/articles/10.3389/fmed.2015.00059

Pillon, N. J., Gabriel, B. M., Dollet, L., Smith, J. A. B., Sardón Puig, L., Botella, J., Bishop, D. J., Krook, A., & Zierath, J. R. (2020). Transcriptomic profiling of skeletal muscle adaptations to exercise and inactivity. *Nature Communications*, *11*(1), 470. https://doi.org/10.1038/s41467-019-13869-w

Poole, J. J. A., & Mostaço-Guidolin, L. B. (2021). Optical Microscopy and the Extracellular Matrix Structure: A Review. *Cells*, *10*(7), 1760. https://doi.org/10.3390/cells10071760

Preussner, J., Zhong, J., Sreenivasan, K., Günther, S., Engleitner, T., Künne, C., Glatzel, M., Rad, R., Looso, M., Braun, T., & Kim, J. (2018). Oncogenic Amplification of Zygotic Dux Factors in Regenerating p53-Deficient Muscle Stem Cells Defines a Molecular Cancer Subtype. *Cell Stem Cell*, *23*(6), 794-805.e4. https://doi.org/10.1016/j.stem.2018.10.011

Pulumati, A., Pulumati, A., Dwarakanath, B. S., Verma, A., & Papineni, R. V. L. (2023). Technological advancements in cancer diagnostics: Improvements and limitations. *Cancer Reports*, *6*(2), e1764. https://doi.org/10.1002/cnr2.1764

Roberson, R. S., Kussick, S. J., Vallieres, E., Chen, S.-Y. J., & Wu, D. Y. (2005). Escape from therapy-induced accelerated cellular senescence in p53-null lung cancer cells

and in human lung cancers. *Cancer Research*, *65*(7), 2795–2803. https://doi.org/10.1158/0008-5472.CAN-04-1270

Roos, W. P., Thomas, A. D., & Kaina, B. (2016). DNA damage and the balance between survival and death in cancer biology. *Nature Reviews. Cancer*, *16*(1), 20–33. https://doi.org/10.1038/nrc.2015.2

Rosenblatt, J. D., & Parry, D. J. (1992). Gamma irradiation prevents compensatory hypertrophy of overloaded mouse extensor digitorum longus muscle. *Journal of Applied Physiology (Bethesda, Md.: 1985)*, *73*(6), 2538–2543. https://doi.org/10.1152/jappl.1992.73.6.2538

Rubenstein, A. B., Smith, G. R., Raue, U., Begue, G., Minchev, K., Ruf-Zamojski, F., Nair, V. D., Wang, X., Zhou, L., Zaslavsky, E., Trappe, T. A., Trappe, S., & Sealfon, S. C. (2020). Single-cell transcriptional profiles in human skeletal muscle. *Scientific Reports*, *10*(1), 229. https://doi.org/10.1038/s41598-019-57110-6

Sakai, H., Sagara, A., Arakawa, K., Sugiyama, R., Hirosaki, A., Takase, K., Jo, A., Sato, K., Chiba, Y., Yamazaki, M., Matoba, M., & Narita, M. (2014). Mechanisms of cisplatin-induced muscle atrophy. *Toxicology and Applied Pharmacology*, *278*(2), 190–199. https://doi.org/10.1016/j.taap.2014.05.001

Saleh, K. K., Xi, H., Switzler, C., Skuratovsky, E., Romero, M. A., Chien, P., Gibbs, D., Gane, L., Hicks, M. R., Spencer, M. J., & Pyle, A. D. (2022). Single cell sequencing maps skeletal muscle cellular diversity as disease severity increases in dystrophic mouse models. *IScience*, *25*(11), 105415. https://doi.org/10.1016/j.isci.2022.105415

Santini, M. P., Malide, D., Hoffman, G., Pandey, G., D'Escamard, V., Nomura-Kitabayashi, A., Rovira, I., Kataoka, H., Ochando, J., Harvey, R. P., Finkel, T., & Kovacic, J. C. (2020). Tissue-Resident PDGFRα+ Progenitor Cells Contribute to Fibrosis versus Healing in a Context- and Spatiotemporally Dependent Manner. *Cell Reports*, *30*(2), 555-570.e7. https://doi.org/10.1016/j.celrep.2019.12.045

Sattar, S., Alibhai, S. M. H., Fitch, M., Krzyzanowska, M., Leighl, N., & Puts, M. T. E. (2018). Chemotherapy and radiation treatment decision-making experiences of older adults with cancer: A qualitative study. *Journal of Geriatric Oncology*, *9*(1), 47–52. https://doi.org/10.1016/j.jgo.2017.07.013

Saul, D., Kosinsky, R. L., Atkinson, E. J., Doolittle, M. L., Zhang, X., LeBrasseur, N. K., Pignolo, R. J., Robbins, P. D., Niedernhofer, L. J., Ikeno, Y., Jurk, D., Passos, J. F., Hickson, L. J., Xue, A., Monroe, D. G., Tchkonia, T., Kirkland, J. L., Farr, J. N., & Khosla, S. (2022). A new gene set identifies senescent cells and predicts senescence-associated pathways across tissues. *Nature Communications*, *13*(1), 4827. https://doi.org/10.1038/s41467-022-32552-1

Scaramozza, A., Park, D., Kollu, S., Beerman, I., Sun, X., Rossi, D. J., Lin, C. P., Scadden, D. T., Crist, C., & Brack, A. S. (2019). Lineage Tracing Reveals a Subset of Reserve Muscle Stem Cells Capable of Clonal Expansion under Stress. *Cell Stem Cell*, *24*(6), 944-957.e5. https://doi.org/10.1016/j.stem.2019.03.020

Scott, R. W., Arostegui, M., Schweitzer, R., Rossi, F. M. V., & Underhill, T. M. (2019). Hic1 Defines Quiescent Mesenchymal Progenitor Subpopulations with Distinct Functions and Fates in Skeletal Muscle Regeneration. *Cell Stem Cell*, *25*(6), 797-813.e9. https://doi.org/10.1016/j.stem.2019.11.004

Seki, E., De Minicis, S., Inokuchi, S., Taura, K., Miyai, K., Van Rooijen, N., Schwabe, R. F., & Brenner, D. A. (2009). CCR2 promotes hepatic fibrosis in mice. *Hepatology (Baltimore, Md.)*, *50*(1), 185–197. https://doi.org/10.1002/hep.22952

Sharkey, A. M., Carey, A. B., Heise, C. T., & Barber, G. (1993). Cardiac rehabilitation after cancer therapy in children and young adults. *The American Journal of Cardiology*, *71*(16), 1488–1490. https://doi.org/10.1016/0002-9149(93)90625-m

Skapek, S. X., Ferrari, A., Gupta, A. A., Lupo, P. J., Butler, E., Shipley, J., Barr, F. G., & Hawkins, D. S. (2019). Rhabdomyosarcoma. *Nature Reviews. Disease Primers*, *5*(1), 1. https://doi.org/10.1038/s41572-018-0051-2

Stepien, D. M., Hwang, C., Marini, S., Pagani, C. A., Sorkin, M., Visser, N. D., Huber, A. K., Edwards, N. J., Loder, S. J., Vasquez, K., Aguilar, C., Kumar, R., Mascharak, S., Longaker, M. T., Li, J., & Levi, B. (2020). Tuning macrophage phenotype to mitigate skeletal muscle fibrosis: Macrophage and FAP Crosstalk in Muscular Polytrauma. *Journal of Immunology (Baltimore, Md. : 1950)*, *204*(8), 2203–2215. https://doi.org/10.4049/jimmunol.1900814

Stubblefield, M. D. (2011). Radiation fibrosis syndrome: Neuromuscular and musculoskeletal complications in cancer survivors. *PM & R: The Journal of Injury, Function, and Rehabilitation*, *3*(11), 1041–1054. https://doi.org/10.1016/j.pmrj.2011.08.535

Sung, H., Ferlay, J., Siegel, R. L., Laversanne, M., Soerjomataram, I., Jemal, A., & Bray, F. (2021). Global Cancer Statistics 2020: GLOBOCAN Estimates of Incidence and Mortality Worldwide for 36 Cancers in 185 Countries. *CA: A Cancer Journal for Clinicians*, *71*(3), 209–249. https://doi.org/10.3322/caac.21660

Theret, M., Saclier, M., Messina, G., & Rossi, F. M. V. (2022). Macrophages in Skeletal Muscle Dystrophies, An Entangled Partner. *Journal of Neuromuscular Diseases*, *9*(1), 1–23. https://doi.org/10.3233/JND-210737

Thomas, K., Engler, A. J., & Meyer, G. A. (2015). Extracellular matrix regulation in the muscle satellite cell niche. *Connective Tissue Research*, *56*(1), 1–8. https://doi.org/10.3109/03008207.2014.947369

Tisdale, M. J. (2001). Loss of skeletal muscle in cancer: Biochemical mechanisms. *Frontiers in Bioscience: A Journal and Virtual Library*, *6*, D164-174. https://doi.org/10.2741/tisdale

Tong, C. K. W., Lau, B., & Davis, M. K. (2020). Exercise Training for Cancer Survivors. *Current Treatment Options in Oncology*, *21*(7), 53. https://doi.org/10.1007/s11864-020-00752-w

Uezumi, A., Fukada, S., Yamamoto, N., Ikemoto-Uezumi, M., Nakatani, M., Morita, M., Yamaguchi, A., Yamada, H., Nishino, I., Hamada, Y., & Tsuchida, K. (2014). Identification and characterization of PDGFRα+ mesenchymal progenitors in human skeletal muscle. *Cell Death & Disease*, *5*(4), e1186. https://doi.org/10.1038/cddis.2014.161

Uezumi, A., Fukada, S., Yamamoto, N., Takeda, S., & Tsuchida, K. (2010). Mesenchymal progenitors distinct from satellite cells contribute to ectopic fat cell formation in skeletal muscle. *Nature Cell Biology*, *12*(2), 143–152. https://doi.org/10.1038/ncb2014

Uezumi, A., Ikemoto-Uezumi, M., Zhou, H., Kurosawa, T., Yoshimoto, Y., Nakatani, M., Hitachi, K., Yamaguchi, H., Wakatsuki, S., Araki, T., Morita, M., Yamada, H.,

Toyoda, M., Kanazawa, N., Nakazawa, T., Hino, J., Fukada, S.-I., & Tsuchida, K. (2021). Mesenchymal Bmp3b expression maintains skeletal muscle integrity and decreases in age-related sarcopenia. *The Journal of Clinical Investigation*, *131*(1), 139617. https://doi.org/10.1172/JCI139617

Uezumi, A., Ito, T., Morikawa, D., Shimizu, N., Yoneda, T., Segawa, M., Yamaguchi, M., Ogawa, R., Matev, M. M., Miyagoe-Suzuki, Y., Takeda, S., Tsujikawa, K., Tsuchida, K., Yamamoto, H., & Fukada, S. (2011). Fibrosis and adipogenesis originate from a common mesenchymal progenitor in skeletal muscle. *Journal of Cell Science*, *124*(Pt 21), 3654–3664. https://doi.org/10.1242/jcs.086629

Vallecillo-García, P., Orgeur, M., Vom Hofe-Schneider, S., Stumm, J., Kappert, V., Ibrahim, D. M., Börno, S. T., Hayashi, S., Relaix, F., Hildebrandt, K., Sengle, G., Koch, M., Timmermann, B., Marazzi, G., Sassoon, D. A., Duprez, D., & Stricker, S. (2017). Odd skipped-related 1 identifies a population of embryonic fibro-adipogenic progenitors regulating myogenesis during limb development. *Nature Communications*, *8*(1), 1218. https://doi.org/10.1038/s41467-017-01120-3

Vallejos, C. A. (2019). Exploring a world of a thousand dimensions. *Nature Biotechnology*, *37*(12), Article 12. https://doi.org/10.1038/s41587-019-0330-9

Venosa, A., Cowman, S., Katzen, J., Tomer, Y., Armstrong, B. S., Mulugeta, S., & Beers, M. F. (2021). Role of CCR2+ Myeloid Cells in Inflammation Responses Driven by Expression of a Surfactant Protein-C Mutant in the Alveolar Epithelium. *Frontiers in Immunology*, *12*. https://www.frontiersin.org/articles/10.3389/fimmu.2021.665818

Vignard, J., Mirey, G., & Salles, B. (2013). Ionizing-radiation induced DNA double-strand breaks: A direct and indirect lighting up. *Radiotherapy and Oncology*, *108*(3), 362–369. https://doi.org/10.1016/j.radonc.2013.06.013

Voyant, C., Julian, D., Roustit, R., Biffi, K., & Lantieri, C. (2014). Biological effects and equivalent doses in radiotherapy: A software solution. *Reports of Practical Oncology and Radiotherapy: Journal of Greatpoland Cancer Center in Poznan and Polish Society of Radiation Oncology*, *19*(1), 47–55. https://doi.org/10.1016/j.rpor.2013.08.004

Wang, J., Xu, Z., Wang, Z., Du, G., & Lun, L. (2021). TGF-beta signaling in cancer radiotherapy. *Cytokine*, *148*, 155709. https://doi.org/10.1016/j.cyto.2021.155709

Wang, L., Lankhorst, L., & Bernards, R. (2022). Exploiting senescence for the treatment of cancer. *Nature Reviews Cancer*, *22*(6), Article 6. https://doi.org/10.1038/s41568-022-00450-9

Wessner, B., Liebensteiner, M., Nachbauer, W., & Csapo, R. (2019). Age-specific response of skeletal muscle extracellular matrix to acute resistance exercise: A pilot study. *European Journal of Sport Science*, *19*(3), 354–364. https://doi.org/10.1080/17461391.2018.1526974

Williams, J. P., Calvi, L., Chakkalakal, J. V., Finkelstein, J. N., O'Banion, M. K., & Puzas, E. (2016). Addressing the Symptoms or Fixing the Problem? Developing Countermeasures against Normal Tissue Radiation Injury. *Radiation Research*, *186*(1), 1–16. https://doi.org/10.1667/RR14473.1

World Health Organization (WHO)—Childhood cancer, 2021. (n.d.).

Wosczyna, M. N., Konishi, C. T., Perez Carbajal, E. E., Wang, T. T., Walsh, R. A., Gan, Q., Wagner, M. W., & Rando, T. A. (2019). Mesenchymal Stromal Cells Are Required for Regeneration and Homeostatic Maintenance of Skeletal Muscle. *Cell Reports*, *27*(7), 2029-2035.e5. https://doi.org/10.1016/j.celrep.2019.04.074

Wright, W. D., Shah, S. S., & Heyer, W.-D. (2018). Homologous recombination and the repair of DNA double-strand breaks. *The Journal of Biological Chemistry*, *293*(27), 10524–10535. https://doi.org/10.1074/jbc.TM118.000372

Xue, M., & Jackson, C. J. (2015). Extracellular Matrix Reorganization During Wound Healing and Its Impact on Abnormal Scarring. *Advances in Wound Care*, *4*(3), 119–136. https://doi.org/10.1089/wound.2013.0485

Yao, L., Rathnakar, B. H., Kwon, H. R., Sakashita, H., Kim, J. H., Rackley, A., Tomasek, J. J., Berry, W. L., & Olson, L. E. (2022). Temporal control of PDGFRα regulates the fibroblast-to-myofibroblast transition in wound healing. *Cell Reports*, *40*(7), 111192. https://doi.org/10.1016/j.celrep.2022.111192

Yin, H., Price, F., & Rudnicki, M. A. (2013). Satellite cells and the muscle stem cell niche. *Physiological Reviews*, *93*(1), 23–67. https://doi.org/10.1152/physrev.00043.2011

Zhang, W., Liu, Y., & Zhang, H. (2021). Extracellular matrix: An important regulator of cell functions and skeletal muscle development. *Cell & Bioscience*, *11*(1), 65. https://doi.org/10.1186/s13578-021-00579-4

Zhang, X., Habiballa, L., Aversa, Z., Ng, Y. E., Sakamoto, A. E., Englund, D. A., Pearsall, V. M., White, T. A., Robinson, M. M., Rivas, D. A., Dasari, S., Hruby, A. J., Lagnado, A. B., Jachim, S. K., Granic, A., Sayer, A. A., Jurk, D., Lanza, I. R., Khosla, S., … LeBrasseur, N. K. (2022). Characterization of cellular senescence

in aging skeletal muscle. *Nature Aging*, *2*(7), Article 7. https://doi.org/10.1038/s43587-022-00250-8

Chapter VI

Supplementary Information

Chapter II

Supplementary Figures and legends

Radiation induces long-term muscle fibrosis and promotes a fibrotic phenotype in fibro-adipogenic progenitors

Nicolas Collao[1], Donna D'Souza[1], Laura Messeiller[1], Evan Pilon[2], Jessica Lloyd[1], Jillian Larkin[1], Matthew Ngu[1], Alexanne Cuillerier[3], Alexander E. Green[3], Yan Burelle[3], and Michael De Lisio[1,4]*

[1]School of Human Kinetics, Faculty of Health Science, [2]Department of Biology, Faculty of Science, [3]Interdisciplinary School of Health Sciences and [4]Department of Cellular and Molecular Medicine, Regenerative Medicine Program, University of Ottawa, Ottawa, ON, Canada

S1

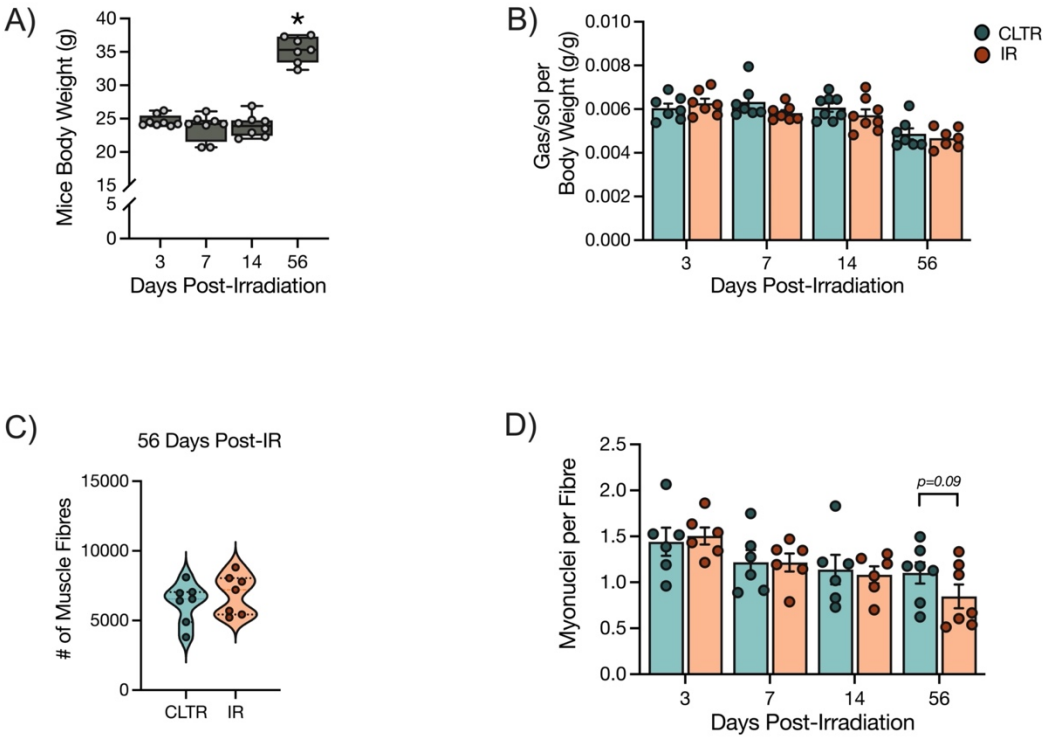

Figure S1. ***Changes in mice body weight, and no changes in muscle fibre number and myonuclei per fibre following radiation.***

(A) Body weight (g), (B) gas/sol weight per body weight (g/g), (C) number of muscle fibres at 56-days post-IR per cross-section, and (D) number of myonuclei per fibre. One-way ANOVA (A), and Paired Student's t-test between CLTR and IR at each timepoint (B-D). *$p < 0.05$ (n=6-8).

S2

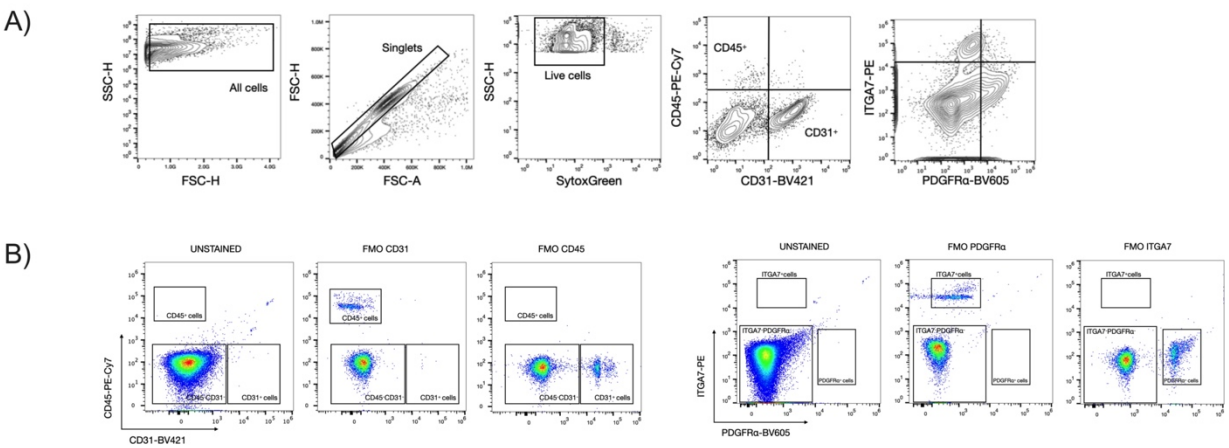

Figure S2. ***Flow cytometer gating strategy***

(A) Flow cytometer gating strategy. (B) Fluorescence minus one (FMO) staining to establish gating strategy.

S3

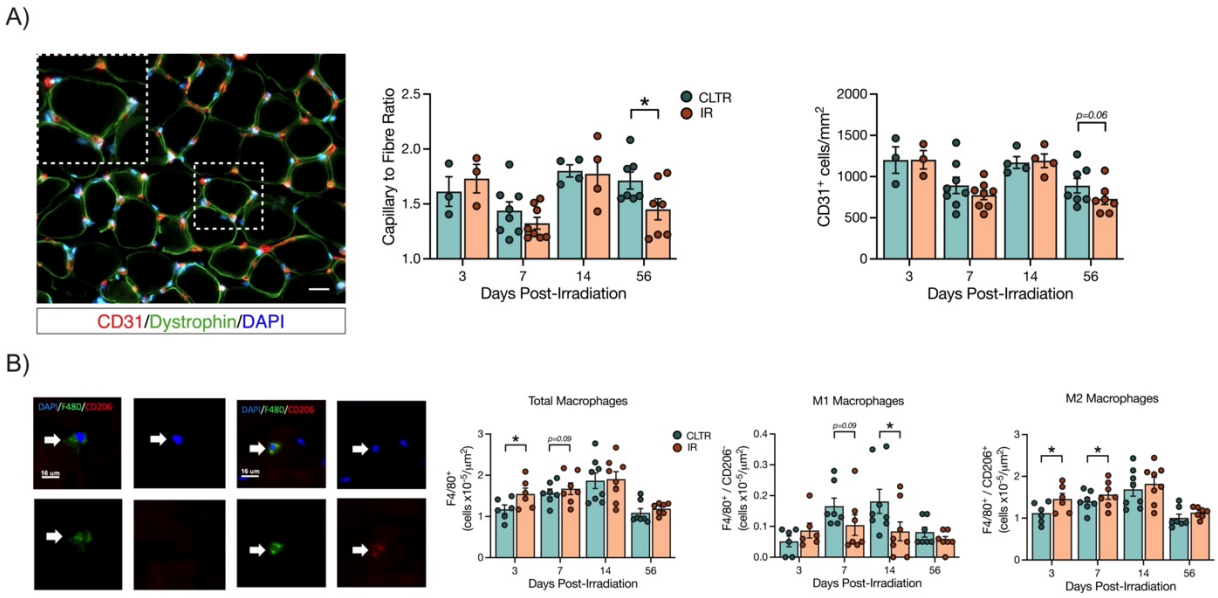

Figure S3. Radiation induces macrophage polarization, decreases vascular endothelial cells content, and reduces PDGFRα content.

(A) Representative image of vascular endothelial cells. $CD31^+$ cells (red), Dystrophin (green), and DAPI (blue). Scale bar 20 µm. Quantification of capillary to fibre ratio, and $CD31^+$ cells per mm^2. (B) Representative image of macrophages staining. $F4/80^+$ cells (green), $CD206^+$ cells (red), and DAPI (blue). Scale bar: 16 µm. Quantification of: Total macrophages ($F4/80^+$) per μm^2. 'M1' macrophages ($F4/80^+/CD206^-$) per μm^2, and 'M2' macrophages ($F4/80^+/CD206^+$) per um^2. *$p < 0.05$, Paired Student's t-test between CLTR and IR at each timepoint (n=3-8).

S4

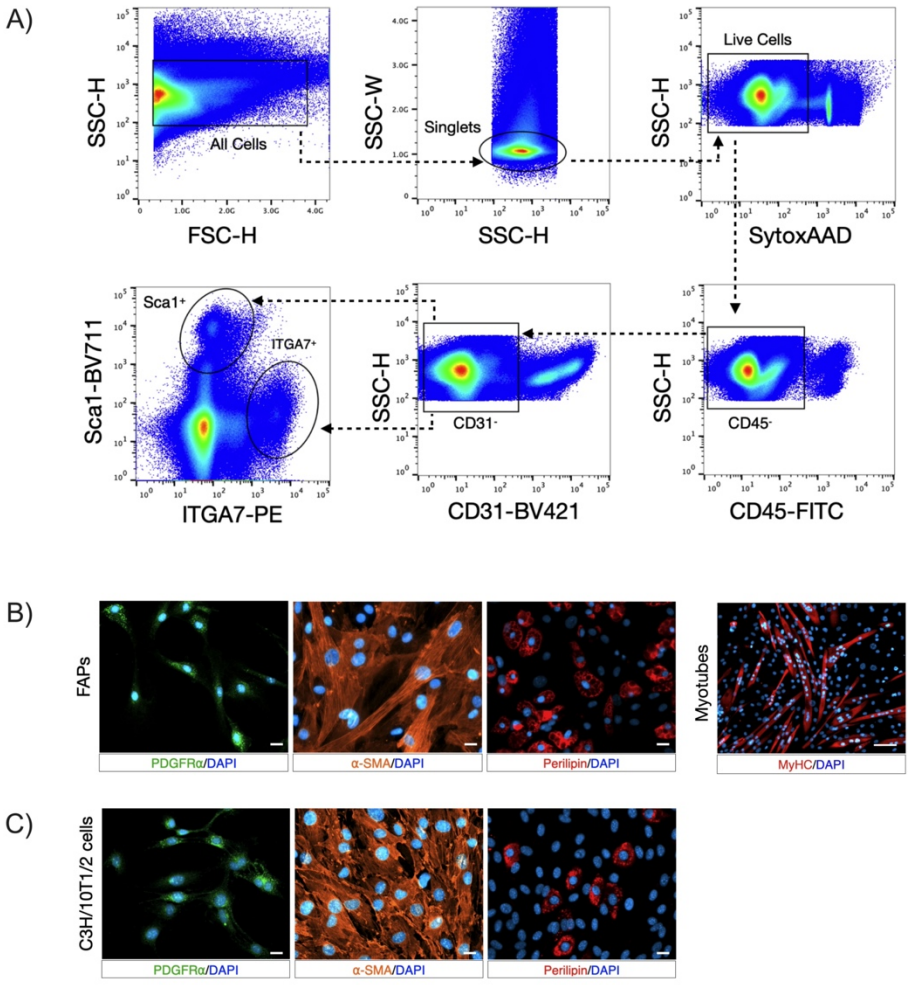

Figure S4. ***FAP, MuSC, and C3H/10T1/2 cell differentiation.***

(A) FACS gating strategy. (B) Representative images of FAPs expressing: PDGFRα (green), fibrogenic FAP differentiation expressing αSMA (orange), adipogenic FAP differentiation expressing Perilipin (red), and DAPI (blue), and MuSCs differentiation expressing MyHC (red), and DAPI (blue). (C) Representative images of C3H/10T1/2 cells

expressing: PDGFRα (green), fibrogenic differentiation αSMA (orange), adipogenic differentiation Perilipin (red), and DAPI (blue). Scale bar: 20 μm.

S5

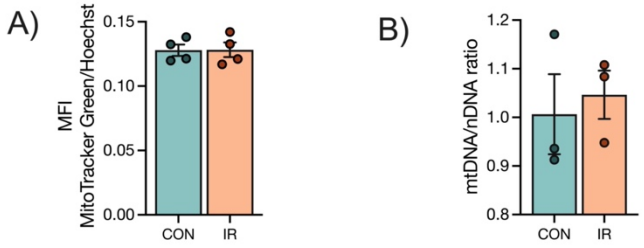

Figure S5. ***No changes in mitochondrial biogenesis followed in vitro radiation.*** (A) MitoTracker Green Fluorescence Intensity normalized by Hoechst Fluorescence Intensity. (B) Mitochondrial DNA to nuclear DNA (mtDNA/nDNA) ratio.

S6

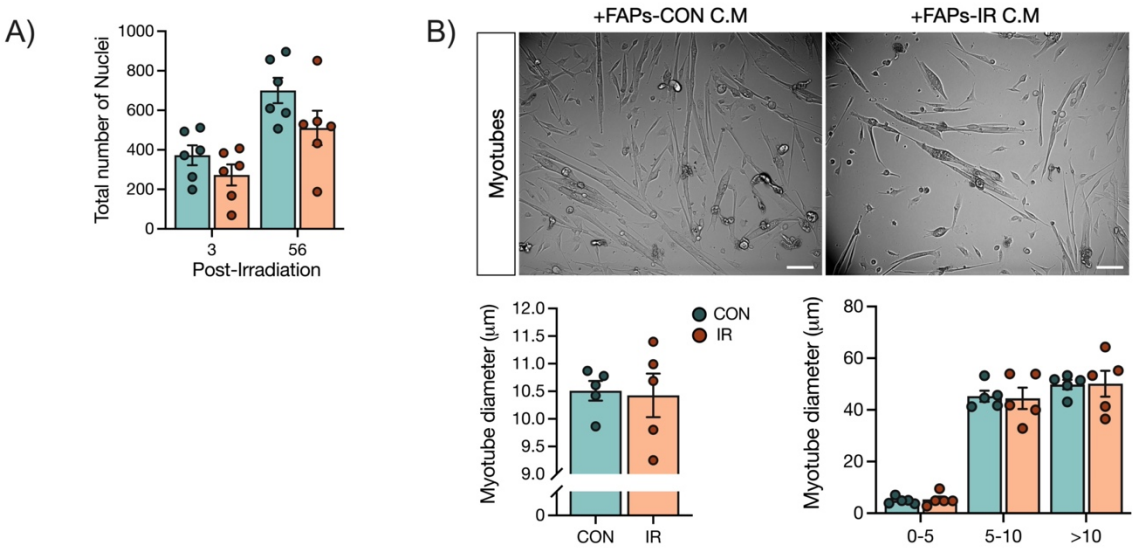

Figure S6. ***Total number of Nuclei is not altered by radiation and no changes in myotube diameter is found when condition media from IR-FAPs is applied.***

(A) Total number of nuclei per field (B) Representative brightfield image of myotube formation used to quantify myotube diameter (µm). Scale bar: 100 µm. Unpaired Student's t-test. (n=5-6).

Chapter II

Extended Methods Section

Histochemical and immunofluorescent analysis

For immunofluorescent analysis, muscle cross-sections were fixed with 2% paraformaldehyde (PFA) for 10 minutes, permeabilized using 0.1% Triton X-100 (Thermo Fisher Scientific) for 10 minutes at room temperature, blocked using either standard block (for Laminin, αSMA,CD31,F4/80 and CD206, 5% Goat Serum, 1% Bovine Serum Albumin, and 0.1% Triton X-100 in 1x PBS), Mouse on Mouse Immunodetection Kit (for Pax7; Cat# BMK-2202, Vector Labs,) or Serum-Free Protein Block (for PDGFRα; Cat# X0909, Agilent) for 1 hour at room temperature. Sections were then incubated overnight at 4°C with primary antibody: rat anti-Laminin (Cat# MA1-06100, Invitrogen), PDGFRα (Cat# AF1062, R&D Systems), αSMA (Cat# A5228, MilliporeSigma), Pax7 (Cat# 528428, DSHB), CD31 (Cat# 14-0311-85, Invitrogen), F4/80 (Cat# 6650, Abcam), CD206 (Cat# 64693, Abcam). After washing 3 times with 0.1% Triton X-100 in PBS 1x, host-specific secondary antibodies were diluted in blocking solution and incubated for 30 minutes at room temperature (Alexa Fluor 594 Goat anti-Rat, A-11012, Invitrogen 1:300) and nuclei were counterstained using 4,6-diamidino-2-phenylindole (DAPI) (Cat# D9542, Sigma Aldrich). Sections were mounted and sealed with fluoromount, cover slipped, then stored in the dark at 4°C until imaging. Cross-sectional area (CSA) was analyzed by semi-automatic macro on Fiji software previously described.[S52] Representative mask from the Gas/sol muscle complex CSA was performed using Imaris software version 9.7.2, Oxford Instruments.

Fluorescence-activated cell sorting (FACS) and Flow cytometer

The IR limb and the CLTR limb were carefully dissected and processed separately. After removing superficial connective and fat tissue, the dissected muscle was washed with cold-PBS and transferred to a Miltenyi GentleMACS C tube (Cat# 130-093-237, Miltenyi Biotec) containing Collagenase B (1.5U/ml, Cat# 11088831001; Roche® Life Science Products,) and Dispase II (2U/ml, Cat# 42613-33-2; Sigma Aldrich) in Ham's F10 media (Cat# 318-050-CL, Wisent Inc, St-Bruno, Canada). Samples were homogenized in the gentleMACS Octo Dissociator (Cat# 130-096-427, Miltenyi Biotec). The homogenate was passed through a 100–µm strainer (Cat# 22-363-549, Fisher Scientific,) and centrifuged at 600 x *g* at 4°C for 10 minutes. Red Blood Cell Lysing Buffer (Hydri-MaxTM; Cat# R7767; Sigma-Aldrich) was added to the cell-pellet and centrifuged at 600 x *g* at 4°C for 5 minutes. Ice-cold FACS buffer (10% FBS, 3mM of EDTA in 1xPBS) was added to the cell-pellet and resuspended. Primary antibodies against CD45 (FITC Rat Anti-Mouse CD45, Cat# 561088, BD Biosciences), CD31 (BV421 Rat Anti-Mouse CD31, Cat# 102423, BioLegend), ITGA7 (anti-Alpha 7 Integrin 647, Cat# 67-0010-05, AbLab Biologics), Ly-6A/E (Sca1) (BV711 Rat Anti-Mouse Ly-6A/E, Cat# 563992, BD Bioscience), and SYTOX™ AADvanced™ (Cat# S10349, Thermo Fisher Scientific) were used for FACS. Antibodies against CD45 (PE-Cy™7 Rat Anti-Mouse CD45, Cat# 552848, BD Bioscience), CD31 (BV421 Rat Anti-Mouse CD31, Cat# 102423, BioLegend), ITGA7 (anti-Alpha 7 Integrin PE, Cat# 53-0010-05, AbLab Biologics), CD140a (PDGFRα, BV605, Cat# 740380, BD Bioscience) and SYTOX™ green (Cat# S34860, Invitrogen) were used for Flow Cytometry. Following incubation at 4°C in the dark for 35 minutes samples were washed prior to analysis. For all antibodies, fluorescence minus one (FMO) and single-stained controls were used for compensation and to establish gates.

Compensation with AbC™ Total Antibody Compensation Bead Kit (Cat# A10497, Thermo Fisher Scientific) was used if required. Attune™ Nxt Acoustic Focusing Flow Cytometer system (Thermo Fisher Scientific) with two excitation lasers (Violet (405 nm) and Blue (488 nm)) was used for flow cytometer analysis. Beckman Coulter MoFlo XDP (32-bit high resolution digital system with five excitation laser lines (UV, 405nm, 488nm, 561nm, and 640nm) cell sorter was used for FACS. Cells were identified as: Endothelial cells ($CD45^-CD31^+$), hematopoietic cells ($CD31^-CD45^+$), MuSCs ($CD45^-CD31^-PDGFR\alpha^-ITGA7^+$), and FAPs ($CD45^-CD31^-ITGA7^-PDGFR\alpha^+$). FCS files were processed in FlowJo™ v10.8 Software (BD Life Sciences).

Protein extraction and western blot analysis

For western blot, whole muscle or cells were lysed in ice-cold RIPA buffer (10 mM Tris, pH 7.4; 150 mM NaCl; 1 mM EDTA; 1 mM EGTA; 1% NP-40; 10% glycerol; 0.1% SDS; 0.5% sodium deoxycholate; 1 mM DTT) containing Complete Protease inhibitor cocktail (Cat# 04693116001, Millipore Sigma) and Phosphatase inhibitor (PhosSTOP) (Cat# 4906837001, Millipore Sigma) for protein extraction. Homogenates were cleared by centrifugation at 14,000 rpm, for 8 minutes at 4°C. Protein was quantified using Bradford assay (Cat# 5000006, Bio-Rad) following the manufacturer's instructions. Protein extracts were subjected to SDS–PAGE, transferred to PVDF membranes (Cat# 162017, Bio-Rad Laboratories), and incubated overnight at 4°C with primary antibodies: Fibronectin (Cat# F3648, MilliporeSigma), p-SMAD3 (Cat# 9520S, Cell Signaling Technology), SMAD3 (Cat# 9523S, Cell Signaling Technology), αSMA (Cat# A5228, MilliporeSigma), Anti-cyclophilinB (Abcam;Waltham, MA; Cat. No. ab16045) or PDGFRα (Cat# AF1062, R&D Systems). Primary antibodies were detected using a secondary

antibody conjugated to horseradish peroxidase: anti-mouse IgG (1:1000, Cat# 7076S, Cell Signaling Technology) or anti-rabbit IgG (Cat# 7074S 1:1000, Cell Signaling Technology). Immunoreactions were visualized by SuperSignal™ West Pico PLUS Chemiluminescent Substrate (Cat# 34579, Thermo Fisher Scientific) using ChemiDoc™ (Bio-Rad Laboratories). Western blot densitometry quantification was performed using Fiji software (ImageJ version 2.0.0-rc/69/1.52n).

Bioenergetic analysis

Bioenergetic analysis was performed according to Agilent's recommendations (Agilent Technologies). Mitochondrial inhibitors were sequentially injected at the following final concentrations: 1 µM oligomycin (Cat# 75351, Sigma-Aldrich), 2 µM FCCP (Cat# C2920, Sigma-Aldrich), 1 µM/1 µM Rotenone/Antimycin (Cat# R8875 and A8674, Sigma-Aldrich), and 50 mM 2-Deoxy-D-Glucose (2-DG) (Cat# D6134, Sigma-Aldrich). Mitochondrial oxygen consumption rate (OCR) and extracellular acidification rate (ECAR) were analyzed. OCR and ECAR were normalized to the number of cells per well for each experimental sample. Immediately after the assay, nuclei were labelled with a live cell stain added directly to cells in full media (NucBlue™ Live ReadyProbes™ Reagent (Hoechst 33342), Cat# R37605, Thermo Fisher Scientific) and a representative field of each well was captured using an EVOS-FL2 Automated Microscope (Thermo Fisher Scientific) and automatically scored with Fiji, ImageJ (National Institutes of Health; USA; v. 1.53c).

DNA isolation and qPCR

Nuclear and mitochondrial DNA was extracted from FAPs using a commercial kit (Cat# BS427, EZ-10 Spin Column Genomic DNA Miniprep Kit; BioBasic) as per the

manufacturer's instructions. DNA was quantified using a NanoDrop Lite Spectrophotometer (Cat# ND-2000, ThermoScientific). Quantitative PCR was used to amplify and detect the levels of nuclear DNA and mtDNA in a 10 µL reaction (5 ng of DNA, 0.25 µM each of Forward and Reverse Primers, and 2.5 µL of Luna® Universal qPCR MasterMix (Cat# M3003S, New England BioLabs) in a BioRad 384 qPCR thermocycler (Cat# CFX384t™ Real-Time System, Bio-Rad) using SybrGreen detection technology. Primers were as follows, for mtDNA amplification – Forward "CCTATCACCCTTGCCATCAT" and Reverse "GAGGCTGTTGCTTGTGTGAC" – and for nuclear DNA amplification – Forward "ATGGAAAGCCTGCCATCATG" and Reverse "TCCTTGTTGTTCAGCATCAC". Results were quantified using the 2^-ΔΔCt method.

MitoTracker Green and TMRM staining

FAPs were irradiated with 1 Gy *in vitro,* MitoTracker™ Green FM (Cat# M7514, Invitrogen), and Tetramethylrhodamine, methyl ester (TMRM) (Cat#T668, Invitrogen) was applied 24-hours post-IR at a final concentration of 200 nM and 25 nM respectively and incubated for 30 minutes. Nuclei were labeled with a live cell stain (NucBlue™ Live ReadyProbes™ Reagent (Hoechst 33342), Cat# 37605, Thermo Fisher Scientific). MitoTracker Green, and TMRM fluorescence intensity was detected by Synergy H1 Multimode Reader (BioTek) and normalized to Hoechst fluorescence intensity to determine intensity per cell.

Myosin heavy chain staining

Myosin heavy chain staining was performed as previous described.[18] Briefly, myotubes were fix with 2% PFA for 15 minutes at room temperature. Myotubes were permeabilized with (0.5% Triton X-100 in 1xPBS) for 10 minutes. Block solution (10%

FBS, 0.1% Triton X-100 in 1x PBS) was applied for 1 hour and primary antibody anti-MyHC (Cat# MF-20, DSHB) was incubated overnight at 4°C. Secondary antibody Alexa Fluor 488-Goat Anti-Mouse (Cat# A11001, Invitrogen) was used to visualized stress fibre formation and nuclei were counterstained with DAPI.

Glycolysis manipulation

The metabolic perturbation was performed by supplementing FAPs media with 100 nM of Oligomycin[S53] and 10 μM of 2-Deoxy-D-Glucose (2-DG)[S54] respectively, or by applying DMEM low glucose (1 g/L) or high glucose (4.5 g/L) respectively.[32, S30] Cells were fixed 24-hours post-*in vitro* IR and αSMA staining was performed.

Extended References

S1. Gawade PL, Hudson MM, Kaste SC, Neglia JP, Wasilewski-Masker K, Constine LS et al. A systematic review of selected musculoskeletal late effects in survivors of childhood cancer. Curr Pediatr Rev 2014;10:249–262.

S2. Paulino AC. Late effects of radiotherapy for pediatric extremity sarcomas. International Journal of Radiation Oncology*Biology*Physics 2004;60:265–274.

S3. Stubblefield MD. Radiation fibrosis syndrome: neuromuscular and musculoskeletal complications in cancer survivors. PM R 2011;3:1041–1054.

S4. Bentzinger CF, Wang YX, Dumont NA, Rudnicki MA. Cellular dynamics in the muscle satellite cell niche. EMBO Rep 2013;14:1062–1072.

S5. Mauro A. Satellite cell of skeletal muscle fibers. J Biophys Biochem Cytol 1961;9:493–495.

S6. Williams JP, Calvi L, Chakkalakal JV, Finkelstein JN, O'Banion MK, Puzas E. Addressing the Symptoms or Fixing the Problem? Developing Countermeasures against Normal Tissue Radiation Injury. Radiat Res 2016;186:1–16.

S7. Amersfoort J, Eelen G, Carmeliet P. Immunomodulation by endothelial cells - partnering up with the immune system? Nat Rev Immunol 2022 doi:10.1038/s41577-022-00694-4.

S8. Verma M, Asakura Y, Murakonda BSR, Pengo T, Latroche C, Chazaud B et al. Muscle Satellite Cell Cross-Talk with a Vascular Niche Maintains Quiescence via VEGF and Notch Signaling. Cell Stem Cell 2018;23:530-543.e9.

S9. Chazaud B. Inflammation and Skeletal Muscle Regeneration: Leave It to the Macrophages! Trends Immunol 2020;41:481–492.

S10. Huntsman HD, Rendeiro C, Merritt JR, Pincu Y, Cobert A, De Lisio M et al. The impact of mechanically stimulated muscle-derived stromal cells on aged skeletal muscle. Exp Gerontol 2018;103:35–46.

S11. Zou K, Huntsman HD, Carmen Valero M, Adams J, Skelton J, De Lisio M et al. Mesenchymal stem cells augment the adaptive response to eccentric exercise. Med Sci Sports Exerc 2015;47:315–325.

S12. Boppart MD, De Lisio M, Zou K, Huntsman HD. Defining a role for non-satellite stem cells in the regulation of muscle repair following exercise. Front Physiol 2013;4:310.

S13. Contreras O, Rebolledo DL, Oyarzún JE, Olguín HC, Brandan E. Connective tissue cells expressing fibro/adipogenic progenitor markers increase under chronic damage: relevance in fibroblast-myofibroblast differentiation and skeletal muscle fibrosis. Cell Tissue Res 2016;364:647–660.

S14. Ieronimakis N, Hays A, Prasad A, Janebodin K, Duffield JS, Reyes M. PDGFRα signalling promotes fibrogenic responses in collagen-producing cells in Duchenne muscular dystrophy. J Pathol 2016;240:410–424.

S15. Pakshir P, Noskovicova N, Lodyga M, Son DO, Schuster R, Goodwin A et al. The myofibroblast at a glance. Journal of Cell Science 2020;133:jcs227900.

S16. Klingberg F, Hinz B, White ES. The myofibroblast matrix: implications for tissue repair and fibrosis. J Pathol 2013;229:298–309.

S17. Mirzaie-Joniani H, Eriksson D, Sheikholvaezin A, Johansson A, Löfroth P-O, Johansson L et al. Apoptosis induced by low-dose and low-dose-rate radiation. Cancer 2002;94:1210–1214.

S18. Feige P, Rudnicki MA. Isolation of satellite cells and transplantation into mice for lineage tracing in muscle. Nat Protoc 2020;15:1082–1097.

S19. Tojkander S, Ciuba K, Lappalainen P. CaMKK2 Regulates Mechanosensitive Assembly of Contractile Actin Stress Fibers. Cell Rep 2018;24:11–19.

S20. Chen H, Vermulst M, Wang YE, Chomyn A, Prolla TA, McCaffery JM et al. Mitochondrial fusion is required for mtDNA stability in skeletal muscle and tolerance of mtDNA mutations. Cell 2010;141:280–289.

S21. Mahdy MAA. Skeletal muscle fibrosis: an overview. Cell Tissue Res 2019;375:575–588.

S22. Biernacka A, Dobaczewski M, Frangogiannis NG. TGF-β signaling in fibrosis. Growth Factors 2011;29:196–202.

S23. Trensz F, Haroun S, Cloutier A, Richter MV, Grenier G. A muscle resident cell population promotes fibrosis in hindlimb skeletal muscles of mdx mice through the Wnt canonical pathway. Am J Physiol Cell Physiol 2010;299:C939-947.

S24. Buras ED, Converso-Baran K, Davis CS, Akama T, Hikage F, Michele DE et al. Fibro-Adipogenic Remodeling of the Diaphragm in Obesity-Associated Respiratory Dysfunction. Diabetes 2019;68:45–56.

S25. Hillsley A, Santoso M, Engels SM, Contreras LM, Rosales AM. A Strategy to Quantify Myofibroblast Activation on a Continuous Spectrum. 2022;2022.03.09.483659.

S26. Vaughan MB, Howard EW, Tomasek JJ. Transforming growth factor-beta1 promotes the morphological and functional differentiation of the myofibroblast. Exp Cell Res 2000;257:180–189.

S27. Hinz B. Formation and function of the myofibroblast during tissue repair. J Invest Dermatol 2007;127:526–537.

S28 Kim EJ, Lee M, Kim DY, Kim KI, Yi JY. Mechanisms of Energy Metabolism in Skeletal Muscle Mitochondria Following Radiation Exposure. Cells 2019;8:E950.

S29. Amorim NML, Kee A, Coster ACF, Lucas C, Bould S, Daniel S et al. Irradiation impairs mitochondrial function and skeletal muscle oxidative capacity: significance for metabolic complications in cancer survivors. Metabolism 2020;103:154025.

S30. Elkalaf M, Anděl M, Trnka J. Low glucose but not galactose enhances oxidative mitochondrial metabolism in C2C12 myoblasts and myotubes. PLoS One 2013;8:e70772.

S31. Shiratori R, Furuichi K, Yamaguchi M, Miyazaki N, Aoki H, Chibana H et al. Glycolytic suppression dramatically changes the intracellular metabolic profile of multiple cancer cell lines in a mitochondrial metabolism-dependent manner. Sci Rep 2019;9:18699.

S32. Liu C, Lin Q, Yun Z. Cellular and molecular mechanisms underlying oxygen-dependent radiosensitivity. Radiat Res 2015;183:487–496.

S33. Negroni E, Kondili M, Muraine L, Bensalah M, Butler-Browne GS, Mouly V et al. Muscle fibro-adipogenic progenitors from a single-cell perspective: Focus on their ‘virtual’ secretome. Front Cell Dev Biol 2022;10:952041.

S34. Dobaczewski M, Bujak M, Li N, Gonzalez-Quesada C, Mendoza LH, Wang X-F et al. Smad3 signaling critically regulates fibroblast phenotype and function in healing myocardial infarction. Circ Res 2010;107:418–428.

S35. Contreras O, Rossi FM, Brandan E. Adherent muscle connective tissue fibroblasts are phenotypically and biochemically equivalent to stromal fibro/adipogenic progenitors. Matrix Biol Plus 2019;2:100006

S36. Etienne J, Liu C, Skinner CM, Conboy MJ, Conboy IM. Skeletal muscle as an experimental model of choice to study tissue aging and rejuvenation. Skelet Muscle 2020;10:4.

S37. Álvarez D, Cárdenes N, Sellarés J, Bueno M, Corey C, Hanumanthu VS et al. IPF lung fibroblasts have a senescent phenotype. Am J Physiol Lung Cell Mol Physiol 2017;313:L1164–L1173.

S38. Zhu Y, Tchkonia T, Pirtskhalava T, Gower AC, Ding H, Giorgadze N et al. The Achilles' heel of senescent cells: from transcriptome to senolytic drugs. Aging Cell 2015;14:644–65

S39. Gambini E, Martinelli I, Stadiotti I, Vinci MC, Scopece A, Eramo L et al. Differences in Mitochondrial Membrane Potential Identify Distinct Populations of Human Cardiac Mesenchymal Progenitor Cells. Int J Mol Sci 2020;21:7467.

S40. Perry SW, Norman JP, Barbieri J, Brown EB, Gelbard HA. Mitochondrial membrane potential probes and the proton gradient: a practical usage guide. Biotechniques 2011;50:98–115.

S41. Murphy MP. How mitochondria produce reactive oxygen species. Biochem J 2009;417:1–13.

S42. Wang Y, Lu M, Xiong L, Fan J, Zhou Y, Li H et al. Drp1-mediated mitochondrial fission promotes renal fibroblast activation and fibrogenesis. Cell Death Dis 2020;11:29.

S43. Li X, Jiang Y, Meisenhelder J, Yang W, Hawke DH, Zheng Y et al. Mitochondria-Translocated PGK1 Functions as a Protein Kinase to Coordinate Glycolysis and the TCA Cycle in Tumorigenesis. Mol Cell 2016;61:705–719.

S44. Wu S-B, Wei Y-H. AMPK-mediated increase of glycolysis as an adaptive response to oxidative stress in human cells: implication of the cell survival in mitochondrial diseases. Biochim Biophys Acta 2012;1822:233–247.

S45. Pala F, Di Girolamo D, Mella S, Yennek S, Chatre L, Ricchetti M et al. Distinct metabolic states govern skeletal muscle stem cell fates during prenatal and postnatal myogenesis. J Cell Sci 2018;131.

S46. Knobloch M, Pilz G-A, Ghesquière B, Kovacs WJ, Wegleiter T, Moore DL et al. A Fatty Acid Oxidation-Dependent Metabolic Shift Regulates Adult Neural Stem Cell Activity. Cell Rep 2017;20:2144–2155.

S47. Ding H, Jiang L, Xu J, Bai F, Zhou Y, Yuan Q et al. Inhibiting aerobic glycolysis suppresses renal interstitial fibroblast activation and renal fibrosis. Am J Physiol Renal Physiol 2017;313:F561–F575.

S48. Wei Q, Su J, Dong G, Zhang M, Huo Y, Dong Z. Glycolysis inhibitors suppress renal interstitial fibrosis via divergent effects on fibroblasts and tubular cells. Am J Physiol Renal Physiol 2019;316:F1162–F1172.

S49. Voyant C, Julian D, Roustit R, Biffi K, Lantieri C. Biological effects and equivalent doses in radiotherapy: A software solution. Rep Pract Oncol Radiother 2014;19:47–55.

S50. Fowler JF. 21 years of biologically effective dose. Br J Radiol 2010;83:554–568.

S51. Emmons R, Ngu M, Xu G, Hernández-Saavedra D, Chen H, DE Lisio M. Effects of Obesity and Exercise on Bone Marrow Progenitor Cells after Radiation. Med Sci Sports Exerc 2019;51:1126–1136.

S52. Karlsen A, Bechshøft RL, Malmgaard-Clausen NM, Andersen JL, Schjerling P, Kjaer M et al. Lack of muscle fibre hypertrophy, myonuclear addition, and satellite cell pool expansion with resistance training in 83-94-year-old men and women. Acta Physiol (Oxf) 2019;227:e13271.

S53. Hao W, Chang C-PB, Tsao C-C, Xu J. Oligomycin-induced bioenergetic adaptation in cancer cells with heterogeneous bioenergetic organization. J Biol Chem 2010;285:12647–12654.

S54. Woodward GE, Hudson MT. The effect of 2-desoxy-D-glucose on glycolysis and respiration of tumor and normal tissues. Cancer Res 1954;14:599–605.

S55. von Haehling S, Coats AJS, Anker SD. Ethical guidelines for publishing in the Journal of Cachexia, Sarcopenia and Muscle: update 2021. J Cachexia Sarcopenia Muscle 2021;12:2259–2261.

Chapter III

Supplementary information

Single-cell transcriptomic analysis of skeletal muscle cellular dynamics following radiation exposure.

Nicolas Collao[1,2], Emma B Johannsen[3,4], Jesper Just[3,4], and Michael De Lisio[1,2,5*]

[1]School of Human Kinetics, Faculty of Health Science, University of Ottawa, Ottawa, ON, Canada, [2]Éric Poulin Centre for Neuromuscular Disease, University of Ottawa, Ottawa, ON, Canada [3]Department of Molecular Medicine, Aarhus University Hospital, Aarhus, DK-8200, Denmark, [4]Department of Clinical Medicine, Aarhus University, Aarhus, DK-8200, Denmark, [5]Department of Cellular and Molecular Medicine, Regenerative Medicine Program, University of Ottawa, Ottawa, ON, Canada

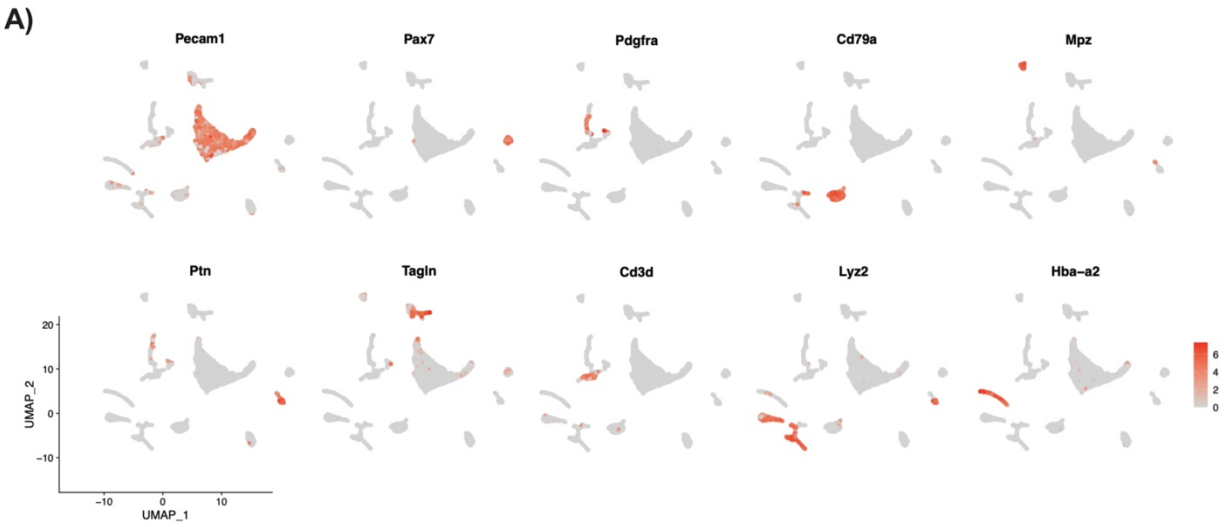

Figure S1. Canonical gene expression in the different cell populations.

(A) Feature plots displaying expression of genes/markers common for the different cell types identified from the scRNA-seq data.

Related to Figure 1.

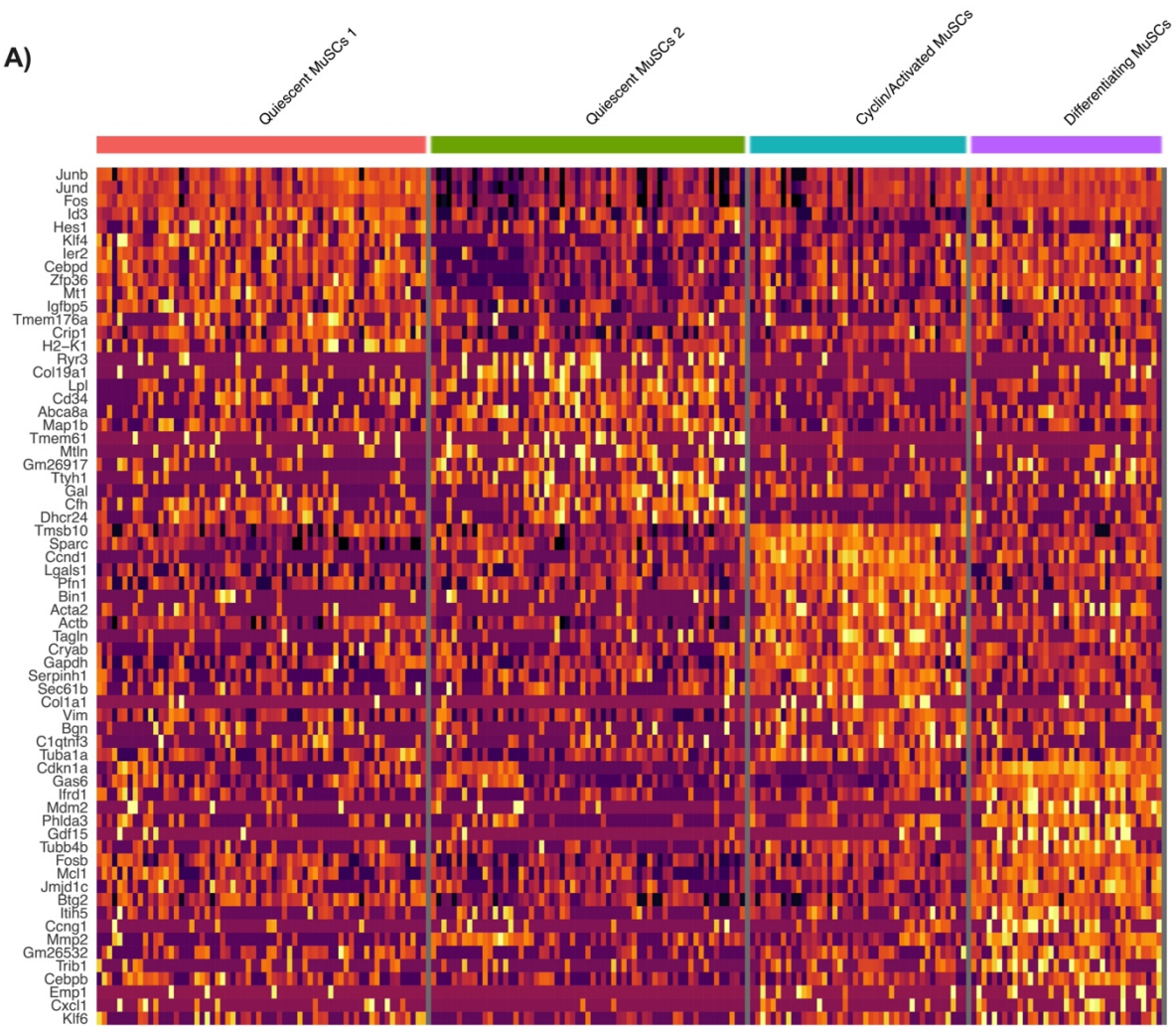

Figure S2. Hierarchical cluster of the top 20 differentially expressed genes in MuSCs subpopulations.

(A) Heatmap of the top 20 genes that are differentially enriched in each MuSCs subcluster.

Related to Figure 2.

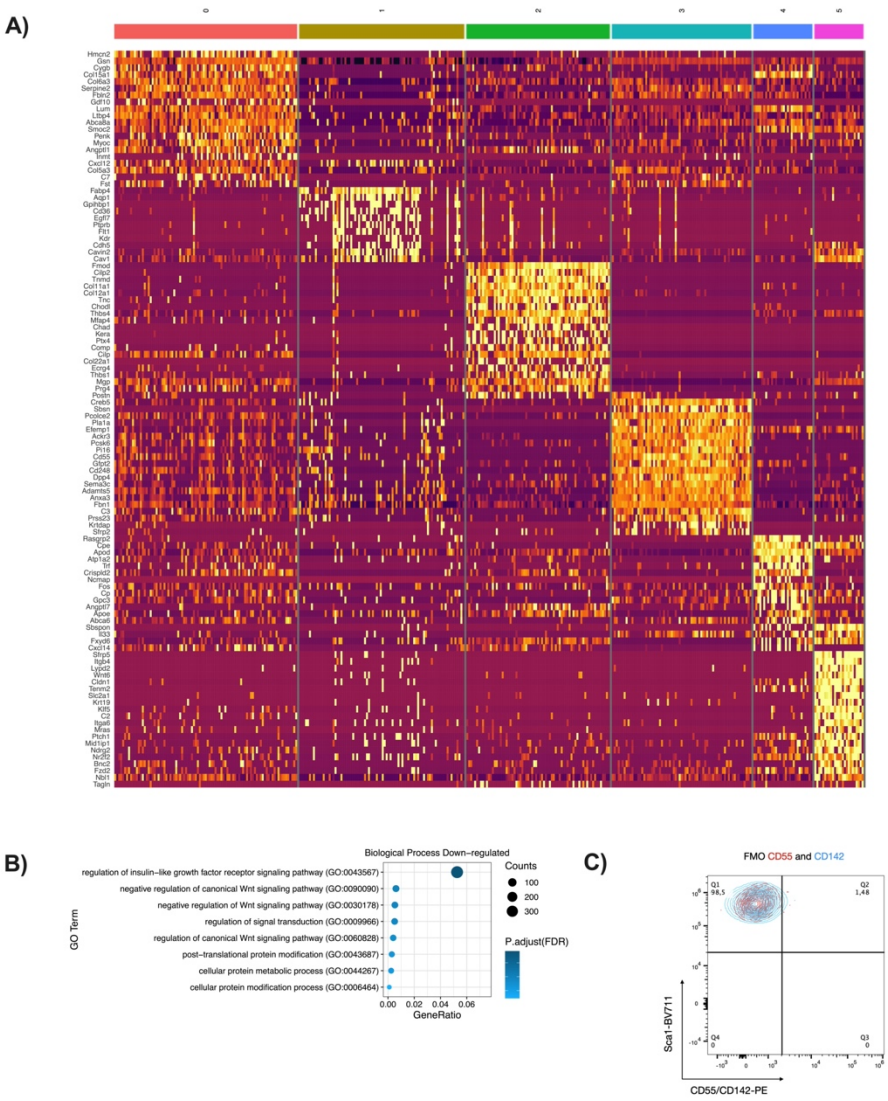

Figure S3. Hierarchical cluster of the top 20 differentially expressed genes in FAP subpopulations and Flow cytometer control.

(A) Heatmap of the top 20 genes that are differentially enriched in each FAP subcluster. (B) GO enrichment analysis of the DEGs in IR versus CON at 24-hours of total FAPs showing down-regulated biological process. (C) Merge flow plot of fluorescence minus one (FMO) for CD55 and CD142 staining.

Related to Figure 3.

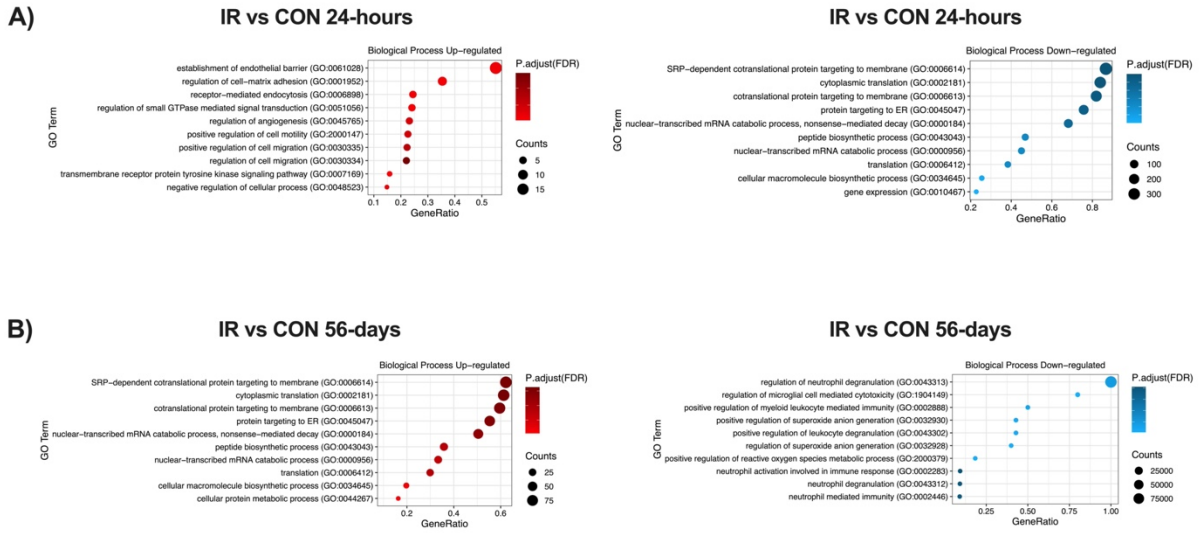

Figure S4. Gene ontology enrichment analysis in all muscle mononuclear cells following radiation exposure.

(A) GO enrichment analysis of the DEGs in IR versus CON at 24-hours in all muscle mononuclear cells showing up- and down-regulated biological process. (B) GO enrichment analysis of the DEGs in IR versus CON at 56-days in all muscle mononuclear cells showing up- and down-regulated biological process.

Related to Figure 6.

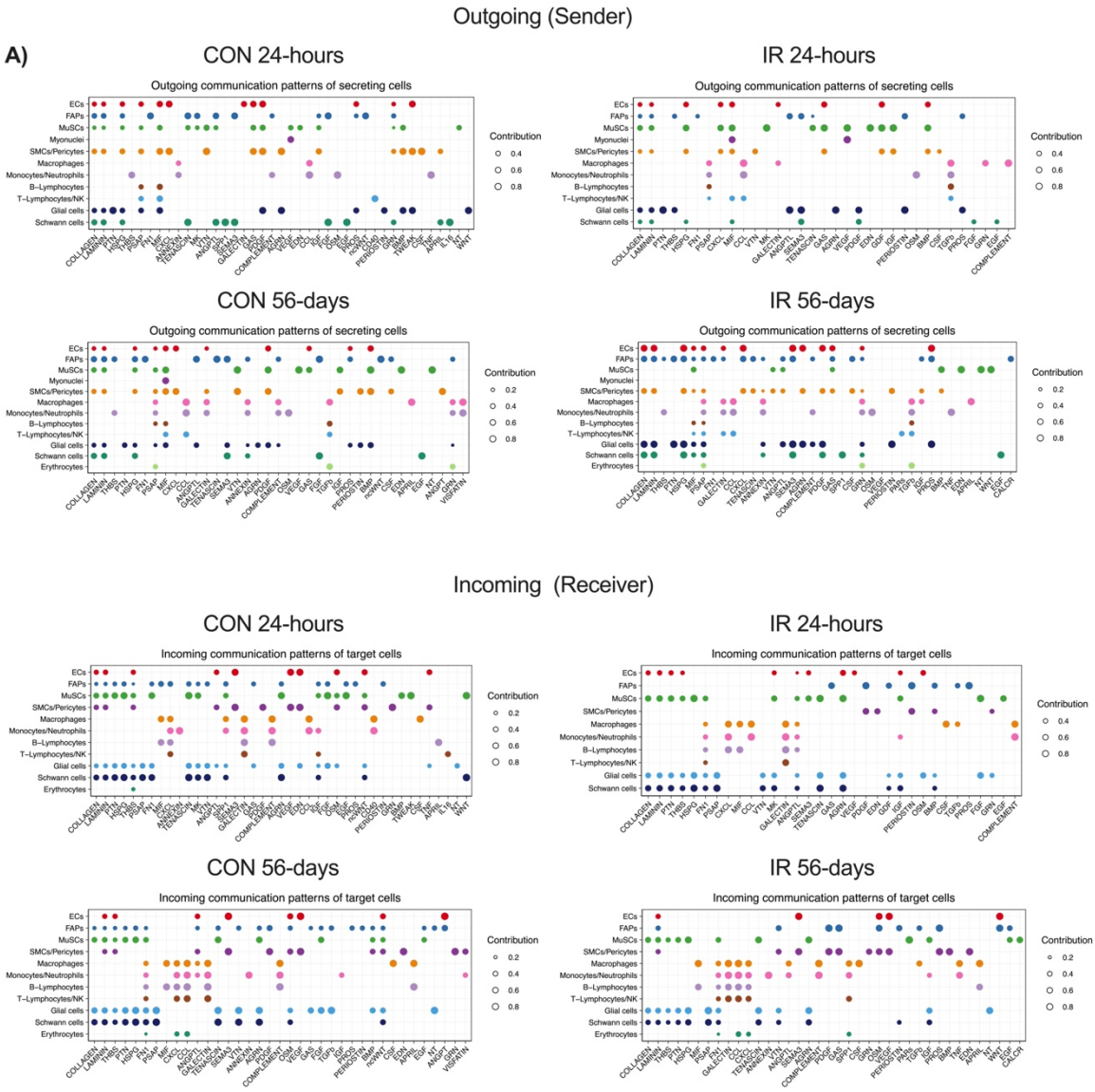

Figure S5. Outgoing and incoming signalling of different pathways.

(A) Dot plot showing the different signal of outgoing (sender), and Incoming (receivers) cells for each listed pathway. The contribution of each cell type to a pathway is proportional to the dot size.

Related to Figure 8.

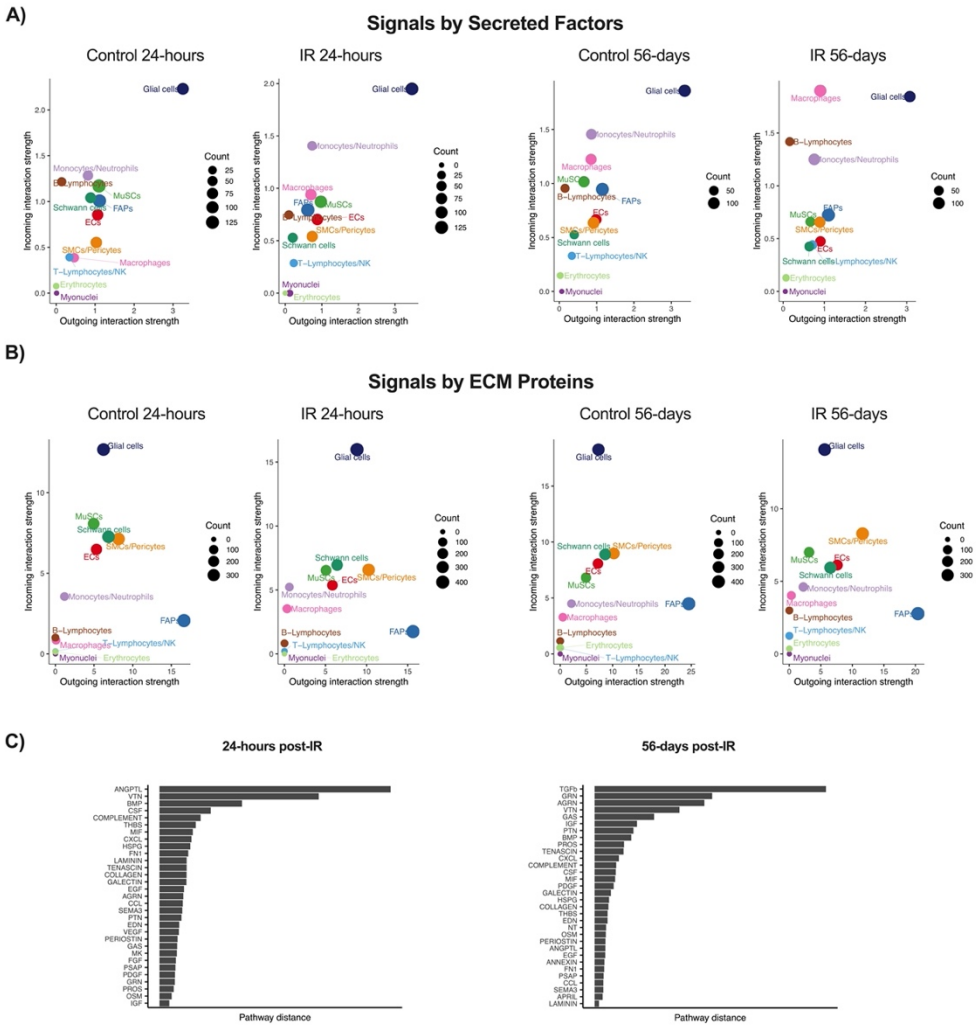

Figure S6. Cell type contribution mediated by secreted factors or ECM proteins.

(A) Scatterplot showing the different cell type contribution to secreted factors and ECM protein. The contribution of each cell type to a pathway is proportional to the dot size. (B) Bar graph showing the Euclidean distance to determine the differences between signalling pathways between IR and CON. A large gray bar or distance implies a large communication difference between the two data sets. Signalling pathways only identified in IR or CON are not considered.

Related to Figure 8.

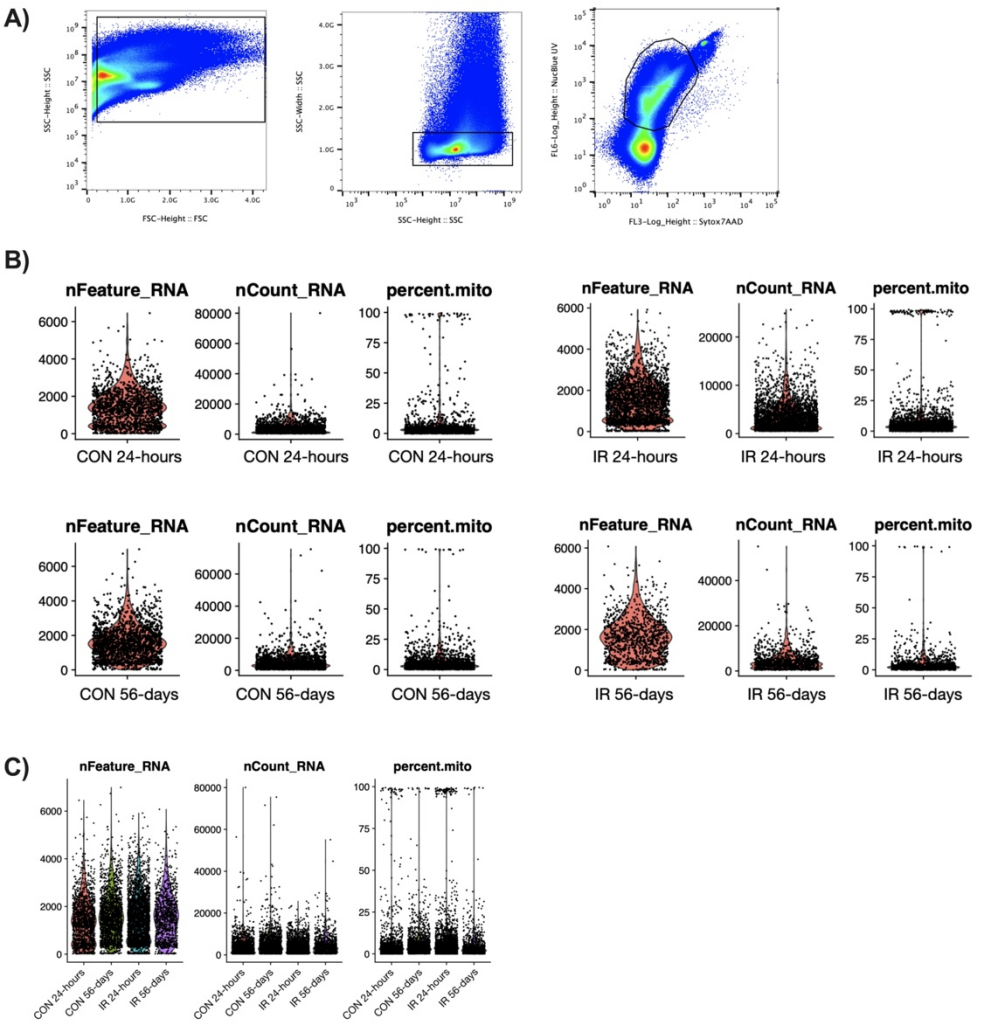

Figure S7. Fluorescence activated cell sorting strategy and quality control for scRNA-seq.

(A) Fluorescence activated cell sorting (FACS) strategy to sort live-mononucleated cells. (B) Violin plots showing the quality control for scRNA-seq per condition including number of genes identified (nFeature_RNA), number of counts (nCount_RNA), and percentage of mitochondrial genes (percent.mito). (C) Integrated quality control.

Related to Method details.

Chapter IV

Supplementary information

Resistance endurance training improves muscle mass and the inflammatory/fibrotic transcriptome in a rhabdomyosarcoma model

Nicolas Collao[1†], Olivia Sanders[1†], Taylor Caminiti[1], Laura Messeiller[1], and Michael De Lisio[1,2*]
[1]School of Human Kinetics, and [2]Department of Cellular and Molecular Medicine, Regenerative Medicine Program, University of Ottawa, Ottawa, ON, Canada

†These authors contribute equal to this work.

*Correspondence to: Michael De Lisio, School of Human Kinetics, and Department of Cellular and Molecular Medicine, Regenerative Medicine Program, University of Ottawa, Ottawa, ON, Canada. Phone: +1 613-562-5800 ext. 6987. Email: mdelisio@uottawa.ca

Supplementary Methods

Protein extraction and western blot analysis

For western blot whole-muscle was prepared as previously described.[S6] The following antibodies were used for detection; MMP-2 Antibody (Cat# 4022S, 1:1000, New England Biolabs), CCR2 Recombinant Rabbit Monoclonal Antibody (Cat# MA5-42780, 1:1000, Thermo Fisher Scientific) and Cyclophilin B (Cat# ab16045, 1:5000, Abcam). Western blot densitometry quantification was performed using Fiji software.

RNA isolation and qPCR

Briefly, RNA isolation was extracted from whole muscle using RNeasy Mini Kit (Cat# 74104, Qiagen) and quantified using a NanoDrop Lite Spectrophotometer (Cat# ND-2000, ThermoFisherScientific). Quantitative PCR was used to amplify and detect the RNA levels in a 10 µL reaction (5 ng of RNA, 0.25 µM each of Forward and Reverse Primers, and 2.5 µL of Luna® Universal qPCR MasterMix (Cat# M3003S, New England BioLabs) in a BioRad qPCR thermocycler (Cat# CFX384tTM Real-Time System, Bio-Rad) using SybrGreen detection technology. Primers were as follows, for MMP-2 - Forward "CCTGGACCCTGAAACCGTG" and Reverse "TCCCCATCATGGATTCGAGAA" and Col3a1 – Forward "CTGTAACATGGAAACTGGGGAAA" and Reverse "CCATAGCTGAACTGAAAACCACC". Results were quantified using the 2^-ΔΔCt method.

Supplementary References

S1. Blanc RS, Kallenbach JG, Bachman JF, Mitchell A, Paris ND, Chakkalakal JV. Inhibition of inflammatory CCR2 signaling promotes aged muscle regeneration and strength recovery after injury. *Nat Commun* 2020;**11**:4167.

S2. Santini MP, Malide D, Hoffman G, Pandey G, D'Escamard V, Nomura-Kitabayashi A *et al.* Tissue-Resident PDGFRα+ Progenitor Cells Contribute to Fibrosis versus Healing in a Context- and Spatiotemporally Dependent Manner. *Cell Reports* 2020;**30**:555-570.e7.

S3. Tidball JG. Regulation of muscle growth and regeneration by the immune system. *Nat Rev Immunol* 2017;**17**:165–178.

S4. DiPasquale DM, Cheng M, Billich W, Huang SA, van Rooijen N, Hornberger TA *et al.* Urokinase-type plasminogen activator and macrophages are required for skeletal muscle hypertrophy in mice. *Am J Physiol Cell Physiol* 2007;**293**:C1278-1285.

S5. von Haehling S, Morley JE, Coats AJS, Anker SD. Ethical guidelines for publishing in the Journal of Cachexia, Sarcopenia and Muscle: update 2019. *J Cachexia Sarcopenia Muscle* 2019;**10**:1143–1145.

S6. Collao N, Akohene-Mensah P, Nallabelli J, Binet ER, Askarian A, Lloyd J *et al.* The role of L-type amino acid transporter 1 (Slc7a5) during in vitro myogenesis. *Am J Physiol Cell Physiol* 2022;**323**:C595–C605.

Supplementary Figure Legends

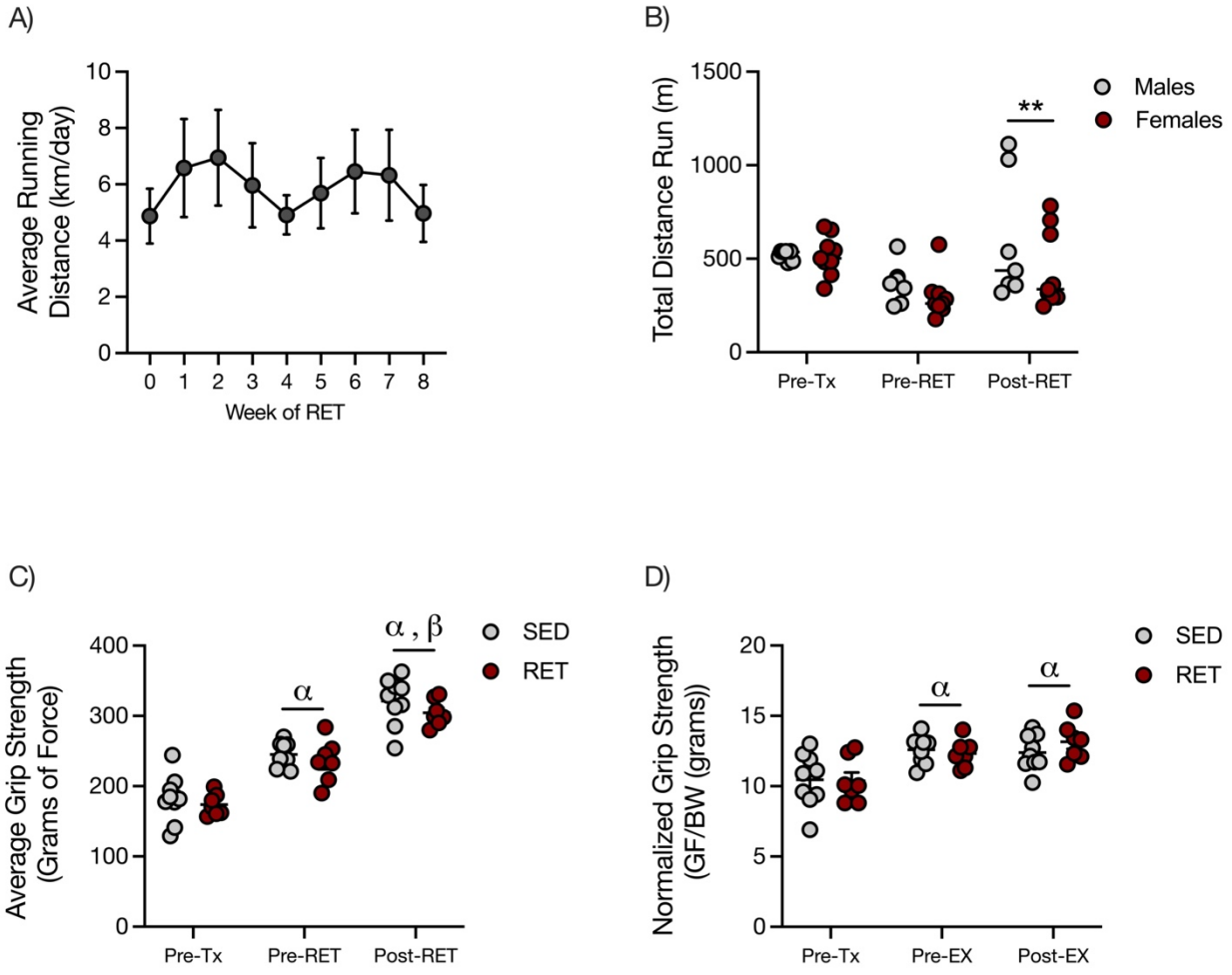

Figure S1. ***Weekly running distance and changes in grip strength and lean mass over the intervention.***

(A) Average running distance (km/day) for RET mice throughout the intervention. (B) Total distance run (m) males and females. (C) Average grip strength (grams of force). (D) Grip strength normalized by body weight. **P<0.001; α = significantly different than Pre-Tx; β = significantly different than Pre-RET. Two-way ANOVA, Sidak posthoc test. N = 7-9 per group.

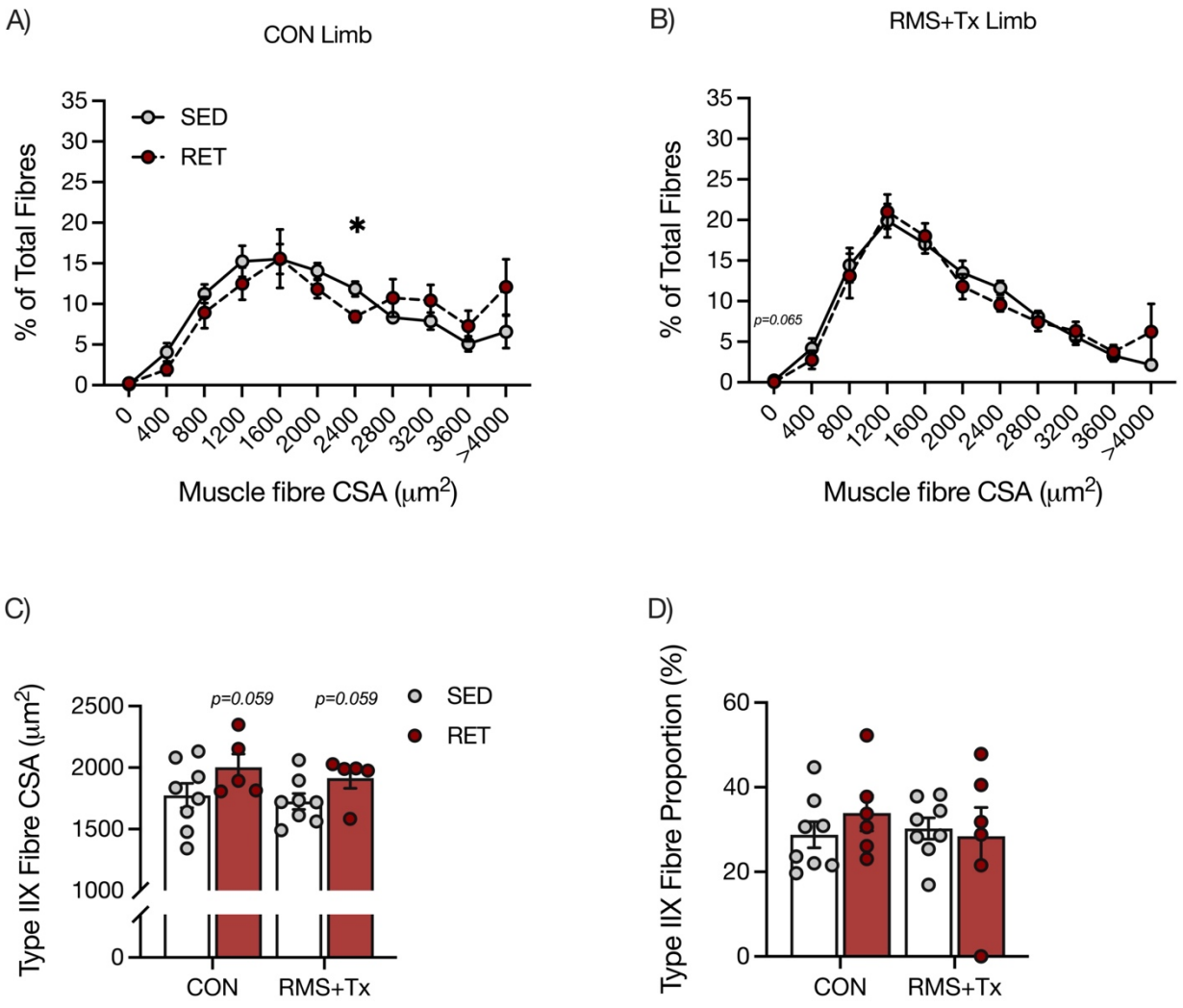

Figure S2. ***Fibre distribution and type IIx fibre characteristics.***

(A) Average percentage of myofibres within each CSA (μm^2) bin in the CON limb. (B) Average percentage of myofibres within each CSA (μm^2) bin in the RMS+Tx limb. (C) Type IIX fibre specific CSA (μm^2). (D) Proportion of Type IIX fibres (% of total fibre #). *P<0.05. Two-way ANOVA, Sidak post hoc test or unpaired t-test for each bin (A-B). N=6-8 per group

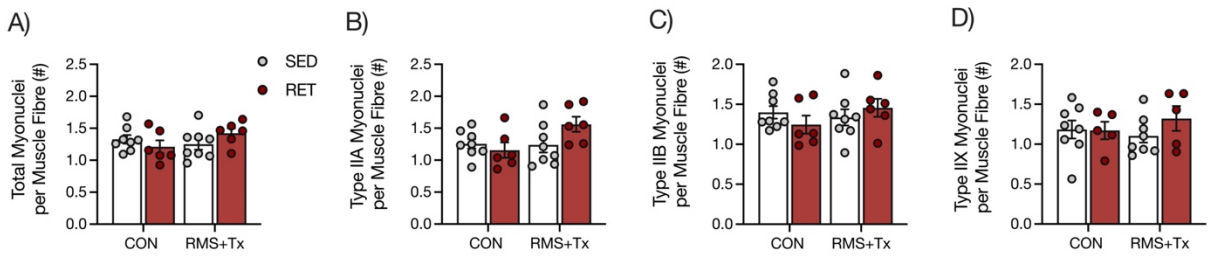

Figure S3. ***Fibre type specific myonuclei per fibre.***

(A) Total nuclei per fibre (#). (B) Nuclei per Type IIA fibre (#). (C) Nuclei per Type IIB fibre (#). (D) Nuclei per Type IIX fibre (#). Two-way ANOVA, Sidak post hoc test. N=6-8 per group.

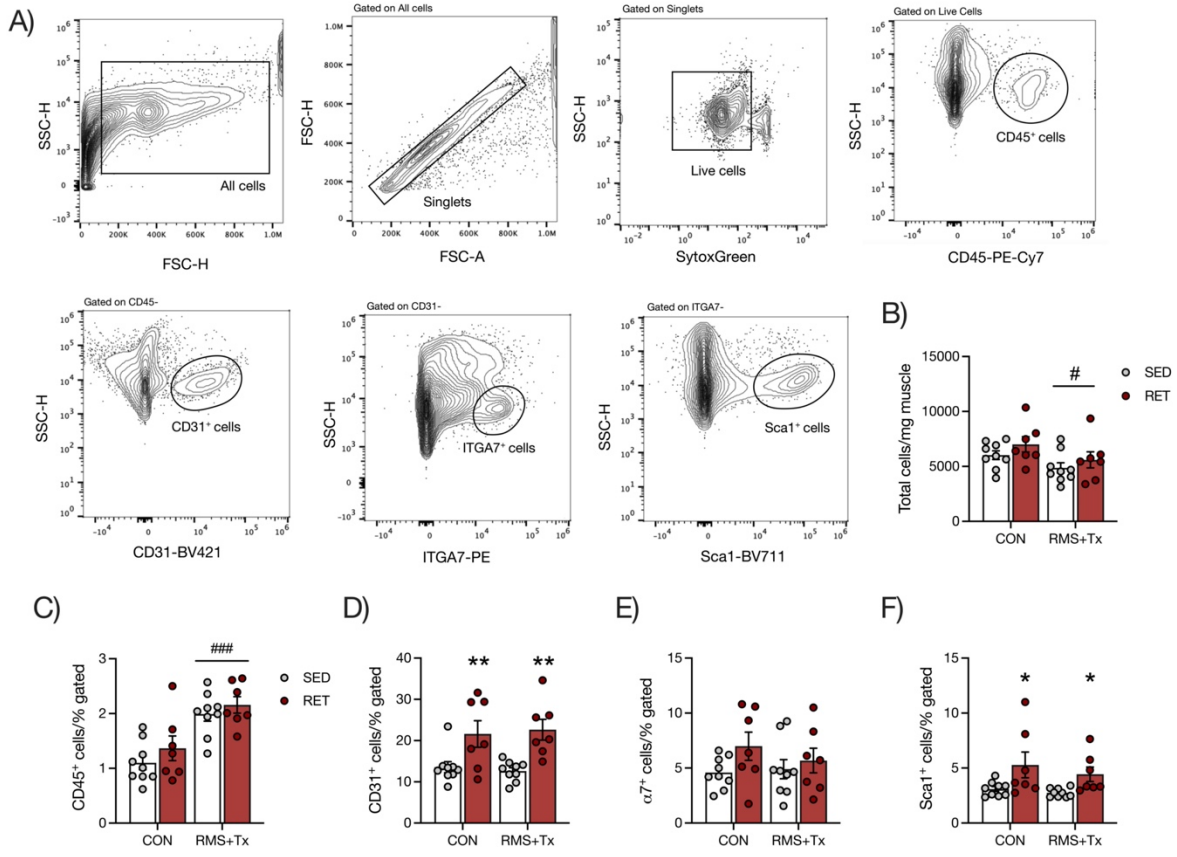

Figure S4. ***Representative flow plots and cell proportions.***

(A) Representative flow plots and gating strategy of cell populations analyzed from GAS. (B) Live cells per mg of muscle weight. (C) Percentage of $CD45^+$ cells gated. (D) Percentage of $CD31^+$ cells gated. (E) Percentage of $\alpha7^+$ cells gated. (F) Percentage of $Sca1^+$ cells gated. *P<0.05 , **P < 0.01; SED vs RET. #P < 0.05, ###P < 0.001; RMS+Tx vs CON. Two-way ANOVA, Sidak post hoc test. N= 7-9 per group.

Supplementary Figure 5.

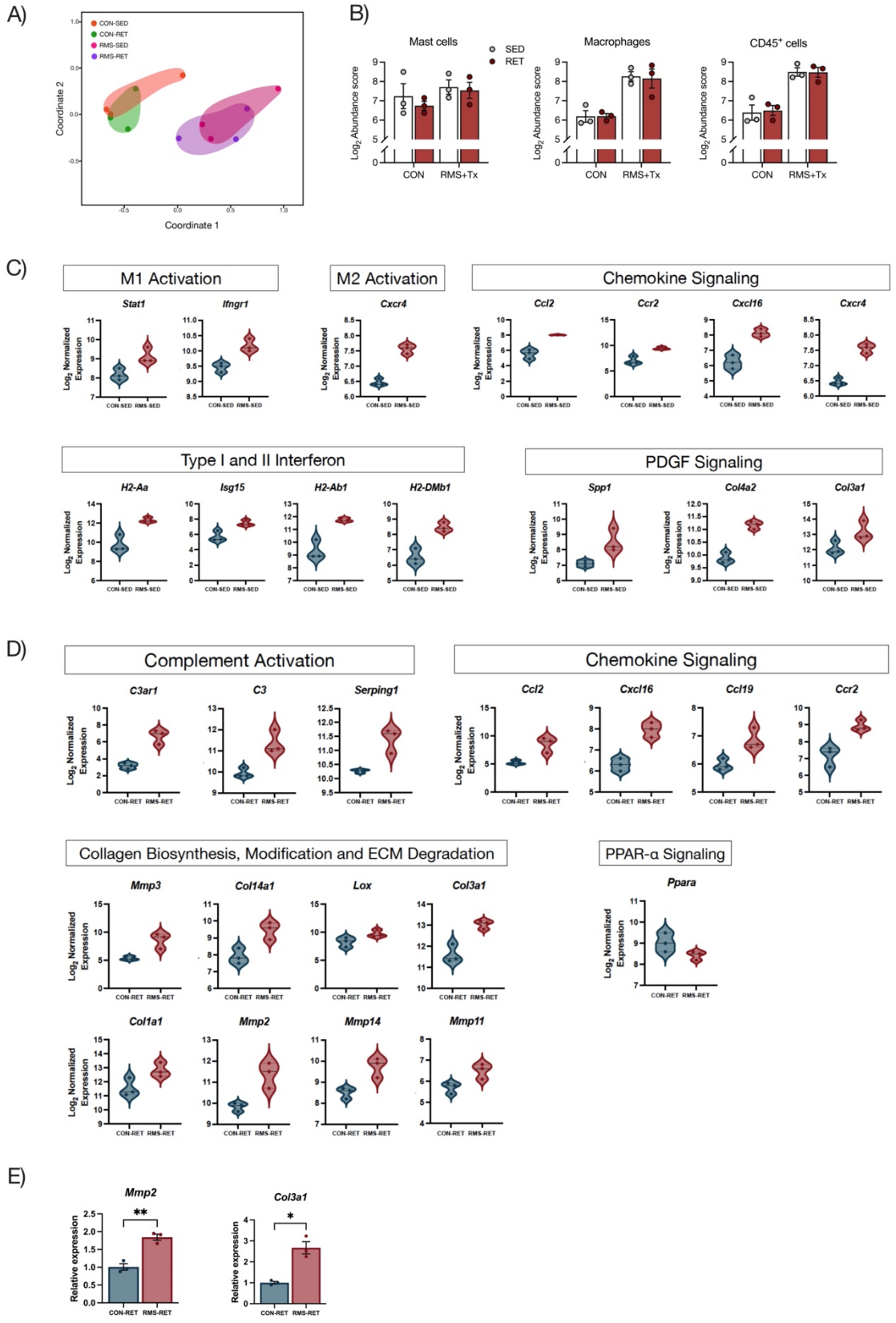

Figure S5. ***mRNA Cell Profiler and isolated gene changes.***

(A) Multidimensional scaling (MDS) plot of CON-SED, CON-RET, RMS-SED, and RMS-RET transcription profile. (B) Cell profiler analysis identifying enrichment of mast cells, macrophages, and CD45 cells. (C) Genes of the Top 10 direct enrichment score from the gene set analysis (GSA) in RMS-SED vs. CON-SED. (D) Genes of the Top 10 direct enrichment score from the gene set analysis (GSA) in RMS-RET vs. CON-RET. (E) Gene expression analysis by qPCR. *P<0.05 , **P < 0.001. N=3 per condition.

Appendix A

Protocols

Some protocols were previously established in the laboratory or created and optimized for this thesis. Some protocols were conducted according to the manufacturer's instructions.

Myosin Heavy chain staining for cultured cells

1. If the cells are grown on coverslips or a Multiwell plate, wash them twice with 1xPBS for 5 minutes.
2. Then, fix the cells with 4% formaldehyde/PBS for 10 minutes at room temperature. After that, wash them three times with 1xPBS for 5 minutes each time.
3. Next, permeabilize the cells with methanol at -20°C for 15 minutes.
4. Then, wash them twice with 1xPBS for 5 minutes each time. Incubate the cells with the primary antibody against myosin heavy chain MF-20 (diluted 1:100 in blocking solution) for 1 hour at room temperature. The antibody concentration is 5ug/ml; dilute it either 1:100 or 1:200 in the block solution. Alternatively, you can incubate the cells overnight at 4°C. The blocking solution consist of 10% FBS, 0.1% triton X in 1x PBS.
5. After incubation with the primary antibody, wash the cells twice with PBS for 5 minutes each time.
6. Then, incubate the cells with the secondary antibody (Alexa Fluor 488 or 594 goat anti-mouse, with 488 being recommended) for 30 minutes at room temperature in the dark. Dilute the secondary antibody in blocking solution (10% FBS, 0.1% triton X in 1xPBS) at a ratio of 1:300.
7. After incubation with the secondary antibody, wash the cells twice with 0.1% triton X in 1xPBS for 5 minutes each time.
8. Finally, counterstain the cells with DAPI for 5 minutes, then wash them twice with 1xPBS for 5 minutes each time.

9. If you are working with a Multiwell plate, add enough ddH2O to cover the wells before mounting.
10. Visualize the cells using Cell Discoverer.

Myosin Heavy chain Staining in CSA

Primaries antibodies:

- BA-D5 (IgG-2b) Myosin Heavy Chain Type I (1:100 dilution). **Type I (647)**
- SC-71(IgG1) Myosin Heavy Chain Type IIA (1:100 dilution). **Type IIA (488)**
- BF-F3 (IgM) Myosin Heavy Chain Type IIB (1:25 dilution). **Type IIB (Cy3)**
- Anti-Dystrophin (IgG) (1:50 dilution) **405**

Secondary antibodies:

- Cy™3 AffiniPure Fab Fragment Goat Anti-Mouse IgM, μ chain specific (**1:50** – 1:800 range)
- Alexa Fluor® 488 AffiniPure Goat Anti-Mouse IgG, Fcγ subclass 1 specific (**1:100** – 1:800 range)
- Alexa Fluor® 647 AffiniPure Goat Anti-Mouse IgG, Fcγ subclass 2b specific (**1:100** – 1:800 range)
- Alexa Fluor 405 Goat Anti-mouse (IgG) **(1:300) 1:50**

Day 1

1. Begin by air drying frozen or freshly cut sections (sections do not require fixation for this protocol).
2. Proceed to block them with M.o.M. for 1 hour at room temperature using a 1:25 (Drops) in 1x PBS solution.
3. Wash the sections with 1xPBS twice for 2 minutes each time, followed by adding M.o.M diluent for 5 minutes at a 1:12.5 in 1xPBS ratio.
4. Apply 1'Ab Dystrophin MANDRA 1:50 1% BSA in PBS overnight at 4 degrees.

Day 2

1. Wash the sections three times for 5 minutes with 1xPBS.

2. Add 2’Ab AF405- 1:50 1% BSA in PBS for 1 hour at room temperature.
3. Wash the sections with 1xPBS three times for 5 minutes each time.
4. Then, incubate them with a mixture of BA-D5 and SC71 for 45 minutes at 37°C in PBS-1%BSA.
5. Wash the sections with 1xPBS three times for 5 minutes each time.
6. Incubate them with a mixture of the following secondary antibodies: anti-mouse IgG2b-Alexa647 (for type I), anti-mouse IgG1-Alexa488 (for type IIA), anti-mouse Cy3 IgM (for type IIX) for 30-40 minutes at 37°C. Dilute the antibodies in PBS containing 0.5% of BSA and 5% of goat serum.
7. Wash the sections with 1xPBS three times for 5 minutes each time.

Note: If you do not use DAPI, proceed to Step 10. If you do use DAPI:

8. Apply it for 5 minutes at room temperature.
9. Then, wash the sections with 1xPBS for 1x5 minutes.
10. After the washes, briefly rinse the sections in water.
11. Finally, mount the sections and store them at 4°C.

It is recommended to create a negative section with only 2'Ab. Please note that if you are using the 405 channel, do not use DAPI as the same light cube is used in the cell discoverer.

Co-Staining CD31 (PCAM-1)/Dystrophin

1. To prepare the sections for immunostaining, allow the frozen sections to thaw and air-dry.
2. Next, fix them in acetone for 10 minutes in the freezer.
3. After removing the acetone, give the sections time to dry, and circle them with immunopen.
4. To create a negative section, wash once with PBS and then three times for five minutes each.

5. For blocking, use 5% BSA (1:20 in 1 x PBS) and leave it for 20 minutes at room temperature.
6. Then, add the 1st antibody, CD31 (clone 390, e-Bioscience, unconjugated) 1:100 in 1% BSA for 30 minutes.
7. After washing with 1% BSA (in 1 x PBS) three times, add the 2nd antibody, AF647 goat anti-rat (1:300) in block and leave it for one hour at room temperature.
8. Once again, wash with 1% BSA (in 1 x PBS) three times, and then add the MOM block for one hour at room temperature.
9. Wash twice with PBS for two minutes each time, and add the MOM block diluent for five minutes.
10. Then, add the 1st antibody, Dystrophin (mouse) 1:100 in 1% BSA for 30 minutes.
11. After washing with 1% BSA (in 1 x PBS) three times, add the 2nd antibody, AF488 goat anti-mouse (1:300) in block and leave it for one hour at room temperature.
12. Finally, wash with 1% BSA (in 1 x PBS) once for five minutes, add DAPI for five minutes at room temperature, and then wash again with 1% BSA (in 1 x PBS) once for five minutes.
13. Mount the sections, cover them with a coverslip, and apply nail polish around the slides to secure them.

Co-Staining with F4/80 and CD206

Day 1:

1. Air-dry the sections and use an immuno-pen to circle them. Create a negative section.
2. Wash the sections once in PBS for 2 minutes, three times.
3. Fix the sections using 2% PFA for 7 minutes at RT.
4. Wash the sections once in PBS for 2 minutes, three times.
5. Use 0.1% Triton x 100 to treat the sections for 10 minutes at RT.
6. Wash the sections once in PBS for 2 minutes, three times.
7. Block the sections using NGS/BSA/triton for 1 hour at RT.
8. Apply F4/80 aRat (1:100) in block for overnight at 4degreesC.
9. Do not apply 1'Ab on the negative section.

Day 2:

1. Wash the sections once in PBS for 2 minutes, five times.
2. Apply AF647 aRat (1:300) in block for 1 hour at RT.
3. Wash the sections once in PBS for 2 minutes, five times.
4. Block the sections using NGS/BSA/triton for 1 hour at RT.
5. Apply C206 aRabbit (1:150) in block for 1 hour at RT.
6. Do not apply 1'Ab on the negative section.
7. Wash the sections once in PBS for 2 minutes, three times.
8. Apply AF594 aRabbit (1:300) in block for 1 hour at RT.
9. Wash the sections once in PBS for 2 minutes, three times.
10. Use DAPI for 5 minutes at RT.
11. Wash the sections once in PBS for 2 minutes, two times.
12. Mount the slides, cover them with a coverslip, and apply nail polish around them.

Co-Staining Pax7/MyoD/Laminin

Day 1:

1. Air-dry the sections and circle them with an immuno-pen. Create a negative section.
2. Wash the sections with 1x PBS three times for 2 minutes each.
3. Fix the sections with 2% PFA for 7 minutes at room temperature.
4. Wash the sections with 1x PBS two times for 2 minutes each.
5. Incubate the sections with 0.1% Triton x 100 for 10 minutes at room temperature.
6. Wash the sections with 1x PBS two times for 2 minutes each.
7. Block the sections with MOM (mouse on mouse) for 1 hour at room temperature.
8. Wash the sections with 1x PBS two times for 2 minutes each.
9. Incubate the sections with Mom block diluent for 5 minutes at room temperature.
10. Incubate the sections with Pax7 mouse [neat] for overnight at 4 degrees Celsius. Do not apply 1'Ab on the negative section.

Day 2:

1. Wash the sections with 1x PBS three times for 5 minutes each.
2. Incubate the sections with AF488 aMouse (1:300) in 5% GS for 1 hour at room temperature.
3. Wash the sections with 1x PBS three times for 5 minutes each.
4. Block the sections with NGS (5%)/BSA(1%)/triton (0.2%) for 1 hour at room temperature.
5. Incubate the sections with MyoD aRabbit (1:100) & Laminin aRat (1:200) in block for overnight at 4 degrees Celsius. Do not apply 1'Ab on the negative section.

Day 3:

1. Wash the sections with 1x PBS three times for 5 minutes each.
2. Incubate the sections with AF594 aRabbit (1:300) & AF647 aRat (1:300) in block for 1 hour at room temperature.
3. Wash the sections with 1x PBS two times for 2 minutes each.
4. Incubate the sections with DAPI for 5 minutes at room temperature.
5. Wash the sections with 1x PBS three times for 5 minutes each.
6. Mount, coverslip, and apply nail polish around the slides.

Co-Staining PDGFRa and Laminin

Day 1:

1. 1.Air-dry sections and circle them with an immuno-pen. Create a negative section.
2. Wash the sections once with PBS and then three times for two minutes each.
3. Fix the sections with 2% PFA for seven minutes at room temperature.
4. Wash the sections again with PBS, twice for two minutes each.
5. Use 0.1% Triton x 100 for 10 minutes at room temperature.
6. Wash the sections three times with PBS for two minutes each.
7. Block with DAKO for 30 minutes at room temperature.
8. Apply PDGFRa aGoat (1:500) in the block and keep it overnight at 4 degrees Celsius. Do not apply 1st antibody on the negative section.

Day 2:

1. Wash the sections once with PBS and then three times for two minutes each.
2. Use AF488 aGoat (1:300) in block for two hours at room temperature.
3. Wash the sections again with PBS, three times for two minutes each.
4. Block with DAKO for 30 minutes at room temperature.
5. Apply Laminin aRat (1:200) in 1 x PBS and keep it overnight at 4 degrees Celsius. Do not apply 1st antibody on the negative section.

Day 3:

1. Wash the sections five times with PBS for two minutes each.
2. Use AF647 aRat (1:300) in 1 x PBS for one hour at room temperature.
3. Wash the sections again with PBS, three times for two minutes each.
4. Mount the slides, cover them with a coverslip, and apply nail polish around them.

Extracting Protein from Adherent Cells

1. Remove the medium from the culture dishes containing the cells and rinse them with ice-cold PBS.
2. Get rid of the PBS and add ice-cold lysis buffer.
3. Use a cold plastic cell scraper to scrape off the cells and collect them in microfuge tubes.
4. Agitate the contents of the microfuge tubes for 30 minutes at 4°C.
5. Centrifuge the tubes at 16000G for 10 minutes at 4°C. Collect the supernatant in a fresh tube and keep it on ice. Discard the pellet.

Western blot

Instructions for Sample Preparation:

1. To perform a protein quantification assay (Bradford assay), remove a small volume of lysate. Determine the protein concentration for each cell lysate.
2. Use an excel spreadsheet to calculate how much protein to load and add an equal volume of 4X Laemmli buffer and ddH20.

3. To denature your samples, boil each cell lysate in sample buffer at 95°C for 5 min. Aliquot and store lysates at -20°C for future use to avoid protein degradation. If stored at -80°C, boil again at 95°C for 5 min. After denaturation, vortex the sample and spin-down.

Instructions for Loading and Running the Gel:

1. Load equal amounts of protein into the wells of the SDS-PAGE gel, along with molecular weight marker.
2. Run the gel for 1-2 hours at 100V at room temperature. The time and voltage may require optimization depending on the protein being sought.

Instructions for Transferring Protein from Gel to Membrane:

1. Choose either nitrocellulose or PVDF as the membrane. Activate PVDF with methanol for 5-10 seconds and rinse with ddH20 before preparing the stack.

2. *Prepare the stack as follows:*

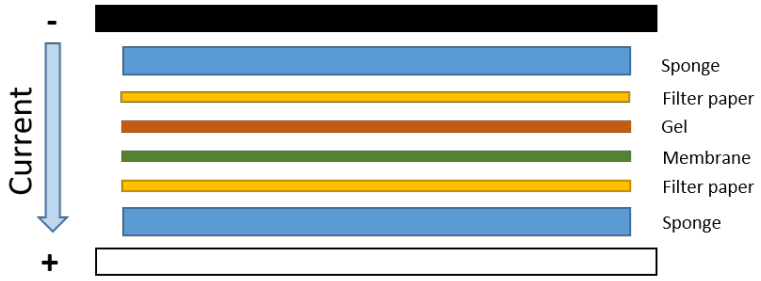

3. Optimize the time and voltage for a 1-hour transfer of 120 V to ensure efficient protein transfer from the gel to the membrane.
4. Before blocking, check the transfer using Ponceau S staining and take a picture for normalization purposes.
5. Wash the membrane three times for five minutes each with T-BST to remove the Ponceau S.
6. To begin antibody staining, block the membrane with 5% milk in TBS-T at room temperature for one hour.
7. Wash the membrane three times for five minutes each with TBS-T.

8. Dilute the primary antibody appropriately in 5% BSA in TBS-T and incubate the membrane overnight at 4°C.
9. Recover the primary antibody, which can be used up to three times.
10. Wash the membrane three times for five minutes each with TBS-T.
11. Incubate the membrane with the recommended dilution of the conjugated secondary antibody in blocking buffer (5% milk in TBS-T) at room temperature for one hour.
12. Wash the membrane three times for five minutes each with TBS-T.
13. Use an ECL kit (1:1 ratio) for signal development for five minutes in the dark.
14. Finally, scan the membrane.

Flow Compensation Beads.

1. To prepare the ABC beads for use, vortex them for 10 seconds as they are stored at 4 degrees Celsius.
2. Next, label the sample tubes correctly with the appropiate fluorochromes and add one drop of the ABC beads to each tube.
3. Then, add 1ul of the desired Antibodies (Ab's) for compensation in the Attune and mix well with a pipette.
4. Incubate the mixture for 15 minutes at room temperature in the dark.
5. Afterward, add 3 ml of 1x PBS or another buffer and centrifuge for 5 minutes at 250g at room temperature.
6. Remove the supernatant, but leave 50ul as the beads are not visible.
7. Resuspend it with 500ul of 1x PBS.
8. Next, vortex the Negative beads stored at 4 degrees Celsius and add one drop to each tube.
9. Vortex everything well and analyze with flow.

Muscle Progenitors Isolation

Protocol modified for scRNA-seq and Flow cytometer (Attune NxT)

Things that you need:

- Ham's F10 Media
- Collagenase B
- Dispase II
- FBS
- 1x PBS
- C tubes
- 25mM EDTA stock solution
- DMEM high Glucose
- P/S
- Twicers and scissors
- 50 and 15ml tubes
- Flow tubes
- Eppendorf tubes

FACS Media (50ml):

- 6ml of 25mM EDTA
- 5ml FBS
- 39ml of 1x PBS

Enzymatic Solution (50ml):

- 0.5 g of Collagenase B (final 1.5U/ml)
- 0.2 g of Dispase II (final 2U/ml)
- 50ml of Ham 's F10

*Note: Prepare fresh from powder stock same day. Mix gently and filter in 0.2um. "warm-up"

(This protocol is for two hindlimbs per MACS tubes)

NOTE: REMEMBER to keep a small piece of GASTROC/SOL for cryosections.

1. Place the muscle already clean (w/o Fat and connective tissue) into a 60mm dish containing 5ml of cold 1xPBS. (Place the dish on ice if you are dissection more mices).
2. Add 5ml of enzymatic solution into the MACS tubes (respectively labeled) and add the peace of muscles.
3. With scissors cut the muscle in small pieces into the MACS tube with the enzymatic solution on it.
4. Close the tube and inverted and place it on ice and go to the MACS gentle machine.
5. Machine: user 1, Slice_FACS, program 27min.
6. After, add 5ml of FBS to each MACS tube and pipette up and down with the pipette gun(10ml).
7. In a 50ml tube Filter the solution with a 100um strainer (*coat first the strainer with FBS), also rinse the MACS tube with 10ml of 1xPBS, close the cap mix it well and pass it to the filter as well.
8. Split the 50ml tube containing your sample into two 15ml tubes and centrifuge **600g 10min 4C** (respectively labeled).
9. Remove the supernatant with the pipette gun (10ml) and add 400ul of Red blood lysis buffer to the first tube (mix well with the p1000) and take all the solution and add it into the second 15ml tube that contain the half of your sample. Mix it well.
10. Add 10ml of cold FACS buffer, mix well
11. Centrifuge **600g 5min 4C**
12. Remove supernatant
13. Resuspend with 1ml FACS buffer

*From here, go the Flow cytometer and the scRNA-seq steps

For Flow cytometer (Attune NxT):

****REMEMBER TO TAKE 50ul for UNSTAINED AND 50ul for FMO for CD55 and CD142**

- After the step (13) take 200ul and split it into two Eppendorf tube (100ul each) (respectively labeled)
- Add to each tube 2ul of PDGFRa BV-605 antibody and wait for 20 min on ice (DARK)

- After the incubation period add:

First tube:

- CD31 BV421: 1ul
- CD45 PE-Cy7: 1ul
- Sca1 BV711: 1.8ul
- **CD55-PE:** 1.8ul

Second tube:

- CD31 BV421: 1ul
- CD45 PE-Cy7: 1ul
- Sca1 BV711: 1.8ul
- **CD142:** 1.8ul

(FOR FMO you can use less antibody 0.5 ul will be enough)

- Incubate for 30min
- After incubation wash the sample adding 1ml of FACS buffer and centrifuge 600g 5min 4C
- After the centrifugation remove the supernatant and add 1ml of FACS Buffer, mix well.
- Filter the sample into a Eppendorf tube with a 50um strainer.
- ****REMEMBER** add 0.3 ul of Sytox GREEN
- Incubate for 10-15min (ice-DARK)
- Maintain the samples on ice and use FLOW

For scRNA-seq

- After resuspending the sample in 1ml of FACS buffer, filter the sample with the 50um yellow strainer into a Flow tube.
- Add 1ml more of FACS buffer (because it's to concentrated to sort it that way)
- *Add 1ul of Sytox 7AAD FIRST and then 4 drops of NucBlue.*
- Wait approx. 10 to 15 min after the Sort
- Sort for Cells positives for NucBlue-Negative for Sytox 7AAD.

Click-iT Plus EdU detection.

Prepare stock solutions.

1. Allow vials to warm to room temperature
2. Add 2 mL DMSO (Component C) or an aqueous solution to Component A to make a 10 mM EdU stock solution. Store at –20°C
3. Make **1X Click-iT® EdU reaction buffer** by transferring the solution (4 mL) in the Component D bottle to 36 mL of deionized water. Store any remaining solution at 2–8˚C
4. Make **10X Click-iT® EdU buffer additive** by adding 2 mL deionized water to Component F and mixing until fully dissolved. Store at –20°C
5. Dilute Hoechst® 33342 (Component G) 1:2,000 in PBS to obtain a 1X solution

Label cells with EdU

1. Plate cells on coverslips and incubate overnight
2. Dilute 10 µL of 10 mM EdU stock solution in 5 mL of prewarmed tissue culture medium to make a 20 µM EdU labeling solution (enough for 10 coverslips)
3. Remove half of the medium from cells
4. Replace with an equal volume of EdU labeling solution (final concentration of 10 µM)
5. Incubate cells under appropriate growth conditions for two hours. NOTE: the choice of incubation time depends on the cell growth rate; thus optimization may be required
6. Proceed immediately to fixation and permeabilization

Fix and permeabilize cells

1. Transfer each coverslip into one well of a 6-well plate
2. Add 1 mL of 3.7% formaldehyde in PBS to each well
3. Incubate for 15 minutes at room temperature
4. Remove formaldehyde and wash twice with 1 mL of 3% BSA in PBS
5. Remove wash solution and add 1 mL of 0.5% Triton® X-100 in PBS to each well
6. Incubate for 20 minutes at room temperature

Detect EdU

1. Make **1X Click-iT® EdU buffer additive** by diluting the 10X solution created above **1:10** in deionized water. Prepare this solution fresh and use the solution on the same day.
2. Prepare Click-iT® Plus reaction cocktail according to the table below. IMPORTANT: add the ingredients in the order listed in the table.
3. Remove permeabilization buffer from cells and wash twice with 1 mL of 3% BSA in PBS
4. Remove the wash solution
5. Add 0.5 mL of Click-iT® Plus reaction cocktail to each well. Rock the plate briefly to ensure even distribution of reaction cocktail
6. Incubate the plate for 30 minutes at room temperature, protected from light
7. Remove the reaction cocktail and wash each well once with 1 mL of 3% BSA in PBS

Reaction components*	**Number of coverslips**						
	1	2	4	5	10	25	50
1X Click-iT® reaction buffer	440 µL	880 µL	1.84 mL	2.25 mL	4.4 mL	10.9 mL	21.9 mL

Copper protectant	10 µL	20 µL	40 µL	50 µL	100 µL	250 µL	500 µL
Alexa Fluor® picolyl azide (Component B)	1.2 µL	2.5 µL	5 µL	6 µL	12.5 µL	31 µL	62 µL
1X Click-iT® EdU buffer additive	50 µL	100 µL	200 µL	250 µL	500 µL	1.25 mL	2.5 mL
Total volume	500 µL	1 mL	2 mL	2.5 mL	5 mL	12.5 mL	25 mL
*Note: Add the ingredients in the order listed in the table.							

Stain DNA

1. Wash each well with 1 mL of PBS. Remove the wash solution
2. Add 1 mL of 1X Hoechst® 33342 solution per well
3. Incubate for 30 minutes at room temperature, protected from light
4. Remove the Hoechst® 33342 solution
5. Wash each well twice with 1 mL of PBS
6. Remove the wash solution
7. OPTIONAL: Perform antibody labeling of the samples at this time, following the recommendations from the manufacturer of the primary and secondary antibody. Note: protected samples from light during these incubations.

Image

1. Cells labeled with Click-iT® Plus EdU are compatible with all methods of slide preparation including wet mount or prepared mounting media

2. Image cells with appropriate filters listed below

Reaction components*	**Number of coverslips**						
	1	2	4	5	10	25	50
1X Click-iT® reaction buffer	440 µL	880 µL	1.84 mL	2.25 mL	4.4 mL	10.9 mL	21.9 mL
Copper protectant	10 µL	20 µL	40 µL	50 µL	100 µL	250 µL	500 µL
Alexa Fluor® picolyl azide (Component B)	1.2 µL	2.5 µL	5 µL	6 µL	12.5 µL	31 µL	62 µL
1X Click-iT® EdU buffer additive	50 µL	100 µL	200 µL	250 µL	500 µL	1.25 mL	2.5 mL
Total volume	500 µL	1 mL	2 mL	2.5 mL	5 mL	12.5 mL	25 mL
*Note: Add the ingredients in the order listed in the table.							

Cell signaling Senescence β-Galactosidase Cell Staining Protocol 9860

A. Solutions and Reagents

Reagents provided are sufficient to stain 125 x 35 mm wells.

Supplied Reagents

10X Fixative Solution #11674

10X Staining Solution #11675

100X Solution A #11676

100X Solution B #11677

X-Gal #11678

Additional Reagents (Not Supplied)

1X PBS

DMF (Dimethylformamide) #12767

Polypropylene tubes

37°C dry incubator (No CO_2)

Phase contrast or light microscope

70% glycerol (optional)

DMSO (Dimethyl Sulfoxide) #12611

B. Solution Preparation

NOTE: All solutions should be prepared just prior to use.

Volumes are for one 35 mm well of a 6-well plate. Volumes in the procedure should be approximately half that of the tissue culture media. (e.g. 1 ml for 35 mm well/plates containing 2 ml of media, 2.5 ml for 60 mm plates containing 5 ml of media, and 5 ml for 100 mm plates containing 10 ml of media).

1. **PBS:** Prepare at least 6 ml 1X PBS per 35 mm well
2. **Fixative Solution:** Dilute the 10X Fixative Solution to a 1X solution with distilled water. You will need 1 ml of the 1X solution per 35 mm well.

3. **Staining Solution:** Redissolve the 10X Staining Solution by heating to 37°C with agitation. Dilute the 10X staining solution to a 1X solution with distilled water. You will need 930 ul of the 1X Staining Solution per 35 mm well.
4. **X-Gal:**

IMPORTANT: Always use **polypropylene** plastic or glass to make and store X-gal. Do not use polystyrene.

Dissolve 20 mg of X-gal in 1 ml DMF to prepare a 20 mg/ml stock solution. Excess X-gal solution can be stored in -20°C in a light resistant container for up to one month.

Note: DMSO can be used in place of DMF.

5. **β-Galactosidase Staining Solution:** For each 35 mm well to be stained, combine the following in a **polypropylene** container:

. 930 µl 1X Staining Solution (See step 3)

a. 10 µl 100X Solution A

b. 10 µl 100X Solution B

c. 50 µl 20mg/ml X-gal stock solution (see Step 4)

IMPORTANT: Due to variations in water pH, please be sure that the β-Galactosidase Staining Solution has a final pH of 6.0 (A pH 5.9-6.1 is acceptable). pH differences can affect staining: A low pH can result in false positives and high pH can result in false negatives. If necessary, use HCl or NaOH to lower or raise pH, respectively.

C. Procedure

1. Remove growth media from the cells.
2. Rinse the plate one time with 1X PBS (2 ml or a 35 mm well plate, or match volume of media)
3. Add 1 ml of 1X Fixative Solution to each 35 mm well. Allow cells to fix for 10-15 min at room temperature.
4. Rinse the plate two times with 1X PBS (SAFE STOP) Alternatively, plates can be left in 1X PBS, covered at +4°C overnight.

5. Add 1 ml of the β-Galactosidase Staining Solution to each 35 mm well (see Solution Preparation Step 5).

Important: Seal plate with parafilm to prevent evaporation. Evaporation can cause crystals to form.

6. Incubate the plate at 37°C at least overnight in a dry incubator (no CO_2).

Note: The presence of CO_2 can cause changes to the pH which may affect staining results.

7. While the β-galactosidase is still on the plate, check the cells under a microscope (200X total magnification) for the development of blue color.
8. For long-term storage of the plates, remove the β-Galactosidase staining solution and overlay the cells with 70% glycerol. Store at 4°C.

CellRox Staining

Detection and quantitation of reactive oxygen species (ROS) in live cells

1. The vial is 2.5mM (with a total of 50ul) and the working concentration is either 5uM or 10uM. To serve as a positive control, use Menadione. The recommended dose is 100uM for 30 minutes (1 hour) at 37C for Flow.
2. To use CellRox, add it at a final concentration of 5uM or 10uM, depending on your cell line, and incubate it for 30 minutes at 37C. Afterward, remove the media and wash the cells thrice with 1xPBS. You can use the cell discoverer for live imaging (with a 508 excitation) and the NucBlue channel.

Note that the absorption/emission is at 485/520. Also, take note that this reagent is formaldehyde-fix compatible for up to 15 minutes.

FAPs Culture (primaries)

Media:

1. 20% FBS

2. DMEM high Glucose Media
3. bFGF (5 ng/ml)
4. 1% P/S (100 U/ml)

C3H/10T1/2 Culture

Media:

1. 10% FBS
2. DMEM high Glucose Media
3. 1% P/S (100 U/ml)

Primary myoblast culture

Media:

1. 20% FBS
2. DMEM high Glucose Media
3. bFGF (5 ng/ml)
4. 1% P/S (100 U/ml)

Culture cells

Changing Media

1. Remove old growth media carefully
2. Rinse the cells with warm 1xPBS
3. Remove and discard 1xPBS
4. Fill the plates with growth Media (10cm well plate with 7-8 ml of media).

Splitting cells

1. Heat the growth media (GM), trypsin 0.25%, and 1x PBS in the water bath.
2. Remove the old growth media from the cells.
3. Rinse the cells with 1x PBS twice.
4. Remove and discard the 1x PBS.
5. Add 1 ml of 0.25% trypsin to the cells.

6. Incubate the cells for 5 minutes in the incubator.
7. Gently tap the plate of cells to ensure that the cells have detached from the dish.
8. Add approximately 3 ml of normal growth media.
9. Triturate the cells about 6 times with the big pipette gun.
10. Remove the cells from the dish and place them into a 15ml falcon tube.
11. Centrifuge the tube for 5 minutes at 500g at 4 degrees Celsius.
12. Remove the supernatant and resuspend the cells with growth media.
13. Split the cells into a new plate.
14. Add media to the plate.

Fibrogenic FAP Differentiation

To differentiate FAPs towards their fibrogenic linage, follow these steps:

1. Incubate the cells in DMEM high glucose, 2% horse serum, and 1% P/S with 5ng/ml of TGFB1 for 3 days.
2. After 3 days, stain the cells with a-SMA.

Note: Store TGFB1 stock (400ng/ml) at -20C.

Preparation of TGFB1

Use Prepotech Cat# 100-21 vial 10ug of recombinant human TGFB1 and reconstitute in 10mM Citric Acid pH 3.0.

aSMA Staining

1. Fix the cells with 4% PFA for 10 minutes at room temperature (RT) or with straight Methanol at RT, and leave it at -20C for 10 minutes.
2. Wash the cells two times with 1x PBS.
3. Permeabilize the cells with 0.5% triton x-100 in PBS for 5 minutes at RT. (If you fix with methanol, the permeabilization step is not necessary).
4. Wash the cells two times with 1xPBS.
5. Block the cells with 10% FBS in 0.1% triton in PBS for 1 hour at RT.

6. Dilute primary Ab aSMA in Block solution and incubate ON 4C or 1hr RT. Dilution 1:300.
7. Wash the cells three times with 0.1% triton x for 5 minutes.
8. Add secondary Ab' (AF 594-Goat Anti-Mouse) diluted in block solution for 30 minutes at RT. Dilution 1:300.
9. Wash the cells three times with 0.1% triton in PBS.
10. Add DAPI for 5 minutes at RT.
11. Wash the cells once with 1x PBS and once with ddH2O.
12. Image.

Adipogenic FAP Differentiation

3. To create Adipogenic Media, mix 5ml of 10x Supl. Adipogenic Media with 45ml of Basal Medium.
4. Then, add 0.5 ml of L-Glutamine to create a final concentration of 2mM.
5. Apply the adipogenic media to the cells for 3 days.
6. Afterward, remove the media and add adipocyte maintenance medium, which consists of Growth Media (normal GM for FAPs 20% FBS, high glucose, 1% P/S) with 1ug/ml of INSULIN for 2 days to mature the adipocytes.
7. Note that the insulin stock concentration is 9.5 to 11.5 mg/ml, so use the 11.5 concentration.

Perilipin Staining

1. To begin Perilipin Staining, fix cells with 4% PFA for 10 minutes at room temperature, or with straight Methanol at room temperature and leave it at -20C for 10 minutes.
2. Wash the cells twice with 1x PBS. If you used methanol to fix, the permeabilization step is not necessary. Otherwise, add 0.5% Triton X-100 in PBS and permeabilize for 5 minutes at room temperature.

3. Wash the cells twice with 1x PBS.
4. Next, block 10% FBS in 0.1% Triton in PBS for 1 hour at room temperature.
5. Dilute Primary Ab Perilipin in block solution and incubate overnight at 4C or for 1 hour at room temperature. The dilution should be 1:300.
6. Wash the cells three times with 0.1% Triton X for 5 minutes.
7. Then, add the secondary Ab diluted in block solution and incubate for 30 minutes at room temperature. The dilution should be 1:300 (AF 594-Goat Anti-Rabbit).
8. Wash the cells three times with 0.1% Triton in PBS.
9. Add DAPI for 5 minutes at room temperature, and then wash the cells once with 1x PBS and once with ddH2O.
10. Image

Radiation Protocol

Here are the steps to follow when using the radiation machine at ACVS:

1. Visit the ACVS website to reserve the radiation machine.
2. Turn on the X-RAD 320 and allow it to warm up.
3. Confirm that the correct filter is in place for either animals or cells.
4. If you are working with mice, bring their cages to the x-ray room using carts and allow them to acclimatize for 30 minutes.
5. Place each mouse in a new, clean, transparent cage. To sedate the mouse, connect the isoflurane and oxygen tube to the cage. This will allow you to use the nose cone in the irradiator to keep the mouse sedated during the irradiation procedure.
6. Carefully remove the sedated mouse from its cage and position it with its nose in the actively pumping nose cone inside the irradiator. Make sure the radiation beam is fully covering the area that you wish to irradiate.
7. Extend the left leg of the mouse outward and tape it gently with skin-safe medical tape.
8. Place the lead body shield over the mouse with the left leg sticking out, ensuring that no other body part of the mouse is exposed to the radiation beam.
9. Close the X-RAD door gently to prevent it from slamming.

10. Use the conversion chart on the radiator to convert 4.8Gy, 8.2Gy or 16Gy to the appropriate MU dosage. Double-check to ensure you have the correct dose and write it down on a sticky note to ensure you give the same dose to each mouse.
11. Hit the enter button to confirm the dose selection.
12. Press the start button to begin the radiation process, then step out of the room.
13. Once the radiation process is complete, the light will go off, and you can gently remove the mouse and put it back in its cage.
14. Monitor the mouse to ensure it wakes up from the sedation without any issues.
15. After administering all the doses, transfer each mouse to a sterile cage to avoid infection and monitor them closely.

Exercise Endurance Test

1. To conduct the test, acclimate the mice to the testing room for half an hour.
2. Place each mouse on a separate lane of the treadmill.
3. Start the test at a speed of 11 m/min and increase it by 1 m/min every two minutes.
4. Encourage the mice to keep running using paintbrush bristles, and do not use electric shock.
5. Consider a mouse to have completed the test if it meets any of the following criteria: (1) resists stimulation, (2) remains on the platform for over two minutes, or (3) stays approximately one body length away from the platform for over five continuous seconds.
6. Record the finishing time and distance of each mouse.

Grip Strength Test Procedure

1. Bring your mice to the testing room and allow them to habituate for 30-60 minutes. Remember to turn over the "Do Not Disturb" sign hanging outside the door to ensure no one will enter during testing.
2. Before taking grip strength measurements, always weigh each mouse to enable grip data normalization using animal body weight. Press the power button to turn on the instrument, then press the Zero key to reset the value to 0.
3. Hold the mouse gently using the proper holding techniques and move it close to the grid. The instrument is ready to use when a numerical value is displayed on the screen.

Gently pull the mouse along a horizontal plane relative to the grid at a steady speed of approximately 2.5 cm/sec until the animal releases the grid. Avoid pulling the mice away too slowly as it may cause premature release of the bar with one or both paws.

4. After the mouse releases the grid, record the value of force displayed on the screen in gram force (GF). The instrument only displays the maximal value, so press the Zero key multiple times to clear the screen. Repeat the process for a maximum of eight consecutive measurements with a 10-second rest period in between each trial.
5. Finally, place the mouse back in its home cage and repeat the test for all mice. When finished, log off the computer, return the mice to their regular housing room, and clean the testing room.

Resistance endurance training (RET) set-up, Monitoring, and Wheel Data Analysis

Please follow the steps below to set up the monitoring system for the mice's running wheels:

1. Request 10 low-profile wireless running wheels with plate numbers 1 and 2 from the behavioural core. (ENV-044 and ENV-047)
2. Insert batteries into the wheels.
3. Bring the cart with the monitoring software, named "Wheel Manager Software SOF-860," into the room where the mice are kept.
4. Ensure that the software picks up the wheels by checking if each wheel's specific number is displayed on the screen.
5. Smooth out the bedding at the bottom of each cage.
6. Place the docking plate at the bottom of each cage and remove any pellets between the dock and the cage floor.
7. Check that the two pegs on the dock are upright, then securely attach each low-profile wheel onto the dock.
8. Use hot glue to attach a 1g magnet (K&J magnetics) to the outer edge of each wheel as close as possible to the outside for maximum resistance.
9. Once the original magnet is securely attached, additional weight can be added incrementally by allowing the magnets' attractive forces to keep them in place.

10. Set the software to count the total revolutions for a 24-hour period.
11. Check the software daily to ensure that it accurately counts the number of revolutions completed by each mouse, and export the data to an Excel sheet each day in case of system failures.
12. Select "file" and "export sensor data."
13. Make sure to select "include sensor headings," "include row labels," and "include column labels" in the export data pop-up.
14. Choose "date/time column" under report format and "revolutions" under activity units.
15. Edit the output file and select a specific location to save it, then press the "ok" button.
16. Each wheel has a conversion factor of 6.0198 cm per revolution, which can be used to calculate the total distance run per day.

scRNA-seq Codes

For all De Lisio's Lab members, the codes are saved in the shared De Lisio Lab OneDrive folder of Nicolas Collao. You can obtain access to it through this link: https://uottawa.sharepoint.com/sites/1600_365_T_DeLisioLab/SharedDocuments/Forms/AllItems.aspx?id=%2Fsites%2F1600_365_T_DeLisioLab%2FSharedDocuments%2FGeneral%2FLab Members%2FNicolasCollao%2FSTUDIES%2FscRNA-seq project%2FCodes and files&viewid=c5150322-ce80-44ba-a722-2197799a95a9

TMRM and Mitotracker Green stain

1. Incubate cells with growth media with indicated dye concentrations.
2. Wash 3x with Phenol Red Free Media.
3. Add 1000 µL of Phenol Red Free Media to empty wells.
4. Read on Plate Reader.
5. Image on Cell Discoverer - MTGFM plates can go for flow cytometry.

6. Add FCCP to a final concentration of 10 µM (1 µL of 10 mM to each well) of FCCP-stained plates.
7. Read on Plate Reader
8. Image on Cell Discoverer.

DNA extraction

For Cultured Animal Cell (Bio-BAsic

1. Centrifuge the appropriate number of cells (>5x10⁶) for 5 minutes at 200 x g (1,200 rpm).
2. Resuspend pellet in 500 µl of PBS Soluon. 2. Wash the cells 2 mes with PBS Soluon.
3. Resuspend pellet in 300 µl of ACL soluon buffer.
4. Add 20 µl of Proteinase K, mix well and Incubate at 55°C for 10 minutes.
5. Cool to room temperature. Vortex for 20 seconds and centrifuge 10,000 x g (12,000 rpm) for 5 minutes.
6. Pipette 200 ul of supernantant to a new Eppendorf tube, add 200ul of AB solution Mix by occasionally inverting tube, and keep for 2 minutes. Then lad all the solution to a EZ-10 Spin Column.
7. Centrifuge at 2,000 x g (4000 rpm) for 2 minutes and discard the flow-through.
8. Add 500 ul of wash solution, and spin at 8,000 g (10,000 rpm) for 1 min.
9. Repeat step 9, wash twice.
10. Discard flow-through. Spin at 8,000 x g (10,000 rpm) for an addional minute to remove residual amount of Wash Soluon.
11. Place the column into a clean 1.5 ml Eppendorf tube. Add 30-50 µl Eluon Buffer into the center part of membrane in the column. Incubate at RT for 2 or 3 minutes. Incubang the tube at 37°C or 50°C for 2 minutes may increase recovery yield. 1
12. Spin at 8,000 x g (10,000 rpm) for 1 minute to elute DNA from the column.
13. For long term storage, keep aliquots of purified genomic DNA at -20 °C.
14. Measure DNA quantity by UV absorption at A260 (1.0 OD unit is equivalent of 50 ug). Assess genomic DNA quality with an analytical 0.7% agarose gel.

yH2AX

1. Wash the cells twice with 1x PBS.
2. Fix the cells with 4% PFA for 10 min at RT.
3. Wash twice with 2x PBS.
4. Permeabilize the cells with 2% triton x-100 in 1x PBS for 10min at RT, or with methanol 15 min 4C.
5. Wash twice with 1x PBS.
6. Block with 1% BSA in PBS for 20min at RT.
7. Incubate with phosphor yH2AX with 5% FBS, 1xPBS and 0.1% Triton-X for 30 min at RT Dark.
8. Wash twice with 1x PBS.
9. Add DAPI for 5 min.
10. Wash twice with 1x PBS.
11. Add ddH2O into the well.
12. Image in the Cell Discoverer.

M3-9-M Rhabdomyosarcoma (RMS) cell line

Media:

1. Glutamax (100x) Stock (Gibco, Cat# 35050-061)
2. Non-essential amino acid (100x) Mem-Neaa (Gibco, Cat# 11140-050)
3. HEPES Buffer (1M stock) (Gibco, Cat# 15630-080)
4. 15% Heat-Inactivated FBS (56C for 30min)
5. RPMI 1640 (500ml, Multicell, Cat# 350-045-CL w/o HEPES, L-Glutamine and Phenol Red.
6. P/S (100 IU/ml)/(100 ug/ml)
7. 50 uM of 2-Mercaptoethanol (55mM stock)

RMS cell line injection

1. To culture RMS M3-9-M cells, use 3-5 10cm plates and allow them to grow until they reach about 80% confluency. These cells grow quickly, so keep an eye on them.

2. Use specific RMS media containing RPMI 1640 and 1% L-glutamine with 10% heat-inactivated fetal bovine serum, HEPES buffer, 1% non-essential amino acids, 1% sodium pyruvate, 1% penicillin/streptomycin, and 50 mM 2-mercaptoethanol to culture the cells.
3. To prepare the cells for injection, lift them from the plate using trypsin, remove the cell debris in the supernatant, and re-suspend them in sterile PBS. Count the number of cells per ml of solution using a cell counter and adjust the volume of PBS accordingly to accurately inject 100,000 cells into each mouse. This should be done on the morning of the injections.
4. Using isoflurane, sedate each mouse and remove the hair on the entire left hindlimb with clippers to ensure accurate location for the injection. Use a sterile insulin syringe to inject the M3-9-M cells into both lobes of the left GAS hindlimb of each mouse.

Chemotherapy Administration (Vincristine)

1. Start by dissolving solid vincristine sulfate (Sigma Aldrich, cat#. V8388) in sterile water and ensure it is combined homogenously to create a 20mg/ml concentration.
2. Store this solution in the -20c freezer for a few weeks. It is best to prepare this stock solution before it is needed and dilute it to the required concentration the day of the vincristine injections.
3. On the day of injection, freshly dilute the stock solution to a concentration of 0.2mg/ml (1:100) in PBS.
4. Weigh each mouse using an electronic scale on the day of the injections to ensure that each dosage is specific for each individual mouse.
   NOTE: It is important to weigh each mouse to ensure they weigh more than 12g during vincristine administration as a lower weight may be fatal.
5. Ensure each mouse receives 1mg/kg of body weight (5ul per gram).
6. Use a sterile standard insulin syringe to inject each mouse I.P.
7. Monitor the mice closely.

RNA Isolation from Mouse Tissue (frozen in liquid nitrogen)

Homogenization:

- Chip frozen tissue to weight of 20 – 25mg
- Transfer 25mg of tissue sample into tube containing 1.0mL Trizol Reagent without delay.
- Homogenize for 30 – 60 seconds at room temperature using glass homogenizer
- Incubate the homogenized sample at room temperature for 5 minutes
- Add 0.2mL of cholorfom per 1.0mL of Trizol Reagent (ie. Add 200µL of chloroform)
- Shake tube vigorously for 15 seconds
- Incubate at RT for 5 minutes
- Centrifuge at 12 000g, 4ºC for 10 minutes
- Transfer upper aqueous phase (450 ul) to new tube and measure volume.

NOTE: RNA from 10cm plate. Wash the cells with 1xPBS and then add 350 ul of RLT buffer. Scape the cells and transferred to a Eppendorf tube. Continue with the steps below.

RNA Purification:

- Add equal volume of 70% ethanol (use isopropanol) to aqueous phase transferred in previous step & mix be pipetting. Do not centrifuge.
    - Note: a precipitate may form after the addition of alcohol in some preparations. This does not affect the procedure.
- Pipette 700µL of the volume into an RNA spin column placed into a 2mL collection tube (provided in kit). Centrifuge at 10 000g for 30-60 seconds at RT. Discard flow through.
- **Optional:** This is the starting point if performing the optional on0column DNase1 digestion. Follow protocol as outline on page 15 of instruction manual from Total RNA Kit 1 from OMEGA
- Pipette 500µL of RNA Wash Buffer I directly into the RNA spin column. Centrifuge at 10 000g for 30-60 seconds at RT and discard flow through.

- Pipette 500µL of RNA Wash Buffer II (RPE) diluted with absolute ethanol into the RNA spin column. Centrifuge at 10 000g for 30-60 seconds at RT. Discard flow though.
- Pipette 350µL of RNA Wash Buffer II (RPE)diluted in absolute ethanol into the RNA spin column. Centrifuge at 10 000g for 30-60 seconds at RT and discard flow though.
- With the 2mL collection tube emptied, centrifuge the RNA spin column at 2 min on max speed to completely dry the matrix. (Note: Lids often tear off, ensure microcentrifuge tube is labelled on side before spinning.)

Eluting RNA:

- Pre-heat 40-70µL of DEPC-treated (or RNase free) water. (ie. Place in microwave for 45-60 seconds)
- Transfer the RNA spin column into a clean 1.5mL collection tube (ie. 1.5mL centrifuge tube – not supplied in kit), and elute RNA with pre-heated 40 - 70µL of DEPC-treated water (or RNase free water). Ensure to add the water directly to the spin column. Centrifuge for 2 minutes at 10 000g.
    - Note: a second elution **may be** necessary if expected yield of RNA is >30ng. Just one is enough.
- Alternatively, RNA may be eluted with a greater volume of water. While additional elutions increase total RNA yield, the concentration will be lower since more that 80% of RNA has been recovered in the first elution. Pre-heating the water to 70ºC before adding it to the column, and incubating the column for 5 min at RT before centrifugation may increase yields.
- Quantify RNA in flow through immediately with nanodrop (blanked with same water/solution used to elute RNA) or store at -80ºC until use.

Beads Homogenizer for Muscle

1. Remove the samples from the -80 and leave them in dry-ice.

2. Label the special tubes for the homogenizer and add “4 beads” into the 2ml homogenizer tube.
3. You can smash the muscle and make it powder to extract as much protein as possible.
4. Use the hammer and the metal container (Burelle’s Lab)
5. Weight the muscle and add RIPA buffer (containing proteases and phosphatases inhibitors, for 10ml of RIPA add one full tablet of phosphatase and proteases inhibitors) based on the weight of the sample. (i.e 50mg of muscle add 500ul of RIPA buffer)
6. Place the homogenizer machine in the -4 degrees room and the samples.
7. Run 2 bouts of 60 sec at max speed with 5 sec in between.
8. After that you can remove the beads and centrifuge at 15000 rpm, 4C for 15 min.
9. Take the supernatant and transfer it into a 1.5 ml Eppendorf tube.
10. Remove 5ul of the sample and add it into a PCR tube for Bradford assay.
11. Flash freeze the sample
12. Storage at -80 degrees.

Note: the beads and the homogenizer tubes can be used again, make sure you cleaned with water and ethanol.

Bradford assay

1. Dilute concentrated bradford reagent (store at 4C) 1:5 in 1x PBS (The bradford reagebet final volume will depend of how many samples do we have)
2. Prepare standar and blank as follow: Create a serial dilution of 2ug/ul BSA stock in PBS. Make the standard curve with 0 – 0.125 – 0.25 – 0.5 – 1 and 2 ug/ul
3. Prepare 1:10 dilutions of the samples. (to your 5ul of your samples add 45ul of ddH20, you can change the dilution factor as you need)
4. Pipette 5ul of each (standard curev and samples already diluted into a 96 WP). Make Duplicates.
5. Add 250 ul of 1x Bradford reagent using the multichannel pipette into the wells containing the standard curve and your samples in duplicate.
6. Insert the plate into the plate reader and read it at 595 wavelengths.
7. Absorbance is in the RAW data.

Appendix B

Resources table

REAGENT	SOURCE	CATALOG #
Antibodies		
FITC Rat Anti-Mouse CD45	BD Biosciences	Cat# 561088
BV421 Rat Anti-Mouse CD31	BioLegend	Cat# 102423
anti-Alpha 7 Integrin 647	AbLab Biologics	Cat# 67-0010-05
anti-Alpha 7 Integrin PE	AbLab Biologics	Cat# 53-0010-05
BV711 Rat Anti-Mouse Ly-6A/E	BD Bioscience	Cat# 563992
PE anti-mouse CD55	BioLegend	Cat# 131803
CD140a, PDGFRα, BV605	BD Bioscience	Cat# 740380
PE Mouse Coagulation Factor III/Tissue Factor	R&D Systems	Cat# FAB3178P
SYTOX™ AADvanced™	Thermo Fisher Scientific	Cat# S10349
SYTOX™ green	Invitrogen	Cat# S34860
PE-Cy™7 Rat Anti-Mouse CD45	BD Bioscience	Cat# 552848
alpha-smooth muscle actin (αSMA)	MilliporeSigma	Cat# A5228
anti-Laminin	Invitrogen	Cat# MA1-06100
PDGFRα	R&D Systems	Cat# AF1062
Pax7	DSHB	Cat# 528428
CD31	Invitrogen	Cat# 14-0311-85
F4/80	Abcam	Cat# 6650

CD206	Abcam	Cat# 64693
Alexa Fluor® 647 AffiniPure Goat Anti-Mouse IgG, Fcγ subclass 2b specific	Cedarlane Laboratories	Cat# 115-605-207
Alexa Fluor® 488 AffiniPure Goat Anti-Mouse IgG, Fcγ subclass 1 specific	Cedarlane Laboratories	Cat# 115-545-205
Cy™3 AffiniPure Fab Fragment Goat Anti-Mouse IgM, μ chain specific	Cedarlane Laboratories	Cat# 115-167020
Alexa Fluor 594 Goat anti-Rat	Invitrogen	Cat# A-11012
Alexa Fluor 488-Goat Anti-Mouse	Invitrogen	Cat# A11001
Alexa Fluor 594-Goat Anti-Mouse	Invitrogen	Cat# A11005
Anti-phospho- Histone H2A.X (Ser139)	Cell Signaling Technology	Cat# 9718T
AbC™ Total Antibody Compensation Bead Kit	Thermo Fisher Scientific	Cat# A10497
Fibronectin	MilliporeSigma	Cat# F3648
p-SMAD3	Cell Signaling Technology	Cat# 9520S
SMAD3	Cell Signaling Technology	Cat# 9523S
Anti-cyclophilinB	Abcam	Cat# ab16045
anti-mouse IgG	Cell Signaling Technology	Cat# 7076S
anti-rabbit IgG	Cell Signaling Technology	Cat# 7074S
anti-MyHC	DSHB	Cat# MF-20
Other reagents		
NucBlue™ Live ReadyProbes™ Reagent (Hoechst 33342)	Thermo Fisher Scientific	Cat# R37605

SYTOX™ AADvanced™	Thermo Fisher Scientific	Cat# S10349
Collagenase B	Roche® Life Science Products	Cat# 11088831001
Dispase II	Sigma Aldrich	Cat# 42613-33-2
Red Blood Cell Lysing Buffer	Sigma-Aldrich	Cat# R7767
Optimal cutting temperature (OCT)	Fisher Scientific	Cat# 4585
liquid nitrogen-cooled isopentane	Sigma-Aldrich	Cat# 277258-1L
Premium Frosted Microscope Slides	Fisher Scientific	Cat# 12-544-2
Click-iT EdU Assay Kits	Thermo Fisher Scientific	Ca# C10337
DMEM High Glucose	Wiset Bioproducts	Cat# 319-005-CL
DMEM low glucose	Wiset Bioproducts	Cat#319-010-CL
Fetal Bovine Serum (FBS)	Thermo Fisher Scientific	Cat# 12483-020
Horse Serum	Thermo Fisher Scientific	Cat# 16050122
Ham's F10 media	Wiset Bioproducts	Cat# 318-050-CL
RPMI media 1640	Wiset Bioproducts	Cat# 350-000CL
Basic fibroblast growth factor (bFGF) 5 ng/ml	MilliporeSigma	Cat# F0291
100 U/ml penicillin/streptomycin (P/S)	Thermo Fisher Scientific	Cat# 15140-122
MesenCult™ Adipogenic Differentiation Kit	Stemcell Technologies	Cat# 05507
Insulin (1 µg/ml)	MilliporeSigma	Cat# I9278
Transforming growth factor beta-1 (TGFβ-1)	PeproTech	Cat# 100-21

4’, 6-diamidino-2-phenylindole (DAPI)	Sigma-Aldrich	Cat# D9542
Triton X-100	Sigma-Aldrich	Cat# 9036-19-5
CellROX™ Green reagents	Thermo Fisher Scientific	Cat# C10444
Senescence-associated β-Galactosidase (SA-β-Gal)	Cell Signaling Technology	Cat# 9860
MitoTracker Green FM	Invitrogen	Cat# M7514
Tetramethylrhodamine, methyl ester (TMRM)	Invitrogen	Cat#T668
Seahorse XFe96 Microplates	Agilent Technologies	Cat# 101085-004
Mouse on Mouse Immunodetection Kit (M.o.M)	Vector Labs	Cat# BMK-2202
Serum-Free Protein Block	Agilent	Cat# X0909
100-µm strainer	Fisher Scientific	Cat# 22-363-549
Protease inhibitor cocktail	Millipore Sigma	Cat# 04693116001
Phosphatase inhibitor (PhosSTOP)	Millipore Sigma	Cat# 4906837001
Bradford assay	Bio-Rad	Cat# 5000006
PVDF membranes	Bio-Rad	Cat# 162017
Oligomycin	Sigma-Aldrich	Cat# 75351
FCCP	Sigma-Aldrich	Cat# C2920
Rotenone	Sigma-Aldrich	Cat# R8875
Antimycin	Sigma-Aldrich	Cat# A8674
2-Deoxy-D-Glucose (2-DG)	Sigma-Aldrich	Cat# D6134

RNA extraction Micro Kit	Qiagen	Cat# 74004
DNA commercial kit	BioBasic	Cat# BS427
Luna® Universal qPCR MasterMix	New England BioLabs	Cat# M3003S
L-glutamine	STEMCELL Technologies	Cat# 07100
HEPES	Gibco	Cat# 15630-080
Non-essential amino acids	Gibco	Cat# 11140-050
Sodium pyruvate	Gibco	Cat# 11360-070
2-mercaptoethanol	Gibco	Cat# 21985-023
Vincristine sulfate	Sigma-Aldrich	Cat# V8388
SuperSignal™ West Pico PLUS Chemiluminescent Substrate	Thermo Fisher Scientific	Cat# 34579
Chromium Next GEM Single Cell 3′ Kit v3.1	10X Genomics	Cat#PN-1000121
NanoString nCounter Mouse Fibrosis V2 panel	NanoString Technologies	Cat# 115000388
Deposited data		
Raw scRNA-seq data and processed matrices	GEO	GSE24165
Experimental models		
C57Bl/6J	The Jackson Laboratory	Cat#000664
CBA	The Jackson Laboratory	Cat#000656
C3H/10T1/2 Clone 8	ATCC	Cat# CCL-226
M3-9-M RMS cells		

Softwares		
CellRanger version v5.0.0	10x Genomics	https://support.10xgenomics.com/single-cell-gene-expression/software/release-notes/3-0
R/RStudio v4.2.1	R CRAN	https://cran.r-project.org/
Seurat R package v4.2.0	R CRAN	https://cran.r-project.org/web/packages/Seurat/index.html
enrichR v3.1	R CRAN	https://cran.r-project.org/web/packages/enrichR/index.html
ClusterProfiler R v3.10.1	Bioconductor	https://bioconductor.org/packages/release/bioc/html/clusterProfiler.html
CellChat v1.6.0		https://github.com/sqjin/CellChat
Ucell v1.0.0		https://github.com/carmonalab/UCell
FlowJo™ v10.8	BD Life Sciences	https://www.flowjo.com/
GraphPad Prism v10	GraphPad Software	https://www.graphpad.com/
Zen Blue v2.6	ZEISS	N/A
Fiji	ImageJ	https://fiji.sc/
nSolver v4.0	NanoString Technologies	https://nanostring.com/
ROSALIND® nCounter Data Analysis	ROSALIND	https://www.rosalind.bio/

Imaris v9.7.2	Oxford Instruments	https://imaris.oxinst.com/
Wheel Manager Software	Med Associates	SOF-860
Others		
X-RAD 320, Precision X-Ray Irradiation	N/A	N/A
Attune™ Nxt Acoustic Focusing Flow Cytometer system	Thermo Fisher Scientific	N/A
MoFlo XDP cell sorter	Beckman Coulter Life Sciences	N/A
Illumina NextSeq 500	Illumina	N/A
GentleMACS Octo Dissociator	Miltenyi Biotec	Cat# 130-096-427
GentleMACS C tube	Miltenyi Biotec	Cat# 130-093-237
Microm HM525 NX Cryostat	Epredia™	Cat# 2210
CellDiscoverer7 microscope	ZEISS	N/A
Seahorse XFe96 Analyzer	Agilent	N/A
ChemiDoc™	Bio-Rad	N/A
EVOS-FL2 Microscope	Thermo Fisher Scientific	N/A
NanoDrop Lite Spectrophotometer	Thermo Fisher Scientific	Cat# ND-2000
Thermocycler (384 qPCR)	Bio-Rad	Cat# CFX384t
Synergy H1 Multimode Reader	BioTek	N/A
EchoMRI-900	EchoMRI LLC	N/A
Wireless running wheels	Med Associates	Cat# ENV-044 and ENV-047
Chatillon DFE II	Columbus Instruments	N/A